

Copyright  
by  
Yongseok Hong  
2009

The Dissertation Committee for Yongseok Hong Certifies that this is the approved  
version of the following dissertation:

**EXPERIMENTAL AND MATHEMATICAL INVESTIGATION OF  
DYNAMIC AVAILABILITY OF METALS IN SEDIMENT**

**Committee:**

---

Danny D. Reible, Co-Supervisor

---

Kerry A. Kinney, Co-Supervisor

---

Howard M. Liljestrand

---

Mary J. Kirisits

---

Lynn E. Katz

---

G. Christopher Shank

**EXPERIMENTAL AND MATHEMATICAL INVESTIGATION OF  
DYNAMIC AVAILABILITY OF METALS IN SEDIMENT**

by

**Yongseok Hong, B.S.E.,; M.S.E**

**Dissertation**

Presented to the Faculty of the Graduate School of

The University of Texas at Austin

in Partial Fulfillment

of the Requirements

for the Degree of

**Doctor of Philosophy**

**The University of Texas at Austin**

**December 2009**

## **Dedication**

To my Lord and my parents

## Acknowledgements

It has been a wonderful journey for the past four and half years in Austin and there are so many individuals who helped me one way or another. First of all, I would like to express my sincere gratitude to my supervisor, Dr. Danny Reible for his advice, patience and encouragement. He has given me the best direction to go whenever I lost my way in research, allowed me to have enough time to consider the research problems, and inspired me to have passion, enthusiasm, humility and self-confidence. I deeply appreciate his support again. Second of all, I would like to express many thanks to my co-supervisor, Dr Kerry Kinney who has encouraged, helped and taken care of me during my Ph.D work. I will not forget her great help. Lastly, special thanks to Dr. Liljestrand's wink which was an oasis during his class. My good friends, David Lampert, Nathan Johnson, Anthony (Tony) Smith, Andrew Davidson, Patrick Macnamra, Shawn Moderow, Brad Eck, Jaehak, Timothy Chess, Fei Yan, Dr. Lu, Matt Jordan, Gabe Trajo, Jinyong, Dr. Chen, Diana should get gratitude from me as well for the many unforgettable good memories.

# EXPERIMENTAL AND MATHEMATICAL INVESTIGATION OF DYNAMIC AVAILABILITY OF METALS IN SEDIMENT

Publication No. \_\_\_\_\_

Yongseok Hong, Ph.D.

The University of Texas at Austin, 2009

Supervisors: Danny D. Reible and Kerry A. Kinney

Contaminated sediments are periodically subjected to resuspension processes during either storm events or due to dredging. In sediments, metals are often contained in insoluble low bioavailability forms. Upon resuspension, however, biogeochemical processes associated with the exposure to more oxic conditions may lead to transformation and release of the metals, giving rise to exposure and risk in the water column. Batch experiments suggested that oxidation of reduced species and corresponding pH decrease were the most importance processes controlling metals release upon sediment resuspension. A mathematical model was implemented to better understand the complex underlying biogeochemical reactions that affect metals release. The model described the metals dynamics and other inter-related important biogeochemical factors well and was successful at predicting the metals release from different sediment reported in the literature.

Tidal and other cyclic variations in oxygen, pH and other relevant parameters in the overlying water may also lead to cyclic transformations and release of metals from surficial sediments. In simulated estuarine microcosm experiments, cyclic variations in pH and salinity due to freshwater/saltwater exchange were shown to lead to cyclic variations in metal release. Both pH and salinity were important factors controlling interstitial dissolved metals concentrations, however, in terms of freely dissolved metals concentrations, which have been considered to be more related with toxicity and bioavailability, pH was the single most important parameter. The mathematical model was extended to the conditions of the cyclic behavior in an estuary and successfully described metals release under such conditions. It is believed that the model can be used to predict the metals behavior in other sediments and conditions by model calibration with a similar experimental approach to that used in this study.

# Table of Contents

<b>Table of Contents.....</b>	<b>viii</b>
<b>List of Tables .....</b>	<b>xi</b>
<b>List of Figures.....</b>	<b>xii</b>
<b>Chapter 1: Introduction .....</b>	<b>1</b>
1.1 Background.....	1
1.2 Problem Identification .....	2
1.3 Research Objectives .....	4
1.4 Modeling and Experimental Approach.....	5
1.4.1 Mathematical Modeling .....	5
1.4.2 Experiments.....	7
1.5 Document Outline .....	8
<b>Chapter 2: Literature Review.....</b>	<b>9</b>
2.1 Heavy Metals in Anoxic Sediments .....	9
2.1.1 Diagenetic Reactions in Anoxic Sediment .....	9
2.1.2 AVS and SEMs.....	11
2.2 Heavy Metals in Aerobic Sediment.....	12
2.3 Summary.....	15
<b>Chapter 3: Experimental and Mathematical Investigation of pH Changes and Metals Release upon Sediment Resuspension .....</b>	<b>17</b>
3.1 Introduction.....	17
3.2 Materials and Experimental Procedures .....	19
3.2.1 General Techniques .....	19
3.2.2 Resuspension Experiments.....	19
3.2.3 Sediment Characterizations and Analytical Techniques.....	20
3.3 Mathematical Modeling of Sediment Resuspension Experiments.....	22
3.3.1 Modeling Oxidation Kinetics of Reduced Sediments .....	22
3.3.2 Modeling pH.....	24
3.3.3 Modeling Metals Complexation with Organics, Oxides and Inorganic Ligands .....	27
3.3.4 Acid Volatile Sulfide (AVS) and Simultaneously Extracted Metals (SEM) Calculation .....	29
3.3.5 Solution Techniques.....	29
3.4 Results and Discussion .....	30
3.4.1 Model Parameters and Initial Conditions .....	30
3.4.2 The Deviation of the Model Fit to Experimental Observations .....	35
3.4.3 Oxidation of Sulfur Species.....	36
3.4.4 Oxidation of Aqueous Phase and Solid Phase Ferrous Iron .....	39
3.4.5 Dissolved Carbonate Concentration and pH changes.....	41
3.4.6 Metals Release from Sediment .....	44
3.4.7 Sensitivity analysis .....	47
3.4.8 Modeling Ni, Zn and Pb Releases under Environmental Conditions .....	50
3.5 Conclusions.....	55

<b>Chapter 4: Experimental Investigation of pH and Salinity Effects on Metals Release and Sediment Early Diagenesis</b> .....	<b>56</b>
4.1 Introduction.....	56
4.2 Methods .....	58
4.2.1 General Methods and Reagents .....	58
4.2.2 Microcosm Experiments.....	58
4.2.3 Ex-situ Sediment Porewater Analysis .....	61
4.2.4 In-situ Porewater Characterizations .....	62
4.2.5 Sediment Analysis .....	63
4.2.6 Flux Calculation .....	64
4.3 Results and Discussion .....	64
4.3.1 General Sediment Properties .....	64
4.3.2 Effect of CdS <sub>(s)</sub> Spiking.....	66
4.3.3 Overlying Water pH and Salinity.....	68
4.3.4 Zn <sub>(aq)</sub> , Cd <sub>(aq)</sub> and Mn <sub>(aq)</sub> Release .....	70
4.3.5 Zn <sup>2+</sup> , Cd <sup>2+</sup> and Mn <sup>2+</sup> Release .....	74
4.3.6 AVS/SEM and Dissolved Cd and Zn Concentrations in Porewater .....	78
4.4 Conclusions.....	80
<b>Chapter 5: Modeling Investigation of pH and Salinity Effects on Metals Release and Sediment Early Diagenesis</b> .....	<b>82</b>
5.1 Introduction.....	82
5.2 Mathematical Modeling.....	84
5.2.1 Governing Equation.....	84
5.2.2 Electrostatic interactions on metals sorption .....	90
5.2.3 Grid Generation and Solution Technique.....	92
5.2.4 Model Parameters and Initial Conditions .....	93
5.3 Results and Discussion .....	97
5.3.1 The Deviation of the Model Fit to Experimental Observations .....	97
5.3.2 Sediment-Water Interactions and Sediment Early Diagenesis.....	98
5.3.3 Metals Behavior.....	106
5.3.4 Sensitivity analysis for the Cd and Zn release to overlying water .....	112
5.3.5 Effect of Diurnal Tidal Flow on Heavy Metals Releases in Estuary.....	115
5.4 Conclusions.....	118
<b>Chapter 6: Conclusions and Recommendations</b> .....	<b>120</b>
6.1 Summary.....	120
6.2 Implications .....	122
6.3 Recommendations for future work.....	123
<b>APPENDIX A: Supporting Information for Chapter 3</b> .....	<b>127</b>
A.1 pH Model Derivation.....	127
A.2 Figures .....	134
A.3 Tables .....	137
<b>APPENDIX B: Supporting Information for Chapter 4</b> .....	<b>138</b>
B.1 Figures .....	138
B.2 Tables.....	144
<b>APPENDIX C: Supporting Information for Chapter 5</b> .....	<b>145</b>

C.2 Figures .....	145
C.2 Tables.....	148
<b>APPENDIX D: Metal – Inorganic Ligands Complexation Reactions .....</b>	<b>149</b>
<b>APPENDIX E: Microcosm Tracer Test .....</b>	<b>151</b>
<b>APPENDIX F: Dissolved Organic Carbon Complexation with Metals.....</b>	<b>154</b>
F.1 The effect of dissolved organic carbon on metals release.....	154
F.2 Extending the proposed model to other sites where high dissolved organic carbon concentrations are expected.....	158
<b>References.....</b>	<b>160</b>
<b>Vita.....</b>	<b>171</b>

## List of Tables

Table 2.1	Factors affecting metals mobility (Adapted from Adriano, 2001).....	16
Table 3.1	Reaction Stoichiometry .....	22
Table 3.2	List of parameters associated with kinetics .....	31
Table 3.3	List of parameters for metal sorption (Lofts and Tipping, 1998; Tipping, 1998).....	32
Table 3.4	Model Initial Conditions.....	34
Table 3.5	Statistical Analysis of the Model Fit .....	36
Table 3.6	Sensitivity of Zn speciation related parameters to final Zn <sub>(aq)</sub> concentrations after 15 days sediment resuspension.....	48
Table 3.7	pH dependent sensitivity of Zn <sub>(aq)</sub> concentrations after 15 days.....	49
Table 3.8	Sensitivity of pH related parameters to final pH after 15 days sediment resuspension.....	50
Table 3.9	Model Initial Conditions.....	51
Table 3.10	Pb, Zn, and Ni sorption constants (Lofts and Tipping, 1998; Tipping, 1998).....	51
Table 3.11	PbS <sub>(s)</sub> , ZnS <sub>(s)</sub> , and NiS <sub>(s)</sub> oxidation rates (Carbonaro et al., 2005) .....	52
Table 4.1	Metal loadings in Anacostia River Sediments.....	65
Table 4.2	Porewater and solid phase characteristics changes by CdS <sub>(s)</sub> spiking.....	67
Table 5.1	Reactions in sediments .....	87
Table 5.2	The effect of surface charge and ionic strength on ‘exp(-2wZ)’ which modifies the strength of sorption to oxides and organics. ....	91
Table 5.3	List of parameters for primary redox reactions .....	94
Table 5.4	List of parameters for the reactions in sediments .....	95
Table 5.5	List of parameters for metal sorption (Lofts and Tipping, 1998; Tipping, 1998).....	96
Table 5.6	The diffusivity of ions at infinite dilution (Handbook of chemicals, CRC) .....	97
Table 5.7	Statistical Analysis of Model Fit.....	98
Table 5.8	Sensitivity of metal speciation related parameters to cumulative metal releases in the overlying water for 120 days. ....	114
Table 5.9	Simulated Estuary Conditions .....	115
Table A.1	Basic characteristics of sediments.....	137
Table B.1	Salts concentration in control, salt, and fresh water.....	144
Table C.1	Sediment Characteristics .....	148
Table F.1	Simulation conditions for resuspension experiments.....	154
Table F.2	Simulation conditions for microcosm experiments .....	155
Table F.3	K <sub>DOC,Me</sub> from WinHumic V(WHAM V) .....	159

## List of Figures

Figure 1.1	Conceptual dynamic environment for sediments.....2
Figure 1.2	The key processes affecting heavy metal speciation and corresponding mathematical approach.....6
Figure 3.1	Temporal sulfur species ( $AVS$ , $S^0$ , $SO_4^{2-}$ ) changes in (a) Anacostia River sediment and (b) Acid Sulfate sediment (Burton et al., 2006) upon resuspension. Symbols and error bars are the mean and standard deviations of duplicate experiments and lines are modeling results. ....37
Figure 3.2	Temporal ferrous iron species ( $Fe^{2+}_{(aq)}$ , $Fe^{2+}_{(s)}$ ) changes in (a) Anacostia River sediment and (b) Acid Sulfate sediments (Burton et al., 2006) upon sediment resuspension. Symbols and error bars are the mean and standard deviations of duplicated experiments and lines are modeling results. ....40
Figure 3.3	Transient pH and total dissolved carbonate species dynamics in (a) Anacostia River sediment and (b) Acid Sulfate sediments (Burton et al., 2006) upon sediment resuspension. Symbols and error bars are the mean and standard deviations of duplicate experiments and lines are modeling results.....42
Figure 3.4	Modeling results of proton production rates (mM/day) and cumulative proton production (mM) from (a), (c) Anacostia River sediment and (b), (d) Acid Sulfate sediments (Burton et al., 2006) resuspension. ....44
Figure 3.5	Dissolved Mg, Ca, Mn and Zn release from (a) ~ (d) Anacostia River sediment and (e) ~ (h) Acid Sulfate sediments (Burton et al., 2006). The broken lines in $Mn_{(aq)}$ graphs are the modeling results from the $pK_{Mn}$ (-1.4) adjustment for humic acid. Symbols and error bars are the mean and standard deviations of duplicated experiments and lines are modeling results. SE stands for standard errors (standard deviation of residuals) between experimental observations and model. ....45
Figure 3.6	Modeling results of temporal metals phase distribution (%) in dissolved ( $M_{(aq)}$ ), adsorbed to organics (M-OC), adsorbed to oxides (M-OX) and solid phases ( $MgCO_3$ , $CaCO_3$ , $MnS$ , $ZnS$ ) from (a) ~ (d) Anacostia River sediment and (e) ~ (h) Acid sulfate Sediments (Burton et al., 2006) resuspension. ....46
Figure 3.7	Transient dissolved (a) Pb, (b) Zn and (c) Ni concentration changes upon sediment resuspension under three different solid densities (dilute slurry = $7.7 \text{ g L}^{-1}$ , mild slurry = $77 \text{ g L}^{-1}$ , dense slurry = $770 \text{ g L}^{-1}$ ). Speciation of (d) Pb, (e) Zn and (f) Ni in dissolved ( $M_{(aq)}$ ), adsorbed to organics (M-OC), adsorbed to oxides (M-OX) and metal sulfides ( $MS_{(s)}$ ) upon sediment resuspension in mild slurry (sediment density = $77 \text{ g L}^{-1}$ ). ....53

Figure 3.8	Transient dissolved oxygen concentrations upon sediment resuspension under three different solid densities (dilute slurry = $7.7 \text{ g L}^{-1}$ , mild slurry = $77 \text{ g L}^{-1}$ , dense slurry = $770 \text{ g L}^{-1}$ ). .....	54
Figure 4.1	Temporal (a) salinity and (b) pH changes in the effluents where control, salt and fresh waters were continuously pumped and where fresh and cycling waters were cyclically pumped once every 8 days. Symbols and error bars are the mean and standard deviation of duplicated experiments respectively. ....	68
Figure 4.2	Effluent salinities and pH relations for 4 different microcosms. Average salinities and pH of duplicated experiments for 100 days were shown in circles symbols (●) with bi-directional standard deviations. Salinity and pH for the effluent of the cycling water microcosm are plotted in hollow squares (□). ....	70
Figure 4.3	Temporal changes of total dissolved (a) $\text{Zn}_{(\text{aq})}$ , (b) $\text{Cd}_{(\text{aq})}$ and (c) $\text{Mn}_{(\text{aq})}$ concentrations/fluxes under the continuous overlying water conditions. Temporal changes of total dissolved (d) $\text{Zn}_{(\text{aq})}$ , (e) $\text{Cd}_{(\text{aq})}$ and (f) $\text{Mn}_{(\text{aq})}$ concentrations/fluxes under cyclic overlying water conditions alternating with fresh and salt water once every 8 days. Symbols and error bars are the mean and standard deviations of duplicated experiments respectively. ....	71
Figure 4.4	Dissolved organic carbon concentrations in the overlying water. Symbols and error bars are the mean and standard deviations of duplicate experiments respectively. ....	74
Figure 4.5	Temporal changes of calculated freely dissolved (a) $\text{Zn}^{2+}$ , (b) $\text{Cd}^{2+}$ and (c) $\text{Mn}^{2+}$ concentrations/flux under the continuous overlying water conditions. Temporal changes of calculated freely dissolved (d) $\text{Zn}^{2+}$ , (e) $\text{Cd}^{2+}$ and (f) $\text{Mn}^{2+}$ concentrations/flux under cyclic overlying water conditions alternating with fresh and salt water once every 8 days. Symbols and error bars are the mean and standard deviations of duplicate experiments, respectively. ....	77
Figure 4.6	Vertical profiles of solid phase AVS/SEMs by 1 M HCl and dissolved phase Zn/Cd concentrations by DGT probe after 130 days sediments exposure to (a) control, (b) salt, (c) fresh and (d) cycling waters. Zn and Cd are considered in calculating SEMs. Symbols and error bars for AVS/SEMs are the mean and standard deviations of duplicated experiments respectively. Porewater $\text{Zn}_{(\text{aq})}$ and $\text{Cd}_{(\text{aq})}$ concentrations are data from single measurement. ....	79
Figure 5.1	Model initial conditions, boundary conditions, uneven grids and overlying water hydraulic conditions. Initial conditions were calculated from measured values using proper extraction and analytical techniques. ....	93
Figure 5.2	Experimental (symbols) and modeling (solid) results of temporal pH (a-c) and salinity (d-f) changes in the effluents for 100 days where fresh and salt	

- waters were continuously pumped and where fresh and cycling waters were cyclically pumped once every 8 days. Symbols and error bars are the mean and standard deviations of duplicated experiments respectively..... 99
- Figure 5.3 Experimental (symbols) and modeling (solid lines) results of vertical profiles of porewater Cl<sup>-</sup> in fresh, salt, and cycling water after 120 days. Symbols and error bars are the mean and standard deviations of duplicate experiments respectively. DMF are as follow: DMF<sub>Cl,salt</sub>=16.7%, DMF<sub>Cl,cycling</sub>=27.4%, DMF<sub>Cl,fresh</sub>=15.7%..... 100
- Figure 5.4 Experimental (symbols) and modeling (solid lines) results of vertical profiles of porewater SO<sub>4</sub><sup>2-</sup> under fresh, cycling, and salt water conditions after 120 days. Symbols and error bars are the mean and standard deviations of duplicate experiments respectively. DMF are as follows: DMF<sub>SO<sub>4</sub>,salt</sub>=16.4%, DMF<sub>SO<sub>4</sub>,cycling</sub>=13.0%, DMF<sub>SO<sub>4</sub>,fresh</sub>=6.0%. Broken lines are SO<sub>4</sub><sup>2-</sup> profiles without sulfate reductions..... 102
- Figure 5.5 Acid volatile sulfide (AVS) and simultaneously extracted metals (SEM) in sediments which are exposed to (a) freshwater, (b) cycling water, and (c) saltwater water for 120 days. Symbols and error bars are the mean and standard deviations of duplicate experiments, respectively. Solid lines are modeling results. Dashed lines are initial conditions. DMF are as follow: DMF<sub>AVS,salt</sub>=18.1%, DMF<sub>AVS,cycling</sub>=17.4%, DMF<sub>AVS,fresh</sub>=19.6%, DMF<sub>SEM,salt</sub>=4.5%, DMF<sub>SEM,cycling</sub>=3.6%, DMF<sub>SEM,fresh</sub>=6.0%..... 103
- Figure 5.6 Experimental (symbols) and modeling (solid lines) results of vertical profiles of porewater pH in (a) fresh, (b) cycling, and (c) salt water after 120 days. pH was determined by microelectrodes. Symbols and error bars are the mean and standard deviations of duplicate experiments respectively. DMF are as follow: DMF<sub>pH,salt</sub>=1.9%, DMF<sub>pH,cycling</sub>=1.9%, DMF<sub>pH,fresh</sub>=3.7%. DMF without correction of diffusion are as follow: DMF<sub>pH,salt</sub>=5.9%, DMF<sub>pH,cycling</sub>=2.8%, DMF<sub>pH,fresh</sub>=3.7%..... 104
- Figure 5.7 Temporal oxygen profile developments at the surficial sediments under (a) freshwater, (b) cycling water, and (c) saltwater..... 105
- Figure 5.8 Experimental (symbols) and modeling (solid) results of temporal Zn<sub>(aq)</sub> (a-c), Cd<sub>(aq)</sub> (d-f), Mn<sub>(aq)</sub> (g-i) concentrations changes in the effluents for 100 days where fresh and salt waters were continuously pumped and where fresh and cycling waters were cyclically pumped once every 8 days. Symbols and error bars are the mean and standard deviations of duplicate experiments respectively. Broken lines indicate the model estimated uncomplexed metal concentration..... 107
- Figure 5.9 Experimental (symbols) and modeling (solid lines) results of vertical profiles of Mn<sub>(aq)</sub> (a-c), Fe<sub>(aq)</sub> (d-f), Zn<sub>(aq)</sub> (g-i) and Cd<sub>(aq)</sub> (j-l) in porewater after 120 days sediments exposure to continuous freshwater, saltwater and to alternating freshwater and saltwater once every 8 days. Mn<sub>(aq)</sub> and Fe<sub>(aq)</sub> were determined from duplicate experiments by voltametric

microelectrodes (solid and hollow diamond) in-situ. For the better description of the vertical profiles of  $Fe_{(aq)}$  (dashed line) under salt water condition, 18.0  $\mu\text{mol/g}$  of reducible iron was assumed to present. Two independent methods, DGT (single measurement, square with dashed line) and centrifugation/filtration (duplicate measurements, solid and hollow triangles), were used to determine porewater Zn and Cd concentrations.

..... 110

Figure 5.10 Temporal profiles of newly precipitated  $FeOOH_{(s)}$  by  $Fe^{2+}$  oxidation at the surficial sediments under (a) freshwater, (b) cycling water, and (c) saltwater..... 111

Figure 5.11 Effect of overlying water current on salinity, pH and metals release in estuary..... 116

Figure 5.12 Quasi steady state dynamics of salinity, pH and metals concentrations . 117

Figure A.1 Dissolved oxygen concentration changes in Anacostia Sediment Resuspension experiment ..... 134

Figure A.2 Redox potential changes in Anacostia Sediment Resuspension experiment ..... 135

Figure A.3 Organic carbon concentration changes in Anacostia Sediment Resuspension experiment ..... 136

Figure B.1 Microcosm dimensions..... 138

Figure B.2 Schematics and experimental setup of microcosms..... 139

Figure B.3 Dissolved Fe concentrations in the overlying water. .... 140

Figure B.4 Vertical profiles of porewater pH,  $Cl^-$  and  $SO_4^{2-}$  concentrations after 130 days sediments exposure to control, salt, fresh and cycling waters. pH and  $Cl^-$  concentrations were determined in-situ using microelectrodes.  $SO_4^{2-}$  concentrations were determined from centrifuged porewater. Symbols and error bars are the mean and standard deviations of duplicated experiments respectively. .... 141

Figure B.5 Vertical profiles of porewater  $Fe_{(aq)}$  and  $Mn_{(aq)}$  determined by voltametric microelectrode and centrifugation..... 142

Figure B.6 Vertical profiles of porewater DOC concentrations. Symbols and error bars are the mean and standard deviations of duplicated experiments respectively. .... 143

Figure C.1 Transient pH,  $Cl^-$  and  $SO_4^{2-}$  profiles developments in sediment porewaters under freshwater, saltwater, and cycling water conditions..... 145

Figure C.2 Phase distribution of Cd, Zn, Fe and Mn to dissolved, particulate organic carbon, oxides, and sulfide (carbonate for  $Fe^{2+}$ ) under fresh water condition. The metals distributions are similar for other overlying water conditions..... 146

Figure C.3 T-Cell exposed to fresh water. Note the dark precipitates right below the surficial sediments..... 147

Figure C.4	T-Cell exposed to Salt water. Note the dark precipitates covering the whole sediment depth.....	147
Figure E.1	Standard curve for food coloring. ....	151
Figure E.2	Tracer test without overlyingwater aeration. ....	152
Figure E.3	Tracer test with overlyingwater aeration. ....	153
Figure F.1	The distribution of Zn in resuspension experiments. ....	155
Figure F.2	The DOC dependent distribution of Zn, Cd, and Cu in fresh and saltwater. Cu is simulated to compare the strength of metal complexation with DOC. Typical DOC concentration in the overlying water was less than 3 mg/L only for the first 10 days. The DOC complexation with Cd and Zn with DOC were not significant. ....	156
Figure F.3	The metal-DOC complex concentrations in sediment porewater where metal sulfides are present. $[M^{2+}]$ were calculated from solubility products of metal sulfides when sulfide concentrations were $10E-6,-7,-8M$ . $[DOC-M]$ were calculated from the $K_d$ which were calculated from Figure F.2 in freshwater composition. In anoxic sediments, sulfide minerals control the solubility of dissolved metals concentrations even when DOC concentration is close to 100 mg/L. ....	157
Figure F.4	Zn speciation when $10^{-6}$ M of Zn is introduced to sediment porewater. $[HS^-]$ were changed from $10^{-9}$ to $10^{-12}$ M. When $[HS^-]$ is greater than $10^{-10}M$ and when DOC is less than 100 mg/L, almost all Zn would be precipitated as $ZnS_{(s)}$ . However, when $[HS^-]$ is less than $10^{-12}M$ , $ZnS_{(s)}$ will not precipitate and aqueous phase complexation will determine Zn speciation. ....	158

## Chapter 1: Introduction

### 1.1 BACKGROUND

Heavy metals, metals that are toxic to humans or animals (Duffus, 2002), are some of the primary contaminants of concern in aquatic sediments. Heavy metals have been used for thousands of years and occur naturally by weathering of parent rocks and metallic minerals. Industrial and metallurgical activities such as mining, smelting and metal finishing, accelerate the heavy metal contamination (Bradl, 2005). Once they are released into the environment, they are not degraded but persist in various forms and eventually are deposited with sediments as permanent sinks and sources for heavy metals in aquatic systems (Wang and Chen, 1997).

In anoxic sediments, the heavy metals are mainly precipitated, co-precipitated or adsorbed to authigenic sulfide minerals that are produced by sulfate reduction. The metal sulfide minerals are insoluble and non-bioavailable, but the contaminated anoxic sediments are periodically subject to resuspension processes during either storm events or due to dredging. When the anoxic sediments are resuspended, biogeochemical processes associated with the exposure to more oxic conditions may lead to transformation and release of the metals, giving rise to exposure and risk in the water column. Furthermore, diurnal tidal flows in estuaries and other cyclic variations in oxygen, pH, salinity and other relevant parameters in the overlying water, may also lead to cyclic transformations and release of metals from surficial sediments. Figure 1.1 summarizes the dynamic environment of sediments.

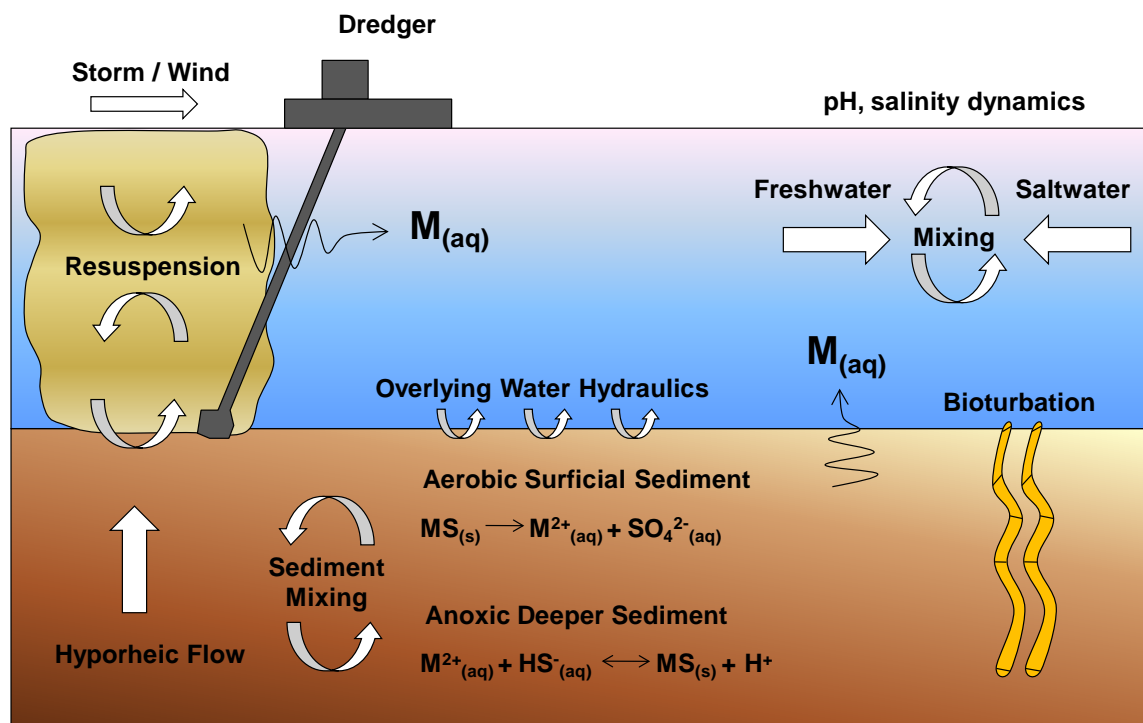


Figure 1.1 Conceptual dynamic environment for sediments

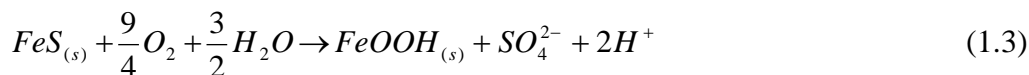
## 1.2 PROBLEM IDENTIFICATION

It has been recognized that total metal concentrations in sediments are a poor estimate of metal toxicity while pore water metal concentrations are often correlated with observed adverse biological effects (Di Toro et al., 1990; Berry et al., 1996; Hansen et al., 1996). Hence, extensive research has been conducted to identify the key partitioning phase that enables us to estimate porewater metal concentrations in sediments. Reactive iron sulfides, such as amorphous iron mono sulfide, mackinwite, greigite and pyrrhotite have been considered to be the dominant phases for scavenging metals and determining the dissolved metal concentration in anoxic sediment.  $FeS_{(s)}$  has a higher solubility product than other heavy metal sulfides ( $CdS_{(s)}$ ,  $NiS_{(s)}$ ,  $CuS_{(s)}$ ,  $ZnS_{(s)}$ ,  $AgS_{(s)}$ ,  $PbS_{(s)}$ )

so that any dissolved heavy metals may displace the  $Fe^{2+}$  and precipitate as a metal sulfide as follows.



As a result, sediments that contain more reactive sulfides than heavy metals may not be toxic because the metals would be bound as relatively insoluble metal sulfides (Ankley et al., 1996). An operational measure of the amount of sulfides available for binding metals is the acid volatile sulfide (AVS) to simultaneously extracted metals (SEM) ratio (Allen et al., 1993) and this measure evaluates the  $H_2S$  evolved and the metals released after treatment of the sediment with a strong acid. However, several processes can expose the anoxic sediment to an oxic environment: (1) resuspension by storm events or mechanical dredging, (2) resuspension by freshwater and salt water mixing from diurnal flow, and (3) enhancement of oxygen diffusion into anoxic sediment by the activity of benthic organisms. Upon contact with aerobic water, reactive iron sulfides, metal sulfides and other reduced species will be oxidized followed by release of the associated heavy metals and acid production in the aqueous phase.



After the oxidation, some of the released heavy metals can be immobilized by strong sorption to particulate organic matter (POM) and oxides (iron, manganese, aluminum oxides) potentially reducing any adverse effects of the sulfide oxidation.

In aerobic sediments, the idea that dissolved metals will be precipitated as insoluble metal sulfides by reactive sulfides is not applicable due to the absence of iron sulfides. Thus resuspended or surficial sediment may exhibit greater dissolved metal toxicity and bioavailability. This can also be problematic in the entire biologically active

zone of sediments because most of the habitat of sediment dwelling organisms may be oxidized by enhanced oxygen diffusion due to organism activity, i.e. bioturbation.

Dissolved metals concentrations in aerobic sediments can be affected by many factors, such as pH, competing cations, complexing ligands, and DOC (dissolved organic carbon), which can vary over several orders of magnitude. In particular, interstitial water pH in estuarine and river sediments can change in the range of 5.5 to 8.5 depending on the biogeochemical reactions and overlying water hydrodynamics (Cai and Wang, 1998; Ringwood and Keppler, 2002). It is important to remember that pH is based on a log scale and metal speciation is very sensitive to pH, so even a change of 0.5 – 1.0 unit can lead to substantial changes in metal speciation. Although the significant impact of pH on metals speciation in sediments is well known, the dynamics of pH variabilities in natural systems have been neglected in many of the current mathematical models that have been developed to study metal dynamics in sediments (Carbonaro et al., 2005; Sevinc et al., 2007; Canavan et al., 2007).

### **1.3 RESEARCH OBJECTIVES**

The purpose of this research was to investigate the release of heavy metals from contaminated sediment as a result of sediment resuspension or cyclic changes in the surrounding environment and to develop a better quantitative description of heavy metal speciation model under those conditions for the management of heavy metal contaminated sediments. A mathematical model is developed incorporating pH changes as a result of biogeochemical reactions and pH dependent metals sorption to sediment particles. Batch experiments and microcosm experiments were conducted to support the

mathematical model framework and to focus on understanding the dynamics of the metal transformation and release processes. Specific objectives include:

1. Develop a mathematical model that can simulate biogeochemical reactions and heavy metals releases upon sediment resuspension.
2. Validate and calibrate the model with experimental observations focused on metals ( $\text{Zn}_{(\text{aq})}$ ,  $\text{Fe}_{(\text{aq})}$ ,  $\text{Mn}_{(\text{aq})}$ ,  $\text{Ca}_{(\text{aq})}$ ,  $\text{Mg}_{(\text{aq})}$ ), AVS, pH,  $\text{O}_2$ ,  $\text{SO}_4^{2-}$ , and total dissolved carbonates.
3. Investigate a heavy metal dynamics under more realistic sediment resuspension events using the calibrated model.
4. Extend the developed model to a more a complicated system, i.e. estuarine sediments that may be subject to cyclic variations of key parameters.
5. Validate and calibrate the model with experimental observations, such as dissolved metals ( $\text{Zn}_{(\text{aq})}$ ,  $\text{Cd}_{(\text{aq})}$ ,  $\text{Mn}_{(\text{aq})}$ ), pH and salinity in the overlying water as well as AVS, SEMs, pH,  $\text{SO}_4^{2-}$ ,  $\text{Cl}^-$ , and metals ( $\text{Zn}_{(\text{aq})}$ ,  $\text{Cd}_{(\text{aq})}$ ,  $\text{Mn}_{(\text{aq})}$ ,  $\text{Fe}_{(\text{aq})}$ ) concentrations in both porewater and sediments.
6. Model the heavy metals release resulting from the cyclic changes in pH and salinity from diurnal tidal flow.

## **1.4 MODELING AND EXPERIMENTAL APPROACH**

### **1.4.1 Mathematical Modeling**

Current models (e.g., Carbonaro et al., 2005) for assessing the potential heavy metal toxicity in sediment include metal sulfides formation, metal sulfides oxidation, and metal partitioning onto organic carbon and iron oxides with vertical diffusive transport. The model incorporates acid volatile sulfides (AVS) and simultaneously extracted metals

(SEM) calculations, which have been used as an indicator of metal toxicity (i.e. toxic if SEM/ AVS > 1)

$$AVS = [FeS_{(s)}] + \sum_{MS} \alpha_{MS} [MS_{(s)}] \quad (1.4)$$

$$SEM = \sum_M (M_{aq} + M_s + M_p + \alpha_{MS} [MS_{(s)}]) \quad (1.5)$$

where  $\alpha_{MS}$  is the fraction of  $MS_{(s)}$  extracted by the AVS/SEMs procedure,  $M_{aq}$  is the porewater (aqueous phase) metal,  $M_s$  is the metal sorbed to solids, either oxides or organic carbon, and  $M_p$  is metal precipitates other than metal sulfides soluble in 1 M hydrochloric acid.

The model (Carbonaro et al., 2005) neglects pH dependent metal sorption to sediment particles, which could have a significant influence on potential heavy metal toxicity. As a result, this research has focused on including those factors explicitly in the proposed model. Figure 1-2 shows the key processes in the proposed model and corresponding mathematical approach.

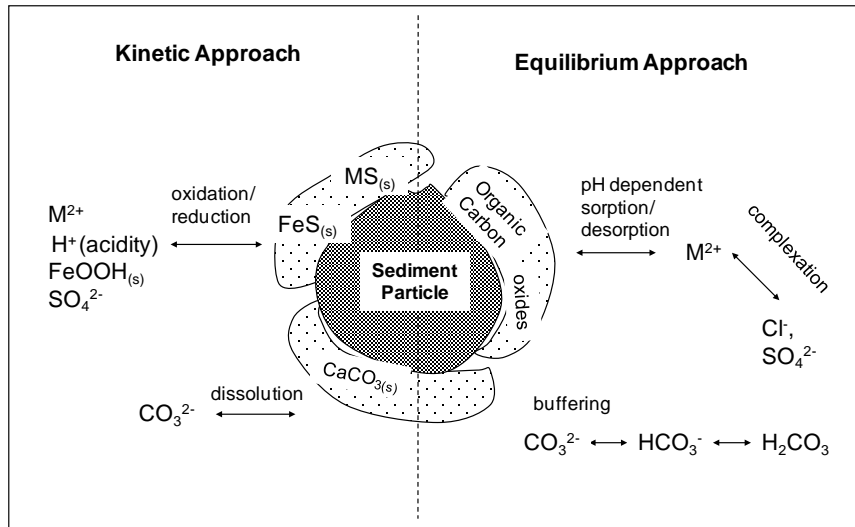


Figure 1.2 The key processes affecting heavy metal speciation and corresponding mathematical approach

The proposed model has several equilibrium sub-models, such as carbonate species acid-base chemistry and metal sorption to organic carbon or oxides. The carbonate species equilibrium and acidity production/consumption by biogeochemical reactions are coupled. The equilibrium and kinetic reactions are decoupled algebraically and transient pH changes are explicitly incorporated as ordinary differential equations.

The partitioning of metals to sediments is assumed to be in equilibrium because the characteristic time of metals sorption to particles is typically faster than other oxidation-reduction biogeochemical reactions. SCAMP (Surface Chemistry Assemblage Model for Particles, Lofts and Tipping, 1998) was used to describe metals sorption to sediments. Humic acid represents sediment organic carbon and the acid extractable iron, manganese, aluminum and silicate are considered as minerals composing sediment particles. To describe metal sorption to humic acids, Model VI (Tipping, 1998) is used. The complete use of the SCAMP approach may lead to hundreds of non-linear equations for a single metal. The approach would be not practical because it is computationally expensive if the distribution needs to be calculated in every time step for transient simulations. To overcome the difficulties, electrostatic interactions and multidentate complexation are neglected and the model is calibrated with experimental observations.

#### **1.4.2 Experiments**

To investigate the dynamic availability of metals, two experiments were conducted. The first was a resuspension experiment employing sediments from the Anacostia River, Washington DC in aerated water. To supply oxygen and mixing, ambient air was continuously bubbled into the sediment slurry. Samples were taken regularly and the particulate and aqueous phases were separated by filtration (0.45  $\mu\text{m}$ ).

pH, O<sub>2</sub>, Zn, Fe<sup>2+</sup>, Mn, Ca, Mg, and SO<sub>4</sub><sup>2-</sup> were analyzed from the aqueous phase and AVS and oxalate extractable Fe<sup>2+</sup> were extracted from the solid phase.

The second experiment was to study the dynamics of heavy metals release from estuary sediments. Estuaries are dynamic systems which can exhibit daily or seasonal pH and salinity fluctuations. CdS<sub>(s)</sub>-spiked Anacostia River sediments were alternately exposed to freshwater (pH=6.8, salinity=1.0 g L<sup>-1</sup>) and saltwater (pH=8.3, salinity=35 g L<sup>-1</sup>). Samples were taken regularly and dissolved metal concentrations (Zn<sub>(aq)</sub>, Cd<sub>(aq)</sub>, Fe<sub>(aq)</sub>, Mn<sub>(aq)</sub>), pH and salinity were determined from overlying water. After 100 days, biogeochemical factors in solid and aqueous phase in sediments were characterized by both in-situ and ex-situ techniques. The experimental observations were used to calibrate and validate the proposed model to build confidence in the model and to help identify processes that must be incorporated within the model to improve predictions.

## 1.5 DOCUMENT OUTLINE

The literature is reviewed in Chapter 2 with a focus on heavy metals behavior in both aerobic and anaerobic sediments as well as conventional modeling approaches for assessing heavy metals toxicity in sediments. In Chapter 3, a mathematical model is developed and verified with lab experiments and further tested with experimental data collected by Burton et al. (2006). In Chapter 4, the effect of cyclic changes in pH and salinity were investigated in microcosm experiments. During the experiments, several controls were applied to elucidate the impact of pH and salinity on metals release. In Chapter 5, the experimental observations in Chapter 4 were further investigated by the model which was extended from Chapter 3. This document is devoted to conclusions and future work in Chapter 6.

## Chapter 2: Literature Review

Heavy metal speciation is closely linked to oxidation reduction reactions in sediments. In Section 2.1, important reduction reactions for heavy metals speciation are reviewed. Several fundamental theories for assessing sediment quality criteria including AVS (acid volatile sulfide) and SEMs (simultaneously extracted metals) are described. The oxidation of anoxic sediments and the sorption of heavy metals to particulate organic carbon, oxides and other minerals are covered in Section 2.2.

### 2.1 HEAVY METALS IN ANOXIC SEDIMENTS

#### 2.1.1 Diagenetic Reactions in Anoxic Sediment

Sediments are complex mixtures of minerals and organic materials that are transported and settle at the bottom of water bodies. After sedimentation, microorganisms utilize organic carbon to obtain energy and to synthesize cellular components. The microorganism will first utilize oxygen ( $O_2$ ) to metabolize organic matter. If dissolved  $O_2$  becomes sufficiently depleted by the aerobes, further organic decomposition continues by use of nitrate ion ( $NO_3^-$ ) as an oxidizing agent (Sorensen, 1982). Upon complete removal of  $O_2$  and  $NO_3^-$ , anaerobic microorganisms use iron, manganese oxides, sulfate, and organic materials as electron acceptors (Lovely, 1991; Thanmdrup et al., 1994) based on the metabolic free energy yield for each reaction.

Sometimes,  $FeOOH_{(s)}$ ,  $MnO_2$  and  $SO_4^{2-}$  are reduced simultaneously (Furrer and Wehrli, 1996), but the reactions generally succeed one another, in the order of their free energy yield until each oxidizing agent is exhausted. Thus, in a typical near-shore marine sediment, oxygen and nitrate are decomposed in the top few centimeters (Boudreau,

1991) and sulfate reduction is dominant in the sediments below. In freshwater sediment, manganese and iron are dominant oxidants while sulfate reduction is not as significant as in marine sediment due to low sulfate concentration (Cai et al., 2002).

The reduced byproducts, such as  $\text{NH}_4^+$ ,  $\text{Mn}^{2+}$ ,  $\text{Fe}^{2+}$  and  $\text{S}^{2-}$  undergo further reactions.  $\text{NH}_4^+$  and  $\text{Mn}^{2+}$  are mainly oxidized by  $\text{O}_2$  because they are produced right below the aerobic zone in the sediment.  $\text{S}^{2-}$  tends to be precipitated with  $\text{Fe}^{2+}$  and/or other relevant metals as AVS, but  $\text{S}^{2-}$  can sometimes reduce  $\text{FeOOH}_{(s)}$  to  $\text{Fe}^{2+}$ . More reactions play important roles in cycling redox sensitive species (Wang, 1996) and these complicated coupled reactions are called secondary redox reactions. The sum of total physical, chemical, and/or biological processes that bring about changes in sediment subsequent to deposition in water is called 'Early Diagenesis' (Berner, 1980).

Diagenesis can be summarized as the primary and secondary redox reactions in addition to precipitation, dissolution and acid-base reactions as well as transport of species in sediment pore water. Although early diagenesis is composed of complex biogeochemical processes, there have been several modeling efforts that successfully reproduced the concentration of redox sensitive species in pore water (Lovely and Klug, 1986; Wang and Van Cappellen, 1996; Furrer and Wehrli, 1996).

During sediment diagenesis, heavy metals will participate in previously described biogeochemical reactions. A particularly important reaction is adsorption or co-precipitation with iron oxide ( $\text{FeOOH}_{(s)}$ ), as metals have a high affinity for this compound. The metals entrained in iron oxide can be released, subsequently increasing the availability due to the reduction of iron oxide (Bousserrhine et al., 1999; Zachara et al., 2001; Cooper et al., 2005). The remobilization or immobilization of heavy metals under iron reducing conditions may be significant but sulfide would control the metal

speciation more strongly than iron oxide under anoxic conditions due to its high affinity for heavy metals.

### 2.1.2 AVS and SEMs

The toxicity of heavy metals in anoxic sediments have been screened by total metal loadings normalized by sediment mass (Sullivan et al., 1985; Persaud et al., 1989; Long and Morgan, 1991; MacDonald et al., 1996), but the toxicity derived from bulk sediment loading has been proven to vary by one or more orders of magnitude among different sediments (Di Toro et al., 1990). Hence, the relevant sediment properties should be taken into account to better assess the toxicity and bioavailability of metals in contaminated sediments.

A key partitioning phase controlling the heavy metal speciation in anoxic sediments is authigenic sulfide minerals. Due to the complexities and difficulties in extracting authigenic sulfide minerals separately, operationally defined AVS (acid volatile sulfide) has been used. AVS represents sulfide that is evolved from acidified sediment by adding 1 M HCl. It usually includes sulfides ( $\text{H}_2\text{S}$ ,  $\text{HS}^-$ ,  $\text{S}^{2-}$ ), amorphous iron sulfide ( $\text{FeS}_{(s)}$ ), mackinawite ( $\text{FeS}_{(s)}$ ) and greigite ( $\text{Fe}_3\text{S}_4_{(s)}$ ). At the same time, the metals that are dissolved in 1M HCl are defined as SEMs (Simultaneously Extracted Metals) (Allen et al., 1993).

Although the detailed heavy metal scavenging mechanisms by AVS are still unclear (Rickard and Morse, 2005), there have been many studies that correlate the toxicity and AVS/SEM in anoxic sediments (Di toro et al., 1990; Di Toro et al., 1992; Ankley et al., 1996; Berry et al., 1996; Hansen et al., 1996; Liber et al., 1996; Berry et al., 2004). In short, if there is more AVS than SEM, the sediment demonstrates less toxicity

due to displacement reactions. However, if there is less AVS than SEMs, there may be significant metal toxicity because there are not enough sulfides to scavenge the free metals. The fundamental assumption for estimating the bioavailability of toxic metals using AVS/SEM is that the reactive sulfide can be used to estimate the dissolved metal ions that would be toxic to aquatic organisms. Since the metal sulfides are usually less soluble than  $\text{FeS}_{(s)}$ , a typical dominant sulfide phase in AVS, dissolved metals will displace  $\text{Fe}^{2+}$  to form more insoluble metal sulfide. Besides AVS, organic carbon has been considered as an additional binding phase sequestering the free metal ions (Mahony et al., 1996). As a result, current sediment quality criteria consider metal sorption to organic carbon in anoxic sediment (EPA, 2005). The metal partitioning to organic carbon will be covered in the next section.

AVS/SEM appears to be a good estimate of heavy metal bioavailability in anoxic sediments. Grabowski et al. (2001) observed seasonal variation of AVS that leads to a misinterpretation of the sediment toxicity depending on the sampling time of a year. The fundamental basis for AVS/ SEM also breaks down during oxidizing conditions when sulfur may be present as sulfates rather than sulfides. Care should be taken when AVS/SEMs is used to assess the sediment toxicity under certain circumstances.

## **2.2 HEAVY METALS IN AEROBIC SEDIMENT**

While AVS/SEM has been considered a simple and conservative approach for predicting the toxicity of heavy metals in anoxic sediment, it has not been applicable to surficial sediment or re-suspended sediment (Chapman et al., 1998; Chapman et al., 1999). The oxidation of AVS has been known to be fast with a half life of less than 4 hours (Nelson, 1978; Di Toro et al., 1996; Simpson et al., 1998; Simpson et al., 2000) in

the presence of oxygen. Once the AVS is oxidized by sediment resuspension, the metals associated with AVS may be released into the water column. Then the availability of heavy metals is determined by oxides or organic carbon in the sediment particles which become the primary metal scavengers (Schwertmann and Taylor, 1989).

In aerobic sediment, the metal toxicity or availability is determined by other binding phases, such as POM (particulate organic carbon), dissolved (colloidal) organic carbon, iron oxide, manganese oxide, aluminum oxide, clays and other minerals. The metal speciation to these phases is further complicated by several sorption-related mechanisms: (1) pH dependence of available sorption sites, (2) heavy metal competition with cations ( $\text{Ca}^{2+}$ ,  $\text{Mg}^{2+}$ ) to sorption sites and (3) complexation of heavy metals with dissolved colloidal organic and or inorganic ligands.

The sorption group consisting of iron, manganese and aluminum oxides (Tessier et al., 1985; Wang and Chen, 1997) has been considered to be the dominant sorption phase for heavy metals due to their high specific surface area and affinity. The heavy metal sorption to iron oxides have been studied widely and the behavior is well described by surface complexation models (Dzombak and Morel, 1990). Besides oxide phase, natural organic carbon is one of the dominant phases that control metal speciation in aerobic sediment as well (Hart, 1981; Fu et al., 1992; Tessier et al., 1993). Even in anoxic sediment, organic carbon seems to play an important role in controlling heavy metal availability (Mahony et al., 1996). Among the natural organic carbon, humic substances, which generally comprise half of the organic carbon (Thurman and Malcom, 1981) are known to be the major component of complexation with trace metals (Schnitzer and Kahn, 1972).

Several mathematical models (Kinniburgh et al., 1996; Tipping, 1998; Gustafsson, 2001) have been suggested to estimate ion binding to humic acid under a variety of experimental conditions. Among the models, 'Model VI' (Tipping, 1998) and 'NICA-Donnan Model' (Kinniburgh, 1996) would be the most comprehensive models that can fit an extensive experimental data set with reasonable accuracy.

Model VI allows for eight different types of sites, some of which are close enough together to behave as bidentate or tridentate sites. It uses a simple empirical electrostatic model to differentiate between generic Coulombic binding and specific binding. Model VI can describe metal-metal competition and assumes that the metal ion affinities are directly related to the proton affinities. The NICA-Donnan model assumes two binding mechanisms; specific interactions between the cation and negatively-charged surface functional groups and nonspecific Coulombic binding to any residual negative charge. And the specific binding is described by NICA model, and the nonspecific binding is described by the Donnan model (Kinniburgh, 1996).

There have been a couple of models that extended the metals – oxides and metals – organics interactions to the assemblage of oxides and minerals, in other words, sediments and soils. SWAMP (Sediment Water Algorithm for Metal Partitioning, Radovanovic and Koelmans, 1998) and SCAMP (Surface Chemistry Assemblage Model for Particles, Lofts and Tipping, 1998) are comprehensive and mechanistic models that can be used to estimate metal distribution in aquatic sediments based on sediment chemical composition and water chemistry. Both of the models assume the sediment is a mixture of pure oxides and humic acid and the metals are binding to each sites without any interactions among the minerals and organics. The total adsorbed metals are calculated by linear addition of metals adsorbed to each phase.

Although oxides and organic carbon seem to control the heavy metal speciation in aerated sediments (Chapman et al., 1999), there are several limitations for applying the mechanistic models to real world problems. In fact, sediment particles most commonly occur as complex aggregates, containing inter-layered and intermeshed iron oxide coating, organic coatings, and discrete manganese oxide particles, often surrounding a clay particle (Luoma and Davis, 1983). As a result, the complex structure of sediments and the interactions among phases are the most uncertain factors and have been neglected. Further research is needed for this topic.

### **2.3 SUMMARY**

In conclusion, the heavy metal release from sediment upon resuspension or heavy metal flux from bottom sediments depends on the oxidation kinetics of authigenic sulfide minerals and the sorption to individual binding phases. The metal sorption is further complicated by water chemistry such as pH, O<sub>2</sub>, competition with other cations and complexation with ligands. The factors that affect heavy metal speciation are summarized in Table 2.1.

Table 2.1 Factors affecting metals mobility (Adapted from Adriano, 2001)

Factors	Process	Mobility into aqueous phase
Low pH	Decrease $M^{2+}$ sorption onto oxides (Fe,Mn,Al) by increasing positively charged surface.	Increase
	Decrease $M^{2+}$ sorption onto organic carbon by protonating surface functional groups.	Increase
	Increase organic carbon sorption onto oxides (Fe,Mn,Al)	Decrease
High pH	Increase $M^{2+}$ sorption onto oxides (Fe,Mn,Al) by increasing negatively charged surface.	Decrease
	Increase $M^{2+}$ sorption onto organic carbon by deprotonating surface functional groups.	Decrease
	Decrease organic carbon sorption onto oxides (Fe,Mn,Al)	Increase
	Increase $M^{2+}$ precipitation as carbonates and sulfide	Decrease
High clay(%)	Increase ion exchange for $M^{2+}$ (at all pH)	Decrease
High POC	Increase $M^{2+}$ sorption to organic carbon	Decrease
High DOC	Increase $M^{2+}$ complexation with DOC	Increase
High $Ca^{2+}, Na^+$	Increase competition for sorption sites	Increase
High $Cl^-$ , $CO_3^{2-}$	Increase $M^{2+}$ complexation with ligands	Increase
High oxides(%)	Increase $M^{2+}$ sorption to oxides	Decrease
Low redox	Decrease dissolved $M^{2+}$ by precipitation of metal sulfide	Decrease

## Chapter 3: Experimental and Mathematical Investigation of pH Changes and Metals Release upon Sediment Resuspension

### 3.1 INTRODUCTION

The mobility and bioavailability of heavy metals have been related to the balance between acid volatile sulfides (AVS) and simultaneously extracted metals (SEM) as operationally determined by 1 M HCl (Allen et al., 1993). The amorphous iron sulfide ( $\text{FeS}_{(s)}$ ), the major metal sulfide species in AVS, is more soluble than other divalent metal sulfides so that the dissolved metals precipitate with sulfide displacing  $\text{Fe}^{2+}$  in  $\text{FeS}_{(s)}$  (Di Toro et al., 1990). Consequently, heavy metals in anoxic sulfidic sediments are often contained in insoluble, low bioavailability forms without significant adverse effects on aquatic organisms.

However, sediments are periodically subjected to oxic conditions during either storm events or due to dredging activities. Moreover, surficial sediments are in contact with aerobic overlying water and oxygen may penetrate from a few millimeters to centimeters by local sediment resuspension (Audry et al., 2006) and/or by enhanced oxygen diffusion from bioturbation (Boudreau, 1997). In aerobic environments, reduced metal sulfides are likely to be oxidized and release soluble forms by biogeochemical processes. Hence, the AVS/SEM approach is not applicable in aerobic sediments (Chapman et al., 1998). During short term resuspension events followed by deposition, the kinetics of the oxidation and release processes are important to define the potential exposure and risk of the metals released into the aqueous phase.

Oxidation of AVS and the resulting pH decrease have been recognized as the primary factor influencing heavy metal remobilization from initially anoxic sediments.

(Burton et al, 2006). Acidification affects the saturation state of minerals (Stumm and Morgan, 1996) and the characteristics of metal sorbing surfaces in sediments (Wang and Chen, 1997). Sometimes, oxidation of metal sulfides, such as  $ZnS_{(s)}$  and  $CdS_{(s)}$ , slowly release metals without significant acidification (Simpson et al., 1998) and biological transformation of metal-associated species are important mechanisms for metal release (Lors et al., 2004) as well. Complexation of metals with dissolved ligands, such as dissolved organic carbon and inorganic anions, enhance heavy metal remobilization (Gao et al., 2003). Resuspension energy and duration by tidal flow may also play an important role in phase partitioning of metals in sediments (Kalnejais et al., 2007).

Sediment resuspension, however, does not necessarily lead to acidification of overlying water due to the buffering capacity of water, typically dilute sediment suspensions and/or lack of acid-producing species in sediments (Saulnier and Mucci, 2000; Cappuyns and Swennen, 2005). Metals release is the consequence of several interrelated biogeochemical processes that the degree of release can be dissimilar under different experimental or sediment conditions. To better understand and predict the degree of acidification and metals release depending upon the sediment characteristics, a resuspension experiment was conducted with Anacostia River (District of Columbia, USA) sediments. In this study, a mathematical model was developed that simulates oxidation of reduced species, dissolution of minerals, pH changes and pH dependent metal sorption. The model was used to interpret the relative importance of individual processes on pH changes and metals release. As a test of the model's ability to describe resuspension in a system other than the test sediment, the model was also used to predict the metals release behavior observed in a different sediment reported by Burton et al. (2006).

## 3.2 MATERIALS AND EXPERIMENTAL PROCEDURES

### 3.2.1 General Techniques

All solutions were prepared by dissolving analytical reagent grade or equivalent analytical purity chemicals in deionized water (18 M $\Omega$ cm<sup>-1</sup>, Millipore). Deionized water was further deaerated by bubbling N<sub>2</sub> gas (99.9%) for at least 3 hours to make ferrous iron and sulfide stock solutions. All the experimental procedures regarding anoxic sediments and chemicals were conducted under 97% N<sub>2(g)</sub> and 3% H<sub>2(g)</sub> atmosphere in an anaerobic chamber (Coy Laboratory Products Inc.). All glass and plastic-ware were soaked in 1M HNO<sub>3</sub> for more than 1 day, rinsed several times with deionized water and dried in an electric drying cabinet (Hamilton) for 1 day at 70 °C before use.

### 3.2.2 Resuspension Experiments

Anacostia sediment (Washington D.C.) was passed through #10 (2 mm) sieve to remove large debris and stored at 4 °C. Polypropylene bottles (3.5 liters) were used for the resuspension reactors. Five hundred grams of wet sediments were suspended in 2.8 liters of artificial river water (Na<sup>+</sup> : 52.9 mg L<sup>-1</sup>, Mg<sup>2+</sup> : 6.6 mg L<sup>-1</sup>, Ca<sup>2+</sup> : 2.0 mg L<sup>-1</sup>, K<sup>+</sup> : 2.0 mg L<sup>-1</sup>, Cl<sup>-</sup> : 97.2 mg L<sup>-1</sup>) and aerated/agitated with the flow rate of 5 L min<sup>-1</sup> for 14 days. The flow rate was controlled by flow meter (Coleparmer) and the compressed air was filtered with a 0.3  $\mu$ m filter (Hepta-Vent<sup>TM</sup> Whatman) to remove any airborne bacteria or particles. The air was pre-bubbled into deionized water to supply humidity and to prevent any volatilization of water from the sediment slurry.

Samples were taken at 0, 1, 2, 4, 6, 12 hours and at 1, 2, 4, 7, 10, 14 days to investigate both the short term and the long term behavior of redox sensitive species. pH, O<sub>2</sub> and ORP (Oxidation Reduction Potential) were determined directly in the sediment

slurry by inserting individual electrodes. Thirty mL sediment slurry samples were collected by polypropylene pipette and filtered through 0.45  $\mu\text{m}$  nitrate cellulose membrane to separate the solid phase. Ten mL of filtrate was transferred to a 24mL scintillation vial, and 14 mL of  $\text{H}_2\text{O}$  were added. The vial was sealed with Teflon lined septum cap immediately, and dissolved inorganic carbon and organic carbon were determined within 1 hour after sampling. Another 5mL of filtrate was transferred to a 15mL centrifuge tube containing a phenanthroline solution to determine dissolved  $\text{Fe}^{2+}$  concentration (Standard Methods, 1998). The rest of the filtrate ( $\approx 10\text{mL}$ ) was acidified with 2% nitric acid to determine dissolved metal (Ca, Mg, Zn, Mn) and anion ( $\text{Cl}^-$ ,  $\text{SO}_4^{2-}$ ) concentrations. From the filter residue, 1.0 grams sediment was transferred to a scintillation vial to measure AVS. Another 1.0 gram of sediment was transferred to a 50 mL polypropylene vial to determine solid phase  $\text{Fe}^{2+}$  by anoxic oxalate extraction (Phillips and Lovely, 1987). The experiments were conducted in duplicate.

### 3.2.3 Sediment Characterizations and Analytical Techniques

Porewater was generated by centrifugation of the sediment (9000 rpm, 20 min, Beckman J2-21) and filtration with 0.45 $\mu\text{m}$  polypropylene membrane.  $\text{Cl}^-$  and  $\text{SO}_4^{2-}$  were determined by Ion Chromatography (Metrohm) and samples were filtered through ion exchange cartridge (OnGuard<sup>®</sup>II 1cc Dionex) to remove any cations that can cause precipitation during anion analysis. Total dissolved inorganic carbon was determined by carbon analyzer (Tekmar Dohrmann Appollo 9000) and dissolved organic carbon was determined by Ultra Violet Absorbance at 270 nm using a potassium hydrogen phthalate standard. Ferrous iron ( $\text{Fe}^{2+}$ ) was measured by colorimetric method using 1,10-phenanthroline (Standard Methods, 1998). Sulfide ( $\text{S}^{2-}$ ) and ammonium ( $\text{NH}_4^+$ )

concentrations were determined with silver sulfide (VWR Symphony) and ammonium (Thermo Orion 9512) ion selective electrodes, respectively. pH was determined by pH electrode (VWR Symphony) calibrated with standard 4.00, 7.02 and 10.05 pH buffers. The ORP was measured by platinum electrode in combination with Ag/AgCl reference electrode (Accumet) calibrated with standard pH 4.00, 7.00 buffer solutions saturated with Quinhydrone. The oxygen concentrations were determined with a oxygen electrode (YSI Incorporated). The concentration of metals, such as Zn, Fe, Mn, Ca, Mg, Na and K, were determined with ICP-AES (Inductively Coupled Plasma Atomic Emission Spectrometer, Spectro) or graphite furnace AAS (Atomic Absorption Spectroscopy, Perkin Elmer).

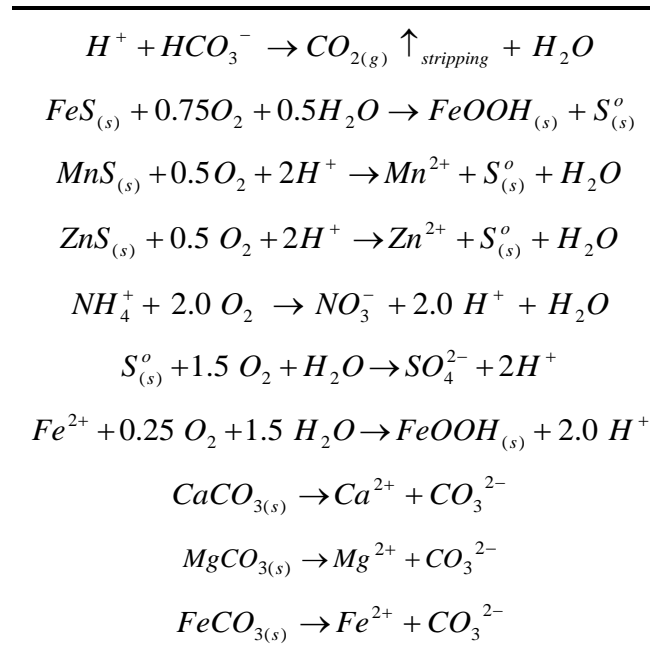
The water content was determined by weight loss after water evaporation from bulk sediment in a 95 °C oven. Total metals in sediment were extracted by microwave digestion in concentrated HNO<sub>3</sub> (EPA, SW 846–3051). Solid phase Fe<sup>2+</sup> and amorphous Fe<sup>3+</sup> were recovered by anoxic oxalate extraction (Philips and Lovely, 1987). AVS and SEM were determined by the diffusion method (Brouwer and Murphy, 1994) with 0.05 M ascorbic acid addition to 1 M HCl to prevent any sulfide oxidation by Fe<sup>3+</sup> during the analysis (Hseih et al., 2002). Solid phase organic and inorganic carbon concentrations were determined using a CHN analyzer (HewlettPackard). All extracts were filtered with 0.45µm polypropylene membrane. The extract concentrations were determined via the same analytical techniques for the pore water analysis with proper dilutions. All the solid phase concentrations were calculated based on dry sediment weight.

### 3.3 MATHEMATICAL MODELING OF SEDIMENT RESUSPENSION EXPERIMENTS

#### 3.3.1 Modeling Oxidation Kinetics of Reduced Sediments

A set of ordinary differential equations (ODE) were developed to describe the oxidation of reduced species upon anoxic sediments resuspension in aerobic overlying water. Table 3.1 summarizes the reaction stoichiometry considered in the model.

Table 3.1 Reaction Stoichiometry



The oxidation kinetics of metal sulfides,  $S_{(s)}^o$  and ammonium are assumed second order as follows (Wang and Van Cappellen, 1996)

$$\frac{d[R]}{dt} = -k_R[R][O_{2(aq)}] \quad (3.1)$$

where [R] represents the concentrations of any reduced species such as FeS, ZnS, MnS,  $S_{(s)}^o$ , and  $NH_4^+$  [M],  $k_R$  represents the rate constant and  $[O_{2(aq)}]$  is dissolved oxygen concentration [M]. Although slower oxidation rates are likely for adsorbed phase

(Szecsody et al., 2004), the oxidation of  $Fe^{2+}$  is assumed to occur at the same rates in both aqueous and adsorbed phases by the following base catalyzed reaction (Lowson, 1982; Stumm and Morgan, 1996)

$$\frac{d[Fe^{2+}]}{dt} = -\left( k_{1,Fe^{2+}} [Fe^{2+}] [O_{2(aq)}] + k_{2,Fe^{2+}} [Fe^{2+}] \frac{[O_{2(aq)}]}{[H^+]^2} \right) \quad (3.2)$$

where  $[Fe^{2+}]$  represents the aqueous and sorbed phase  $Fe^{2+}$  concentration [M],  $k_{1,Fe^{2+}}$  [ $M^{-1} T^{-1}$ ] and  $k_{2,Fe^{2+}}$  [ $M T^{-1}$ ] are the rate constants. The first term of equation (3.2) dominates ferrous iron oxidation when pH is between 3 and 5 and the second term is important when the pH is greater than 5 (Lowson, 1982). Under most environmental conditions, therefore, only the second term is significant.

Sediment usually contains carbonate minerals such as  $CaCO_{3(s)}$ ,  $MgCO_{3(s)}$  and  $FeCO_{3(s)}$  that buffer the pH of pore water in sediment (Jourabchi et al., 2005). The dissolution kinetics of  $CaCO_{3(s)}$  and  $MgCO_{3(s)}$  has been investigated with well characterized minerals (Chou et al., 1989); however, it is difficult to generalize the kinetics due to the lack of sufficient data under wide environmental conditions (Stumm and Morgan, 1996). Hence, the following kinetic expression is used to describe the dissolution kinetics of three different carbonate minerals,  $CaCO_{3(s)}$ ,  $MgCO_{3(s)}$  and  $FeCO_{3(s)}$  (Archer et al., 1998)

$$\frac{d[MeCO_3]}{dt} = -k_{MeCO_3} [MeCO_3] \left( 1 - \frac{\{Me^{2+}\} \{CO_3^{2-}\}}{K_{MeCO_3}} \right)^{4.5} \quad (3.3)$$

where  $[MeCO_3]$  represents the concentrations of carbonate bearing minerals such as  $CaCO_{3(s)}$ ,  $MgCO_{3(s)}$  and  $FeCO_{3(s)}$  [M],  $k_{MeCO_3}$  represents the dissolution rate constant [ $T^{-1}$ ],  $K_{MeCO_3}$  represents the solubility products of minerals [ $M^{-2}$ ],  $\{Me^{2+}\}$  means the activity of dissolved metals, such as  $Ca^{2+}$ ,  $Mg^{2+}$ , and  $Fe^{2+}$  [M],  $\{CO_3^{2-}\}$  is the activity of dissolved carbonate concentration [M]. Once the carbonate is dissolved, it will be

redistributed to bicarbonate and carboxylic acid. The carbonate species and protons are considered to be in equilibrium at all times because acid base reactions are relatively fast compared to the oxidation of reduced species or the dissolution of minerals (Schulz et al., 2006).

Due to the continuous aeration of sediment slurry, the dissolved  $CO_{2(aq)}$  was continuously stripped from the slurry. The  $CO_{2(aq)}$  stripping disturbs the equilibrium of dissolved carbonate species and increases the pH. This was an artifact of aerating sediments and rarely happens in natural environments; however, including this reaction is important in modeling pH. This reaction is included as a first order ODE as follows

$$\frac{d[CO_{2(aq)}]}{dt} = -k_{CO_2} ([CO_{2(aq)}] - [CO_{2(aq),atm}]) \quad (3.4)$$

where  $[CO_{2(aq)}]$  represents the concentration of dissolved carbon dioxide in sediment slurry [M],  $[CO_{2(aq),atm}]$  represents the concentration of dissolved carbon dioxide that is in equilibrium with atmospheric  $CO_{2(g)}$  [M],  $k_{CO_2}$  represents the gas transfer rate [ $T^{-1}$ ].

### 3.3.2 Modeling pH

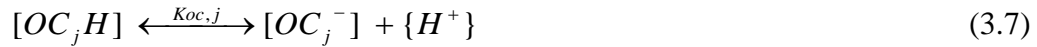
The model for pH changes includes the buffering capacities of both carbonate species and surface functional groups of organics and oxides. Please refer to APPENDIX A for a more detailed derivation and list or discussion of assumptions. Only a brief description is included here. The carbonate species follows the equilibrium reactions



where  $\{CO_{2(aq)}\}$  is the activity of dissolved carbon dioxide or carbonic acid,  $\{H^+\}$  is the activity of protons,  $\{HCO_3^-\}$  is the activity of dissolved bicarbonate,  $\{CO_3^{2-}\}$  is the

activity of dissolved carbonate concentrations.  $K_{CO,a1}$  and  $K_{CO,a2}$  represents the first and second proton dissociation constant for carbonic acid [M].

The solid phase organic carbon is modeled as humic acids composed of carboxylic and phenolic functional groups, which are further divided into 4 sites with different proton binding strengths (Tipping, 1998). The following reaction represents the proton binding to the  $j^{\text{th}}$  site



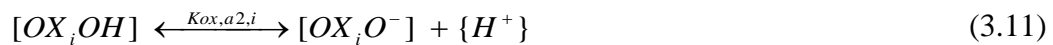
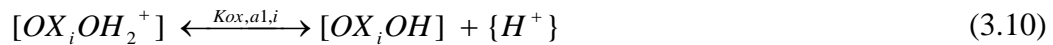
where  $[OC_jH]$  represents the concentration of neutralized  $j^{\text{th}}$  humic acid [M],  $[OC_j^-]$  represents the concentration of deprotonated  $j^{\text{th}}$  site [M], and  $K_{OC,j}$  represents proton dissociation constants for the  $j^{\text{th}}$  site [M]. The total concentration of humic acids was assumed to be a fraction of the total organic carbon (10%) and the concentration of individual species were distributed as assumed by Tipping (1998).  $K_{OC,j}$  can be estimated by

$$pK_{oc,j} = pK_{cb} + \Delta pK_{cb} * (2j - 5) / 6 \quad \text{for } j = 1, 2, 3, 4 \quad (3.8)$$

$$pK_{oc,j} = pK_{ph} + \Delta pK_{ph} * (2j - 13) / 6 \quad \text{for } j = 5, 6, 7, 8 \quad (3.9)$$

where  $pK_{cb}$  and  $pK_{ph}$  represent intrinsic proton dissociation constants for carboxylic and phenolic functional groups respectively,  $\Delta pK_{cb}$  and  $\Delta pK_{ph}$  represent distribution term that modifies  $pK_{oc,j}$ .

The oxides have amphoteric surface hydroxyl groups that can both associate and dissociate protons (Lofts and Tipping, 1998). The proton reactions for oxides can be written generally as



where  $[OX_iOH_2^+]$  represents the concentrations of protonated 'i' oxide molecule,  $[OX_iOH]$  represents the concentrations of neutralized 'i' oxide molecule,  $[OX_iO^-]$  represents the concentrations of deprotonated 'i' oxide molecule,  $K_{OX,a1,i}$ ,  $K_{OX,a2,i}$  represents the first and second proton dissociation constants for oxide 'i' [M].

The temporal behavior of proton and total carbonate concentrations can be expressed as follows

$$\frac{d[H^+]}{dt} = \Gamma * \left\{ \begin{array}{l} (1 - \alpha_0 + \alpha_2)\Sigma rxn_{CO_2} + (-\alpha_0 + \alpha_2)\Sigma rxn_{HCO_3} \\ + (-1 - \alpha_0 + \alpha_2)\Sigma rxn_{CO_3} + \Sigma rxn_{H^+} \end{array} \right\} \quad (3.12)$$

$$\frac{\partial [C_{t,CO_2}]}{\partial t} = \{ \Lambda * (-1 + \alpha_0 - \alpha_2) + 1 \} \Sigma rxn_{CO_2} + \{ \Lambda * (\alpha_0 - \alpha_2) + 1 \} \Sigma rxn_{HCO_3} \quad (3.13)$$

$$+ \{ \Lambda * (1 + \alpha_0 - \alpha_2) + 1 \} \Sigma rxn_{CO_3} - \Lambda * \Sigma rxn_{H^+}$$

where  $[C_{t,CO_2}]$  represents total dissolved carbonate species concentration [M],  $\alpha_0$ ,  $\alpha_1$ ,  $\alpha_2$  are fractions of  $\{CO_{2(aq)}\}$ ,  $\{HCO_3^-\}$ ,  $\{CO_3^{2-}\}$  among total carbonate concentrations (Snoeyink and Jenkins, 1980) respectively [-],  $\Sigma rxn_{CO_2}$ ,  $\Sigma rxn_{HCO_3}$ ,  $\Sigma rxn_{CO_3}$ ,  $\Sigma rxn_{H^+}$  represent the summation of  $CO_{2(aq)}$ ,  $HCO_3^-$ ,  $CO_3^{2-}$ ,  $H^+$  production rate from biogeochemical reactions  $[M T^{-1}]$ ,  $\Gamma$  and  $\Lambda$  represent the coefficient for protons and dissolved total carbonates which are defined as follows

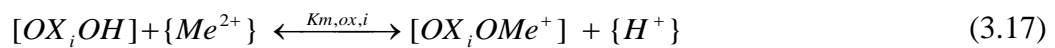
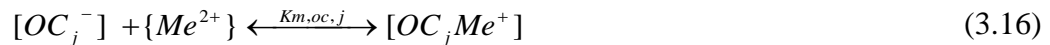
$$\Gamma = \left( \begin{array}{l} 1 + [C_{t,CO_2}] \left[ \begin{array}{l} (1 - \alpha_0 + \alpha_2) \frac{\partial \alpha_0}{\partial H} + (-\alpha_0 + \alpha_2) \frac{\partial \alpha_1}{\partial H} \\ + (-1 - \alpha_0 + \alpha_2) \frac{\partial \alpha_2}{\partial H} \end{array} \right] \\ + \sum_{i=1}^k \left\{ [C_{t,OX,i}] \left[ \begin{array}{l} (1 - \beta_{0,i} + \beta_{2,i}) \frac{\partial \beta_{0,i}}{\partial H} + (-\beta_{0,i} + \beta_{2,i}) \frac{\partial \beta_{1,i}}{\partial H} \\ + (-1 - \beta_{0,i} + \beta_{2,i}) \frac{\partial \beta_{2,i}}{\partial H} \end{array} \right] \right\} \\ + \sum_{j=1}^l \left\{ [C_{t,OC,j}] \left( \chi_{1,j} \frac{\partial \chi_{0,j}}{\partial [H^+]} - \chi_{0,j} \frac{\partial \chi_{1,j}}{\partial [H^+]} \right) \right\} \end{array} \right)^{-1} \quad (3.14)$$

$$\Lambda = \Gamma * C_{t,CO_2} * \left( \frac{\partial \alpha_0}{\partial H} + \frac{\partial \alpha_1}{\partial H} + \frac{\partial \alpha_2}{\partial H} \right) \quad (3.15)$$

where  $\beta_{0,i}$ ,  $\beta_{1,i}$ ,  $\beta_{2,i}$  are fractions of  $[OX_iH_2^+]$ ,  $[OX_iH]$ ,  $[OX_i^-]$  among total 'i' oxide surface [-].  $\chi_{0,j}$ ,  $\chi_{1,j}$  are fractions of  $[OC_jH]$ ,  $[OC_j^-]$  among total  $j^{th}$  surface of humic acid [-].  $C_{t,OX}$  is the total surface hydroxyl functional group concentration for oxide,  $C_{t,OC}$  is the total surface functional groups concentration for organics,  $\partial\alpha/\partial H$ ,  $\partial\beta/\partial H$ ,  $\partial\chi/\partial H$  represent the derivative of fractions for carbonate, oxide and organics with respect to proton concentration.

### 3.3.3 Modeling Metals Complexation with Organics, Oxides and Inorganic Ligands

The oxides and organic carbon surfaces that are part of the pH model are considered to participate in metal sorption as well. The freely dissolved metals are assumed to complex with the surface functional groups of organics and oxides. Only monodentate complexation (Radovanovic and Koelmans, 1998) is considered as follows



where  $\{Me^{2+}\}$  represents the activity of freely dissolved metals [M],  $K_{m,oc,j}$  represents  $j^{th}$  metal sorption constants for organic carbon [ $M^{-1}$ ],  $K_{m,OX,i}$  represents the metal sorption constants for 'i' oxide [-]. The surface complexation sites are considered to be of 8 types which are described in pH model. The  $K_{m,oc,j}$  for these organics sites can be calculated as (Tipping, 1998)

$$pK_{m,oc,j} = pK_{MC} - (2j - 5) / 6 * \Delta LK_1 \quad \text{for } j=1, 2, 3, 4 \quad (3.18)$$

$$pK_{m,oc,j} = (3.39 pK_{MC} + 1.15) - (2j - 13) / 6 * \Delta LK_1 \quad \text{for } j=5, 6, 7, 8 \quad (3.19)$$

where  $K_{MC}$  represents the intrinsic metal sorption constant for carboxylic function group and  $\Delta LK_1$  is fixed at 2.8 (Tipping, 1998).

Inorganic ligands, such as  $SO_4^{2-}$  and  $Cl^-$ , have been known to increase the solubility of metals concentration by complexation and their role was calculated via relationships of the form



where  $\{L^z\}$  represents the activity of dissolved anion ligands with charge z [M],  $K_L$  represents the stability constants for inorganic ligands [ $M^{-1}$ ]. The metal complexation reactions with inorganic ligands and stability constants are summarized in APPENDIX D.

Davies equation was used to correct the activity of monoprotic and biprotic dissolved ionic species as follows (Stumm and Morgan, 1996)

$$\log \gamma_{monoprotic} = \left( -\frac{0.509I^{0.5}}{1 + I^{0.5}} + 0.15I \right) \quad (3.21)$$

$$\log \gamma_{biprotic} = 4 \left( -\frac{0.509I^{0.5}}{1 + I^{0.5}} + 0.15I \right) \quad (3.22)$$

$$I = 0.5 * \sum_i (C_i Z_i^2) \quad (3.23)$$

where  $\gamma$  represents activity coefficient [-], I represents ionic strength [-], C is the concentration of ionic species and Z is the charge of the ionic species [M]. The

electrostatic interactions at the surface are neglected due to the uncertainties of electric double layer in a complex sediment system (Davis et al., 1998; Pivovarov, 1998).

### 3.3.4 Acid Volatile Sulfide (AVS) and Simultaneously Extracted Metals (SEM)

#### Calculation

AVS represents sulfide that is evolved from acidified sediment by adding 1 M HCl. It usually includes sulfides ( $H_2S$ ,  $HS^-$ ,  $S^{2-}$ ), amorphous iron sulfide ( $FeS_{(s)}$ ), mackinawite ( $FeS_{(s)}$ ) and some fraction of metal sulfides ( $Cd_{(s)}$ ,  $NiS_{(s)}$ ,  $PbS_{(s)}$ ,  $ZnS_{(s)}$ ,  $CuS_{(s)}$ ) (Carbonaro et al., 2005). At the same time, the metals that are dissolved in 1M HCl are defined as SEMs (Simultaneously Extracted Metals) (Allen et al., 1993). The AVS and SEM were calculated as follows (Carbonaro et al., 2005)

$$AVS = [FeS_{(s)}] + [HS^-_{(aq)}] + \sum_{MeS} \alpha_{MeS} [MeS_{(s)}] \quad (3.24)$$

$$SEM = \sum_{Me} (Me_{(aq)} + Me_{(OX)} + Me_{(POC)} + \alpha_{MeS} [MeS_{(s)}]) \quad (3.25)$$

where  $FeS_{(s)}$  is amorphous iron sulfide,  $HS^-_{(aq)}$  is dissolved hydrogen sulfide,  $\alpha_{MeS}$  is metal sulfide extraction efficiency in 1 M HCl,  $MeS_{(s)}$  is metal sulfide,  $Me_{(aq)}$  is dissolved metal concentrations,  $Me_{(OX)}$  is metals adsorbed to oxides,  $Me_{(POC)}$  is metal adsorbed to particulate organic carbon.

### 3.3.5 Solution Techniques

The equations compose a set of coupled ODEs constrained by equilibrium conditions. The ODEs are integrated implicitly using ODEs solver 'DVIDE' (Brown et al., 1989) with time step of  $10^{-4}$  days and tolerances of  $10^{-12}$ . The ODEs constitute a stiff system of equations because the coupled system exhibits extremely different relaxation

times (Zeebe et al., 1999) and sparse Jacobian matrix. In between the integration time step, the equilibrium equations are solved to calculate the heavy metals partitioning to sediment surface and aqueous ligands. The metal sorption model is a set of nonlinear algebraic equations and Fixed Point Iteration is used to solve the equations (Burden and Faires, 2005). By repeating this procedure, the governing equation is solved for the time period of interest.

### **3.4 RESULTS AND DISCUSSION**

From the Anacostia River sediment resuspension experiment, the following time dependent factors were characterized: AVS,  $O_{2(aq)}$ , dissolved organic carbon, redox potential,  $Fe^{2+}_{(aq)}$ ,  $Fe^{2+}_{(s)}$ ,  $HCO_3^{-}_{(aq)}$ , pH,  $SO_4^{2-}_{(aq)}$ ,  $Ca_{(aq)}$ ,  $Mg_{(aq)}$ ,  $Mn_{(aq)}$ , and  $Zn_{(aq)}$ . The dissolved oxygen and organic carbon concentrations as well as redox potentials are available in APPENDIX A and the others will be shown and discussed below.

#### **3.4.1 Model Parameters and Initial Conditions**

Model parameter values were calibrated with the experimental results from Anacostia River sediment when reliable values were not available from the literature. Table 3.2 summarizes the constants related to the kinetics and solubility products of minerals and Table 3.3 shows constants related to proton and metal binding to organics and oxides. The rate for carbon dioxide exchange between water and air was fitted to dissolved carbonate concentrations. The elemental sulfur oxidation rate was estimated from AVS and  $SO_4^{2-}$  experimental data in Anacostia River sediment resuspension experiments. The oxidation rate of manganese sulfide was assumed to be the same as that of ferrous iron sulfide assuming coprecipitation of these species.

Table 3.2 List of parameters associated with kinetics

Parameter	Value	Units	Description	Reference
$k_{\text{CO}_2}$	5.0E+1	day <sup>-1</sup>	Carbone dioxide transfer rate	Calibrated
$k_{\text{FeS}}$	9.9E+4	M <sup>-1</sup> day <sup>-1</sup>	FeS <sub>(s)</sub> oxidation rate	(a)
$k_{\text{MnS}}$	9.9E+4	M <sup>-1</sup> day <sup>-1</sup>	MnS <sub>(s)</sub> oxidation rate	Calibrated
$k_{\text{S}^0}$	1.0E+3	M <sup>-1</sup> day <sup>-1</sup>	S <sub>(s)</sub> <sup>0</sup> oxidation rate	Calibrated
$k_{1,\text{Fe}^{2+}}$	0.103	M <sup>-1</sup> day <sup>-1</sup>	Fe <sup>2+</sup> oxidation rate ( 3<pH<5)	(b)
$k_{2,\text{Fe}^{2+}}$	4.3E-9	M day <sup>-1</sup>	Fe <sup>2+</sup> oxidation rate ( 5<pH)	(c)
$k_{\text{ZnS}}$	3.2E+2	M <sup>-1</sup> day <sup>-1</sup>	ZnS <sub>(s)</sub> oxidation rate	(a)
$k_{\text{NH}_4^+}$	1.4E+4	M <sup>-1</sup> day <sup>-1</sup>	NH <sub>4</sub> <sup>+</sup> oxidation rate	(d)
$k_{\text{MeCO}_3}$	0.25	day <sup>-1</sup>	Carbonate minerals dissolution rate	Calibrated
$K_{\text{CaCO}_3}$	4.5E-9	M <sup>2</sup>	Solubility product of CaCO <sub>3</sub>	(c)
$K_{\text{FeCO}_3}$	2.0E-11	M <sup>2</sup>	Solubility product of FeCO <sub>3</sub>	(c)
$K_{\text{MgCO}_3}$	3.6E-8	M <sup>2</sup>	Solubility product of MgCO <sub>3</sub>	(c)
$K_{\text{CO}_2,\text{a}1}$	5.0E-7	M	Carbonic acid protonation constant	(c)
$K_{\text{CO}_2,\text{a}2}$	5.0E-11	M	Bicarbonate protonation constant	(c)
$\alpha_{\text{FeS}}^{(\text{f})}$	1.0	-	S <sup>2-</sup> extraction efficiency from FeS <sub>(s)</sub>	(e)
$\alpha_{\text{ZnS}}$	0.9	-	S <sup>2-</sup> extraction efficiency from ZnS <sub>(s)</sub>	(e)

(a) Carbonaro et al.,2005, (b) Lawson, 1982 (c) Stumm and Morgan, 1996, (d) Wang and Van Cappellen, 1996, (e) Allen et al., 1993, (f) Used for MnS<sub>(s)</sub> assuming coprecipitation.

Table 3.3 List of parameters for metal sorption (Lofts and Tipping, 1998; Tipping, 1998)

Parameters	Humic Acid	FeOOH <sub>(s)</sub>	Description
$n_{cb}$ (mmol g <sup>-1</sup> ) <sup>(a)</sup>	3.3	-	Specific site density of carboxylic functional group
$\Gamma_{max}$ (μmol m <sup>-2</sup> )	-	8.33	Site density for oxides
SSA (m <sup>2</sup> g <sup>-1</sup> ) <sup>(b)</sup>	-	600	Oxides specific surface area
pK <sub>cb</sub> (-)	4.1	-	Proton dissociation constant for carboxylic group
pK <sub>ph</sub> (-)	8.8	-	Proton dissociation constant for phenolic group
ΔpK <sub>cb</sub> (-)	2.1	-	Distribution term that modifies pK <sub>cb</sub>
ΔpK <sub>ph</sub> (-)	3.6	-	Distribution term that modifies pK <sub>ph</sub>
pK <sub>ox,a1</sub> (-)	-	6.26	First protonation constant for oxides
pK <sub>ox,a2</sub> (-)	-	9.66	Second protonation constant for oxides
pK <sub>Mg</sub> (-)	-0.7	5.3	Mg <sup>2+</sup> sorption constant
pK <sub>Ca</sub> (-)	-0.7	7.3	Ca <sup>2+</sup> sorption constant
pK <sub>Mn</sub> (-)	-0.6	4.6	Mn <sup>2+</sup> sorption constant
pK <sub>Fe2+</sub> (-)	-1.3	5.78 <sup>(c)</sup>	Fe <sup>2+</sup> sorption constant
pK <sub>Zn</sub> (-)	-1.5	1.8 <sup>(d)</sup>	Zn <sup>2+</sup> sorption constant
ΔpK <sub>Me</sub> <sup>(e)</sup> (-)	-	-1.5	Distribution term that modifies pK <sub>Me</sub> for oxides
ΔLK <sub>1</sub> (-)	2.8	-	Distribution term that modifies pK <sub>Me</sub> for organics

(a) Specific site density of phenolic functional group can be calculated by  $0.5 \times n_{cb}$ .

(b) Specific site densities of oxides (mol g<sup>-1</sup>) were calculated by multiplying  $\Gamma_{max}$  by SSA. Total available sorption sites (M) in the system was calculated by multiplying specific site densities (mol g<sup>-1</sup>) by bulk density (g L<sup>-1</sup>).

(c) Estimated from the equilibrium constant for the first hydrolysis reaction constant of Fe<sup>2+</sup>

(d) Modified with ΔpK<sub>Me</sub> to describe strong Zn sorption to 9 % of total sorption site.

(e) Me stands for Zn.

The model initial conditions for Anacostia Sediment were determined from the measured values shown in APPENDIX A. The solid density in the reactor was calculated by dividing dry sediment mass by total liquid volume. For modeling purposes, the solid phase concentrations ( $\text{mole g}^{-1}$ ) were converted to molar concentrations by multiplying by the solid density in the slurry ( $\text{g L}^{-1}$ ). All the kinetic parameters were shown based on the solid phase molar concentrations. The  $\text{ZnS}_{(s)}$  and  $\text{MnS}_{(s)}$  were determined by the metals extracted during AVS measurement. The  $\text{FeS}_{(s)}$  was calculated by subtracting the  $\text{ZnS}_{(s)}$  and  $\text{MnS}_{(s)}$  from AVS. The  $\text{Fe}^{2+}_{\text{available}}$  (total dissolved and sorbed  $\text{Fe}^{2+}$ ) was estimated to satisfy the measured dissolved  $\text{Fe}^{2+}$ . The  $\text{FeCO}_{3(s)}$  was calculated by subtracting  $\text{FeS}_{(s)}$ ,  $\text{Fe}^{2+}_{\text{available}}$  and  $\text{Fe}^{2+}_{\text{non-available}}$  from total  $\text{Fe}^{2+}$ , which was oxalic acid extractable  $\text{Fe}^{2+}$ .  $\text{S}^0_{(s)}$  was assigned to zero assuming the sediment was initially fully reduced.  $\text{NH}_4^+_{(aq)}$  was calculated from porewater  $\text{NH}_4^+_{(aq)}$  concentration by mixing porewater with artificial river water assuming mass conservation. The  $\text{Ca}_{\text{available}}$ ,  $\text{Mg}_{\text{available}}$ , and anions were estimated from the measured initial dissolved concentrations.

Active fractions of iron oxides and organics vary in literature, i.e. 2~100% of total iron (Sevinc Sengor et al, 2007; Radovanovic and Loelmans, 1998) and 30~100 % of total organic carbon (Shi et al., 2007). In this study, the anoxic oxalate extractable iron was considered to be the dominant iron oxide phase based on Lofts and Tipping (1998) and 50% of the iron was assumed to be active by calibrating model to be consistent with the initial metals distribution. Similarly, 11% of the measured total organic matter was considered to be active as humic acid to be consistent with the final total metals partitioning between sediment and water. Since proposed model does not consider possible multipdentate sorption and electrostatic interactions, these fractions are likely to be site specific and reflective of both the active surface area and neglected processes.

This fraction may need to be reevaluated when this model is applied to other sediments.  $\text{CaCO}_{3(s)}$  and  $\text{MgCO}_{3(s)}$  concentrations were estimated by calibrating the model to measured pH, dissolved Ca and Mg concentrations. The sediment porewater was oversaturated with  $\text{Ca}^{2+}$  and  $\text{CO}_3^{2-}$  from thermodynamic calculations, indicating the presence of  $\text{CaCO}_{3(s)}$ .

Table 3.4 Model Initial Conditions

Parameters	Unit	Anacostia	Acid Sulfate <sup>(a)</sup>
Water Content	%	53.0	70.0
Solid Density	$\text{g L}^{-1}$	76.7	52.6
$\text{Fe}^{2+}_{(s), \text{non-available}}$	$\mu\text{mol g}^{-1}$	10.8	10.8
$\text{FeS}_{(s)}$	$\mu\text{mol g}^{-1}$	42.4	215.0
$\text{Fe}^{2+}_{\text{available}}$	$\mu\text{mol g}^{-1}$	5.2	76.1
$\text{Fe}^{2+}_{(s) \text{ sorbed}}$	$\mu\text{mol g}^{-1}$	5.2	19.0
$\text{FeCO}_{3(s)}$	$\mu\text{mol g}^{-1}$	0.00	57.0
$\text{S}^0_{(s)}$	$\mu\text{mol g}^{-1}$	0.00	11.3
$\text{ZnS}_{(s)}$	$\mu\text{mol g}^{-1}$	8.5	1.2
$\text{MnS}_{(s)}$	$\mu\text{mol g}^{-1}$	3.9	3.5
$\text{CaCO}_{3(s)}$	$\mu\text{mol g}^{-1}$	23.5	70.3
$\text{MgCO}_{3(s)}$	$\mu\text{mol g}^{-1}$	13.0	81.8
$\text{FeOOH}_{(s) (b)}$	$\text{mg g}^{-1}$	10	16.5
Humic Acid <sup>(b)</sup>	$\text{mg g}^{-1}$	7.7	5.2
$\text{Ca}^{2+}_{\text{available}}$	$\mu\text{mol g}^{-1}$	30.0	0.0
$\text{Mg}^{2+}_{\text{available}}$	$\mu\text{mol g}^{-1}$	13.0	26.6
$\text{Na}^{+}_{\text{available}}$	$\mu\text{mol g}^{-1}$	156.5	342.2
$\text{NH}_4^+$	mM	0.16	0.16
$\text{Cl}^-$	mM	0.27	11.8
$\text{SO}_4^{2-}$	mM	0.00063	2.4
$\text{HCO}_3^-$	mM	0.7	0.7
pH		6.5	6.3

(a) Burton et al., 2006, (b) Assumed to be 50% of oxalic acid extratable ferric iron and 11% of organic matter are active in metals sorption.

Initial conditions for the experiments of Burton et al. (2006) were inferred from that source. Total metal concentrations were used to estimate  $\text{ZnS}_{(s)}$  and  $\text{MnS}_{(s)}$  instead of

SEM. Chromium reducible  $S^0_{(s)}$  was used for the elemental sulfur. Initial conditions from the Anacostia sediment were used for  $Fe^{2+}_{\text{non-available}}$  and  $NH_4^+_{(aq)}$ , which were not reported. All calibrated parameters were held constant at the values estimated from the Anacostia sediment experiments. Table 3.4 summarizes the model initial conditions for both experiments.

### 3.4.2 The Deviation of the Model Fit to Experimental Observations

For the quantitative description of the proposed model predictability, the deviation of the model fit (DMF) to experimental observations is calculated from the standard error (SE) divided by the median of experimental observations as follows

$$DMF = \frac{SE}{\text{median}(Y_E)} * 100 \quad (3.26)$$

$$SE = \sqrt{\frac{1}{N} \sum_{i=1}^N (Y_E - Y_M)^2} \quad (3.27)$$

where DMF is the acronym for the deviation of the model fit,  $N$  is the number of data points from experiment,  $Y_E$  is the mean of duplicated experimental observations and  $Y_M$  is the value of model prediction. Typically, the SE has been used to find the optimal fitting parameters that minimize the SE. The number of fitting parameters, which is the degrees of freedom, is subtracted from the number of data points. Here, most model parameters are set from literature sources, a few parameters are calibrated to particular physical phenomena, and the standard error is used as an indication of the performance of the model reliability.

As a result, SE is used to suggest a quantitative description of the model fit in this study because it has same unit as the evaluated geochemical factors. Furthermore, the SE is normalized by the median of experimental observations to provide a relative deviation of SE from the experimental observations. Care should be taken when interpreting the

deviation of the model fit (DMF), because the use of the median may overestimate the error for data with values that are greater than the median and may underestimate the error when the data values are smaller than the median. Table 3.5 summarizes the SE, median and the deviation of the model fit for various model parameters. The table will be used in the later discussion.

Table 3.5 Statistical Analysis of the Model Fit

Parameter	Units	Anacostia River sediment			Acid Sulfate sediment <sup>(a)</sup>		
		SE	Median	DMF (%) <sup>(c)</sup>	SE	Median	DMF (%)
AVS	$\mu\text{mol g}^{-1}$	3.0	27.90	10.07	22.4	109.92	20.4
$\text{S}_{(s)}^0$	$\mu\text{mol g}^{-1}$	N.A.	-	-	61.9	82.44	75.0
$\text{SO}_4^{2-}$	mM	0.13	2.04	6.57	3.9	8.19	47.9
$\text{Fe}_{(aq)}^{2+}$	$\text{mg L}^{-1}$	0.13	0.39	32.8	40.79	43.62	93.51
$\text{Fe}_{(s)}^{2+}$	$\text{mg g}^{-1}$	0.35	1.53	22.83	-	-	-
pH	$\log \{\text{H}^+\}$	0.23	5.99	3.8	0.27	4.93	5.6
$\text{HCO}_3^-$	mM	0.061	0.35	17.7	0.082	0.28	28.89
$\text{Mg}_{(aq)}$	$\text{mg L}^{-1}$	5.1	15.72	32.0	20.3	87.90	23.1
$\text{Ca}_{(aq)}$	$\text{mg L}^{-1}$	19.7	75.0	26.2	23.2	64.25	36.1
$\text{Mn}_{(aq)}$	$\text{mg L}^{-1}$	7.57	1.27	595.9	6.37	2.38.	268.33
$\text{Mn}_{(aq)}$ <sup>(b)</sup>	$\text{mg L}^{-1}$	0.53	1.27	41.5	2.04	2.38	86.0
$\text{Zn}_{(aq)}$	$\text{mg L}^{-1}$	0.08	0.30	26.8	0.09	0.78	11.4

(a) Burton et al., 2006, (b)  $\text{pK}_{\text{Mn}}$  is changed to increase the model fit.

(c) Acronym for the deviation of the model fit.

### 3.4.3 Oxidation of Sulfur Species

Sulfur species are the most important factors controlling heavy metals availability and redox status of sediments. Experimental and modeling results for the sulfur species in Anacostia sediment are shown in Figure 3.1 (a). Initially, the sediment contained  $54 \mu\text{mol g}^{-1}$  of AVS; however, the AVS rapidly decreased to  $10 \mu\text{mol g}^{-1}$  after 4 hours, and the residual AVS was slowly reduced to  $2 \mu\text{mol g}^{-1}$  after 200 hours. The decrease of AVS did

not directly increase  $\text{SO}_4^{2-}$  suggesting production of intermediate sulfur species in the sediments.

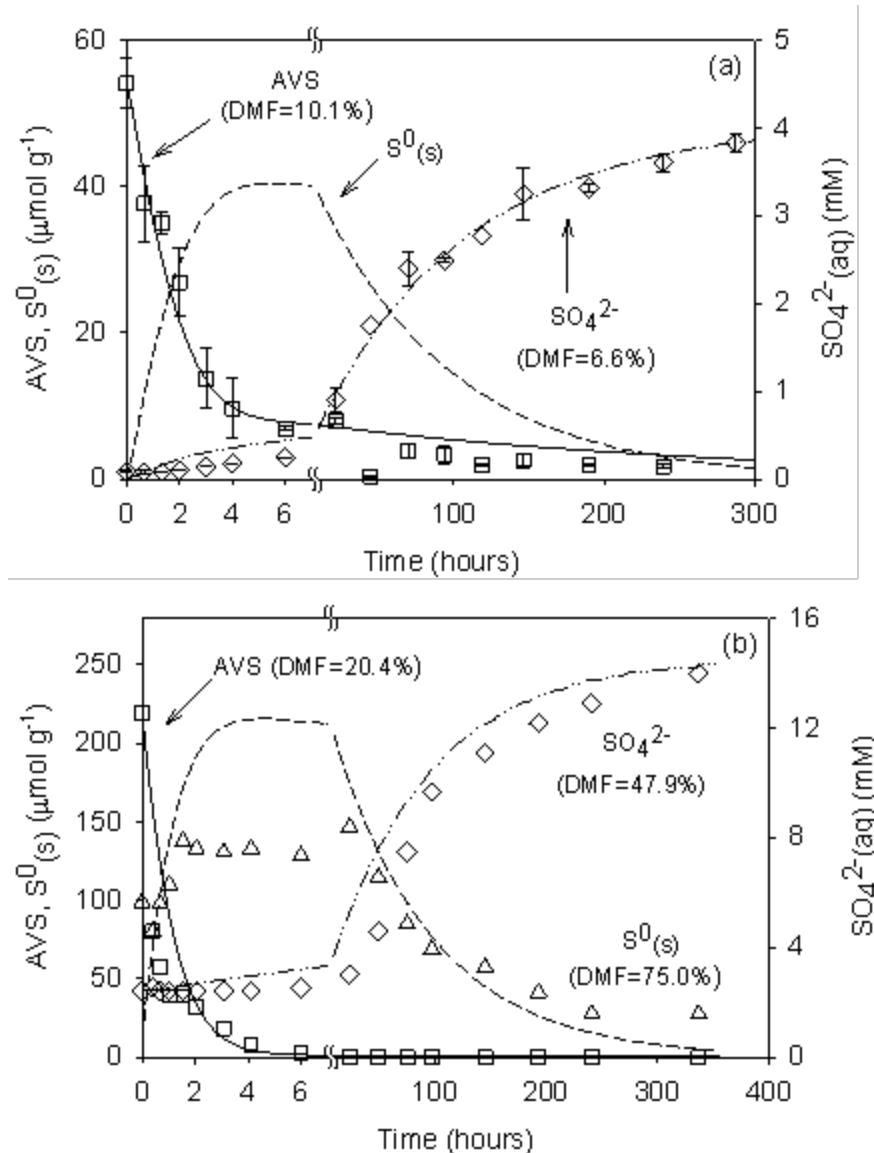


Figure 3.1 Temporal sulfur species (AVS,  $\text{S}^0$ ,  $\text{SO}_4^{2-}$ ) changes in (a) Anacostia River sediment and (b) Acid Sulfate sediment (Burton et al., 2006) upon resuspension. Symbols and error bars are the mean and standard deviations of duplicate experiments and lines are modeling results.

The rapid decrease of AVS at the beginning of experiments was likely due to the oxidation of  $\text{FeS}_{(s)}$  which composes 90% of AVS in the model. The slow oxidation of  $\text{ZnS}_{(s)}$  (Simpson et al., 1998), with a kinetic rate 2 orders of magnitude smaller than that of  $\text{FeS}_{(s)}$  (Carbonaro et al., 2005), explained the slow oxidation of residual AVS. The biphasic AVS oxidation was also consistent with other experimental observations (Simpson et al., 2000). The dynamics of AVS oxidation to  $\text{SO}_4^{2-}{}_{(aq)}$  was modeled as a two step processes which closed the sulfur mass balance successfully.  $\text{S}^0_{(s)}$  was considered to be the dominant byproduct of AVS oxidation, which slowly oxidized to  $\text{SO}_4^{2-}$  producing significant acidity.

Similar dynamics of sulfur species were observed in experiments of Burton et al. (2006) while no significant residual AVS was observed due to lower metal sulfides (i.e.  $\text{ZnS}_{(s)}$ ) concentrations compared to Anacostia sediment. The standard error and deviation of the model fit were generally higher than those of Anacostia River sediment; however the values were not significant. These goodness of model fits indicated that the proposed model simulated the sulfur species behavior well using same parameters from Anacostia sediment experiments but with the experiment-specific initial conditions. Figure 3.1 (b) shows the experimental and modeling results.

The mechanistic pathway of  $\text{FeS}_{(s)}$  oxidation has been relatively well described by a surface complexation oxidation model (Nelson, 1978; Di Toro et al., 1996). The model assumed dissociation of  $\text{FeS}_{(s)}$  to  $\text{Fe}^{2+}$  and  $\text{S}^{2-}$  at the particle surface and subsequent oxidation of  $\text{Fe}^{2+}$  to  $\text{Fe}^{3+}$  catalyzing the transformation  $\text{S}^{2-}$  to  $\text{S}^0_{(s)}$  under neutral to acidic condition and precipitating  $\text{FeOOH}_{(s)}$ . The reported half life of  $\text{S}^0_{(s)}$  in aerobic soil was 10 ~ 25 days for the rapid initial oxidation phase and 100 ~ 300 days for the later slow oxidation phase (Slaton et al., 2001). Compared to the reported half life,  $\text{S}^0_{(s)}$  in

experimental sediments was rapidly oxidized to sulfate with a 4 day half life. This could be either due to the larger specific surface area of  $S^0_{(s)}$  in sediments or bacterial oxidation of  $S^0_{(s)}$  as an electron donor by chemolithotrophic metabolism which is energetically favorable (Madigan et al., 2003). More comprehensive study is necessary to better understand this specific process. Although the proposed model has combined these oxidation mechanisms for both  $FeS_{(s)}$  and  $S^0_{(s)}$  into the second order reaction constant, the dynamics of sulfur species in the two sediments were well described by identical model kinetic parameters.

#### 3.4.4 Oxidation of Aqueous Phase and Solid Phase Ferrous Iron

The time dependent concentration changes of  $Fe^{2+}$  in the aqueous phase and the solid phase for both experiments are shown in Figures 3.2 (a) and (b). It should be noted that aqueous phase  $Fe^{2+}$  dynamics were different in the two experiments. In the Anacostia sediment slurry, dissolved  $Fe^{2+}$  was detected only for the first couple of hours, which was consistent with Saulnier and Mucci (2000). The rapid decrease of dissolved  $Fe^{2+}$  seemed to be caused by the rapid oxidation of  $Fe^{2+}$  in the aqueous phase and sorbed phase. Residual oxalate extractable  $Fe^{2+}$  was observed in the solid phase even after 250 hours aeration. The deviations of the model fit were 32.8 % and 32.8 % for  $Fe^{2+}_{(aq)}$  and  $Fe^{2+}_{(s)}$ , respectively, indicating the experimental observations were modeled well by the base-catalyzed  $Fe^{2+}$  oxidation model (Stumm and Morgan, 1996).

From the observations of Burton et al. (2006), initial dissolved  $Fe^{2+}$  behavior was similar with Anacostia River sediment slurry although the concentrations were ten times greater. Interestingly, dissolved  $Fe^{2+}$  concentration was increased up to 80 mg/L between 100 and 200 hours which was modeled as a result of the dissolution of siderate ( $FeCO_{3(s)}$ ) as well as the desorption of  $Fe^{2+}$  from solid phase by pH decrease.

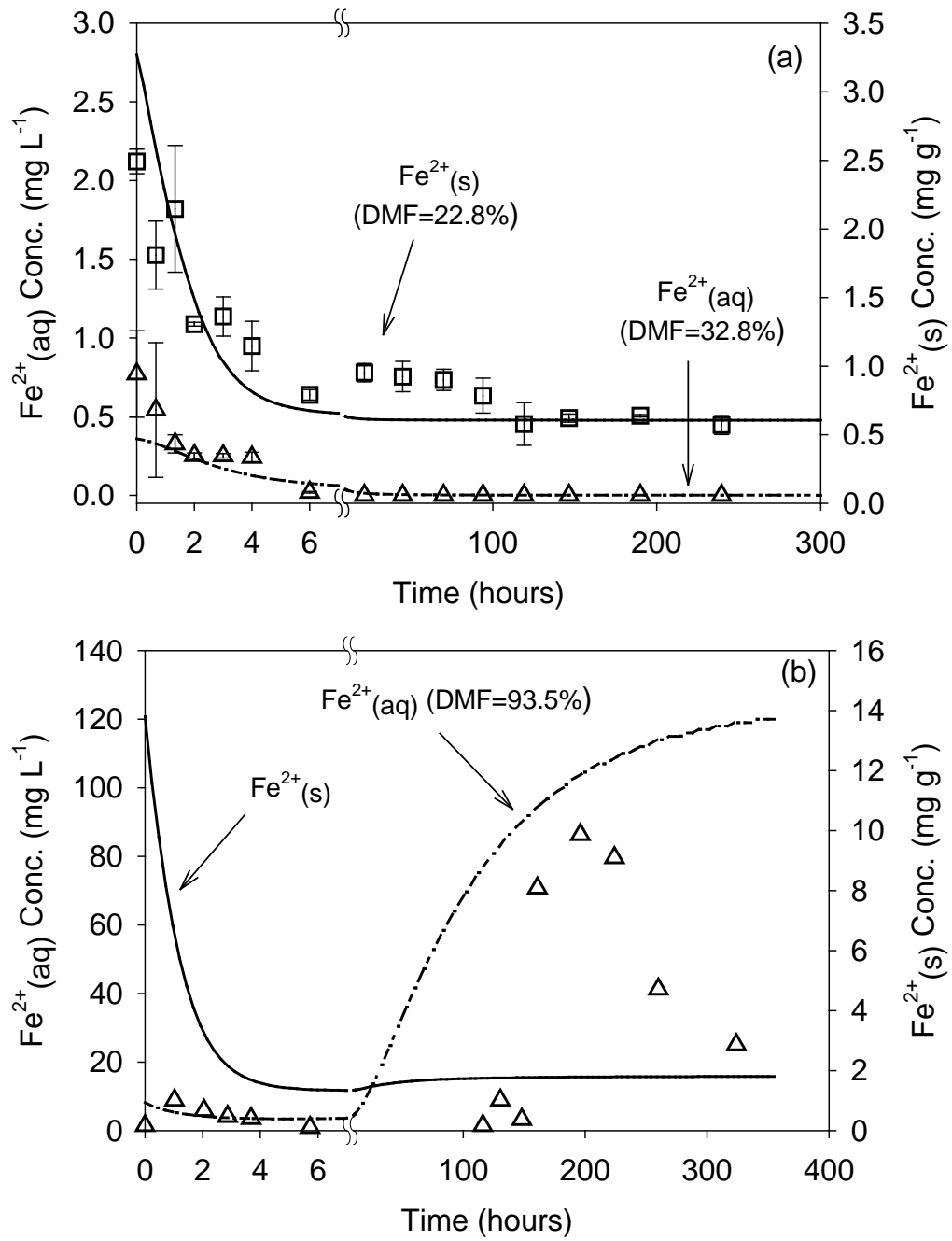


Figure 3.2 Temporal ferrous iron species ( $\text{Fe}^{2+}_{(\text{aq})}$ ,  $\text{Fe}^{2+}_{(\text{s})}$ ) changes in (a) Anacostia River sediment and (b) Acid Sulfate sediments (Burton et al., 2006) upon sediment resuspension. Symbols and error bars are the mean and standard deviations of duplicated experiments and lines are modeling results.

Dissolved  $\text{Fe}^{2+}$  decreased again after 200 hours and the model did not describe the later behavior well and the deviation of the model fit was 93.5 which is higher than that of Anacostia River sediments.

The ferrous iron oxidation model estimated half life of dissolved  $\text{Fe}^{2+}$  at pH 4 was 300 days under well oxygenated system whereas the observed half life was approximately 6 days. These modeling and experimental results suggested that dissolved  $\text{Fe}^{2+}$  was likely to be oxidized by other mechanisms, the most probably by bacterial activity, such as acidophilic chemolithotroph that needs a large amount of  $\text{Fe}^{2+}$  to metabolize (Madigan et al., 2003). The bacterial reaction is not included in this model and more research is required to better describe  $\text{Fe}^{2+}$  oxidation in acidic sediment suspension.

#### **3.4.5 Dissolved Carbonate Concentration and pH changes**

The oxidation of reduced species produced protons and decreased pH. Figure 3.3 (a) and (b) show the pH and dissolved carbonate concentrations in both experiments. The dissolved carbonate concentration was initially 0.8 mM in both experiments and decreased to below the instrument detection limit within 10 hours reducing the buffering capacity of the aqueous phase for the next 14 days experiment. The pH in Anacostia sediment slurry was initially 6.5 then decreased to 5.8 and increased to 6.5 again during the first one hour period that was not captured by the model. The reason for the rapid pH decrease must be caused by oxidation of  $\text{Fe}^{2+}$  followed by production of acidity which is not fully buffered by the carbonate in aqueous phase.

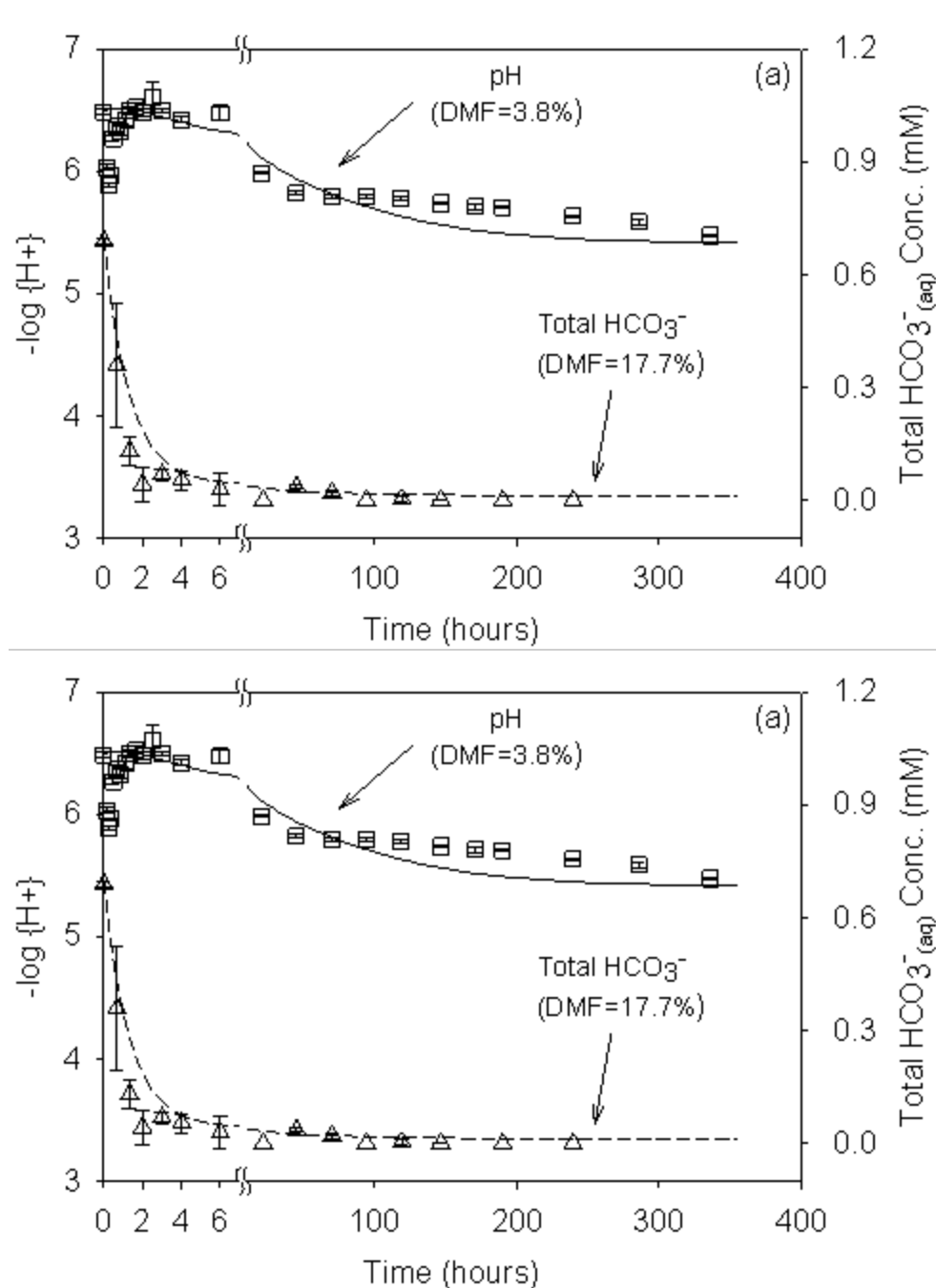


Figure 3.3 Transient pH and total dissolved carbonate species dynamics in (a) Anacostia River sediment and (b) Acid Sulfate sediments (Burton et al., 2006) upon sediment resuspension. Symbols and error bars are the mean and standard deviations of duplicate experiments and lines are modeling results.

The later increase of pH may come from carbon dioxide stripping or dissolution of carbonate from carbonate bearing minerals from the sediment slurry. Carbon dioxide stripping from the aqueous phase increases pH because the carboxylic acid that is in equilibrium with carbon dioxide is continuously produced from bicarbonate or carbonate consuming protons. Similar carbonate species and pH behavior was observed in Burton et al. (2006) after the first hour.

Figure 3.4 (a) and (b) shows the comparison of acidity (proton concentrations) production rates from the oxidation of AVS,  $\text{Fe}^{2+}$  and  $\text{NH}_4^+_{(\text{aq})}$ . The acidity production rates for  $\text{Fe}^{2+}$  were the highest for the first couple of hours which were  $0.004 \text{ M day}^{-1}$  and  $0.014 \text{ M day}^{-1}$  for Anacostia sediment and for Burton et al. (2006), respectively. The initial pH changes must be more affected by the oxidation of ferrous iron than any other species due to its rapid oxidation kinetics under neutral pH. After the rapid oxidation of  $\text{Fe}^{2+}$ , acidity production from sulfur species oxidation dominated for the rest of the experimental period.

After the initial changes, the pH slowly decreased to 5.5 and 3.7 for Anacostia sediment and Burton et al. (2006) respectively during 14 days of aeration. The sediment of Burton et al. (2006) had 4 times more AVS than the Anacostia Sediment which would produce 4 times more acidity from the oxidation. Figure 3.4 (c) and (d) shows the cumulative produced acidity from the oxidation of AVS,  $\text{Fe}^{2+}$  and  $\text{NH}_4^+_{(\text{aq})}$ . Approximately, 0.006 M of acidity is produced from sulfide in Anacostia sediment while 0.023 M of acidity is produced from sulfide in Burton et al. (2006). The acidity produced from ferrous iron or ammonium is not significant compared to sulfide which suggests the importance of sulfide in controlling the long term pH changes in the event of sediment resuspension.

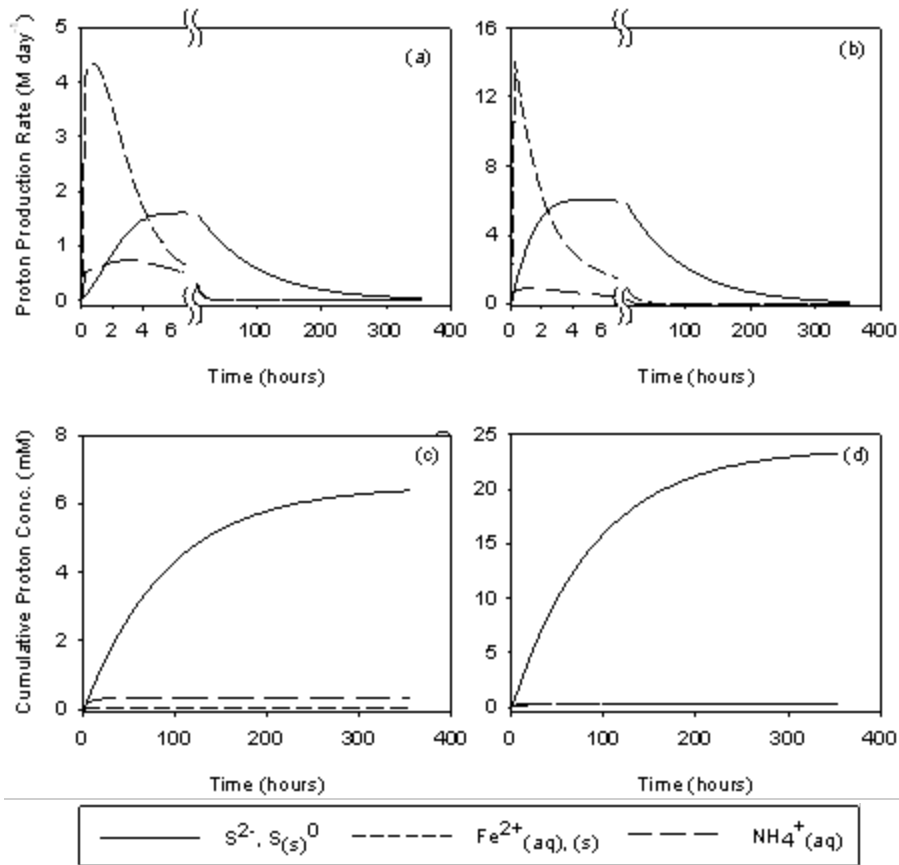


Figure 3.4 Modeling results of proton production rates (mM/day) and cumulative proton production (mM) from (a), (c) Anacostia River sediment and (b), (d) Acid Sulfate sediments (Burton et al., 2006) resuspension.

### 3.4.6 Metals Release from Sediment

The dissolved metal concentrations and modeling results are shown in Figure 3.5. Most of the aqueous phase metals (Mg, Ca, Mn, Zn) concentrations were elevated by the sediment resuspension. The metal release was the result of many interrelated reactions, such as metal sulfide oxidation followed by pH decrease and pH dependent sorption to oxides and organics. The modeling included these underlying processes and described the metals release behavior well except Mn, which probably originated from processes not

incorporated in the model or uncertainty in sorption parameters. (Lofts and Tipping, 1998). For the Mn, the deviation of the model fit decreased from 596 % to 41.5 % in Anacostia River sediments and from 268 % to 86.0 % in Acid Sulfate sediment when  $pK_{Mn}$  of humic acid was increased from -0.6 to -1.4 which was close to those of  $Fe^{2+}$  and  $Zn^{2+}$ .

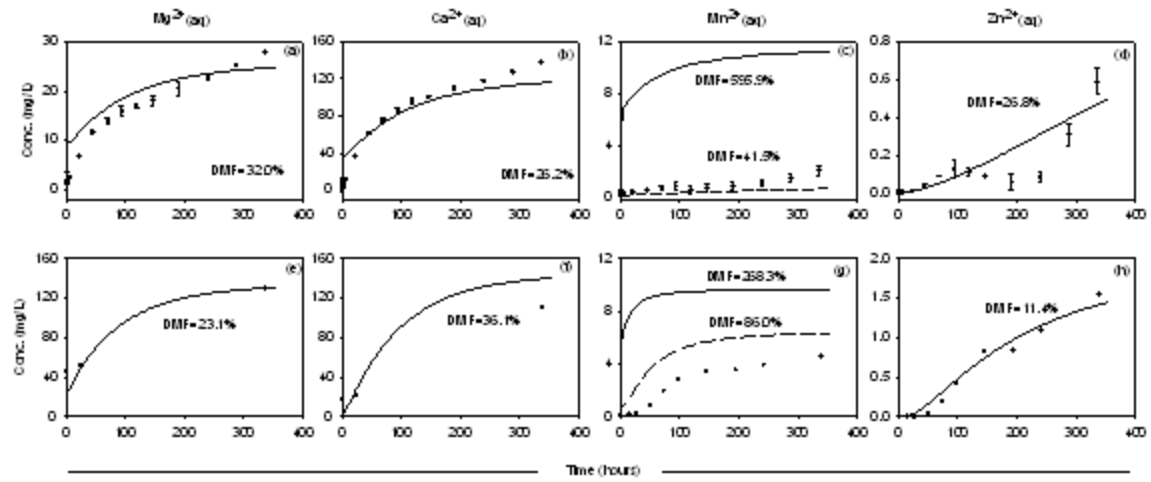


Figure 3.5 Dissolved Mg, Ca, Mn and Zn release from (a) ~ (d) Anacostia River sediment and (e) ~ (h) Acid Sulfate sediments (Burton et al., 2006). The broken lines in  $Mn_{(aq)}$  graphs are the modeling results from the  $pK_{Mn}$  (-1.4) adjustment for humic acid. Symbols and error bars are the mean and standard deviations of duplicated experiments and lines are modeling results. SE stands for standard errors (standard deviation of residuals) between experimental observations and model.

The phase distribution of metals in solid, adsorbed to organics/oxides, and aqueous phase is shown in Figure 3.6. The modeling results explain the metal behaviors upon anoxic sediment resuspension in aerobic overlying water. The Mg and Ca were initially precipitated as  $MgCO_{3(s)}$  and  $CaCO_{3(s)}$  which were dissolved to buffer the acidity produced by the oxidation of reduced species. Once Mg and Ca were released, they were mainly associated with particulate organic carbon which was modeled as humic acid,

because humic acid had more available sorption sites than oxides did, which were not protonated in acidic conditions. Note that all metals are not adsorbed to oxides.

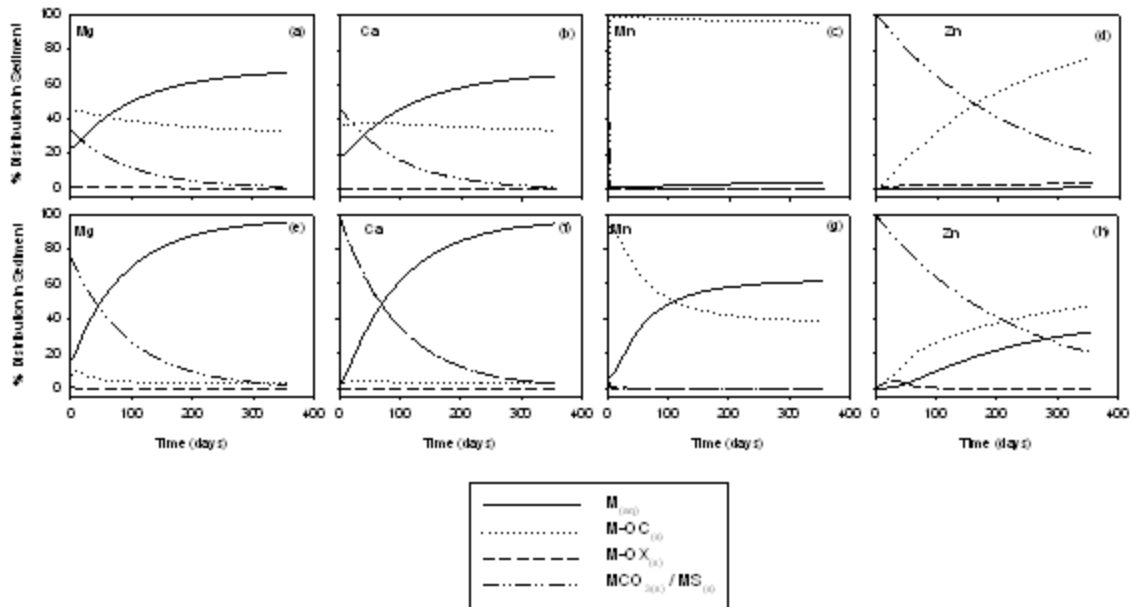


Figure 3.6 Modeling results of temporal metals phase distribution (%) in dissolved ( $M(aq)$ ), adsorbed to organics ( $M-OC$ ), adsorbed to oxides ( $M-OX$ ) and solid phases ( $MgCO_3$ ,  $CaCO_3$ ,  $MnS$ ,  $ZnS$ ) from (a) ~ (d) Anacostia River sediment and (e) ~ (h) Acid sulfate Sediments (Burton et al., 2006) resuspension.

Mn and Zn showed similar modeling results. The Mn and Zn existed as  $MnS_{(s)}$  and  $ZnS_{(s)}$  initially and were released by oxidation of the metal sulfides. The oxidation kinetic rate of  $FeS_{(s)}$  was used for  $MnS_{(s)}$  assuming co-precipitation of Mn in  $FeS_{(s)}$ . The  $MnS_{(s)}$  was oxidized rapidly while  $ZnS_{(s)}$  was resistant to oxidation leaving 20% unoxidized sulfide phase after 14 days aeration. Unlike other metals, Zn was strongly associated with sediments, especially in organic phases even in acidic conditions. Consequently, only 1~ 30% of Zn was released while 10% ~ 50% of Mn was released as

a result of oxidation and more than 80% was released for  $Mg^{2+}$  and  $Ca^{2+}$  in both experiments.

### 3.4.7 Sensitivity analysis

Heavy metals releases are the consequence of many interrelated biogeochemical reactions and identification of the most important processes and parameters are critical in evaluating the metals release upon sediment resuspension. A sensitivity study was conducted using the Anacostia River sediment resuspension experiments for baseline or reference conditions. The sensitivity of parameters in this study is defined as the ratio of ‘change of input’ and ‘change of output’ as follows

$$Sensitivity = absolute\ of\ \frac{\left(\frac{Y - Y_{base}}{Y_{base}}\right)}{\left(\frac{X - X_{base}}{X_{base}}\right)} \quad (3.28)$$

where  $X_{base}$  is the base-line input value,  $X$  is the changed input value,  $Y_{base}$  is the base-line output value, and  $Y$  is the changed output value. During the simulation only one input parameter was changed while all other parameters were fixed. The simulation considers Zn as the metal species of interest because Zn was the dominant heavy metal in the Anacostia River sediment.  $Y$  is the dissolved metal ( $Zn_{(aq)}$ ) concentrations after 15 days sediment resuspension and  $X$  is the Zn speciation related input parameters and initial conditions of sediments. Table 3.6 summarizes the sensitivity of  $X$  to  $Y$ .

Parameters are listed from the most sensitive parameters to the least sensitive parameters to dissolved Zn concentrations after 15 days. These results are specific to the Anacostia River sediments since all the parameters were derived from the site; however, the relative rankings of the sensitivities of individual parameters are likely to hold more general and be somewhat site independent.

Table 3.6 Sensitivity of Zn speciation related parameters to final  $Zn_{(aq)}$  concentrations after 15 days sediment resuspension

Parameters	Description	% change of X	% change of Y	Sensitivity
pH	Final pH after 15 days	16	190	11.54
$pK_{OC,Zn}$	Zn sorption constant to humic acid	33	117	3.51
$pK_{Fe,Zn}$	Zn sorption constant to ferric iron	34	89	2.61
Humic acid	Active humic acid content	50	73	1.46
$ZnS_{(s)}$	Initial $ZnS_{(s)}$ concentration	50	56	1.13
$kZnS$	$ZnS_{(s)}$ oxidation rate	69	61	0.89
FeOOH	Active ferric oxide content	50	32	0.64

The most obvious result is that dissolved  $Zn_{(aq)}$  concentration is strongly dependent on pH. Undoubtedly, pH is the master variable that controls the surface characteristics of organics and oxides that play an important role in metals speciation in oxidized sediments. In particular, the pH changes around neutral condition had dramatic impact on metals release because the point of zero charges of ferric oxide is close to neutral. The sensitivity to pH is investigated in more detail (i.e. under various pH conditions) in Table 3.7.

Table 3.7 pH dependent sensitivity of  $Zn_{(aq)}$  concentrations after 15 days

pH		$Zn_{(aq)}$ conc. (M)		Sensitivity
$X_{base}$	$X$	$Y_{base}$	$Y$	
9	8	1.17E-07	1.34E-07	1.31
8	7	1.34E-07	1.01E-06	52.30
7	6	1.01E-06	5.44E-06	30.70
6	5	5.44E-06	1.65E-05	12.20
5	4	1.65E-05	1.92E-05	0.82
4	3	1.92E-05	2.20E-05	0.58

The pH changes of sediments and overlying water are affected by many biogeochemical reactions. Oxidation of many reduced species in sediments tends to produce acidity and decrease pH. Hence, more simulations were conducted to figure out which process or what parameters are the most important in controlling pH upon sediment resuspension. In this simulation,  $Y$  is the pH after 15 days sediment resuspension and  $X$  is the pH related input parameters and initial conditions of sediments. Table 3.8 summarizes the sensitivity of  $X$  to  $Y$ . Parameters are listed from the most sensitive parameters to the least sensitive parameters.

The  $CaCO_{3(s)}$  content in sediments which buffers the pH by dissolution is the most important parameter and  $FeS_{(s)}$  content which produces most of the acidity by oxidation is the second most important parameter. The  $FeS_{(s)}$  were estimated from AVS measurement while  $CaCO_{3(s)}$  were fitted from measured pH and  $Ca_{(aq)}$  concentrations. Experimental quantification of  $CaCO_{3(s)}$  could decrease model fitting parameters and model uncertainties considerably.

Table 3.8 Sensitivity of pH related parameters to final pH after 15 days sediment resuspension

Parameters	Description	% change of X	% change of Y	Sensitivity
CaCO <sub>3(s)</sub>	Initial CaCO <sub>3(s)</sub> concentrations	20	14	0.68
FeS <sub>(s)</sub>	Ferrous sulfide concentrations	20	12	0.62
FeOOH <sub>(s)</sub>	Active ferric oxide content	20	7	0.34
k <sub>S0</sub>	Elemental sulfur oxidation rate	20	2	0.09
k <sub>CaCO3</sub>	Calcium carbonate dissolution rate	20	2	0.09
Fe <sup>2+</sup> total	Total ferrous iron content	20	2	0.10
HCO <sub>3</sub> <sup>-</sup>	Dissolved carbonates concentrations	20	1	0.06
Humic acid	Active humic acid content	20	1	0.04

### 3.4.8 Modeling Ni, Zn and Pb Releases under Environmental Conditions

Further simulations were conducted to investigate different heavy metals (Pb, Zn, Ni) release behaviors under conditions in which natural buffering and the dilute nature of the sediment in the resuspension event limited the influence of pH changes. A dilute slurry simulation, in which the particle concentration was 7.7 g L<sup>-1</sup>, represents resuspension by storm events which usually suspend sediment particles into a large volume of overlying water column. Additional conditions in which particle concentrations were 77 g L<sup>-1</sup> and 770 g L<sup>-1</sup>, were investigated to compare heavy metal dynamics for different solid densities. The denser slurries are expected to occur in the vicinity of sediment-water interface where sediments are suspended by tidal flow.

During the simulation, pH was fixed to an initial condition since the natural system is well buffered by carbonates and DOC as well as a continuous resupply of

buffering capacity is expected in actual resuspension events. Initial conditions and parameters were used from Anacostia River sediment data in previous section. Initial conditions which are dependent upon solid densities are summarized in Table 3.9. Additional model parameters were collected from the literature and shown in Table 3.10 and 3.11.

Table 3.9 Model Initial Conditions

Parameters	Unit	Simulation 1	Simulation 2	Simulation 3
		Dilute Slurry	Mild Slurry	Dense Slurry
Solid Density	g L <sup>-1</sup>	7.7	77.0	770.0
FeS <sub>(s)</sub>	mM	0.33	3.3	33.0
Fe <sup>2+</sup> <sub>available</sub>	mM	0.04	0.4	4.0
NH <sub>4</sub> <sup>+</sup>	mM	0.02	0.2	2.0
PbS <sub>(s)</sub>	mM	0.05	0.5	5.0
ZnS <sub>(s)</sub>	mM	0.05	0.5	5.0
NiS <sub>(s)</sub>	mM	0.05	0.5	5.0

Table 3.10 Pb, Zn, and Ni sorption constants (Lofts and Tipping, 1998; Tipping, 1998)

Parameters	Humic Acid	FeOOH <sub>(s)</sub>
pK <sub>Pb</sub> (-)	2.0	-0.2
pK <sub>Zn</sub> (-)	-1.5	1.8
pK <sub>Ni</sub> (-)	1.1	4.0

\* Considered to adsorb strongly to 9% of total sorption sites

Table 3.11  $\text{PbS}_{(s)}$ ,  $\text{ZnS}_{(s)}$ , and  $\text{NiS}_{(s)}$  oxidation rates (Carbonaro et al., 2005)

Parameter	Units	Value
$k_{\text{PbS}}$	$\text{M}^{-1} \text{day}^{-1}$	960
$k_{\text{ZnS}}$	$\text{M}^{-1} \text{day}^{-1}$	320
$k_{\text{NiS}}$	$\text{M}^{-1} \text{day}^{-1}$	3200

Three different heavy metals, Pb, Zn, and Ni, showed similar release patterns under different solid densities although the released concentrations were very different among metals, which are shown in Figure 3.7 (a), (b), and (c). Generally, higher dissolved metals concentrations were observed in thicker solid density due to higher total metals concentrations in the system. The highest dissolved concentration was observed for  $\text{Ni}_{(aq)}$  ( $7.7 \times 10^{-6} \sim 3.1 \times 10^{-5} \text{ M}$ ) while many orders of magnitude smaller concentrations were observed for  $\text{Pb}_{(aq)}$  ( $1.0 \times 10^{-9} \sim 1.1 \times 10^{-8} \text{ M}$ ) and  $\text{Zn}_{(aq)}$  ( $1.2 \times 10^{-6} \sim 2.4 \times 10^{-6} \text{ M}$ ) indicating significantly different partitioning of metals to the solid phase. From Figure 3.7 (d), (e), (f), the phase distribution of individual metals can be investigated. The oxidation kinetics of  $\text{PbS}_{(s)}$  was faster than that of  $\text{ZnS}_{(s)}$ . However, the affinity of Pb to oxide was greater than that of Zn. As a result, the aqueous phase  $\text{Pb}_{(aq)}$  concentration was 2 orders of magnitude smaller than  $\text{Zn}_{(aq)}$  because released  $\text{Pb}_{(aq)}$  was significantly scavenged by sediment particles.  $\text{NiS}_{(s)}$  oxidation kinetics were the fastest and the Ni affinity to sediment particle was weaker than Pb and Zn. Zn and Pb strongly adsorbed to oxide phase while Zn was more adsorbed to organics. Consequently, the highest dissolved  $\text{Ni}_{(aq)}$  concentration was observed.

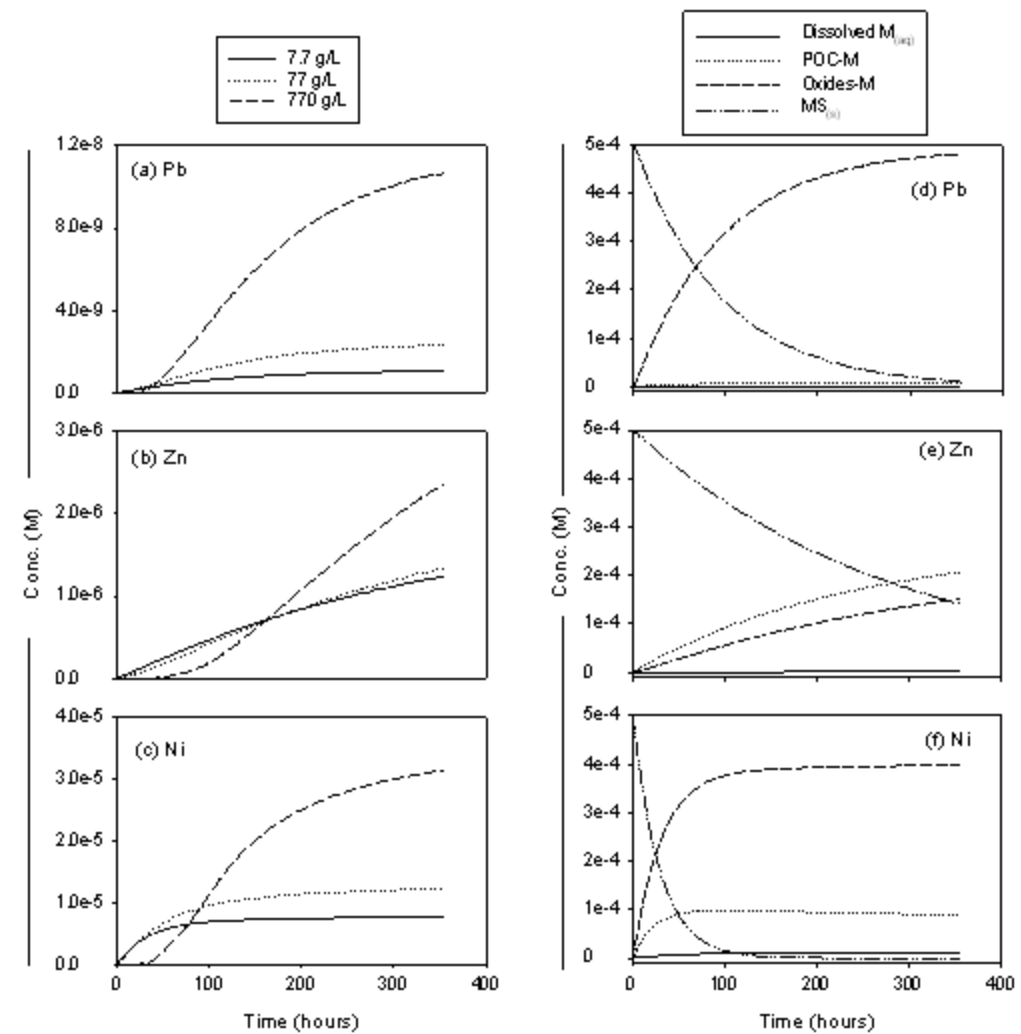


Figure 3.7 Transient dissolved (a) Pb, (b) Zn and (c) Ni concentration changes upon sediment resuspension under three different solid densities (dilute slurry =  $7.7 \text{ g L}^{-1}$ , mild slurry =  $77 \text{ g L}^{-1}$ , dense slurry =  $770 \text{ g L}^{-1}$ ). Speciation of (d) Pb, (e) Zn and (f) Ni in dissolved ( $M_{(aq)}$ ), adsorbed to organics (M-OC), adsorbed to oxides (M-OX) and metal sulfides ( $MS_{(s)}$ ) upon sediment resuspension in mild slurry (sediment density =  $77 \text{ g L}^{-1}$ ).

In the dense slurry, initial (0 ~ 50 hours) dissolved metals concentrations were smaller than other slurries. This was due to oxygen depletion in the dense slurry which

had higher oxygen demand. The oxygen was consumed by the oxidation of many reduced species, such as  $\text{FeS}_{(s)}$ ,  $\text{NH}_4^+_{(aq)}$ , and  $\text{Fe}^{2+}_{(s), (aq)}$  and the oxygen resupply was not fast enough to sustain the initial oxygen concentration. Figure 3.8 shows the oxygen concentrations in the three different slurries. The oxygen concentrations in the dense slurry were lower than those of in the mild and dilute slurry. The decrease of oxygen concentration in the aqueous phase can be a potential issue to fish or other organisms in the overlying water, if the oxygen transfer to sediment slurry is not fast enough to sustain the dissolved oxygen concentrations.

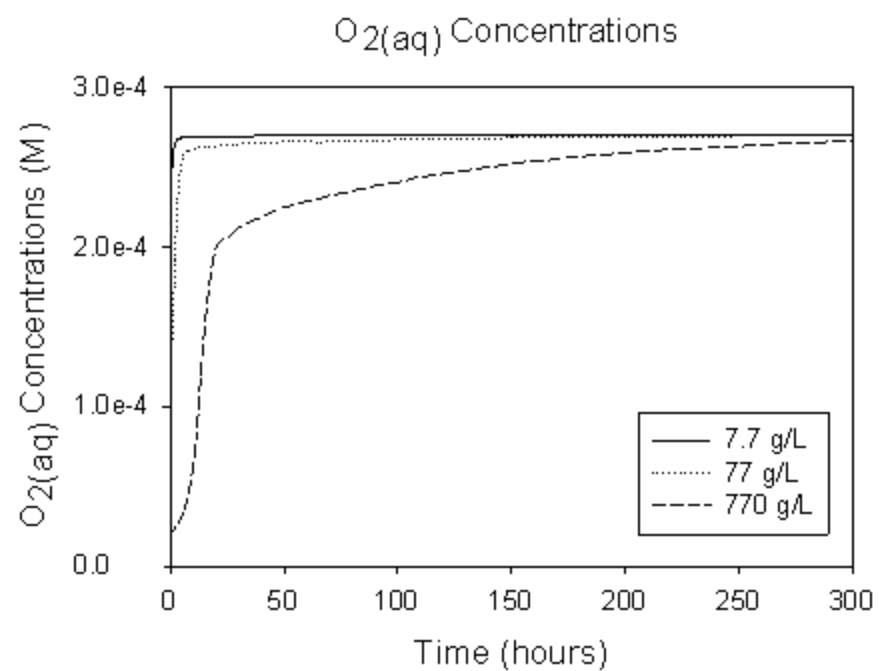


Figure 3.8 Transient dissolved oxygen concentrations upon sediment resuspension under three different solid densities (dilute slurry =  $7.7 \text{ g L}^{-1}$ , mild slurry =  $77 \text{ g L}^{-1}$ , dense slurry =  $770 \text{ g L}^{-1}$ ).

### 3.5 CONCLUSIONS

This research focused on identifying the importance of individual biogeochemical processes such as reduced species oxidation, carbonate minerals dissolution and metals sorption to sediment by acidification followed by heavy metal release under sediment resuspension. The oxidation of ferrous iron produces the most acidity for the first few hours, but the acidity was buffered by both the dissolved carbonate species and sediment surface. The dissolved and solid phase ferrous iron concentration dynamics were well described by the proposed model under the assumption that dissolved and sorbed  $\text{Fe}^{2+}$  are oxidized at the same rate. The AVS were first oxidized to  $\text{S}^0_{(s)}$  within 6 hours without producing acidity. The  $\text{S}^0_{(s)}$  is further oxidized to sulfate with the production of acidity that decreases the pH depending on the initial AVS concentration. The two step oxidation process of sulfide species were described well with the proposed model. The pH dependent Ca, Mg, Zn release from sediment was well described by the mathematical model except Mn which could only be modeled when the sorption constant is changed. Sensitivity analysis showed that pH was the most important parameter for metals release. Further simulations have showed that the oxidation kinetics of metals sulfides and the affinity of metals to either organics or oxides are the controlling factors for the solubility of metals in a well buffered solution. The model does not consider the electrostatic interactions between metals and sediment surface and possible multidentate sorptions. Despite these shortcomings, the model captures the major oxidation process of reduced species and metals release. This is likely due to the relatively low pH ultimately achieved in the experiments. At low pH, the sorption of metals to oxide is negligible and organics controls the dissolved metals concentration, which makes the sorption behavior simpler to describe with proposed model.

## Chapter 4: Experimental Investigation of pH and Salinity Effects on Metals Release and Sediment Early Diagenesis

### 4.1 INTRODUCTION

Free metals ( $M^{2+}_{(aq)}$ ) activity has been often provides a better indication of toxicity than total dissolved concentrations in the aqueous phase (Lofts et al., 2004) or total metal loadings in sediments (Di Toro et al., 1990). The Free Ion Activity Model (FIAM) (Morel, 1993) and the Biotic Ligand Model (BLM) (Thakali et al., 2006; Di Toro et al., 2001), a more generalized concept of FIAM, have been developed and used to indicate the toxicity of dissolved heavy metals in aquatic environments. In sediments, Acid Volatile Sulfide (AVS) and particulate organic carbon have been compared with Simultaneously Extracted Metals (SEM) to screen heavy metals toxicity (USEPA, 2005). The AVS/SEM concept has been recently linked with the BLM model to increase the model prediction of toxicity (Di Toro et al., 2005).

In terms of toxicity and bioavailability, assessing sediment heavy metal contamination in dynamic environments has been considered a challenging task, especially for estuarine sediments due to the fluctuations of biogeochemical factors, such as pH, salinity, dissolved oxygen, particle concentrations, and dissolved organic carbon (Chapman and Wang, 2001), which affect the activity of free heavy metals. There are only a few investigations of metals release that involve dynamic changes of biogeochemical factors. Low dissolved oxygen concentration and low redox potential in the overlying water increased heavy metal flux from sediment presumably by degradation of particulate organic carbon and dissolution of ferromanganese particles associating heavy metals (Riedel et al., 1997; Shine et al., 1998). Wave and current induced small

scale sediment resuspension has been known as an important factor in releasing heavy metals into the overlying water (Catwell et al., 2002; Kalnejais et al., 2007). Sediment disturbance and pH (5.5 ~ 8.0) were more important than dissolved oxygen (3 ~ 8 mg L<sup>-1</sup>) and salinity (15 ~ 45 g L<sup>-1</sup>) in heavy metals release from estuarine sediments (Atkinson et al., 2007). Dissolved organic carbons (DOC) played an important role in controlling dissolved metal solubility by complexation (Turner et al., 2002; Shank et al., 2004). A strong effect on the mortality of aquatic organisms related to both pH and salinity was observed in estuarine sediments (Riba et al., 2004).

Metals release from estuarine sediment, however, is not influenced by one single parameter but affected by many parameters that are changing simultaneously. The dynamic changes of salinity and pH, which are believed to be the master variables controlling the availability of heavy metals in sediments, can be the consequence of mixing between well buffered salt water and poorly buffered freshwater (Cai and Wang, 1998; Mosely et al., 2004). This estuarine mixing usually leads to daily or seasonal cycling changes of pH and salinity (Ringwood and Keppler, 2002; Liu et al., 2007) which may affect heavy metals release significantly. Understanding the relative importance of these key factors would be critical for assessing the metals toxicity in a dynamic estuary environment. This research specifically has focused on identifying the relative importance of pH and salinity on metals release from sediments and metals distribution in sediments. .

## 4.2 METHODS

### 4.2.1 General Methods and Reagents

All solutions were prepared by dissolving analytical reagent grade or equivalent analytical purity chemicals in deionized water ( $18 \text{ M}\Omega\text{cm}^{-1}$ , Millipore). Deionized water was further deaerated by bubbling  $\text{N}_2$  gas (99.9%) for 12 hours to make ferrous iron and sulfide stock solutions. All the experimental procedures for anoxic sediments and chemicals which are sensitive to oxygen were conducted under 97%  $\text{N}_{2(\text{g})}$  and 3%  $\text{H}_{2(\text{g})}$  atmosphere in anaerobic chamber (Coy Laboratory Products Inc.). All glass and plasticware were soaked in 1M  $\text{HNO}_3$  for more than 1 day, rinsed several times with deionized water and dried in an electric drying cabinet (Hamilton) for 1 day at  $70^\circ\text{C}$  before use.

### 4.2.2 Microcosm Experiments

Anacostia River sediment (Washington, D.C) was passed through a #10 (2 mm) sieve to remove large debris and stored at  $4^\circ\text{C}$  until used. As a complementary heavy metal, cadmium was spiked to Anacostia River sediment (Washington, D.C.) as  $\text{CdS}_{(\text{s})}$ . Spiking sediment with heavy metals as an ionic form can cause significant sediment chemistry changes, such as pH decrease, redox potential increase, iron and manganese displacement in solid (Hutchins et al., 2007, 2008). To minimize these undesirable artifacts, a freshly precipitated amorphous  $\text{CdS}_{(\text{s})}$ , which is assumed to be the dominant cadmium phase in anoxic sediments, was spiked into Anacostia River sediment targeting  $40 \mu\text{mol Cd g}^{-1}$  and aged for 2 weeks with mixing under anaerobic condition. To precipitate  $\text{CdS}_{(\text{s})}$ , equimolar quantities of  $\text{Na}_2\text{S}\cdot 9\text{H}_2\text{O}_{(\text{s})}$  and  $\text{CdCl}_2 \cdot 2\frac{1}{2}\text{H}_2\text{O}_{(\text{s})}$  were dissolved in de-aerated Millipore water and mixed and aged for 3 days for complete formation of solid phase in an anaerobic glove box (Bowles et al., 2002). The dissolved

sulfide and cadmium concentrations were checked with Iodine titration (Standard Method, 1998) and commercial standard before precipitation.

The CdS<sub>(s)</sub> spiked Anacostia sediment was transferred to 4 different microcosms (T shape-cells, see APPENDIX B). After 1 week of sediment consolidation in a nitrogen glove box, the cells were moved to the atmosphere and exposed continuously to one of the following environments: 1. control water (high pH $\approx$  8.5, low salinity $\approx$  0.45 g L<sup>-1</sup>), 2. salt water (high pH $\approx$  8.3, high salinity  $\approx$  30.0 g L<sup>-1</sup>), 3. freshwater (low pH $\approx$  6.5, low salinity $\approx$  0.3 g L<sup>-1</sup>) and 4. cycling water, which alternates fresh and salt water once every 8 days. The purpose of control water was to separate the effect of salinity from pH on metals release. If the freshwater and control water cells were compared, the effect of pH can be evaluated because the only difference is pH. In a similar way, if the saltwater and control water cells were compared, the effect of salinity can be evaluated because their pH is similar but the salinity is different. Cycling water was to investigate the effect of cyclic changes of overlying waters in metals release, which simulated estuarine sediments. The long cycling period was selected to allow complete exchange of fresh and saltwater between cycles. After 96 days, the cycling period was adjusted to 1 day to simulate more realistic conditions.

The saltwater was made by dissolving 35 grams of Instant Ocean® sea salts in 1 liter of de-ionized Millipore® water. The saltwater was diluted by a factor of 150 to make ordinary freshwater (Stumm and Morgan, 1996). Additional 3.15 mM of NaHCO<sub>3</sub> was dissolved in the freshwater to make control water. The control water was well buffered similar with saltwater but the salinity was close to freshwater. The concentrations of cations and anions in saltwater were analyzed with ICP-AES and IC with dilutions. The carbonate concentration in the salt water was estimated from titration. The ions

concentrations in freshwater and control water were estimated from salt water's ion concentrations considering the dilution. The measured concentrations of ions are available in APPENDIX B.

A multi-channel peristaltic pump (Ismatec™) and tygon tubing (0.44mm diameter, Cole-Parmer) were used to flow the waters into the microcosms at the flow rate of 0.26 mL min<sup>-1</sup>. A gallon of gas tight collapsible water bags were used as reservoir to prevent pH changes by carbon dioxide exchange between water and atmosphere. The average depth and volume of overlying water were 1.0 cm and 0.206 liters, respectively. Calculated hydraulic residence time was 12.9 hours. A preliminary tracer test showed that the overlying water behaved as a well mixed system (See Appendix E).

During the experiments, the effluents from individual cells were collected to determine pH and salinity in the overlying water. pH was measured by pH electrode (VWR Symphony) calibrated with standard 4.00, 7.02 and 10.05 pH buffers. The changes of liquid junction potential due to different ionic strengths are well known problems in measuring pH in salt water. Ionic strength corrected buffer solutions were prepared according to the procedure developed by Baumann (1973) and used to calibrate pH electrode in high ionic strength saltwater. For the freshwater and control water, standard buffer solutions were used to calibrate the pH electrode. Conductivity was determined by Conductivity Electrode (VWR Symphony) calibrated with 0.001M, 0.01M, 0.1M KCl solutions. The conductivity was converted to salinity by a pre-established linear relationship which is salinity (g/L) equals 0.688×conductivity (mS/cm).

Samples were taken once every 4 days from the control, saltwater, and freshwater pumped microcosms, and once every 2 days from cycling water microcosm to determine dissolved metals concentrations and DOC. The samples were filtered through 0.45µm

polypropylene membrane and acidified with 1% HNO<sub>3</sub> for dissolved Zn<sub>(aq)</sub>, Cd<sub>(aq)</sub>, Mn<sub>(aq)</sub>, and Fe<sub>(aq)</sub> analysis with GFAAS with proper dilutions. To eliminate the effect of background salts concentration on individual metals concentration, matrix modifiers (NH<sub>4</sub>H<sub>2</sub>PO<sub>4</sub>, Mg(NO<sub>3</sub>)<sub>2</sub>, Palladium) were added to the sample as per the GFAAS manufacturer's recommendations.

After 100 days, dissolved metals concentrations in porewater were analyzed in-situ by commercial electrodes, voltammetric microelectrodes and DGT (Diffusive Gradient in Thin Film). After 120 days, the sediments were extruded from the microcosm and sliced with 1cm resolution to determine solid phase AVS/SEM. Dissolved metals (Fe, Mn, Cd, Zn), ionic species and DOC concentrations were also determined from porewaters generated by centrifugation and filtration to compare the concentrations measured by different in-situ and ex-situ techniques.

#### 4.2.3 Ex-situ Sediment Porewater Analysis

Porewater was generated by centrifugation of sediment at the conclusion of the experiment in 500 mL polycarbonate bottles using Beckman J2-21 centrifuge (9000 rpm, 20 min). The porewater was gently transferred to a 15 mL syringe and was filtered with 0.45µm polypropylene membrane. Porewater Cl<sup>-</sup> and SO<sub>4</sub><sup>2-</sup> concentrations were determined with an ion chromatography (Metrohm) and samples were pre-filtered through cartridge (OnGuard<sup>®</sup> II 1cc Dionex) to remove any interfering metals.

Total dissolved inorganic carbon was determined with a carbon analyzer (Tekmar Dohrmann Appollo 9000) and dissolved organic carbon was determined by Ultra Violet Absorbance at 270 nm using a potassium hydrogen phthalate standard. Ferrous iron (Fe<sup>2+</sup>) was measured colorimetrically using 1,10-phenanthroline (Standard Methods,

1998). Some of the porewater samples were acidified immediately after generation with 1% concentrated HNO<sub>3</sub> to determine dissolved Zn, Cd, Fe, Mn, Ca, Mg, Na and K concentrations with ICP-AES (Spectro) and GFAAS (Perkin Elmer) depending on the concentrations.

Porewater was diluted with sulfide anti oxidant buffer (SAOB) solution containing 2 M NaOH, 0.1M ascorbic acid and 0.1 M ethylene diamine tetra acetic acid (EDTA) to determine total dissolved sulfides (H<sub>2</sub>S, HS<sup>-</sup>, S<sup>2-</sup>, FeS<sub>(aq)</sub>) with silver sulfide (VWR Symphony) ion selective electrodes. Ammonium (NH<sub>4</sub><sup>+</sup>) concentrations were determined with ammonium (Thermo Orion 9512) ion selective electrodes with pH adjusting solution (Thermo Orion). The electrodes were calibrated with 10<sup>-6</sup> ~ 10<sup>-2</sup> M S<sup>2-</sup> and NH<sub>4</sub><sup>+</sup> standards, respectively. Oxidation reduction potential (ORP) was measured with a fabricated platinum electrode in combination with Ag/AgCl reference electrode (Accumet) calibrated with Quinhydrone saturated pH 4.00, 7.00 buffer solutions.

#### **4.2.4 In-situ Porewater Characterizations**

Cd, Zn, Fe and Mn concentrations in porewater at the conclusion of the experiments were also determined in-situ by diffusive gradient thin film (DGT) probes for sediments purchased from DGT Research LTD. The probes had been deaerated in 0.1 M NaCl for 24 hours and deployed in sediment for 24 hours to allow dissolved metals diffusion and sorption to the ion exchange resin. After retrieval, the resins were removed from probes and sliced with 1cm resolution. The sorbed metals were leached in 1 M HNO<sub>3</sub> for 24 hours and the dissolved metals concentrations were determined with GFAAS. The porewater metals concentrations were calculated from the eluted metals concentrations assuming Fick's first law of diffusion in a diffusive film, infinite sorption

capacity of the ion exchange resin (Zhang and Davison, 1995) and no depletion of dissolved metals in porewater.

Dissolved  $O_2$ ,  $Mn^{2+}$ ,  $Fe^{2+}$ , and  $S^{2-}$  concentrations were obtained by voltammetric microelectrodes (Brendeland Luther, 1995) using a single axis automated micromanipulator (Analytical Instrument Systems, Flemmington, NJ). Microelectrodes were prepared in the laboratory using the method of Brendel and Luther (1995). At the beginning of each profiling event, electrodes were calibrated for oxygen using a two point calibration, and the method of standard additions was used for iron, manganese, and sulfide in synthetic seawater with 2mM acetate or HEPES buffers. Scan parameters and detection limits were the same as those reported in Brendel and Luther (1995). Calibration checks were performed on electrodes after each profile. Triplicate scans were made at each depth and duplicate electrodes were spaced 2-3cm apart.

Porewater pH and chloride were determined with a micro pH electrode (MI-405, Microelectrodes, INC.) and a needle chloride electrode (665-27, Diamond General Development Corp.) in conjunction with an external reference electrode.

#### **4.2.5 Sediment Analysis**

The water content was determined by weight loss after drying in 95 °C oven for 24 hours. Total metals in sediment were extracted by microwave digestion in concentrated trace metal grade  $HNO_3$  (EPA, SW 846–3051). Reactive solid phase  $Fe^{2+}$  and  $Fe^{3+}$  were recovered by anoxic oxalate extraction (Philips and Lovely, 1987). Hydroxylamine hydrochloride extraction (Tessier, 1979) determined the metals associated with easily reducible iron and manganese in sediments. AVS and SEM were measured by the diffusion method (Brouwer et al., 1994) with 0.05 M ascorbic acid

addition to 1 M HCl to prevent Fe<sup>3+</sup> interference (Hseih et al., 2002). Solid phase organic and inorganic carbon concentrations were determined using CHN analyzer (HewlettPackard). All the extractions were duplicated and the extracts were filtered with a 0.45µm polypropylene membrane. The concentrations of individual metals were determined by the same analytical techniques for the porewater analysis with proper dilutions. All the solid phase concentrations were calculated based on dry sediment weight.

#### 4.2.6 Flux Calculation

The concentration of overlying water species, such as dissolved metals and organic carbon, are affected by the overlying flow. In order to generalize to other flow rates, assuming that release processes do not change, the measured water concentrations were converted to flux by the following equation

$$Flux = \frac{Q \times C}{A} \quad (4.1)$$

where  $Q$  is the flow rate (0.26 mL min<sup>-1</sup>) of overlying water by peristaltic pump,  $C$  is the overlying water concentration of species, and  $A$  is the exposed sediment surface area (120 cm<sup>2</sup>). All plots showing overlying water concentrations are plotted as flux using an additional axis on the right side of the plots.

### 4.3 RESULTS AND DISCUSSION

#### 4.3.1 General Sediment Properties

The Anacostia River (Washington, D.C.) is a freshwater watershed located within the Potomac River Drainage Basin, which discharges to the Chesapeake Bay. The typical

grain size distribution of surficial sediments were found to be 45.7 ~ 74.2 % fine sands, 6 ~ 34.2% silts and 10 ~ 16.1 % clays (ASTM D422). Due to the historical discharge of sewage, the sediment is contaminated with polychlorinated byphenyls (500 ~ 2000  $\mu\text{g kg}^{-1}$ ), polynuclear aromatic hydrocarbons (10000 ~ 30000  $\mu\text{g kg}^{-1}$ ) and heavy metals (Reible et al., 2006).

From the CHN analysis, total organic carbon and inorganic carbon were 7.0 ( $\pm 2.8$ ) % and 1.05 ( $\pm 0.21$ ) % respectively and the major solid phase metals loadings by various extraction methods are summarized in Table 4.1. The numbers are averages of duplicate samples and standard deviation is shown inside the bracket.

Table 4.1 Metal loadings in Anacostia River Sediments

Species	Value
Total Fe ( $\text{mg g}^{-1}$ )	53.42 (6.65)
Total Mn ( $\text{mg g}^{-1}$ )	0.24 (0.022)
Total Zn ( $\text{mg g}^{-1}$ )	0.70 (0.087)
Total Al ( $\text{mg g}^{-1}$ )	12.33 (3.98)
H.H*.extractable Fe ( $\text{mg g}^{-1}$ )	21.8 (0.75)
H.H. extractable Mn ( $\text{mg g}^{-1}$ )	0.23 (0.056)
H.H. extractable Zn ( $\text{mg g}^{-1}$ )	0.65 (0.07)
SEM Zn ( $\text{umol g}^{-1}$ )	8.48 (0.76)
Oxalate extractable Fe <sup>2+</sup> ( $\text{mg g}^{-1}$ )	3.05 (0.07)
Oxalate extractable Fe <sup>3+</sup> ( $\text{mg g}^{-1}$ )	20.85 (1.22)

\*H.H. Hydroxylamine Hydrochloride.

Total iron was 5 % by mass and 50% of total iron were available by both hydroxylamine hydrochloride and oxalic acid extractions, presumably leaching iron from easily reducible phases, such as amorphous iron oxides. Approximately, 15% of readily reducible iron presented as  $\text{Fe}^{2+}$ . Total manganese was 200 times less than iron; however, almost all manganese was recovered by hydroxylamine hydrochloride indicating that most of the manganese presented as easily reducible or associated in exchangeable and carbonate phases (Tessier et al., 1979).

Total zinc concentration ( $0.7 \text{ mg g}^{-1}$ ) was the highest and the other metals, such as copper ( $0.092 \text{ mg g}^{-1}$ ), lead ( $0.18 \text{ mg g}^{-1}$ ), cadmium ( $0.003 \text{ mg g}^{-1}$ ) and nickel ( $0.042 \text{ mg g}^{-1}$ ) and similar trends were observed in SEM analysis as well. Approximately, 80% of total zinc was extracted both by 1 M HCl (SEM) and by hydroxylamine hydrochloride. Previous studies suggested that 1 M HCl (Allen et al., 1993) and hydroxylamine hydrochloride (Peltier et al., 2005) could extract 20% and 95% of Zn from  $\text{ZnS}_{(s)}$  respectively. Higher Zn extractions efficiency by 1 M HCl suggested that significant portion of Zn was not associated with  $\text{ZnS}_{(s)}$ .

#### 4.3.2 Effect of $\text{CdS}_{(s)}$ Spiking

To check sediment porewater chemistry changes by  $\text{CdS}_{(s)}$  spiking, porewaters were extracted from the sediments before and after spiking; then important parameters were characterized and compared in Table 4.2. Generally, the pH was decreased from 7.56 to 6.9 and redox potential was increased from -159 mV to -44.9 mV indicating  $\text{Fe}^{3+}/\text{Fe}^{2+}$  redox couple controlled the porewater redox chemistry.  $\text{CdS}_{(s)}$  spiking raised Na and Cl concentrations and increased conductivity from  $1.27 \text{ mS cm}^{-1}$  to  $8.4 \text{ mS cm}^{-1}$  as well. Most of the metals concentrations in porewater were elevated, but the concentrations of

heavy metals, such as zinc and cadmium were not changed. The minor changes of porewater Zn and Cd concentrations suggested that most of the metals are strongly associated with sediments. The porewater was deficient of sulfate and relatively high AVS was observed compared to other freshwater sediments.

Table 4.2 Porewater and solid phase characteristics changes by CdS<sub>(s)</sub> spiking

	Species	Before Spiking	After Spiking
Porewater	pH	7.56	6.9
	Conductivity (mS cm <sup>-1</sup> )	1.27	8.40
	ORP (mV, SHE)	-159.3	-44.9
	Fe <sup>2+</sup> (M)	5.62 E-4	2.10 E-3
	Mn <sub>(aq)</sub> (M)	4.75 E-5	1.03 E-4
	Cd <sub>(aq)</sub> (M)	N.D. <sup>(a)</sup>	1.33 E-7
	Zn <sub>(aq)</sub> (M)	4.95 E-8	N.D. <sup>(a)</sup>
	Ca <sub>(aq)</sub> (M)	3.37 E-3	8.53 E-3
	Mg <sub>(aq)</sub> (M)	1.49 E-3	2.49 E-3
	K <sub>(aq)</sub> (M)	2.66 E-4	4.19 E-4
	Na <sub>(aq)</sub> (M)	2.16 E-3	4.82 E-2
	S <sup>2-</sup> (M)	N.D. <sup>(a)</sup>	N.D. <sup>(a)</sup>
	Cl <sup>-</sup> (M)	3.15 E-3	9.20 E-2
	SO <sub>4</sub> <sup>2-</sup> (M)	7.27 E-6	4.29 E-7
Sediment	Water Content (%)	55.3 (0.4)	51.5 (0.2)
	AVS (μmol g <sup>-1</sup> )	54.0 (4.3)	88.7 (6.2)
	SEM <sub>Cd</sub> (μmol g <sup>-1</sup> )	0.005 (0.003)	41.12 (1.84)
	Cd by H. H.(μmol g <sup>-1</sup> )	0.01 (0.001)	11.18 (2.09)
	Total Cd <sup>(b)</sup> (μmol g <sup>-1</sup> )	0.01 (0.001)	41.14(1.44)

(a)N.D.: Not Detected

(b)Determined by Microwave Digestion with concentrated nitric acid

Both microwave digestion and 1 M HCl (SEM) extracted 41.1 μmol g<sup>-1</sup> of Cd from sediments whereas only 11.2 μmol g<sup>-1</sup> of Cd (25% of total extracted Cd) was

extracted by hydroxylamine hydrochloride. The partial extraction of Cd was considered to be due to the limitations of hydroxylamine hydrochloride extraction, the incomplete formation of  $\text{CdS}_{(s)}$  during precipitation, and/or oxidation of  $\text{CdS}_{(s)}$  during sediment mixing and aging. The recovery of sulfide as AVS from  $\text{CdS}_{(s)}$  was 87 % which was close to the observation of Carbonaro et al. (2005).

### 4.3.3 Overlying Water pH and Salinity

The effluents from 4 different microcosms were analyzed for pH and conductivity with electrodes. The four individual microcosms are named as control, salt, fresh and cycling microcosms below for convenience. Figure 4.1 shows the effluent salinity and pH for 100 days.

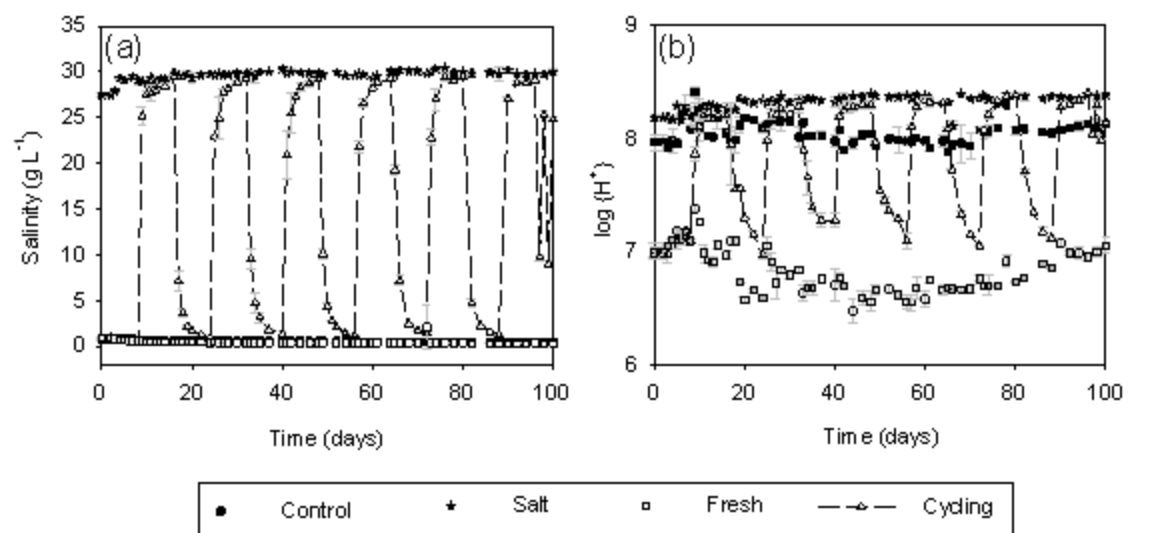


Figure 4.1 Temporal (a) salinity and (b) pH changes in the effluents where control, salt and fresh waters were continuously pumped and where fresh and cycling waters were cyclically pumped once every 8 days. Symbols and error bars are the mean and standard deviation of duplicated experiments respectively.

Salinities in control and fresh microcosms were slightly increased from the influent salinities possibly due to salts release from sediment. However, the effluent salinities were relatively stable at 0.59 ( $\pm 0.089$ ), 29.6 ( $\pm 0.56$ ) and 0.46 ( $\pm 0.25$ ) g L<sup>-1</sup> in control, salt and fresh water microcosms, respectively, which were similar with influent salinities. The effluent salinity in the cycling microcosm changed to the influent salinity within 3 days. The overlying waters were gently aerated with filtered ambient air without disturbing the surficial sediment to mix the overlying water well and to supply enough oxygen. A tracer test verified the completely mixed reactor behavior in the overlying water with the help of aeration (See the Appendix E). After 93 days of the experiment, daily cycling was implemented and the surface water salinity cycled between 10 and 25 g L<sup>-1</sup> as a result.

The effluent pH of control, salt and fresh water microcosms were relatively stable at 8.1 ( $\pm 0.1$ ), 8.3 ( $\pm 0.1$ ) and 6.8 ( $\pm 0.2$ ), respectively, for much of the experiment although a shift from 6.5 to 6.8 was noted in the fresh water microcosm. The relatively constant effluent pH in salt and control water microcosms was due to the strong buffering capacity of carbonate while the pH changes of fresh water (0.044mM HCO<sub>3</sub><sup>-</sup>) seemed to be due to the interaction between weakly buffered overlying water and surficial sediment. When fresh water replaced salt water, the pH decreased from 8.3 to 7.2 slowly while the pH increased from 7.3 to 8.3 rapidly within 2 days when salt water was pumped to the fresh water. Short term cycling of overlying water changed pH between 8.0 and 8.3. This non linear behavior was due to the weak acid base chemistry of carbonate species in the overlying water. The salinity and pH in cycling cell are further plotted in Figure 4.2.

This observation, dramatic pH increases in the early stage of freshwater mixing with saltwater, has been often examined in other estuarine waters (Cai and Wang, 1998; Mosely et al., 2004).

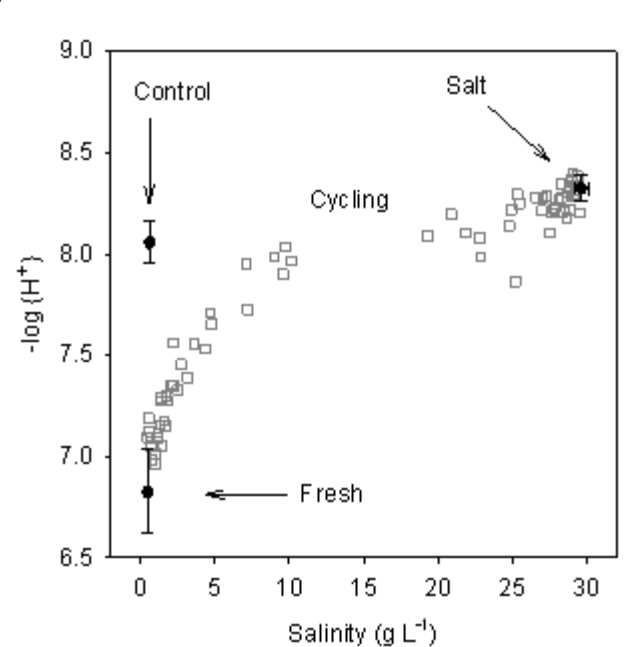


Figure 4.2 Effluent salinities and pH relations for 4 different microcosms. Average salinities and pH of duplicated experiments for 100 days were shown in circles symbols (●) with bi-directional standard deviations. Salinity and pH for the effluent of the cycling water microcosm are plotted in hollow squares (□).

#### 4.3.4 $Zn_{(aq)}$ , $Cd_{(aq)}$ and $Mn_{(aq)}$ Release

The metals associated with solid phase either by sorption or precipitation were subject to be released to the overlying water by desorption, oxidation or dissolution depending on the initial conditions of metals. Figure 4.3 (a), (b) and (c) shows time dependent dissolved  $Zn_{(aq)}$ ,  $Cd_{(aq)}$  and  $Mn_{(aq)}$  concentrations and fluxes to the overlying water where control, salt and fresh waters were continuously pumped into. The metals releases from cycling water microcosms are shown in Figure 4.3 (d), (e) and (f).

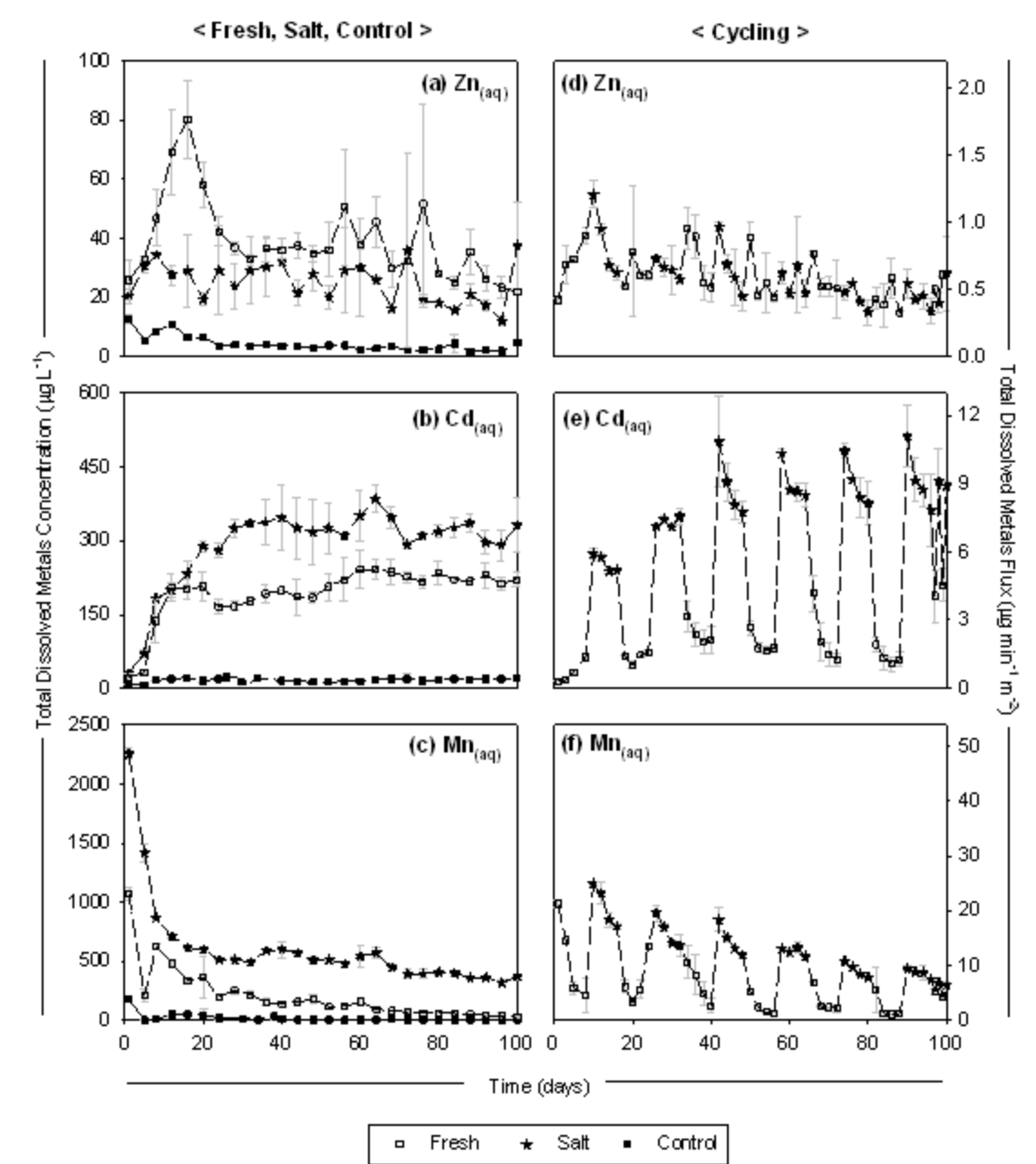


Figure 4.3 Temporal changes of total dissolved (a)  $\text{Zn}_{(\text{aq})}$ , (b)  $\text{Cd}_{(\text{aq})}$  and (c)  $\text{Mn}_{(\text{aq})}$  concentrations/fluxes under the continuous overlying water conditions. Temporal changes of total dissolved (d)  $\text{Zn}_{(\text{aq})}$ , (e)  $\text{Cd}_{(\text{aq})}$  and (f)  $\text{Mn}_{(\text{aq})}$  concentrations/fluxes under cyclic overlying water conditions alternating with fresh and salt water once every 8 days. Symbols and error bars are the mean and standard deviations of duplicated experiments respectively.

In general, the lowest concentrations of metals were detected in the control water microcosm while more metals were released in freshwater or saltwater conditions depending on the metal. Relatively stable  $Zn_{(aq)}$  concentrations were observed under all conditions except the peak  $Zn_{(aq)}$  concentration in fresh water microcosms around 15 days. Although large standard deviations and scattered data were observed, more  $Zn_{(aq)}$  was released under freshwater than salt water conditions. The  $Zn_{(aq)}$  was assumed to be adsorbed to exchangeable phase or to be bound to oxides phase rather than present as  $ZnS_{(s)}$  because hydroxylamine hydrochloride extracted almost all Zn that was recovered by 1 M HCl (SEM). The stable release of  $Zn_{(aq)}$  during the experimental period appeared to be caused by the continuous release of  $Zn_{(aq)}$  from the large pool of exchangeable solid phases.

The Cd concentrations were started from few  $\mu\text{g/L}$  and gradually approached to steady concentrations of 400  $\mu\text{g/L}$  and 250  $\mu\text{g/L}$  in saltwater and freshwater which were two orders of magnitude higher than Cd concentration in control microcosms. Both pH and salinity affected the Cd release significantly and unlike Zn, more Cd was released under saltwater conditions due to complexation with chlorides in the saltwater. This observation was consistent with the previous batch experiments [37]. The Cd was spiked as  $CdS_{(s)}$  initially and the existence of this phase was further verified by the hydroxylamine hydrochloride extraction. The slow release of Cd was considered to be due to slow oxidation of  $CdS_{(s)}$  at the aerobic surficial sediments followed by the diffusional flux of Cd to the overlying water.

A sharp increase followed by a decrease of  $Mn_{(aq)}$  were observed in both fresh and salt water microcosms indicating a large initial flux of  $Mn_{(aq)}$  and depletion of Mn pool at the surficial sediments. After 20 days, stable Mn concentrations were measured at

600  $\mu\text{g L}^{-1}$  (13  $\mu\text{g min}^{-1} \text{m}^{-2}$ ) and 100  $\mu\text{g L}^{-1}$  (2.2  $\mu\text{g min}^{-1} \text{m}^{-2}$ ) in salt and freshwater microcosms, respectively. More Mn was released under salt water than freshwater, similar to Cd.

In cycling water microcosms,  $\text{Zn}_{(\text{aq})}$  release was similar with saltwater and freshwater microcosms; however, a significant difference was observed for  $\text{Cd}_{(\text{aq})}$  when sediments were exposed to saltwater and freshwater alternately. More  $\text{Cd}_{(\text{aq})}$  was released during saltwater inundation and less  $\text{Cd}_{(\text{aq})}$  was released under the freshwater condition. Furthermore, Cd seemed to be depleted at the surficial sediment by the rapid release of  $\text{Cd}_{(\text{aq})}$  under saltwater leading to less  $\text{Cd}_{(\text{aq})}$  release in freshwater portions of the cycle compared to the microcosms where freshwater was continuously pumped.  $\text{Mn}_{(\text{aq})}$  release behavior was similar with  $\text{Cd}_{(\text{aq})}$  showing more release under saltwater and less release under freshwater conditions.

Dissolved  $\text{Fe}_{(\text{aq})}$  concentration in the overlying water is shown in APPENDIX B and the released concentration was not significant due to the oxidation of  $\text{Fe}^{2+}$  at the aerobic surficial sediments. Unlike Mn, only 10 ~ 50  $\mu\text{g L}^{-1}$  (0.2 ~ 1.1  $\mu\text{g min}^{-1} \text{m}^{-2}$ ) of Fe was detected in the overlying water over the experimental period, which were many orders of magnitude less than porewater  $\text{Fe}^{2+}$  concentrations. Significant amount of  $\text{Fe}^{2+}$  were apparently oxidized and precipitated as iron oxide at the surficial sediments supplying additional binding sites for metals sorption.

Dissolved organic carbon (DOC) in the overlying water was also determined over the course of the experiment and shown in Figure 4.4.

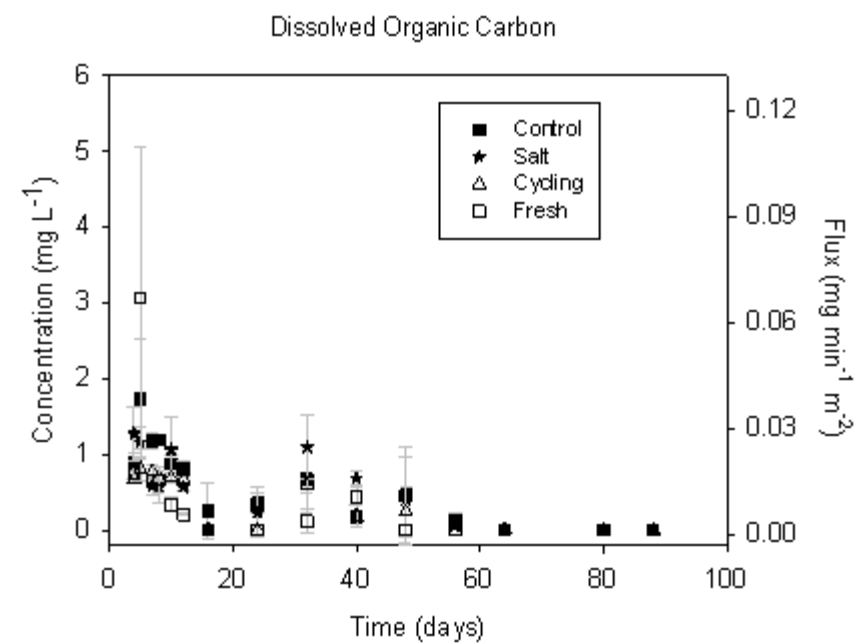


Figure 4.4 Dissolved organic carbon concentrations in the overlying water. Symbols and error bars are the mean and standard deviations of duplicate experiments respectively.

Generally, 1 ~ 3 mg L<sup>-1</sup> (0.02 ~ 0.07 mg min<sup>-1</sup> m<sup>-2</sup>) of DOC were released from sediment for the first 10 days and concentrations asymptotically approached instrument detection limits. The generally low levels limited the influence of organic matter on metals complexation in the overlying water.

#### 4.3.5 Zn<sup>2+</sup>, Cd<sup>2+</sup> and Mn<sup>2+</sup> Release

As indicated above, the release of total Cd<sub>(aq)</sub>, Zn<sub>(aq)</sub>, Fe<sub>(aq)</sub> and Mn<sub>(aq)</sub> was influenced by pH and salinity. To separate the individual effect of pH, cations and anions, the freely dissolved metals (M<sup>2+</sup>) concentrations were calculated. The freely dissolved metals concentration has also been linked more closely to adverse effects. The total

dissolved metals were assumed to include metals both in dissolved form and associated with inorganic ligands as follows

$$\Sigma\{M\} = \{M^{2+}\} + \{MOH^+\} + \dots + \{MSO_4\} + \dots + \{MCl^+\} + \dots \quad (4.2)$$

where,  $\Sigma\{M\}$  represents the total dissolved metals concentrations determined by GFAAS,  $\{M^{2+}\}$  represents the freely dissolved metals activity and  $\{MOH^+\}$ ,  $\{MSO_4\}$ ,  $\{MCl^+\}$  represent metals complexed with  $OH^-$ ,  $SO_4^{2-}$ ,  $Cl^-$ . Note that dissolved organic carbon (DOC) is not considered in this calculation because of the low levels of DOC in this experiment. The effect of organic matter and generalization of this approach to such conditions is described further in Appendix F.

The complexed metals concentrations can be estimated from concentrations of ligands and concentrations of freely dissolved metals using known stability constants, which are available in APPENDIX D. The ligand concentrations were estimated from the salinity and the activity coefficients were calculated by the Davies equations (Stumm and Morgan, 1996) as follows

$$\log \gamma_{monoprotic} = \left( -\frac{0.509I^{0.5}}{1+I^{0.5}} + 0.15I \right) \quad (4.3)$$

$$\log \gamma_{biprotic} = 2 \left( -\frac{0.509I^{0.5}}{1+I^{0.5}} + 0.15I \right) \quad (4.4)$$

$$I = 0.5 * \sum_i (C_i Z_i^2) \quad (4.5)$$

where  $\gamma$  represents activity coefficient,  $I$  represents ionic strength,  $C_i$  is the concentration of ionic species  $i$  and  $Z$  is the charge of the ionic species of  $i$ . The freely dissolved metals concentrations can be calculated as follows

$$\{M^{2+}\} = \frac{\Sigma\{M\}}{1 + K_{OH} \gamma_{OH} [OH^+] + \dots + K_{SO_4} \gamma_{SO_4} [SO_4^{2-}] + \dots + K_{Cl} \gamma_{Cl} [Cl^-] + \dots} \quad (4.6)$$

where,  $K_{OH}$ ,  $K_{SO_4}$ ,  $K_{Cl}$  represent the stability constants,  $\gamma_{OH}$ ,  $\gamma_{SO_4}$ ,  $\gamma_{Cl}$  represent the activity coefficients of  $OH$ ,  $SO_4^{2-}$ ,  $Cl$  calculated from the Davies Equations.

Figure 4.5 shows calculated freely dissolved  $Zn^{2+}$ ,  $Cd^{2+}$  and  $Mn^{2+}$  concentrations from control, salt, fresh waters and cycling water microcosms. More  $Zn^{2+}$  was released under freshwater conditions whereas similar  $Zn^{2+}$  was released under salt water and in the similar pH controls. The stabilized  $Zn^{2+}$  concentration in freshwater was around  $35 \mu\text{g L}^{-1}$  ( $0.76 \mu\text{g min}^{-1} \text{m}^{-2}$ ) which was slightly less than the total  $Zn_{(aq)}$  concentration, however, only 20 % of  $Zn_{(aq)}$  was released as  $Zn^{2+}$  in salt water and the other 80% was released as complexed species. In the cycling cell, more  $Zn^{2+}$  was released under freshwater conditions while less  $Zn^{2+}$  was released under salt water conditions. As noted earlier, there was little difference between salt and fresh water in terms of total Zn.

$Cd^{2+}$  behavior was similar to  $Zn^{2+}$  under fresh and control water but the effect of ligand complexation was more significant under salt water conditions leading to the much higher total Cd release under those conditions. Only less than 1 % of released  $Cd_{(aq)}$  was  $Cd^{2+}$  under saltwater while 70% of  $Cd_{(aq)}$  was  $Cd^{2+}$  under freshwater and control water conditions.  $Cd^{2+}$  has been known to make a strong complex with  $Cl^-$  (Turner et al, 2004) in salt water. As a result, the release pattern of  $Cd^{2+}$  in the cycling microcosms was the opposite of  $Cd_{(aq)}$ . More  $Cd^{2+}$  was released under freshwater while more total  $Cd_{(aq)}$  was released under saltwater. The greater mass release of total  $Cd_{(aq)}$  under salt water conditions may still lead to enhanced dissolved  $Cd^{2+}$  in other areas if fresh and salt water mixing reduces the proportion complexed to  $Cl^-$ .

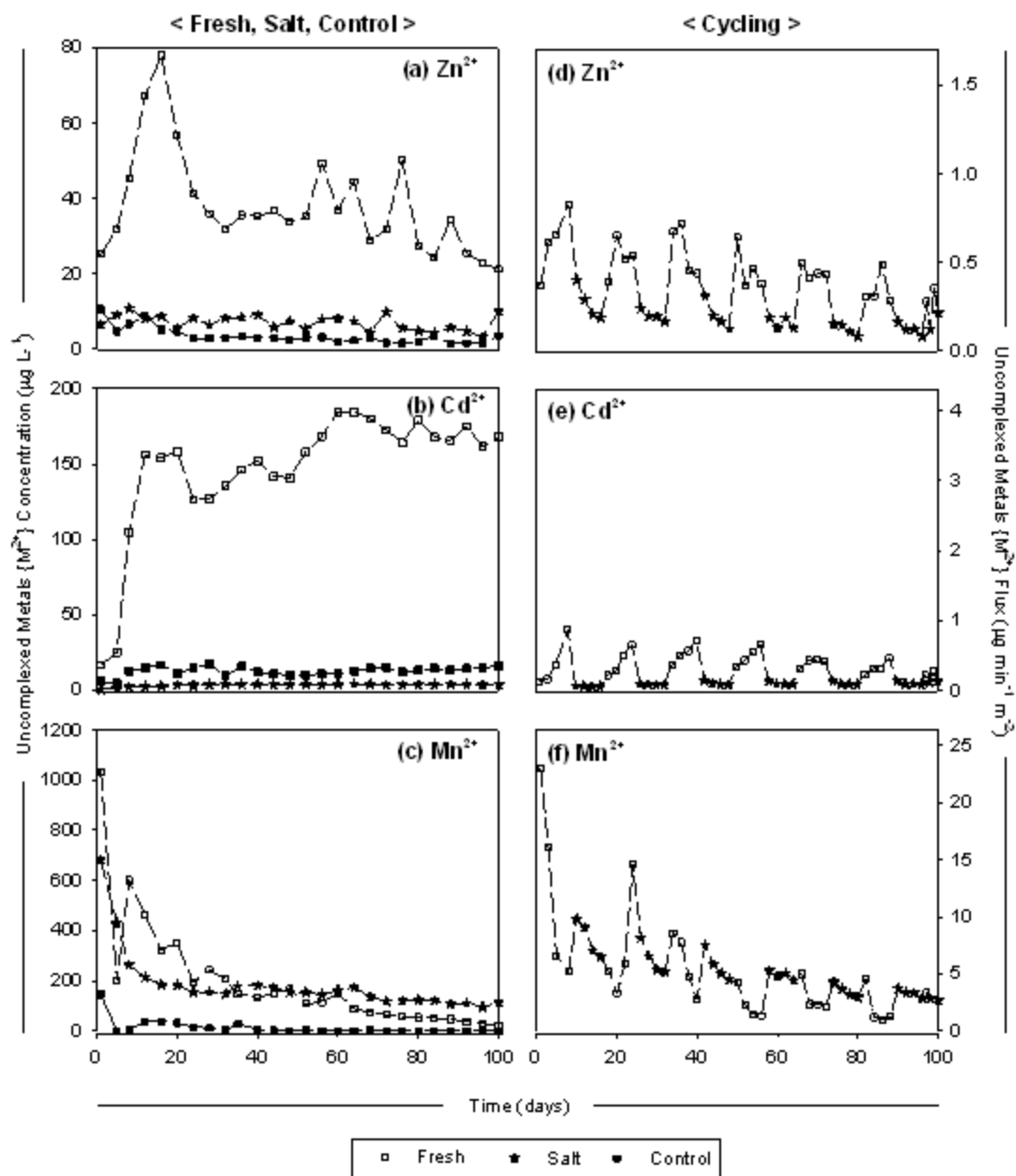


Figure 4.5 Temporal changes of calculated freely dissolved (a)  $Zn^{2+}$ , (b)  $Cd^{2+}$  and (c)  $Mn^{2+}$  concentrations/flux under the continuous overlying water conditions. Temporal changes of calculated freely dissolved (d)  $Zn^{2+}$ , (e)  $Cd^{2+}$  and (f)  $Mn^{2+}$  concentrations/flux under cyclic overlying water conditions alternating with fresh and salt water once every 8 days. Symbols and error bars are the mean and standard deviations of duplicate experiments, respectively.

As with  $Zn^{2+}$  and  $Cd^{2+}$ , more  $Mn^{2+}$  was released under freshwater conditions for the initial stage of the experiment, however, after 30 days, more  $Mn^{2+}$  was released under saltwater conditions. More than 90% of  $Mn_{(aq)}$  was released as  $Mn^{2+}$  in freshwater and control water while approximately only 20% of  $Mn_{(aq)}$  was released as  $Mn^{2+}$  under saltwater conditions. In cycling water microcosm, there was more  $Mn^{2+}$  release under salt water than control water which was not observed for  $Zn^{2+}$  and  $Cd^{2+}$ . More release of  $Mn^{2+}$  under salt water seemed to be due to the competition of  $Mn^{2+}$  with  $Ca^{2+}$  and  $Mg^{2+}$ . The sorption strength of  $Mn^{2+}$  to oxides and organics is not as strong as those of  $Zn^{2+}$  and  $Cd^{2+}$  for which sorption is strong enough to not be affected by  $Ca^{2+}$  and  $Mg^{2+}$  (Lofts and Tipping, 1998).

#### **4.3.6 AVS/SEM and Dissolved Cd and Zn Concentrations in Porewater**

Initially, the sediments were vertically homogeneous but the anoxic surficial sediments were oxidized by oxygen diffusing from the aerobic overlying water. Figure 4.6 shows the vertical profiles of AVS/SEM measured by 1 M HCl and dissolved Zn/Cd concentrations determined by DGT probes. Only Zn and Cd were considered in determining SEM because Mn is bound to sulfide more weakly than Fe and Mn is not included in the AVS/SEM model (Di Toro et al., 2005).

The AVS profiles were characterized as decreased concentrations at the surficial sediments and relatively constant concentrations at depths greater than 2 cm. Slight increases at depth under salt water and cycling waters were due to the diffusion of sulfate from the overlying water and subsequent sulfate reduction by bacterial activities. In all cases, there were sufficient AVS at depth to exceed the measured SEM. Based on the AVS/SEM model, the sediments below 2 cm are expected to be nontoxic and dissolved

metals concentrations should not be detected. In the upper centimeter, the segment averaged AVS was approximately equal to SEM and so dissolved metals and increased metal toxicity might be present, particularly if AVS levels in the upper few mm of sediment are substantially lower than the average over the upper cm.

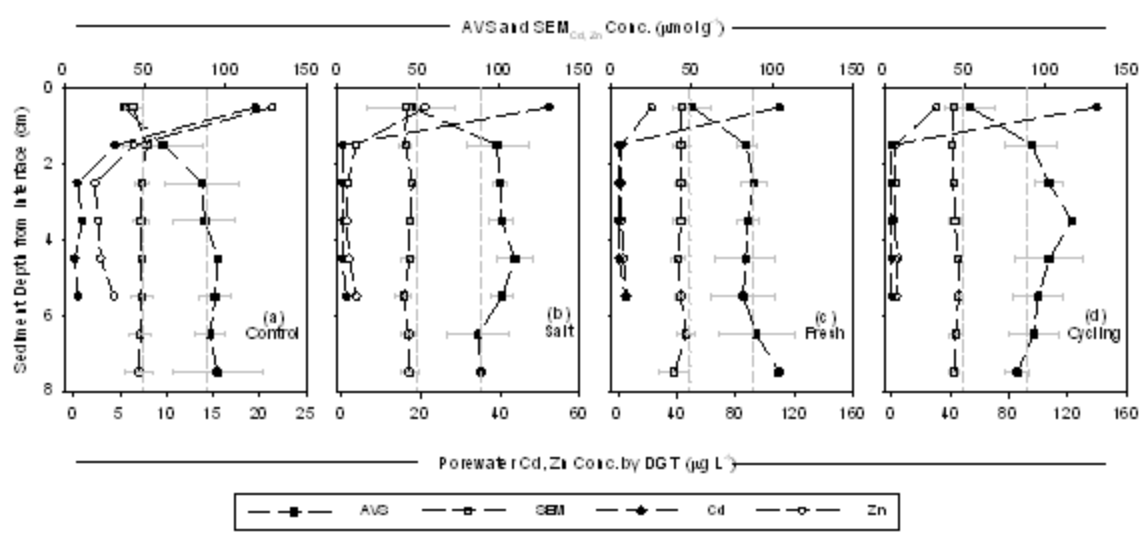


Figure 4.6 Vertical profiles of solid phase AVS/SEMs by 1 M HCl and dissolved phase Zn/Cd concentrations by DGT probe after 130 days sediments exposure to (a) control, (b) salt, (c) fresh and (d) cycling waters. Zn and Cd are considered in calculating SEMs. Symbols and error bars for AVS/SEMs are the mean and standard deviations of duplicated experiments respectively. Porewater  $Zn_{(aq)}$  and  $Cd_{(aq)}$  concentrations are data from single measurement.

Porewater concentrations in the upper centimeter were significantly higher than in the deeper sediments, as measured by DGT. The vertical profiles of  $Zn_{(aq)}$  and  $Cd_{(aq)}$  were characterized by elevated concentrations in the surficial sediments followed by less than  $1 \mu\text{g L}^{-1}$  concentrations in the deeper anoxic sediments. The measured  $Zn_{(aq)}$  concentrations at the surficial sediments were  $21.4 \mu\text{g L}^{-1}$ ,  $21.1 \mu\text{g L}^{-1}$ ,  $22.7 \mu\text{g L}^{-1}$  and

30.4  $\mu\text{g L}^{-1}$  for control, salt, fresh and cycling microcosms which were close to the overlying water  $\text{Zn}_{(\text{aq})}$  concentrations except for the control. The  $\text{Cd}_{(\text{aq})}$  concentrations at the surficial sediments were 19.6  $\mu\text{g L}^{-1}$ , 52.3  $\mu\text{g L}^{-1}$ , 139.8  $\mu\text{g L}^{-1}$  and 110.2  $\mu\text{g L}^{-1}$  for control, salt, fresh and cycling conditions, respectively. The  $\text{Cd}_{(\text{aq})}$  concentrations under salt water conditions were significantly lower than the  $\text{Cd}_{(\text{aq})}$  in the overlying water. Porewater  $\text{Fe}^{2+}_{(\text{aq})}$ ,  $\text{Mn}_{(\text{aq})}$ , DOC, pH,  $\text{Cl}^-$  and  $\text{SO}_4^{2-}$  concentrations were also measured and are shown in APPENDIX B and will be discussed in Chapter 5.

#### 4.4 CONCLUSIONS

$\text{Cd}_{(\text{aq})}$ ,  $\text{Zn}_{(\text{aq})}$ , and  $\text{Mn}_{(\text{aq})}$  release behavior to the overlying water and subsequent metals distribution in both porewater and solid phase were investigated with  $\text{CdS}_{(\text{s})}$  spiked Anacostia River sediment (Washington, D.C.) under control (high pH, low salinity), fresh (low pH, low salinity), salt (high pH, high salinity) and cycling (alternating fresh and salt water) water conditions. Complexation with anions and competition with cations in salt water were the most important release mechanisms for total Cd and Mn, respectively, while pH was the most important factor for total dissolved  $\text{Zn}_{(\text{aq})}$  release. pH was the controlling factor for the freely dissolved concentration of metals, such as  $\text{Zn}^{2+}$  and  $\text{Cd}^{2+}$ , released from the sediments and both pH and salinity dominated  $\text{Mn}^{2+}$  release. The release patterns of metals were all different depending upon their initial conditions. Total dissolved  $\text{Zn}_{(\text{aq})}$  release behavior was characterized by a steady flux from large pool of exchangeable phase and total dissolved  $\text{Cd}_{(\text{aq})}$  release was described by initial small release approaching a plateau gradually due to slow oxidation of  $\text{CdS}_{(\text{s})}$ . A sharp increase followed by immediate decrease was observed for total Mn possibly depleting the pool of Mn at the surficial sediment. Iron release was not

significant compared to its porewater concentrations due to fast  $\text{Fe}^{2+}$  oxidation at the surficial sediments. Based on AVS/SEM model, the sediments were considered to be nontoxic except possibly very near the sediment-water interface. Elevated  $\text{Zn}_{(\text{aq})}$  and  $\text{Cd}_{(\text{aq})}$  concentrations were detected in the surficial sediment (<2 cm) via DGT further supporting this conclusion.

## Chapter 5: Modeling Investigation of pH and Salinity Effects on Metals Release and Sediment Early Diagenesis

### 5.1 INTRODUCTION

Recent studies have showed that freely dissolved metals ( $M^{2+}$ ) are better indicators of metals toxicity and bioavailability than total metals loading in soils or sediments (Lofts et al., 2004). Hence, the toxicity or bioavailability of heavy metals has been estimated by the ratio of acid volatile sulfide (AVS) to simultaneously extracted metals (SEM) (Di Toro et al., 1990). Metals availability is also affected by complexation by anions and organic matter in the porewater as well as solid phase organic carbon (Mahony et al., 1996). Surficial sediments, however, are generally in contact with aerobic overlying water, which can lead to rapid oxidation of AVS (within 6 hours under aerobic conditions, Simpson et al., 2000) and limiting the applicability of the AVS/SEM approach (Chapman et al., 1999).

The depth of partially oxidized sediments depends on site characteristics, such as bioturbation (Boudreau, 1997) and tidal flow in coastal areas (Robert et al., 2004; Audry et al., 2006), which enhance oxygen diffusion, but is typically limited to centimeters in fine grained sediment deposits. The surficial sediments are usually characterized by sharp gradients of redox sensitive species and pH due to the mineralization of labile organic matter and the oxidation of reducing byproducts such as  $NH_4^+$ ,  $Mn^{2+}$ ,  $Fe^{2+}$  and  $FeS_{(s)}$  (Cai et al., 2002). The chemical gradients affect metal sorption-desorption and precipitation-dissolution behavior significantly (Stumm and Morgan, 1996) which are also often complicated by complexation reactions with inorganic ligands and DOM

(dissolved organic matter) as well as competition with alkaline earth metals such as  $\text{Ca}^{2+}$  and  $\text{Mg}^{2+}$  (Chapman et al., 1999; Turner et al., 2004).

Due to the complex interactions between metals and sediments, there have been many biogeochemical models to better understand factors affecting metal speciation. Steady state models (Wang and Van Cappellen, 1996; Canavan et al., 2007) or transient models (Smith and Jaffé, 1998; Carbonaro et al., 2005; Sevinç Şengör et al., 2007) have been used to understand the effect of biogeochemical processes on heavy metals behaviors in sediments. Due to the importance of pH in sediments (Soetaert et al., 2007), models for pH have been developed to estimate and understand the effect of biogeochemical processes on porewater pH distributions (Boudreau, 1987; Boudreau, 1991; Jourabchi et al., 2005; Zeebe, 2007). However, none of the models have generally been tested and used to predict heavy metal behavior in sediments exposed to dynamic environments, i.e. estuary where seasonal and/or daily fluctuations of oxygen, pH, salinity and DOC are observed at the sediment-water interface (Cai and Wang, 1998; Ringwood and Keppler, 2002; Atkinson et al., 2007).

The purpose of this research is to develop a better quantitative model of heavy metal speciation in sediments under dynamic environments where pH and salinity are subject to dynamic changes. A mathematical model is developed to simulate biogeochemical reactions, transient pH and salinity gradients in sediment porewater as well as metal-sediments interactions. The model is tested with experimental results of the effects of pH and salinity on metal distribution in sediments and an overlying water column. The experiments to which the model was calibrated and compared are described in Chapter 4. The model is then used to predict the behavior of metals in estuarine dynamics believed to be representative of those that might be observed in the natural

environment. The model can be employed as a predictive tool for the management of metal contaminated sediments.

## 5.2 MATHEMATICAL MODELING

For the purpose of constructing a conceptual model, the sediment is divided into an overlying water, an oxic layer and an anoxic layer. In the anoxic layer,  $\text{NO}_3^-$ ,  $\text{MnO}_{2(s)}$ ,  $\text{FeOOH}_{(s)}$ , and  $\text{SO}_4^{2-}$  are reduced to  $\text{N}_{2(g)}$ ,  $\text{Mn}^{2+}$ ,  $\text{Fe}^{2+}$  and  $\text{HS}^-$ , respectively when bacteria decompose organic matter. The reduced sulfide is precipitated as either  $\text{FeS}_{(s)}$  or  $\text{MS}_{(s)}$ , where M represents a heavy metal contaminant, depending on their solubility. The reduced aqueous species ( $\text{NH}_4^+$ ,  $\text{Fe}^{2+}$ ,  $\text{HS}^-$ ) are transported by advection and molecular diffusion while solid species, such as  $\text{FeS}_{(s)}$ ,  $\text{MS}_{(s)}$ , and organic/oxides bound metals are transported only by bioturbation simulated as a diffusion-like sediment reworking process. In the aerobic layer, metal sulfides and other reduced species are oxidized producing acidity and releasing metals into the aqueous phase. The released metals are transferred to the either overlying water or anoxic sediments depending on concentration gradients although most of the metals are rapidly scavenged by organics and oxides. The overlying water column is modeled as a completely mixed reactor considering advective mass flux in the influent and effluent as well as the diffusive mass flux between sediment and overlying water. It is assumed that the mass transfer is limited by sediment side diffusion.

### 5.2.1 Governing Equation

In driving the mass balance equations, one-dimensional vertical transport of redox species is assumed by adopting the sediment-water interface as the origin (Berner, 1980). The redox species can be transported in pore water by advection and diffusion and they

also can be carried by solid phase mixing via bioturbation, here modeled as a diffusion-like process (Carbonaro et al., 2005). The oxidation, reduction, precipitation, and dissolution are included in the reaction term (R) and the adsorption, desorption and complexation of species are included in the equilibrium term (E). The general mathematical equation is

$$\frac{\partial[C_{i,b}]}{\partial t} = \frac{\partial}{\partial z} \left( -v_{i,w} \Phi [C_{i,w}] + D_{i,w} \Phi \frac{\partial[C_{i,w}]}{\partial z} + D_{i,s} \rho_s \frac{\partial[C_{i,s}]}{\partial z} \right) + \sum (R_i + E_i) \quad (5.1)$$

where  $i$  is species representative,  $[C_{i,b}]$  is concentration of species  $i$  in bulk sediment [ $\text{mol L}^{-3}$ ],  $[C_{i,w}]$  is concentration of species  $i$  in pore water [ $\text{mol L}^{-3}$ ],  $[C_{i,s}]$  is concentration of species  $i$  in solid phase [ $\text{mol M}^{-1}$ ],  $v_{i,w}$  is Darcy velocity in pore water [ $\text{L T}^{-1}$ ],  $D_{i,w}$  is diffusion coefficient of species  $i$  in porewater [ $\text{L}^2 \text{T}^{-1}$ ],  $D_{i,s}$  is diffusion coefficient of species  $i$  in solid species [ $\text{L}^2 \text{T}^{-1}$ ],  $\Phi$  is porosity [-],  $\rho_s$  is dry sediment density [ $\text{M L}^{-3}$ ],  $R_i$  is diagenetic kinetic reactions related with species  $i$  [ $\text{mol L}^3 \text{T}^{-1}$ ] and  $E_i$  is equilibrium sorption and complexation with inorganic ligands affecting phase distribution of species  $i$  [ $\text{mol L}^3 \text{T}^{-1}$ ]. Note that for comparison to the experimental system, there is no bioturbation or other mechanism for sediment reworking.

The porewater diffusion coefficient of species  $i$  in fine grained sediment is described by the model of Boudreau (1997) where the effective diffusion coefficient is equal to the molecular diffusion coefficient in infinite dilution divided by a hindrance parameter due to tortuosity. The effective diffusion coefficient is as follows

$$D_{i,pw} = \frac{D_{i,aq}}{1 - \ln(\Phi^2)} \quad (5.2)$$

where  $D_{i,aq}$  is the molecular diffusivities of ions in dilute aqueous solution [ $\text{L}^2 \text{T}^{-1}$ ]. Effect of salinity on trace metals diffusion has not been considered due to minor effect (Li and

Gregory, 1974); however, the effect of temperature on ions diffusivity is corrected by following equation (Zhang and Davison, 1995)

$$\text{Log } D_T = \frac{\{1.37 \times (T - 25) + 8.36 \times 10^{-4} \times (T - 25)^2\}}{(109 + T)} + \text{Log} \left( D_{25} \times \frac{(273 + T)}{298} \right) \quad (5.3)$$

where  $D_T$  and  $D_{25}$  are the diffusivity of an ion at  $T^\circ\text{C}$  and  $25^\circ\text{C}$  [ $\text{L}^2 \text{T}^{-1}$ ]. The model assumes that bioturbation, a transport mechanism due to benthic organism activities at the surficial sediments, is described by a quasi-diffusive process. The diffusion coefficient of species  $i$  associated with particles is assumed to decrease exponentially in depth and change with respect to temperature by Arrhenius relationship using  $\theta$  approximation (Di Toro, 2001). The overall equation is

$$D_{i,s}(z) = D_{i,s} \theta_D^{(T-20)} e^{-z/z_{D_{i,s}}} \quad (5.4)$$

where  $D_{i,s}(z)$  is depth dependent diffusion coefficient of particles that associate species  $i$  [ $\text{L}^2 \text{T}^{-1}$ ],  $D_{i,s}$  is the diffusivity of particles that associate species  $i$  [ $\text{L}^2 \text{T}^{-1}$ ],  $z_{D_{i,s}}$  is the particle mixing depth of species  $i$  [L] which was 8 cm in this experiment, and  $\theta_D$  is temperature coefficient [-] which was set to 1.117 (Di Toro., 2001). The diffusion processes only consider physical and chemical diffusion of species  $i$ .

In sediments, microorganisms utilize organic matter to obtain energy (catabolism) and to synthesize cellular components (anabolism). The microorganism will initially utilize oxygen ( $\text{O}_2$ ) to metabolize organic matter. If dissolved  $\text{O}_2$  becomes sufficiently depleted by the aerobes, further organic decomposition continues by utilizing  $\text{NO}_3^-$ ,  $\text{MnO}_2$ ,  $\text{FeOOH}$  and  $\text{SO}_4^{2-}$  as electron acceptors according to the maximum energy yield and availability of the oxidants. These biogeochemical reactions are called primary redox reactions (Cai et al., 2002) and are shown in Table 5.1.

Table 5.1 Reactions in sediments

Primary Redox Reactions
$O.C.^{(a)} + 1.2O_2 \rightarrow HCO_3^- + 1.1H^+ + 0.1NO_3^- + 0.01HPO_4^{2-} + 0.1H_2O$
$O.C. + 0.86NO_3^- \rightarrow 0.48N_2 + HCO_3^- + 0.16H^+ + 0.01HPO_4^{2-} + 0.58H_2O$
$O.C. + 2.0MnO_2 + 2.98H^+ \rightarrow 2.0Mn^{2+} + HCO_3^- + 0.1NH_3 + 0.01HPO_4^{2-} + 2.0H_2O$
$O.C. + 4FeOOH_{(s)} + 6.98H^+ \rightarrow 4Fe^{2+} + HCO_3^- + 0.1NH_3 + 0.01HPO_4^{2-} + 6.0H_2O$
$O.C. + 0.5SO_4^{2-} \rightarrow 0.5HS^- + HCO_3^- + 0.52H^+ + 0.1NH_3 + 0.01HPO_4^{2-}$
Secondary Redox Reactions and Precipitation/Dissolution Reactions
$Fe^{2+} + 0.25O_2 + 1.5H_2O \rightarrow FeOOH_{(s)} + 2H^+$
$HS^- + 2.0O_2 \rightarrow H^+ + SO_4^{2-}$
$MeS_{(s)}^{(b)} + 2.0O_2 \rightarrow Me^{2+} + SO_4^{2-}$
$NH_4^+ + 2.0O_2 \rightarrow NO_3^- + 2.0H^+ + H_2O$
$CH_4 + 2.0O_2 \rightarrow CO_2 + 2.0H_2O$
$^{(b)}MeS_{(s)} + H^+ \leftrightarrow Me^{2+} + HS^-$
$^{(c)}MeCO_{3(s)} \leftrightarrow Me^{2+} + CO_3^{2-}$

(a) O.C. :  $(CH_2O)(NH_3)_{0.1}(H_3PO_4)_{0.01}$

(b) Me :  $Fe^{2+}, Mn^{2+}, Cd^{2+}, Zn^{2+}$

(c) Me :  $Ca^{2+}, Mg^{2+}, Fe^{2+}$

The rate expression for primary redox reactions is assumed to be a Monod-type expression as follows (Choi et al., 2006)

$$R = \alpha \chi_{EA} k_{EA} \left( \frac{[C_{ED}]}{[C_{ED}] + K_{ED}} \right) \left( \frac{[C_{EA}]}{[C_{EA}] + K_{EA}} \right) \quad (5.5)$$

where  $R$  is the degradation rate of an electron donor (O.C.) and acceptor [ $\text{mol L}^{-3} \text{T}^{-1}$ ],  $\alpha$  is a stoichiometric coefficient relating consumptions of electron donor and acceptors as well as productions of reduced species that are shown in Table 5.1,  $\chi_{EA}$  is an indicator coefficient (equals to 1 when the electron acceptor is being utilized and 0 when it is not),  $k_{EA}$  is the maximum substrate utilization rate [ $\text{mol L}^{-3} \text{T}^{-1}$ ],  $[C_{ED}]$  and  $[C_{EA}]$  are the electron donor (organic matter) and the electron acceptor concentrations [ $\text{mol L}^{-3}$ ]

respectively,  $K_{ED}$  and  $K_{EA}$  is the half saturation coefficient for organic matter and electron acceptor [ $\text{mol L}^{-3}$ ] respectively. It is assumed that bacteria utilize only one electron acceptor which is energetically the most favorable in a mixed electron acceptors environment. However, once the most energy yielding electron acceptor concentration drops below a threshold concentration, the next available electron acceptor which may yield the highest energy in the given environment will be metabolized by bacteria.

After this sequential oxidation of organic carbon, several reduced species, such as  $\text{NH}_4^+$ ,  $\text{Mn}^{2+}$ ,  $\text{Fe}^{2+}$  and  $\text{HS}^-$  are produced and transported to aerobic layer. The reduced species are oxidized by various species, including oxygen, manganese oxide and iron oxide and these oxidation reactions are called secondary redox reactions (Cai et al., 2002). They are summarized in Table 5.1 as well and the rate expression is

$$R = k_{rd,ox} [C_{rd}] [C_{ox}] \quad (5.6)$$

where  $R$  is the degradation rate of reductant and oxidant [ $\text{mol L}^{-3} \text{T}^{-1}$ ] which are stoichiometrically related,  $k_{rd,ox}$  is the second order rate coefficient [ $\text{L}^3 \text{mol}^{-1} \text{T}^{-1}$ ],  $[C_{rd}]$  and  $[C_{ox}]$  is the reductant and oxidant concentrations [ $\text{mol L}^{-3}$ ] respectively. The ferrous iron is oxidized in aqueous phase by the following base catalyzed reaction

$$\frac{d[Fe^{2+}]}{dt} = -k_{Fe^{2+}} [OH^-] [Fe^{2+}] [O_{2(aq)}] \quad (5.7)$$

where  $[Fe^{2+}]$  is aqueous and solid phase  $\text{Fe}^{2+}$  concentration [ $\text{mol L}^{-3}$ ],  $[OH^-]$  and  $[O_{2(aq)}]$  are aqueous phase hydroxide and oxygen concentrations [ $\text{mol L}^{-3}$ ],  $k_{Fe^{2+}}$  is the rate constant [ $\text{mol}^{-2} \text{L}^6 \text{T}^{-1}$ ]. Only the neutral and high pH form of Equation 3.2 is employed here consistent with the pH measurements in this system. Metals precipitate with sulfide to form metal sulfides shown in Table 5.1. To model this precipitation, the degree of saturation is defined and the dissolution/precipitation rate is calculated as follows (Şengör et al., 2007)

$$R_i = k_{MS} \{Me^{2+}\} \{HS^-\} \frac{SI}{|SI| + 0.5}, \quad SI = \log \left( \frac{\{Me^{2+}\} \{HS^-\}}{K_{sp,MeS}} \right) \quad (5.8)$$

where  $SI$  is the saturation index,  $\{Me^{2+}\}$  is the dissolved metals concentrations, such as Fe, Mn, Cd, Zn [M],  $\{HS^-\}$  is the bisulfide concentration [ $\text{mol L}^{-3}$ ],  $K_{sp,MS}$  is the solubility product of metal sulfides [ $\text{mol}^2 \text{L}^{-6}$ ],  $k_{MS}$  is the precipitation/dissolution rate [ $\text{mol L}^{-3} \text{T}^{-1}$ ]. The calculated rates are incorporated into the governing mass balance equation considering stoichiometric change of the species by the reactions.

$\text{CaCO}_{3(s)}$ ,  $\text{MgCO}_{3(s)}$ ,  $\text{FeCO}_{3(s)}$  are known to control and buffer the porewater pH in sediment from geochemical reactions (Zeebe, 2007; Chapter 3) as follows (Archer et al., 1998)

$$\Omega = \frac{\{Me^{2+}\} \{CO_3^{2-}\}}{K_{sp,MeCO_3}} \quad (5.9)$$

$$\frac{d[MeCO_3]}{dt} = k_{MeCO_3,precip} (\Omega - 1) \quad \text{if } \Omega > 1 \quad (5.10)$$

$$\frac{d[MeCO_3]}{dt} = k_{MeCO_3,diss} [CaCO_3] (1 - \Omega)^{4.5} \quad \text{if } \Omega > 1 \quad (5.11)$$

where  $\Omega$  is the degree of saturation,  $k_{MeCO_3,precip}$  and  $k_{MeCO_3,diss}$  are the precipitation rate [ $\text{mol L}^{-3} \text{T}^{-1}$ ] and dissolution rate [ $\text{T}^{-1}$ ] of  $\text{MeCO}_{3(s)}$ ,  $K_{sp,MeCO_3}$  is the  $\text{MeCO}_{3(s)}$  solubility products,  $\{Me^{2+}\}$  are the activities of dissolved metals, such as  $\text{Ca}^{2+}$ ,  $\text{Mg}^{2+}$ , and  $\text{Fe}^{2+}$  [ $\text{mol L}^{-3}$ ], and  $\{CO_3^{2-}\}$  is the activity of carbonate [ $\text{mol L}^{-3}$ ]. Once the carbonate is dissolved from the sediment, it will be redistributed to bicarbonate and carbonic acid by consuming protons to meet the equilibrium relations. These acid base reactions are assumed to be in equilibrium each other all the time because those reactions are relatively fast compared to the oxidation of reduced species or dissolution of minerals (Zeebe, 2007).

The Davies equation was used to correct the activity of monoprotic and biprotic dissolved ionic species as follows (Stumm and Morgan, 1996)

$$\log \gamma_{monoprotic} = \left( -\frac{0.509I^{0.5}}{1+I^{0.5}} + 0.15I \right) \quad (5.12)$$

$$\log \gamma_{biprotic} = 4 \left( -\frac{0.509I^{0.5}}{1+I^{0.5}} + 0.15I \right) \quad (5.13)$$

$$I = 0.5 * \sum_i (C_i Z_i^2) \quad (5.14)$$

where  $\gamma$  represents activity coefficient [-],  $I$  represents ionic strength [-],  $C$  is the concentration of ionic species and  $Z$  is the charge of the ionic species.

The calculation of flux to the overlying water was calculated as described in Chapter 4 (Section 4.2.6). AVS and SEM calculations were shown in Chapter 4 (Section 3.3.4). pH changes and the modeling of metal complexation were modeled as described in Chapter 3 (Section 3.3.2 and 3.3.3).

## 5.2.2 Electrostatic interactions on metals sorption

In the current application, the assumption of negligible electrostatic interactions is more problematic because of the near neutral pH. The potential effect of the neglect of electrostatic interactions was assessed by examining their maximum influence. The total surface charge for humic acid is 4.95 meq/g humics and for iron oxide is 8.33  $\mu\text{mol}/\text{m}^2$  oxide (Lofts and Tipping, 1998). These charges will partially offset and, in addition, will be offset by the ionic strength of the interstitial water. The modification of partitioning due to electrostatics is modeled as

$$\frac{[\equiv SOM^+]\{H^+\}}{[\equiv SOH]\{M^{2+}\}} = K_{int,ox} \exp(-2w_{ox}Z_{ox}) \quad (5.15)$$

$$w_{ox} = P_{ox} \log_{10} I \quad (5.16)$$

for oxide surfaces where  $P_{ox} = -1.46E-6 \text{ m}^2\text{oxide}/\text{eq}$  (Lofts and Tipping, 1998), and,

$$\frac{[\equiv OCM^+]}{[\equiv OC^-]\{M^{2+}\}} = K_{int,oc} \exp(-2w_{oc}Z_{oc}) \quad (5.17)$$

$$w_{oc} = P_{oc} \log_{10} I \quad (5.18)$$

for humic surfaces where  $P_{oc} = -330 \text{ g humic / eq}$  (Tipping, 1998).

The neglect of electrostatic effects is effectively the assumption that the exponential term is near unity. The exponential term at various ionic strengths and net surface charges are shown below considering the entire potential range of surface charges (i.e. not the net charge which is likely to be much less in absolute magnitude ).

Table 5.2 The effect of surface charge and ionic strength on ‘exp(-2wZ)’ which modifies the strength of sorption to oxides and organics.

		I (ionic strength)			
		0.001	0.01	0.1	0.6
$Z_{ox}$ (eq/m <sup>2</sup> oxide)	-8.33E-06	1	1	1	1
	-4.17E-06	1	1	1	1
	-2.08E-06	1	1	1	1
	2.08E-06	1	1	1	1
	4.17E-06	1	1	1	1
	8.33E-06	1	1	1	1
$Z_{oc}$ (eq/g humics)	0	1	1	1	1
	-0.001	7	4	2	1
	-0.002	52	14	4	1
	-0.003	380	52	7	2
	-0.004	2752	196	14	2
	-0.005	19930	735	27	2

As indicated in the table, the neglect of electrostatic effects is appropriate at high ionic strength and low surface charge which is likely to be the case at low pH. If the net charge at the surface is high and ionic strength is low, however, this assumption breaks down. For better approximation at high surface charge and low ionic strength, electrostatic effects must be included.

### 5.2.3 Grid Generation and Solution Technique

Slow oxygen diffusion followed by large gradients in redox sensitive species was expected in the surficial sediments. To decrease any possible numerical errors around the thin aerobic layer, an uneven spatial grid was generated. The governing equations were discretized to a set of ordinary differential equations (ODEs) by the ‘Method of Lines’ in uneven spatial grid using central differencing scheme as follows (Boudreau, 1997)

$$\begin{aligned} \frac{\partial [C_{i,b}]_j}{\partial t} = & D_{i,w} \Phi \left( \frac{2[C_{i,w}]_{j-1}}{\Delta x_j (\Delta x_j + \Delta x_{j+1})} - \frac{2[C_{i,w}]_j}{\Delta x_j \Delta x_{j+1}} + \frac{2[C_{i,w}]_{j+1}}{\Delta x_{j+1} (\Delta x_j + \Delta x_{j+1})} \right) \\ & + D_{i,s} \rho_s \left( \frac{2[C_{i,s}]_{j-1}}{\Delta x_j (\Delta x_j + \Delta x_{j+1})} - \frac{2[C_{i,s}]_j}{\Delta x_j \Delta x_{j+1}} + \frac{2[C_{i,s}]_{j+1}}{\Delta x_{j+1} (\Delta x_j + \Delta x_{j+1})} \right) \quad (5.19) \\ & + \sum (R_i + E_i)_j \end{aligned}$$

where  $j$  is the  $j^{th}$  node in uneven spatial grid,  $\Delta x_j$  is the length of  $j^{th}$  grid. It was assumed that porosity and diffusion coefficients are homogeneous in each grid. The grid generation and species specific boundary conditions are shown in Figure 5.1.

The set of ODEs were separated with advection, diffusion, reaction and equilibrium terms because they cannot be solved simultaneously due to the coupled equilibrium assumption of heavy metal sorption with kinetic reactions and diffusive transport. The diffusion and reaction terms are first integrated by the ODEs solver (DVODE) with the time step of 0.01 day. The heavy metal aqueous phase concentration would not be in equilibrium with the adsorbed phases after the integration due to diffusion or reaction of metals from diagenesis. Therefore, the metal distributions are solved to calculate the equilibrium partitioning of heavy metals to each phase before integrating the equations for the next time step. The equilibrium metal distribution model is a set of nonlinear algebraic equations at each spatial grid point. Fixed Point Iteration is

used to solve the equations (Burden and Faires, 2005). By repeating this procedure, the governing equation is solved for the time of interest.

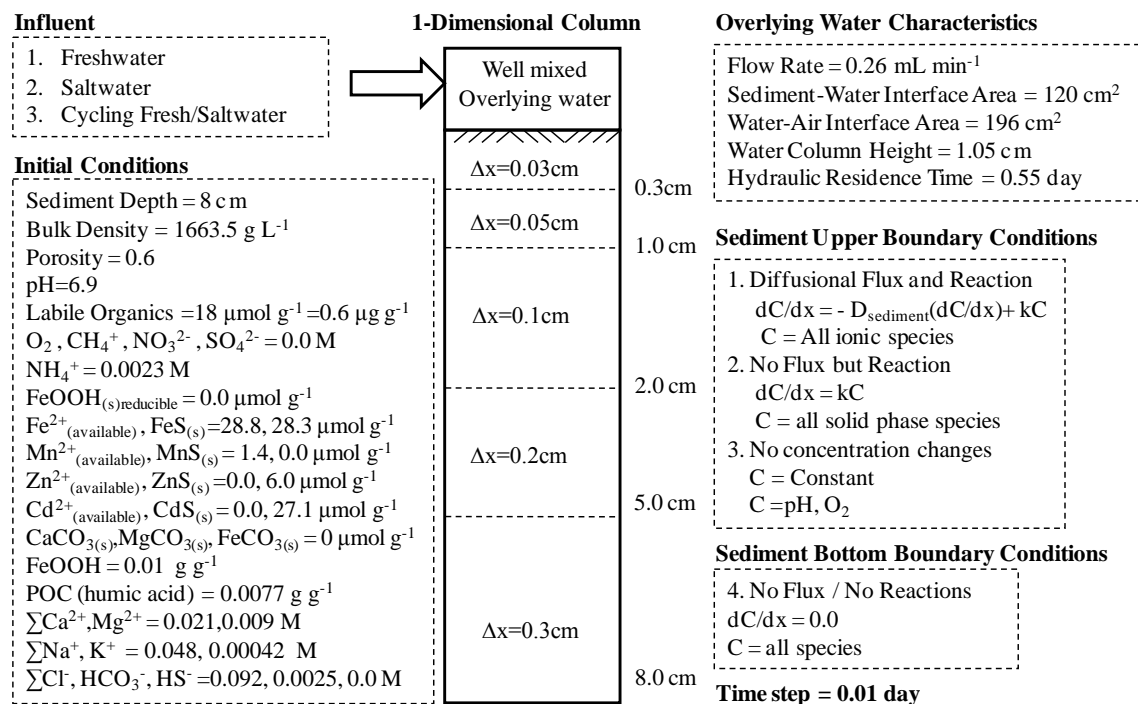


Figure 5.1 Model initial conditions, boundary conditions, uneven grids and overlying water hydraulic conditions. Initial conditions were calculated from measured values using proper extraction and analytical techniques.

## 5.2.4 Model Parameters and Initial Conditions

Biogeochemical reactions in sediments are highly complex so that model parameters have uncertainties (Şengör et al., 2007). However, efforts have been taken to categorize parameters that have high uncertainties and site specificities as well as parameters that should not change significantly from site to site. Parameters for primary redox reactions were considered to be changeable because microbial activities are likely to be site specific. Parameters for secondary redox reactions, metals sorption, and ions

diffusion related parameters were considered to be unchangeable because they are thermodynamic or intrinsic characteristics of chemicals.

Table 5.3 ~ Table 5.6 show parameters for primary redox reactions, secondary redox reactions, metals partitioning, and ions diffusion and their source. The parameters listed in Table 5.3 were collected from references while maximum substrate utilization rate and threshold concentration of sulfate were calibrated with experimental observations for the qualitative model fit. Metal sulfide oxidation rates in Table 5.4 were estimated by fitting the model to experimental data fixing all other parameters due to the lack of reliable data. Model initial conditions and boundary conditions were estimated from measured value and are shown in APPENDIX B. Figure 5.1 suggests model initial conditions and boundary conditions.

Table 5.3 List of parameters for primary redox reactions

	Parameters	Values	Reference
Maximum substrate utilization rate (M day <sup>-1</sup> )	K <sub>O2</sub>	1.1E-4	(a)
	K <sub>NO3-</sub>	4.1E-3	(b)
	K <sub>FeOOH</sub>	8.8E-5	(b)
	K <sub>SO42-</sub>	2.0E-4	Calibrated
Half saturation constant (M)	K <sub>CH2O</sub>	1.0E-4	(a)
	K <sub>O2</sub>	2.0E-5	(b)
	K <sub>NO3-</sub>	2.0E-5	(b)
	K <sub>FeOOH</sub>	2.0E-6	(b)
Threshold concentration (M)	K <sub>SO42-</sub>	1.0E-5	(b)
	O <sub>2</sub> lim	5.0E-7	(b)
	NO <sub>3</sub> <sup>-</sup> lim	6.0E-7	(b)
	FeOOH lim	9.0E-5	(b)
	SO <sub>4</sub> <sup>2-</sup> lim	8.0E-05	Calibrated

(a) Choi et al., 2006, (b) Jaffe et al., 2001

Table 5.4 List of parameters for the reactions in sediments

Parameter	Units	Value	Description	Reference
$k_{\text{FeS},\text{O}_2}$	$\text{M}^{-1} \text{day}^{-1}$	9.9E+4	$\text{FeS}_{(s)}$ oxidation rate	(a)
$k_{\text{MnS},\text{O}_2}$	$\text{M}^{-1} \text{day}^{-1}$	9.9E+4	$\text{MnS}_{(s)}$ oxidation rate	(d)
$k_{\text{Fe}^{2+}}$	4.3E-9	$\text{M day}^{-1}$	$\text{Fe}^{2+}$ oxidation rate ( $5 < \text{pH}$ )	(b)
$k_{\text{ZnS},\text{O}_2}$	$\text{M}^{-1} \text{day}^{-1}$	60.0	$\text{ZnS}_{(s)}$ oxidation rate	Calibrated
$k_{\text{CdS},\text{O}_2}$	$\text{M}^{-1} \text{day}^{-1}$	12.0	$\text{CdS}_{(s)}$ oxidation rate	Calibrated
$k_{\text{HS}^-, \text{O}_2}$	$\text{M}^{-1} \text{day}^{-1}$	4.4E+2	$\text{HS}^-_{(aq)}$ oxidation rate	(c)
$k_{\text{NH}_4^+, \text{O}_2}$	$\text{M}^{-1} \text{day}^{-1}$	1.4E+4	$\text{NH}_4^+_{(aq)}$ oxidation rate	(c)
$k_{\text{S}_0, \text{O}_2}$	$\text{M}^{-1} \text{day}^{-1}$	1.0E+3	$\text{S}_{(s)}^0$ oxidation rate	(d)
$k_{\text{MeCO}_3, \text{dis}}$	$\text{day}^{-1}$	0.25	Carbonate bearing minerals dissolution rate	(d)
$k_{\text{CaCO}_3, \text{pre}}$	$\text{M day}^{-1}$	1.0E-5	Carbonate bearing minerals precipitation rate	(c)
$k_{\text{MeS}}$	$\text{M}^{-1} \text{day}^{-1}$	1.0E+6	$\text{MeS}_{(s)}$ precipitation/dissolution rate	(e)
$K_{\text{SP}, \text{CaCO}_3}$	$\text{M}^2$	4.5E-9	Solubility product of $\text{CaCO}_{3(s)}$	(b)
$K_{\text{MgCO}_3}$	$\text{M}^2$	3.6E-8	Solubility product of $\text{MgCO}_{3(s)}$	(b)
$K_{\text{SP}, \text{FeCO}_3}$	$\text{M}^2$	2.0E-11	Solubility product of $\text{FeCO}_{3(s)}$	(b)
$K_{\text{SP}, \text{FeS}}$	$\text{M}^2$	1.1E-3	Solubility product of $\text{FeS}_{(s)}$	(b)
$K_{\text{SP}, \text{MnS}}$	$\text{M}^2$	1.47	Solubility product of $\text{MnS}_{(s)}$	(b)
$K_{\text{SP}, \text{CdS}}$	$\text{M}^2$	4.4E-15	Solubility product of $\text{CdS}_{(s)}$	(b)
$K_{\text{SP}, \text{ZnS}}$	$\text{M}^2$	1.2E-11	Solubility product of $\text{ZnS}_{(s)}$	(b)
$K_{\text{CO}, \text{a1}}$	M	5.01E-7	Carbonic acid protonation constant	(b)
$K_{\text{CO}, \text{a2}}$	M	5.01E-11	Bicarbonate protonation constant	(b)

(a) Carbonaro et al., 2005 (b) Stumm and Morgan, 1996 (c) Wang and Van Cappellen, 1996 (d) Chapter 3, Resuspension Experiment (e) Sevinc. Sengor et al., 2007

Table 5.5 List of parameters for metal sorption (Lofts and Tipping, 1998; Tipping, 1998)

Parameters	Humic Acid	FeOOH <sub>(s)</sub>	Description
$n_{cb}$ (mmol g <sup>-1</sup> ) <sup>(a)</sup>	3.3	-	Specific site density of carboxylic functional group
$\Gamma_{max}$ (μmol m <sup>-2</sup> )	-	8.33	Site density for oxides
SSA (m <sup>2</sup> g <sup>-1</sup> ) <sup>(b)</sup>	-	600	Oxides specific surface area
pK <sub>cb</sub> (-)	4.1	-	Proton dissociation constant for carboxylic group
pK <sub>ph</sub> (-)	8.8	-	Proton dissociation constant for phenolic group
ΔpK <sub>cb</sub> (-)	2.1	-	Distribution term that modifies pK <sub>cb</sub>
ΔpK <sub>ph</sub> (-)	3.6	-	Distribution term that modifies pK <sub>ph</sub>
pK <sub>ox,a1</sub> (-)	-	6.26	First protonation constant for oxides
pK <sub>ox,a2</sub> (-)	-	9.66	Second protonation constant for oxides
pK <sub>Mg</sub> (-)	-0.7	5.3	Mg <sup>2+</sup> sorption constant
pK <sub>Ca</sub> (-)	-0.7	7.3	Ca <sup>2+</sup> sorption constant
pK <sub>Mn</sub> (-)	-0.6	4.6	Mn <sup>2+</sup> sorption constant
pK <sub>Fe2+</sub> (-)	-1.3	5.78 <sup>(c)</sup>	Fe <sup>2+</sup> sorption constant
pK <sub>Zn</sub> (-)	-1.5	1.8 <sup>(d)</sup>	Zn <sup>2+</sup> sorption constant
pK <sub>Cd</sub> (-)	-1.3	2.0 <sup>(d)</sup>	Cd <sup>2+</sup> sorption constant
ΔpK <sub>Me</sub> (-) <sup>(e)</sup>	-	-1.5	Distribution term that modifies pK <sub>Me</sub> for oxides
ΔLK <sub>1</sub> (-)	2.8	-	Distribution term that modifies pK <sub>Me</sub> for organics

(a) Specific site density of phenolic functional group is calculated by  $0.5 \times n_{cb}$ .

(b) Specific site densities of oxides (mol g<sup>-1</sup>) were calculated by multiplying  $\Gamma_{max}$  by SSA. Total available sorption sites (M) in the system was calculated by multiplying specific site densities (mol g<sup>-1</sup>) by bulk density (g L<sup>-1</sup>).

(c) Estimated from the equilibrium constant for the first hydrolysis reactions of Fe<sup>2+</sup>.

(d) Modified with ΔpK<sub>Me</sub> to describe strong Zn and Cd sorption to 9 % of total sorption site.

(e) Me stands for Zn and Cd.

Table 5.6 The diffusivity of ions at infinite dilution (Handbook of chemicals, CRC)

Species	25 °C	20 °C	Unit
O <sub>2</sub> , Ca <sup>2+</sup> , K <sup>+</sup> , Na <sup>+</sup> , NH <sub>4</sub> <sup>+</sup> , CO <sub>2</sub> , HCO <sub>3</sub> <sup>-</sup> , CO <sub>3</sub> <sup>2-</sup> , SO <sub>4</sub> <sup>2-</sup> , NO <sub>3</sub> <sup>-</sup> , H <sub>2</sub> S, S <sup>2-</sup> , HS <sup>-</sup>	1.0 E-4	8.7 E-5	m <sup>2</sup> d <sup>-1</sup>
Cl <sup>-</sup>	1.8 E-4	1.57 E-4	m <sup>2</sup> d <sup>-1</sup>
H <sup>+</sup>	8.0 E-4	6.96 E-4	m <sup>2</sup> d <sup>-1</sup>
Fe <sup>2+</sup> , Mn <sup>2+</sup> , Cd <sup>2+</sup> , Zn <sup>2+</sup>	6.2 E-5	5.4 E-5	m <sup>2</sup> d <sup>-1</sup>

Note : The diffusivity of particles that associate with heavy metals at 25 °C was assumed to be 1.0E<sup>-8</sup> m<sup>2</sup> d<sup>-1</sup> (Carbonaro, 2005). The predicted results were not sensitive to this value.

### 5.3 RESULTS AND DISCUSSION

#### 5.3.1 The Deviation of the Model Fit to Experimental Observations

The deviation of the model fit to experimental observations is calculated from the standard error (SE) divided by the median of experimental observations which were described in 3.4.2. All graphs are shown with SE which can be understood as the uncertainty that the model has in estimating the experimental observations. Table 5.7 summarizes the SE, median and the deviation of the model fit. The table will be used in the later discussion.

Table 5.7 Statistical Analysis of Model Fit

Factors	Units	Freshwater			Cycling water			Saltwater		
		SE	MDN	DMF %	SE	MDN	DMF %	SE	MDN	DMF %
Overlying Water										
pH	$-\log \{H^+\}$	0.22	6.8	3.2	0.3	8.1	3.7	0.18	8.5	2.1
Salinity	$g L^{-1}$	0.23	0.4	57.6	1.7	19.3	9.0	0.80	30.0	2.7
Zn <sub>(aq)</sub>	$\mu g L^{-1}$	16.4	36.0	45.6	9.2	25.5	36.0	10.0	26.7	37.6
Cd <sub>(aq)</sub>	$\mu g L^{-1}$	94.4	207.0	45.6	175	223	78.3	54.9	318	17.3
Mn <sub>(aq)</sub>	$\mu g L^{-1}$	119	144.5	82.0	305	384	79.5	126	510	24.7
Sediment										
pH <sup>(a)</sup>	$-\log \{H^+\}$	0.25	6.7	3.7	0.13	6.7	1.9	0.13	6.8	1.9
pH	$-\log \{H^+\}$	0.25	6.7	3.7	0.19	6.7	2.8	0.40	6.8	5.9
SO <sub>4</sub> <sup>2-</sup> <sub>(aq)</sub>	$\log M$	0.25	-4.3	6.0	0.32	-2.4	13.0	0.28	-1.7	16.4
Cl <sub>(aq)</sub>	$\log M$	0.29	-1.8	15.7	0.22	-0.8	27.4	0.05	-0.3	16.7
AVS	$\mu mol g^{-1}$	16.6	84.6	19.63	16.4	94.1	17.4	18.1	99.8	18.2
SEM	$\mu mol g^{-1}$	2.6	43.4	6.0	1.6	43.6	3.6	2.0	44.2	4.5
Fe <sub>(aq)</sub>	mM	1.07	0.14	770.3	0.32	0.6	52.6	2.2	3.5	64.0
Fe <sub>(aq)</sub> <sup>(b)</sup>	mM		-			-		1.04	3.5	28.7
Mn <sub>(aq)</sub>	mM	0.09	0.01	897.2	0.03	0.04	69.5	0.11	0.17	64.4

(a) Carbonate species diffusion coefficients are increased to fit the experimental observations, (b) Reducible ferric iron is increased to fit the experimental observations. Note : MDN and DMF stand for median and the deviation of model fit respectively. Units for SE and MDN are same as parameters and unit for DMF is %.

### 5.3.2 Sediment-Water Interactions and Sediment Early Diagenesis

Sediments were vertically homogeneous and fully reduced at the beginning of the experiments. Well aerated overlying water oxidized the reduced species in the surficial sediments producing protons and changing pH in sediment porewater. The pH in the overlying water was modeled based upon the water balance. Figure 5.2 (a), (b) and (c) show modeled time dependent pH changes in three different overlying water conditions,

continuous freshwater and saltwater overflow as well as the cycling of fresh and salt water every 8 days.

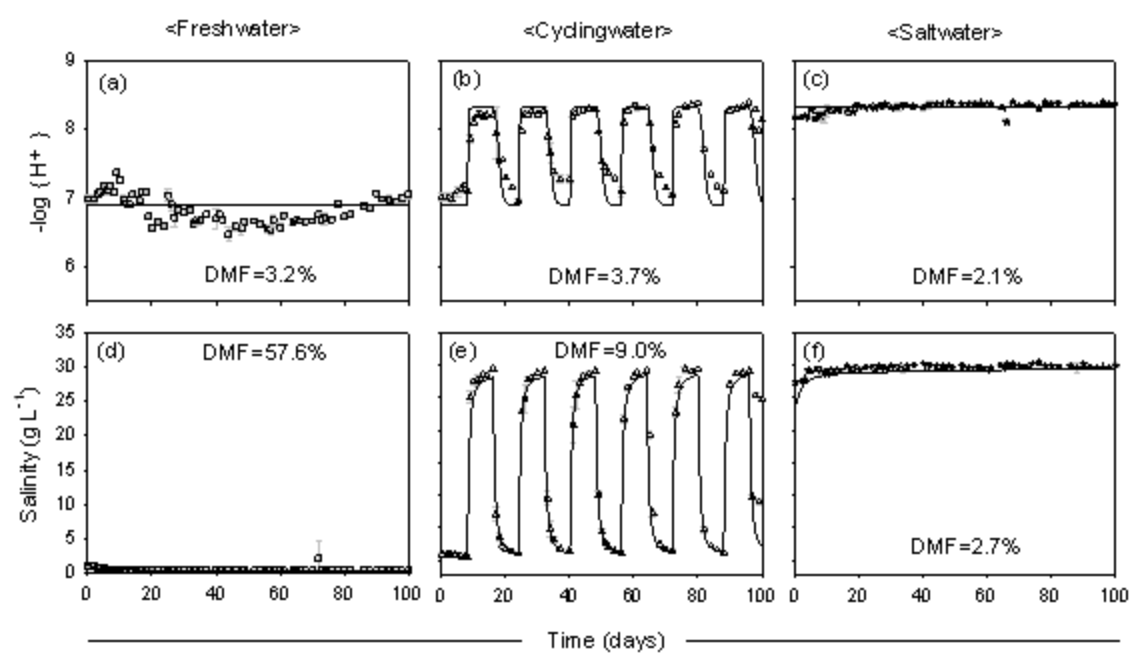


Figure 5.2 Experimental (symbols) and modeling (solid) results of temporal pH (a-c) and salinity (d-f) changes in the effluents for 100 days where fresh and salt waters were continuously pumped and where fresh and cycling waters were cyclically pumped once every 8 days. Symbols and error bars are the mean and standard deviations of duplicated experiments respectively.

The deviations of the model fit were less than 4 % for pH under all overlying water conditions indicating the model followed the measured pH well. Rapid oxidation of reduced species such as  $Fe^{2+}$ ,  $FeS_{(s)}$  and  $S^0_{(s)}$  could have produced significant acidity but seemed to be buffered by sediments and overlying water.

Similar to pH, the model followed the measured salinities very well with standard errors less than  $1.7\ g\ L^{-1}$ . The graphs are shown in Figure 5.2 (d), (e) and (f). The salts' behavior could be described by mixing of salts in the influent and effluent as well as

diffusional salts exchange between sediment and well mixed overlying water. The modeled pH and salinity was considered as a fixed boundary condition for sediments.

Under these pH and salinity conditions, porewater pH and salt concentrations showed different profiles in each microcosm. Figure 5.3 shows measured and modeled chloride concentrations in sediments after 120 days.

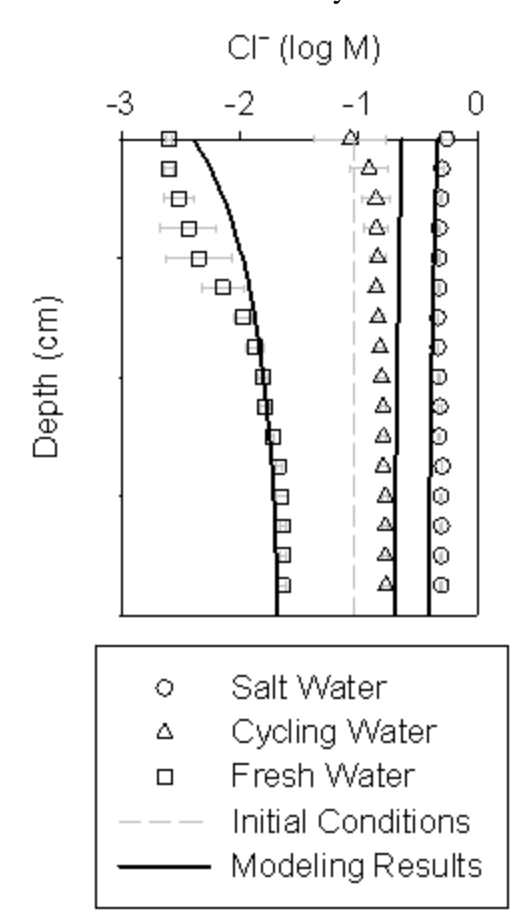


Figure 5.3 Experimental (symbols) and modeling (solid lines) results of vertical profiles of porewater  $\text{Cl}^-$  in fresh, salt, and cycling water after 120 days. Symbols and error bars are the mean and standard deviations of duplicate experiments respectively. DMF are as follow:  $\text{DMF}_{\text{Cl,salt}}=16.7\%$ ,  $\text{DMF}_{\text{Cl,cycling}}=27.4\%$ ,  $\text{DMF}_{\text{Cl,fresh}}=15.7\%$ .

First of all, chloride concentration profiles provide insights into the diffusional ion transport process in the microcosms. Initially, porewater chloride concentration was around  $10^{-1}$ M which was lower than salt water and higher than freshwater. Under freshwater conditions, chloride ions have diffused from the porewater to the overlying water by the concentration gradient and the reverse occurs with saltwater. For the cycling water cell, the chloride concentration at the sediment surface changes in response to the introduced water. In deeper sediment, the chloride concentration approaches the average of freshwater and saltwater chloride concentrations. These transient chloride behaviors in sediment porewater are available in APPENDIX C.

Similar diffusion processes should apply to the sulfate ion although a difference in the profiles would be expected due to the consumption of sulfate by microbial reduction in anoxic sediment. Figure 5.4 shows measured and modeled  $\text{SO}_4^{2-}$  concentrations in sediments after 120 days. Initially,  $4.29 \text{ E-}7 \text{ M}$  sulfate was present in porewater, which was far less than the sulfate concentration in both freshwater and saltwater. Consequently, continuous sulfate diffusion from overlying water to the sediments occurred. Under freshwater conditions, sulfate ions appeared to be reduced to sulfide at depths less than 2 cm. The model results showed an increase in AVS within 2 cm of the surface and effectively constant AVS thereafter, which was also observed experimentally. A thin black layer of sediment approximately 1 cm in thickness, presumably composed of ferrous iron precipitates, was observed below the aerobic layer through the transparent microcosm during experiments, which supports the modeling results (see the pictures in APPENDIX C).

Similar processes were observed in both salt and cycling water microcosms. AVS in both salt and cycling microcosms increased by 15%, which is shown in Figure 5.5 (b)

and (c). However, the sulfate ion concentration in salt water was too high to be affected by sulfate reduction so that linear sulfate ion profile was observed in salt water microcosm. In the cycling cell, surficial sediment's sulfate concentration was similar to the overlying water sulfate concentration while deeper sediment's sulfate concentration was close to fresh water microcosms due to the sulfate loss by sulfate reduction. Time dependent sulfate concentration profiles are available in APPENDIX C as well.

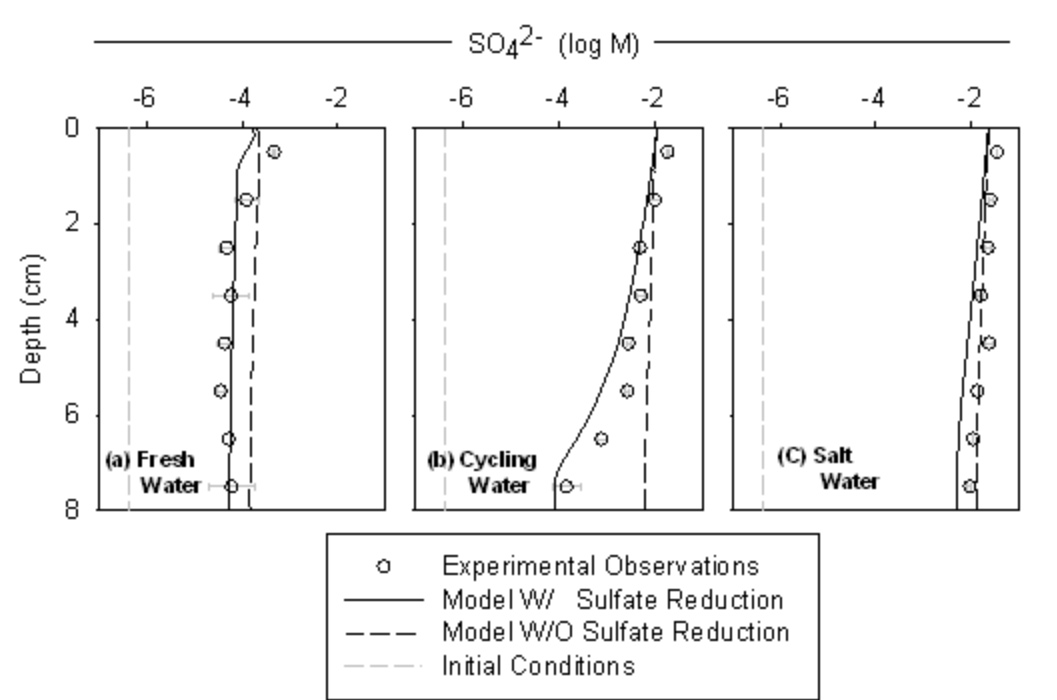


Figure 5.4 Experimental (symbols) and modeling (solid lines) results of vertical profiles of porewater  $\text{SO}_4^{2-}$  under fresh, cycling, and salt water conditions after 120 days. Symbols and error bars are the mean and standard deviations of duplicate experiments respectively. DMF are as follows:  $\text{DMF}_{\text{SO}_4, \text{salt}}=16.4\%$ ,  $\text{DMF}_{\text{SO}_4, \text{cycling}}=13.0\%$ ,  $\text{DMF}_{\text{SO}_4, \text{fresh}}=6.0\%$ . Broken lines are  $\text{SO}_4^{2-}$  profiles without sulfate reductions.

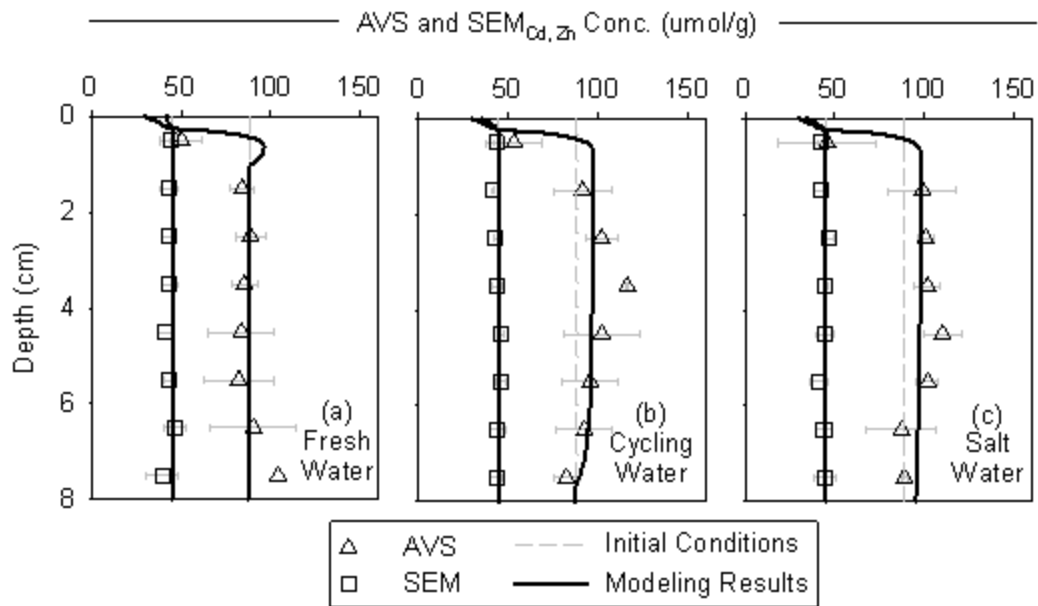


Figure 5.5 Acid volatile sulfide (AVS) and simultaneously extracted metals (SEM) in sediments which are exposed to (a) freshwater, (b) cycling water, and (c) saltwater water for 120 days. Symbols and error bars are the mean and standard deviations of duplicate experiments, respectively. Solid lines are modeling results. Dashed lines are initial conditions. DMF are as follow:  $DMF_{AVS,salt}=18.1\%$ ,  $DMF_{AVS,cycling}=17.4\%$ ,  $DMF_{AVS,fresh}=19.6\%$ ,  $DMF_{SEM,salt}=4.5\%$ ,  $DMF_{SEM,cycling}=3.6\%$ ,  $DMF_{SEM,fresh}=6.0\%$ .

pH profile developments in Figure 5.6 were more complicated than chloride and sulfate because they were controlled by complicated acid base chemistry as well as biogeochemical reactions in sediments. The diffusion coefficient of a proton is almost 4 times greater than that of chloride so that if proton was not affected by other reactions, pH in sediment should remain the same as the pH in the overlying water. However, during the microcosm experiments, pH only changed from the surface to 4cm in sediments and pH in deeper sediments was not different from the initial condition of 6.9.

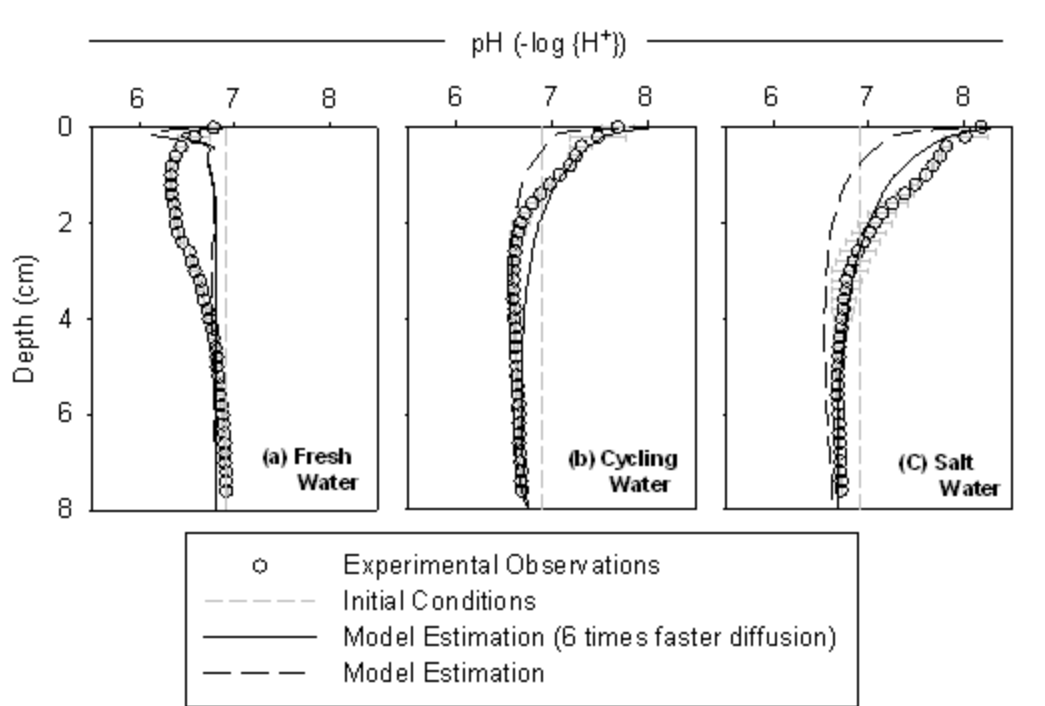


Figure 5.6 Experimental (symbols) and modeling (solid lines) results of vertical profiles of porewater pH in (a) fresh, (b) cycling, and (c) salt water after 120 days. pH was determined by microelectrodes. Symbols and error bars are the mean and standard deviations of duplicate experiments respectively. DMF are as follow:  $DMF_{pH,salt}=1.9\%$ ,  $DMF_{pH,cycling}=1.9\%$ ,  $DMF_{pH,fresh}=3.7\%$ . DMF without correction of diffusion are as follow:  $DMF_{pH,salt}=5.9\%$ ,  $DMF_{pH,cycling}=2.8\%$ ,  $DMF_{pH,fresh}=3.7\%$ .

The pH profiles were initially modeled with the reactions in Table 5.1 as well as proton and carbonate species diffusion from the overlying water. However, modeled pH at the surficial sediments deviated from the experimentally measured pH. The reason for this deviation may be due to the uncertainties in the production of carbonates and protons by the hypothetical reactions in Table 5.1. The organic carbon is assumed to follow Redfield ratio of carbon (106), nitrogen (16), and phosphate (1) which has been considered as the global elemental composition of marine organic matter. The stoichiometric production and consumption of proton and carbonates are strongly

dependent on the organic carbon composition which was highly uncertain in this experiment.

As a result, model predicted pH profiles were fitted to experimental observations by using 6 times faster diffusion coefficients of carbonate. The fitted pH profiles followed the experimental observations well except that pH between 0 and 2 cm under freshwater conditions. This deviation may be the result of other biogeochemical reactions that are not considered in this model as well as the experimental errors. Modeling results of pH dynamics in porewater are available in APPENDIX C.

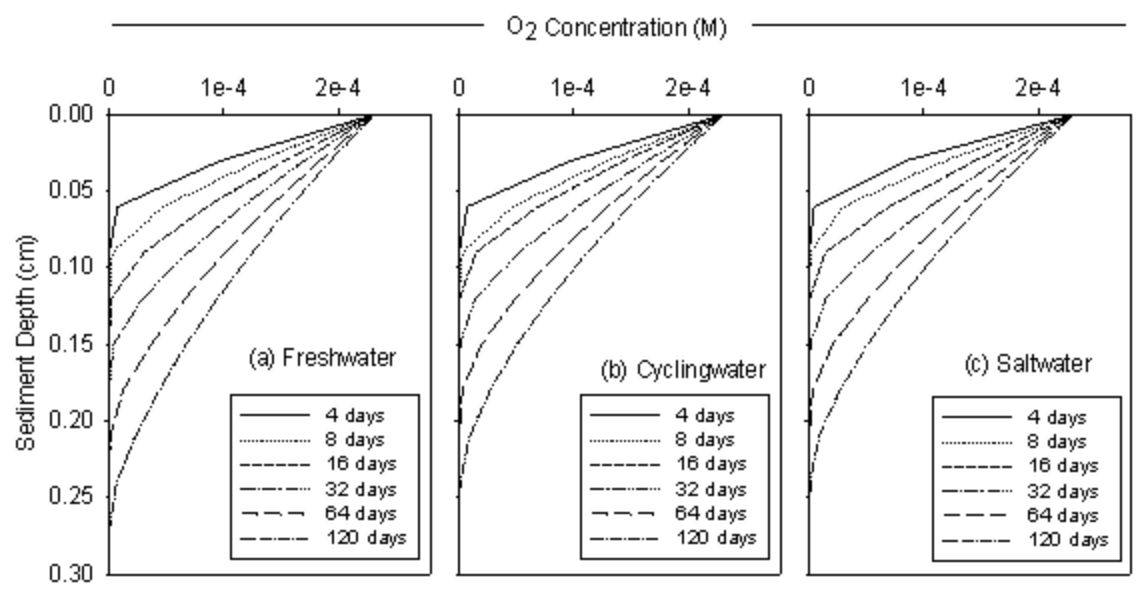


Figure 5.7 Temporal oxygen profile developments at the surficial sediments under (a) freshwater, (b) cycling water, and (c) saltwater.

Under all experimental conditions, a thin aerobic layer (few mm) was observed suggesting rapid oxygen depletion in sediments. Figure 5.7 shows a time dependent thin aerobic layer development, which only extended a few millimeters from the sediment

water interface. The oxygen penetrated slightly deeper with time due to the oxidation of reduced species at the surficial sediments. These thin layers were easily observed by color difference under all experimental conditions. Since this thin layer of aerobic sediments would have the most substantial impact on the metals release into the overlying water, the surficial sediments' pH, which were identical with the overlying water pH, were far more sensitive to metals release than the pH profiles in Figure 5.6. Further discussion is available in the next section.

### 5.3.3 Metals Behavior

Iron, manganese, zinc and cadmium behavior was investigated in both overlying water and sediment porewater.  $Zn^{2+}$  and  $Cd^{2+}$  were believed to be precipitated as metal sulfide due to their low solubility in the presence of AVS while metals such as  $Fe^{2+}$  and  $Mn^{2+}$  were elevated in the porewater due to their abundance and higher solubility. These metals showed different release behaviors depending on their initial conditions, oxidative chemical reactions, competitive sorption to sediment particles, and complexation with anions in overlying water. Moreover, 120 days of sediments exposure to three different overlying waters led to different profiles of metals in sediments. Experimental and modeling results of total dissolved  $Zn_{(aq)}$ ,  $Cd_{(aq)}$  and  $Mn_{(aq)}$  release in the overlying waters are shown in Figure 5.8.

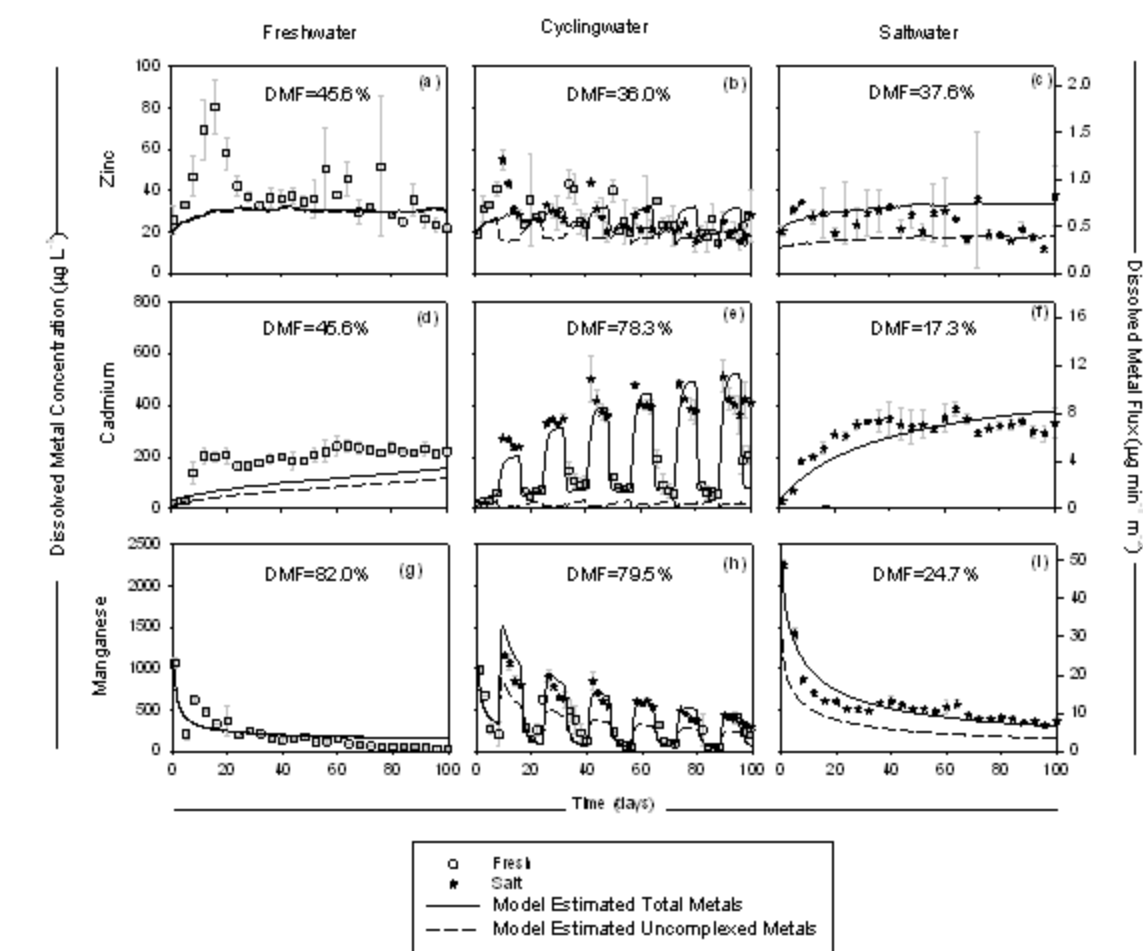


Figure 5.8 Experimental (symbols) and modeling (solid) results of temporal  $\text{Zn}_{(\text{aq})}$  (a-c),  $\text{Cd}_{(\text{aq})}$  (d-f),  $\text{Mn}_{(\text{aq})}$  (g-i) concentrations changes in the effluents for 100 days where fresh and salt waters were continuously pumped and where fresh and cycling waters were cyclically pumped once every 8 days. Symbols and error bars are the mean and standard deviations of duplicate experiments respectively. Broken lines indicate the model estimated uncomplexed metal concentration.

More  $\text{Zn}_{(\text{aq})}$  was released to the freshwater than saltwater although more  $\text{Cd}_{(\text{aq})}$  and  $\text{Mn}_{(\text{aq})}$  were released to saltwater than freshwater in experiments. These contrasting metal dependent release behaviors were captured successfully by the proposed model. Iron oxide controls the metal solubility in the surficial sediments. Release of  $\text{Fe}_{(\text{aq})}$  was

not significant due to rapid oxidation of ferrous iron at the surficial sediments. The modeling results of metals partitioning to sulfide, oxides, organics and aqueous phases are available in APPENDIX C.

From the modeling study, more metals were released under saltwater condition when oxides controlled the metals sorption. The surface charge changes more drastically in oxides than in organics under changes in pH. The iron oxides have two proton association constants and the surface charge changes considerably around the two proton association constants. However, the proton association constants of organics are distributed over a wide range and pH changes between 6.5 and 8 do not alter the surface charge distribution as much as in oxide. As a result, more  $Zn_{(aq)}$  is released under freshwater conditions due to  $Zn_{(aq)}$  desorption from oxides during protonation of the oxides surface. The same reasoning could be applied to  $Cd_{(aq)}$  although the greater Cd complexation with chloride results in a release of more  $Cd_{(aq)}$  under saltwater conditions. The greater  $Mn_{(aq)}$  release under saltwater conditions is likely due to the  $Mn^{2+}$  competition with  $Ca^{2+}$  and  $Mg^{2+}$  for sorption sites. For example,  $Mn^{2+}$  affinity constant to FeOOH is approximately 1 order of magnitude greater than that of  $Mg^{2+}$  but the Mg concentration was many orders of magnitude greater than Mn under salt water conditions. Similar competition of  $Ca^{2+}$  and  $Mg^{2+}$  for  $Cd^{2+}$  and  $Zn^{2+}$  sorption was expected; however, the effect seemed to be negligible because the affinities of  $Cd^{2+}$  and  $Zn^{2+}$  to oxides are many orders of magnitude higher than that of Ca and Mg which are shown in Table 5.5. The model estimated free metals concentrations support these explanations.

In this study, the release of metals to overlying water is controlled by a very thin layer of sediments (2~3 mm) in which oxic conditions apply and for which exchange with the surface is reasonably rapid. Deeper in the sediments, the exchange (diffusion) to

the surface is negligible and the metals are associated with sulfides in the porewater and in the sediment phase. It is important to note, however, that bioturbation by burrowing organisms could create microenvironments that are more oxic and in which metals are more available and potentially toxic.

Porewater  $\text{Fe}_{(\text{aq})}$ ,  $\text{Mn}_{(\text{aq})}$ ,  $\text{Zn}_{(\text{aq})}$  and  $\text{Cd}_{(\text{aq})}$  concentrations were also experimentally characterized and investigated using the mathematical model. The concentrations of  $\text{Fe}_{(\text{aq})}$  and  $\text{Mn}_{(\text{aq})}$  were determined by voltametric microelectrodes in-situ and modeling results are shown in Figure 5.9 (a) ~ (g).

All the profiles followed gradual increase of concentration from the surficial sediments to deeper sediments. Rapid release of  $\text{Mn}_{(\text{aq})}$  followed by slower diffusion from deeper sediments seemed to deplete the Mn at the surficial sediments. No significant release of  $\text{Fe}_{(\text{aq})}$  was observed under all experimental conditions due to the oxidation of  $\text{Fe}^{2+}_{(\text{aq})}$  at the surficial sediments. The overlying water  $\text{Fe}_{(\text{aq})}$  concentrations are available in APPENDIX B. The model-estimated half life of ferrous iron at pH 6.5 ~ 8.0 was  $0.7 \sim 7.0\text{E-}4$  hours which were many orders or magnitude less than the hydraulic residence time (13 hours) suggesting complete oxidation of ferrous iron in the overlying water. Red precipitates, presumably  $\text{FeOOH}_{(\text{s})}$ , were observed at the surficial sediments and modeling results in Figure 5.10 support this explanation. The newly precipitated  $\text{FeOOH}_{(\text{s})}$  were included in  $\text{FeOOH}_{(\text{s})}$  which was active in metals sorption and had increased approximately 100 % sorption sites at the surficial sediments for metals after 120 days.

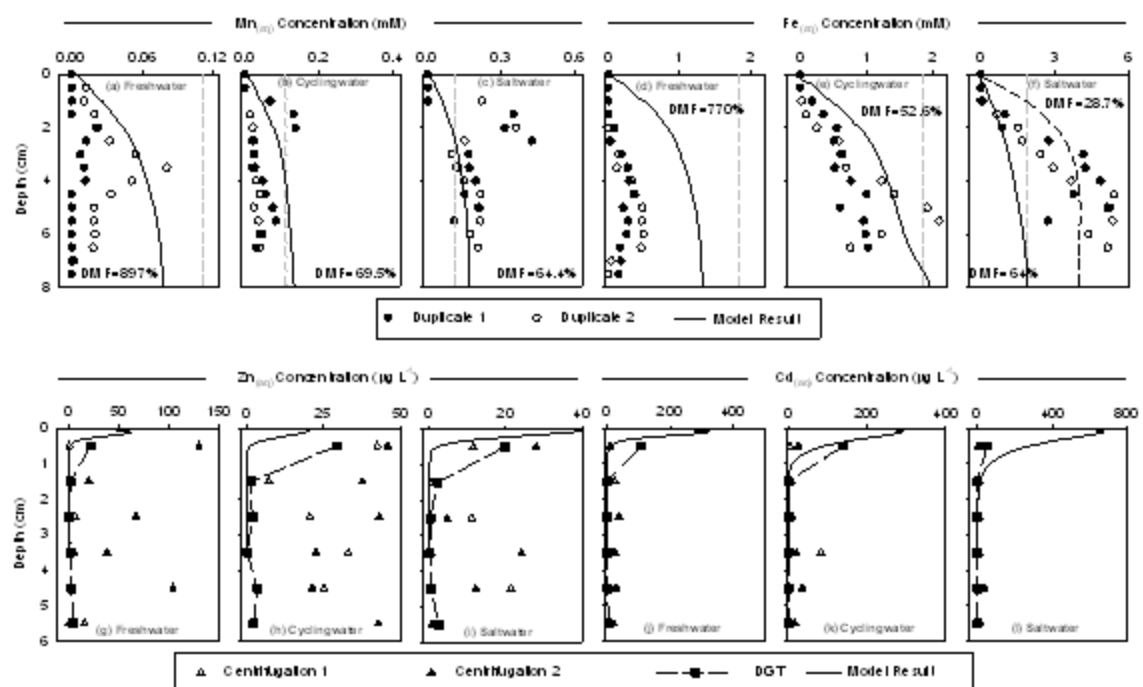


Figure 5.9 Experimental (symbols) and modeling (solid lines) results of vertical profiles of  $Mn_{(aq)}$  (a-c),  $Fe_{(aq)}$  (d-f),  $Zn_{(aq)}$  (g-i) and  $Cd_{(aq)}$  (j-l) in porewater after 120 days sediments exposure to continuous freshwater, saltwater and to alternating freshwater and saltwater once every 8 days.  $Mn_{(aq)}$  and  $Fe_{(aq)}$  were determined from duplicate experiments by voltametric microelectrodes (solid and hollow diamond) in-situ. For the better description of the vertical profiles of  $Fe_{(aq)}$  (dashed line) under salt water condition,  $18.0 \mu\text{mol/g}$  of reducible iron was assumed to present. Two independent methods, DGT (single measurement, square with dashed line) and centrifugation/filtration (duplicate measurements, solid and hollow triangles), were used to determine porewater Zn and Cd concentrations.

The measured  $Fe_{(aq)}$  and  $Mn_{(aq)}$  concentrations in the deeper sediments were very contrasting under different overlying water conditions. The measured  $Fe_{(aq)}$  concentration was between  $0.2 \sim 0.5 \text{ mM}$  at depth of 5 cm while  $1.0 \sim 2.0 \text{ mM}$  and  $3.0 \sim 5 \text{ mM}$  of  $Fe_{(aq)}$  were detected under cycling and saltwater conditions, respectively. Millimolar level of ferrous iron concentrations have often been observed in the porewater of estuarine sediments and salt water sediments (Burton et al., 2006b).

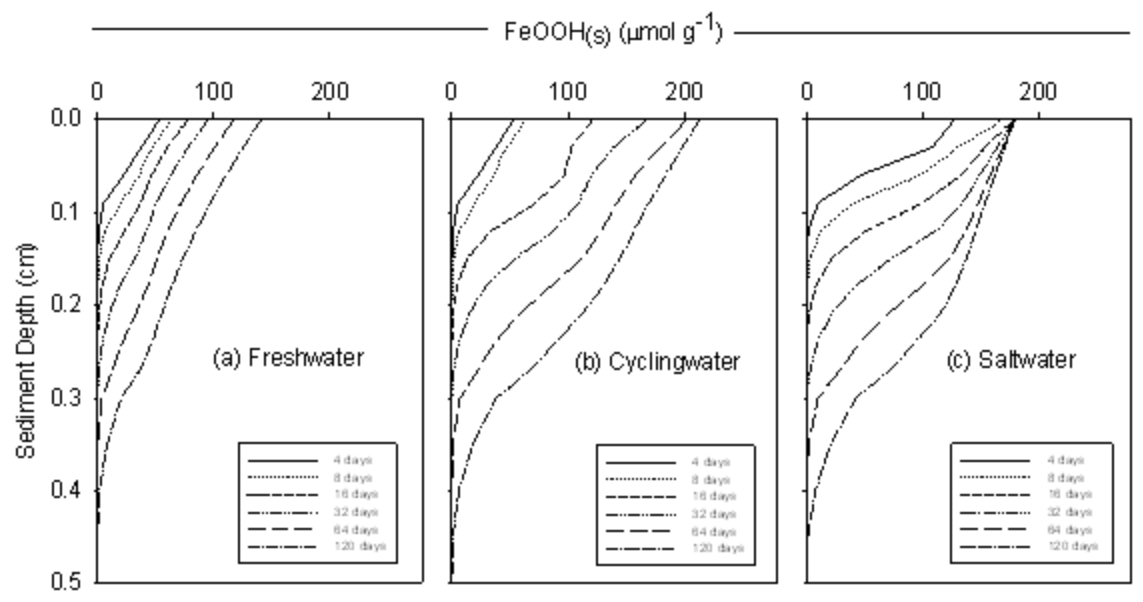


Figure 5.10 Temporal profiles of newly precipitated  $\text{FeOOH}_{(s)}$  by  $\text{Fe}^{2+}$  oxidation at the surficial sediments under (a) freshwater, (b) cycling water, and (c) saltwater.

The elevated ferrous iron concentration under cycling and salt water conditions was initially considered to be due to the increased sulfate concentrations in porewater which complexes with ferrous iron (Stumm and Morgan, 1996). However, the proposed model, which calculates the porewater  $\text{Fe}_{(aq)}$  concentrations considering competitive  $\text{Fe}_{(aq)}$  sorption to sediments and complexation with inorganic ligands such as  $\text{SO}_4^{2-}$ , could not capture the elevated porewater  $\text{Fe}_{(aq)}$  concentrations under salt water conditions.

The model assumes that bacteria only utilize the electron acceptor that is energetically most favorable. Due to the initial abundance of  $\text{Fe}^{2+}$  in sediments, it was assumed that ferric iron reduction had been inhibited by  $\text{Fe}^{2+}$  (Roden et al., 1999) and zero concentration of reducible ferric iron was assigned for the modeling. Consequently, sulfate reduction was assumed to be the most favorable reaction in salt/cycling water microcosms while methanogenesis was expected in the freshwater microcosm. However,

it has been reported that sulfate reduction could facilitate microbial iron reduction (Komlos et al., 2008) which is energetically or thermodynamically unfavorable. Assuming sulfate reduction facilitates ferric iron reduction, the elevated ferrous iron concentration in porewater was simulated in the model using increased reducible ferric iron concentrations in sediments (18.0  $\mu\text{mol/g}$ ). Another possibility was stronger ferrous iron complexation with anions and a greater effect of competitive sorption with other cations. The ferrous iron sorption constants were estimated from the linear relationship between sorption constants and first hydrolysis constant (Lofts and Tipping, 1998).

Porewater Zn and Cd concentrations were determined by DGT probes as well as centrifugation/filtration. Centrifugation gave rise to inconsistent results, presumably due to artifacts of processing such as increased suspended colloidal matter. DGT results should be treated as semi-quantitative due to coarse sectioning and uncertain desorption rates of metals in the matrix surrounding the DGT. Figure 5.9 (g) ~ (l) show measured and modeled Zn and Cd concentration profiles. Both model and DGT measured porewater concentrations were elevated at the surface. Porewater Zn and Cd concentrations were in a  $\mu\text{g/L}$  levels, which can be easily disturbed by mixing sediments.

#### **5.3.4 Sensitivity analysis for the Cd and Zn release to overlying water**

Heavy metals releases are the consequence of many interrelated biogeochemical reactions and identification of the most important processes and parameters are critical in evaluating the metals release during cycling change of surrounding environments. The sensitivity of parameters to metals release is defined as the ratio of ‘change of input’ and ‘change of output’ as follows

$$\text{Sensitivity} = \text{absolute of } \frac{\left( \frac{Y - Y_{base}}{Y_{base}} \right)}{\left( \frac{X - X_{base}}{X_{base}} \right)} \quad (5.20)$$

where  $X_{base}$  is the base-line input value,  $X$  is the changed input value,  $Y_{base}$  is the base-line output value, and  $Y$  is the changed output value.

During the simulation only one input parameter was changed while all other parameters were fixed.  $Y$  is the cumulative mass of Zn and Cd release to the overlying water for 120 days and  $X$  is the metal release related input parameters. Table 5.8 summarizes the sensitivity of  $X$  to  $Y$ .

Generally, sorption related parameters, such as oxides and organic carbon contents, were equally important for metal release. The metal sulfide oxidation kinetic rates were more important than the sorption related parameters. The sensitivities of  $\text{CdS}_{(s)}$  and  $\text{ZnS}_{(s)}$  oxidation kinetic rates were around 0.9 and 0.65, respectively, regardless of overlying water conditions indicating the importance of the rates. Note that the change of  $\text{CdS}_{(s)}$  oxidation kinetic rate didn't affect Zn release at all, and vice versa.

Table 5.8 Sensitivity of metal speciation related parameters to cumulative metal releases in the overlying water for 120 days.

	Parameters	Values		Cd <sub>(aq)</sub>		Zn <sub>(aq)</sub>		abs (X <sub>base</sub> -X) /X	Cd	Zn	Sensitivity	
		X <sub>base</sub>	X	Y <sub>base</sub>	Y	Y <sub>base</sub>	Y		abs (Y <sub>base</sub> -Y) /Y	abs (Y <sub>base</sub> -Y) /Y	Cd	Zn
				mol	mol	mol	mol	%	%	%	-	-
Saltwater	FeOOH <sub>(s)</sub> (g/g)	0.01	0.008	6.41E-05	6.58E-05	1.25E-05	1.29E-05	20	3	3	0.13	0.16
	O.C. (g/g)	0.0077	0.00616	6.41E-05	6.38E-05	1.25E-05	1.25E-05	20	0	0	0.02	0.00
	k <sub>CdS</sub> (M <sup>-1</sup> day <sup>-1</sup> )	12	9.6	6.41E-05	5.23E-05	1.25E-05	1.25E-05	20	18	0	0.92	0.00
	k <sub>ZnS</sub> (M <sup>-1</sup> day <sup>-1</sup> )	60	48	6.41E-05	6.40E-05	1.25E-05	1.09E-05	20	0	13	0.01	0.64
Freshwater	FeOOH <sub>(s)</sub> (g/g)	0.01	0.008	2.44E-05	2.62E-05	1.20E-05	1.26E-05	20	7	5	0.37	0.25
	O.C. (g/g)	0.0077	0.00616	2.44E-05	2.46E-05	1.20E-05	1.23E-05	20	1	3	0.04	0.13
	k <sub>CdS</sub> (M <sup>-1</sup> day <sup>-1</sup> )	12	9.6	2.44E-05	1.99E-05	1.20E-05	1.20E-05	20	18	0	0.92	0.00
	k <sub>ZnS</sub> (M <sup>-1</sup> day <sup>-1</sup> )	60	48	2.44E-05	2.44E-05	1.20E-05	1.05E-05	20	0	13	0.00	0.63
Cyclingwater	FeOOH <sub>(s)</sub> (g/g)	0.01	0.008	4.75E-05	4.92E-05	1.04E-05	1.07E-05	20	4	3	0.18	0.14
	O.C. (g/g)	0.0077	0.00616	4.75E-05	4.72E-05	1.04E-05	1.03E-05	20	1	1	0.03	0.05
	k <sub>CdS</sub> (M <sup>-1</sup> day <sup>-1</sup> )	12	9.6	4.75E-05	3.89E-05	1.04E-05	1.04E-05	20	18	0	0.91	0.00
	k <sub>ZnS</sub> (M <sup>-1</sup> day <sup>-1</sup> )	60	48	4.75E-05	4.77E-05	1.04E-05	9.11E-06	20	0	12	0.02	0.62

### 5.3.5 Effect of Diurnal Tidal Flow on Heavy Metals Releases in Estuary

An estuary is a semi-enclosed coastal body of water that has a free connection with the open sea and within which sea water is measurably diluted with fresh water derived from land drainage (Pritchard, 1967). Hence, estuarine sediments are exposed to overlying water whose interstitial salinities are neither truly fresh nor truly saline and the water may cycle between these two extremes depending upon the tides. The proposed model was used to simulate a more realistic estuary. Estuarine hydrodynamics are complex and often needs complicated model. In this simulation, the overlying water is simply assumed to follow a box model which is internally well mixed with simple mass balance on the influent and effluent. The influent was changed from saltwater to freshwater or freshwater to saltwater once every 12 hours simulating diurnal tidal flow. Table 5.9 summarizes the two overlying water conditions in the estuary. Other model conditions were as described in Chapter 4.

Table 5.9 Simulated Estuary Conditions

Current Speed	Cycling Period (day)	Residence Time in the model (day)	Description
Fast	0.5	0.1	Complete change of overlying water to either saline or fresh water
Slow	0.5	0.4	Incomplete change of overlying water to either saline or fresh water

The modeling results of salinity, pH, and released metals concentrations under these two different conditions are shown in Figures 5.11 which contains 100 days dynamics and Figure 5.12 which shows dynamics between 90 and 100 days providing quasi steady state conditions.

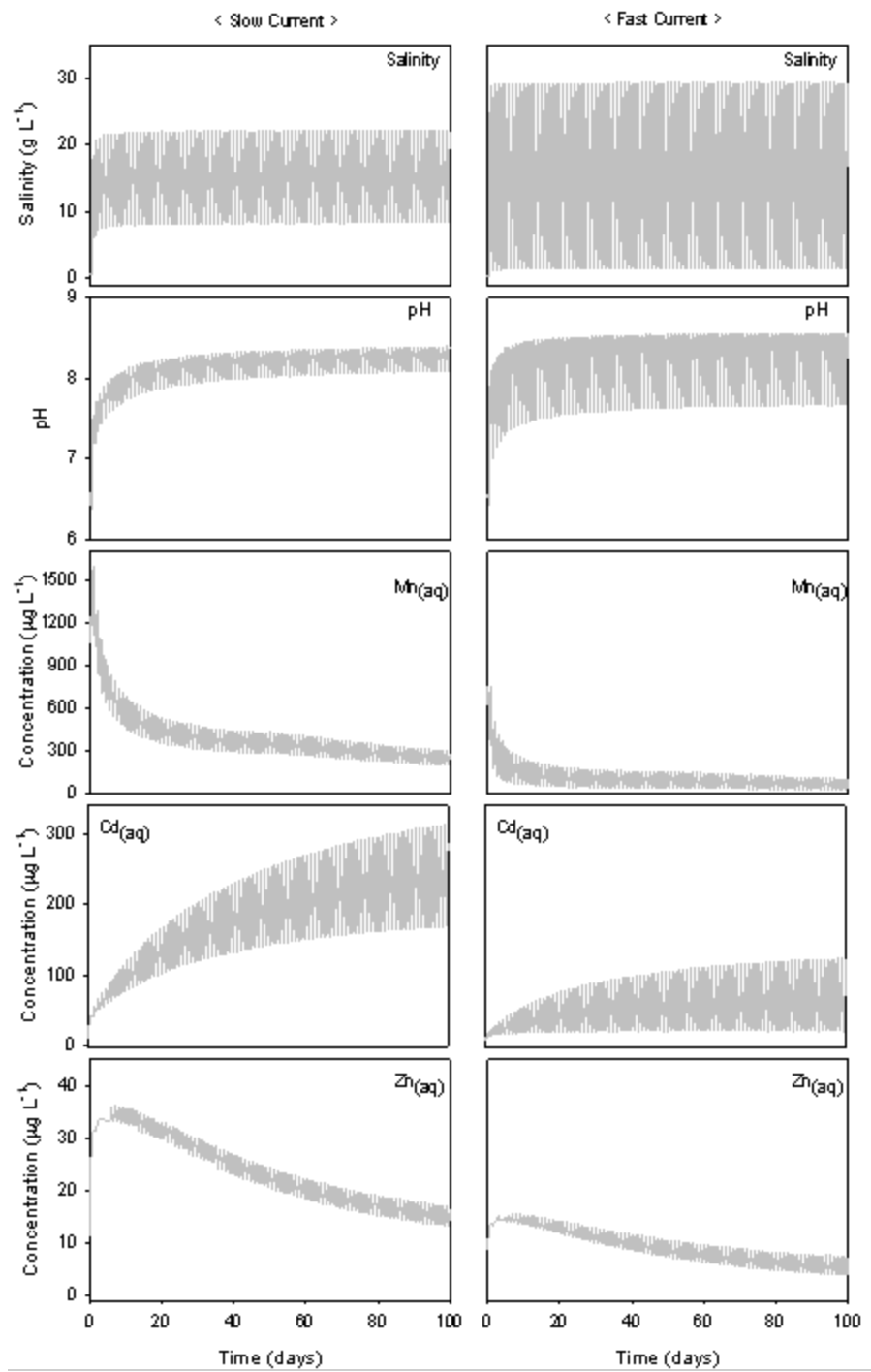


Figure 5.11 Effect of overlying water current on salinity, pH and metals release in estuary.

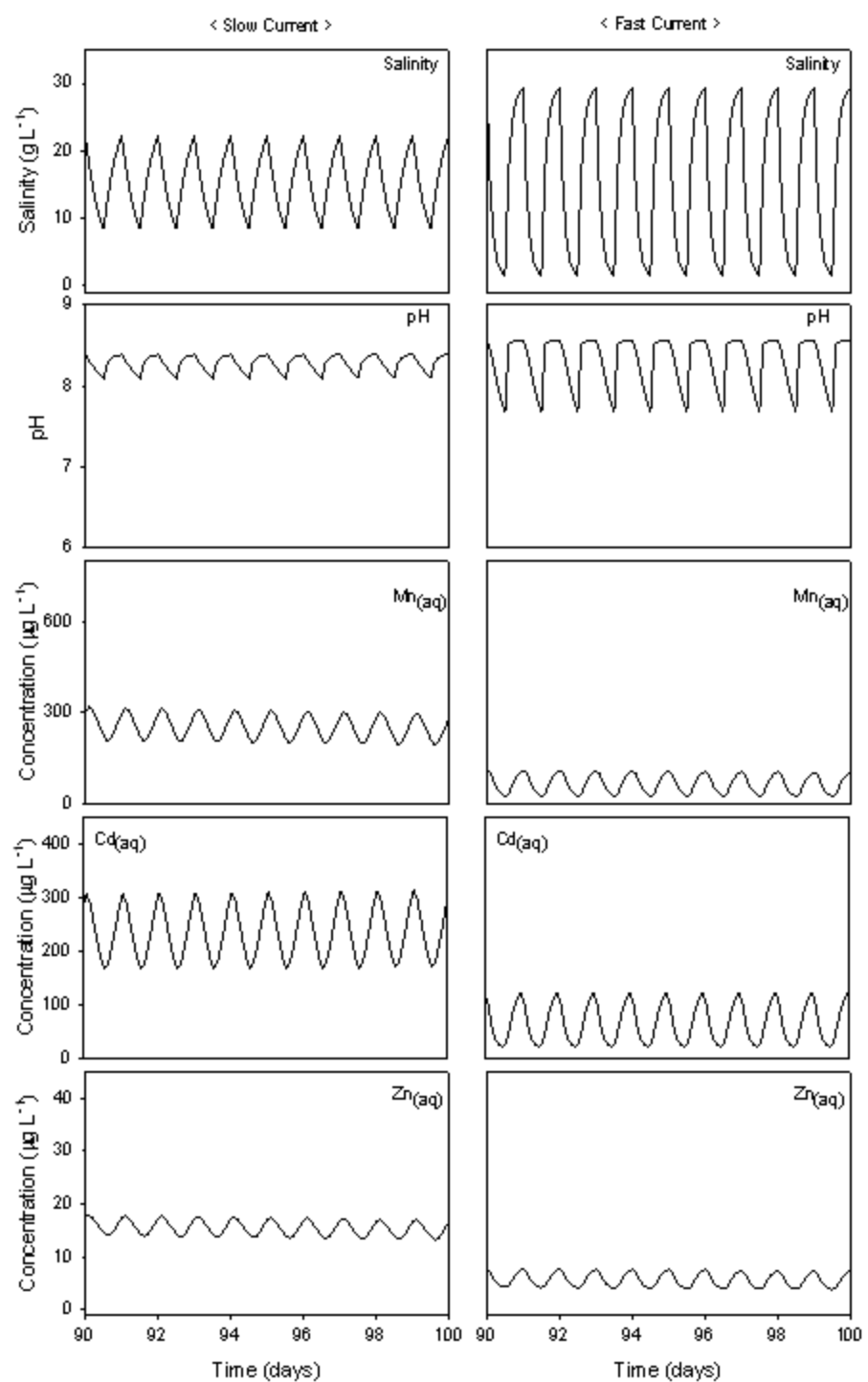


Figure 5.12 Quasi steady state dynamics of salinity, pH and metals concentrations

The salinity changed between 1 and 30 g L<sup>-1</sup> under fast current while slow current changed the salinity only between 8 and 23 g L<sup>-1</sup> due to incomplete exchange during the tidal cycle. Despite the complete change of overlying water, the pH only fluctuated between 7.5 and 8.3 under fast current and was relatively stable at around 8.1 with slow currents. Generally, lower metals concentrations were observed in fast current because metals were flushed out quickly by the tide. Cd<sub>(aq)</sub> showed the biggest fluctuation by tidal flow which concentration changed between 150 and 320 µg L<sup>-1</sup> in slow current and between 10 and 100 µg L<sup>-1</sup> in fast current.

#### 5.4 CONCLUSIONS

The effect of overlying water pH and salinity on metals release and early diagenesis has been investigated in freshwater, saltwater and cycling estuarine sediments. A model is proposed and used to better understand the underlying processes that affect metals release. As shown previously, key conditions in the overlying water include pH and salinity. The overlying water pH and salinity were modeled as boundary conditions for sediments. It was observed that the thin layer of aerobic sediments had the most substantial impact on AVS oxidation and the metals release into the overlying water. Diffusion was the dominant transport process in sediments and evidences of sulfate reduction were observed under saltwater and cycling water by the decrease of porewater sulfate concentrations and increase of AVS. Changes of porewater pH were observed in the first few centimeters and no pH changes were observed or predicted deeper in the sediments due to the strong buffering capacity of the sediments. More Zn (dissolved and complexed) was released under freshwater condition while more Cd and Mn were released under saltwater condition suggesting oxides control the metals solubility at the

surficial sediments and modeling results further supported this conclusions. As indicated previously, truly dissolved metal concentrations of all metals are expected to be higher under freshwater conditions. Porewater Cd/Zn concentrations were characterized in-situ using DGT probes. DGT results showed elevated porewater Zn and Cd concentrations at the surface. The model showed a similar trend although the vertical resolution of the measurements limited the ability to directly compare model to observations.

## Chapter 6: Conclusions and Recommendations

### 6.1 SUMMARY

The purpose of this research was to investigate the release of heavy metals from contaminated sediment as a result of sediment resuspension or cyclic changes in the surrounding environment and to develop a better quantitative description of heavy metal speciation model under those conditions for the management of heavy metal contaminated sediments. The work concentrated on understanding the dynamics of the metal transformation and release processes and identifying the significance of these processes in the environment.

In chapter 3, sediment from Anacostia River (Washington D.C) was suspended in aerobic artificial river water for 14 days to investigate the dynamics of pH, dissolved metals concentrations, acid volatile sulfides (AVS) and dissolved/solid phase  $\text{Fe}^{2+}$ . To better understand and predict the underlying biogeochemical processes, a mathematical model was developed considering oxidation of reduced species, dissolution of minerals, pH changes and pH dependent metals sorption to sediment. Some of the species oxidation rates were adjusted to fit observations. The proposed model and parameters were further tested by predicting, without further calibration, the experimental observations of Burton et al. (2006). The model described the dynamics of AVS,  $\text{Fe}^{2+}$ ,  $\text{S}^0_{(s)}$ , pH, dissolved carbonates concentrations and metals release well. Accurate predictions of Mn release required adjustment of sorption partitioning coefficient, presumably due to the presence of Mn scavenged by phases not accounted for in the original model. The oxidation of AVS (and the resulting release of sulfide bound metals) was consistent with a two step

process, a relatively rapid AVS oxidation to elemental sulfur ( $S^0_{(s)}$ ) and a slow oxidation of  $S^0_{(s)}$  to  $SO_4^{2-}_{(aq)}$  with an associated decrease in pH from neutral to acidic conditions.

More experiments were conducted (Chapter 4) to investigate the relative importance of pH and salinity on metals behaviors in estuarine sediment. Anacostia River sediment contaminated with zinc was spiked with freshly precipitated amorphous cadmium sulfide and transferred to microcosms. The surficial sediments were exposed to salt and fresh water continuously as well as cycled between fresh and saltwater in separate microcosms. Zinc and cadmium release as well as that of other species were observed for 100 days. The total zinc release was relatively insensitive to fresh and saltwater cycling while the total cadmium release was dominated by release during saltwater cycles. Equilibrium modeling, however, indicated that the freely dissolved portion of both metals was greatest during freshwater cycles. Complexation with anions and competitive sorption with cations controlled total cadmium release while the lower pH of freshwater controlled total zinc release. These results were consistent with measurements of sulfides as a function of depth in the sediments and porewater concentrations.

A mathematical model developed in Chapter 3 was extended and applied to experimental observations of Chapter 4 to better understand the experimental observations of saltwater/freshwater cycling. The derivation and results were discussed in Chapter 5. The model investigated the effect of overlying water pH and salinity fluctuation on metal-sediment interactions to provide a tool capable of predicting metals behaviors under these conditions. The model considers pH and salinity dependent metals sorption to sediment particles as well as biogeochemical reactions, transient pH and salinity gradients development in sediment porewater. The model captured the

importance of sub millimeters aerobic surficial layer of sediments on metals release as well as pH and salinity dependent metal release behaviors well. The model reproduced vertical profiles of pH,  $\text{Cl}^-$ ,  $\text{SO}_4^{2-}$ ,  $\text{Mn}_{(\text{aq})}$  and  $\text{Fe}_{(\text{aq})}$  in the porewater and solid phase AVS and SEMs as well. The results were consistent with oxides being the dominant sorption phases for metals at the surficial sediments while AVS controlled Zn, Cd and Mn solubility in anoxic sediments.

## 6.2 IMPLICATIONS

AVS/SEM approach has been suggested to indicate concentration of metal mixtures (Cd, Zn, Pb, Ni, Cu, Ag) in sediments which are protective for the presence of benthic organisms (USEPA, 2005). The approach is applicable to a variety of sediments, such as river, marine, lakes and wetlands, because AVS/SEM accounts for the varying biological availability of heavy metals in different sediments considering sulfides as the major heavy metal scavenging species. However, this approach relies strongly on the equilibrium partitioning of heavy metals under stable sediment conditions while natural aquatic sediments generally are subject to changing conditions. Moreover, the approach does not capture the potential toxicity and bioavailability of heavy metals at the oxidized surficial sediment layer, which may be relevant to the microenvironment that microorganism could create in the deeper sediment by bioturbation.

This research was motivated to support the risk assessment of metal contaminated sediments under these dynamics conditions. Experiments have showed that bulk AVS/SEM does not indicate metals release

1. at surficial sediments where sulfides can be oxidized by aerobic overlying water

2. during resuspension events when sulfide oxidation can influence the entire volume of sediments resuspended
3. during dynamic cycling of surficial conditions (e.g. pH and salinity changed by the freshwater and saltwater mixing) at the sediment water interface.

The static view of sediments presented by AVS/SEM can be misleading and a more sophisticated analysis was necessary to understand the risks posed by metals in these complicated environments.

A model was developed to address these concerns and provided an excellent tool for metals oxidation and release under the experimental conditions studied. The model was used to predict metals release under a variety of realistic conditions and the results suggest that the metals release and risk can be significant under certain conditions even when the AVS/SEM ratio is  $\gg 1$  over most of the sediment layer. Although proposed mathematical model may not include some of the detailed microscopic mechanisms of metals speciation and biogeochemical reactions, the model captured the major behaviors of metals and dominant factors affecting metals speciation under chemically complicated sediment system. This model can be used to estimate the future behavior of contaminants and assess the risks of contaminated sediments. To have better confidence in the model and parameters, calibrating the model with suggested experiments in Chapter 3 and 4 are recommended when this model is applied to other sites because some of the kinetic parameters are likely to be site specific.

### **6.3 RECOMMENDATIONS FOR FUTURE WORK**

#### **Effects of DOC on metals release**

In this study, only the effects of pH and salinity on metals are investigated while dissolved organic carbon (DOC), which can greatly affect metals behaviors, are not included. DOC has high density of many functional groups and strongly associates with dissolved metals in aquatic environments. Heavy metals, such as Cu and Pb, tend to adsorb strongly to organic carbon (Lofts and Tipping, 1998) whose concentrations are also dynamic in estuaries by freshwater and saltwater mixing (Cai and Wang, 1998). It may be more realistic and interesting to address the relative importance of pH, salinity and DOC on metals release in sediments.

### **Effects of bioturbation on metals release**

Bioturbation is the mixing and transport processes associated with the normal life-cycle behavior of benthic organisms (Reible and Mohanty, 2002). Bioturbation seemed to increase oxygen diffusion to anoxic sediments and enhance bioavailability of some heavy metals via oxidation of AVS (Peterson et al., 1996). Investigating how the bioturbation affects the biogeochemical reactions and metals release would be important in assessing metal contaminated sediments. Moreover, bioavailability and toxicity of metals can be investigated at the same time by sacrificing the benthic organisms from the experiments. The proposed model can be used to understand the experimental data with minor modifications because bioturbation has traditionally been modeled as diffusion process, which is already included in the model.

### **Extension of the model to field observations**

The proposed model has described the dynamics of biogeochemical factors and metals behaviors under controlled lab conditions; however, the model should be tested

with and used for field observations to verify the model applicability to real environment. The actual environment may be more complicated by site specific hydrodynamics. Porewater advection, which is not considered in this study, is often observed in estuary and hyporheic area by tidal pumping or groundwater discharge. Porewater advection changed vertical redox boundaries (Himmelheber et al., 2008) which were closely linked with metals behaviors in sediments. There are a few studies focused on metal release under these conditions (Liu et al., 2001; Simpson et al., 2004); however, more study is necessary to identify how the hydrodynamics will affect the biogeochemical reactions as well as metals release in sediments. The proposed model can be used for this purpose with minor modifications because it already includes advection term or the proposed model can be implemented into more complicated hydrodynamic transport models.

### **The roles of microorganisms in oxidation of elemental sulfur and ferrous iron in acidic sediment slurry.**

In Chapter 3, many reduced species were oxidized and were reasonably modeled. The model didn't differentiate chemical and biological reactions but lump those two reactions into one. However, this approach could not model the dissolved ferrous iron dynamics very well when sediment slurry was acidic. There are many studies regarding ferrous iron oxidation in acidic solution (pH 3~ 4) by acidophilic chemolithotroph (*Thiobacillus ferrooxidans*). Very little energy is generated from the oxidation of ferrous iron so that small population of active bacteria can oxidize large amount of ferrous iron. Similarly, the elemental sulfur could be oxidized by sulfur bacteria, which are common in sediments. The oxidation of these two species is likely to be affected by microorganisms in sediments. More thorough experimental research, applying molecular biology

techniques and sterilizing sediments with radiation, are needed to reveal the underlying biological oxidation mechanisms of these species.

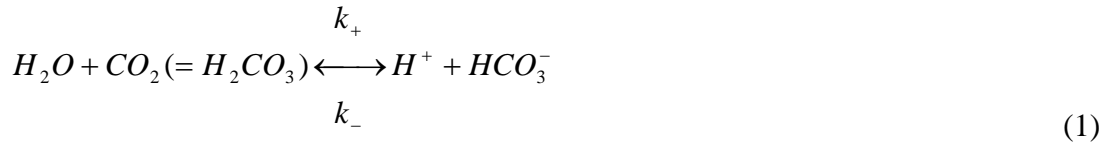
### **Suggested approaches to improve generality and predictability of the proposed model**

The proposed biogeochemical model consists of many sub models to describe metals sorption/desorption, precipitation/dissolution, complication, oxidation/reduction, and advection/diffusion. Every mechanism is important for metals and every sub model is the simplification of complex chemistry and has some uncertainties. In particular the sorption model doesn't include the electrostatic interactions which are considered in the original model (Lofts and Tipping, 1998). The proposed mode can be improved by including the electrostatic interactions or full inclusion of SCAMP (Lofts and Tipping, 1998). In addition, model uncertainties can be minimized by tiered approaches, such as isotherm experiments to check the sorption model and to evaluate sorption related parameters, resuspension experiments to assess kinetics related parameters, culminating microcosm experiments to ensure the overall performance of full biogeochemical model.

## APPENDIX A: Supporting Information for Chapter 3

### A.1 PH MODEL DERIVATION

To describe the pH changes and corresponding carbonate species distribution in sediment slurry, following reactions are considered for proton association/dissociation with carbonate species.



Where  $k_+$  is the forward reaction rate constant,  $k_-$  is the backward reaction rate constant. The oxides, such as iron, manganese and aluminum oxides have amphoteric surface that both dissociate and associate the protons as follows.



where, 'i' denotes any oxides. The organics in sediments are assumed to be humic acid which has 8 discrete sites with different strength of proton sorption. Following reactions are assumed



for  $j^{\text{th}}$  site out of 8. The equilibrium constants that describe the above reactions are as follows.

$$K_{CO,a1} = \frac{[HCO_3^-][H^+]}{[CO_2]} \quad K_{CO,a2} = \frac{[CO_3^{2-}][H^+]}{[HCO_3^-]}$$

$$K_{OX,a1,i} = \frac{[OX_iH][H^+]}{[OX_iH_2^+]} \quad K_{OX,a2,i} = \frac{[OX_i^-][H^+]}{[OX_iH]}$$

$$K_{OC,j} = \frac{[OC_j^-][H^+]}{[OC_jH]}$$

where  $K_{CO,a1}$  is the equilibrium constant for carboxylic acid dissociation,  $K_{CO,a2}$  is the equilibrium constant for bicarbonate dissociation,  $K_{OX,a1,i}$  and  $K_{OX,a2,i}$  are the first and second proton dissociation constants for oxide 'i',  $K_{OC,j}$  is the proton binding constants for  $j^{\text{th}}$  site in humic acid.

Then, the set of differential equations that describe the temporal concentration changes of proton ( $H^+$ ), carboxylic acid ( $CO_{2(aq)}$ ), bicarbonate ( $HCO_3^-$ ), carbonate ( $CO_3^{2-}$ ), protonated oxide 'i' surface ( $OX_iH_2^+$ ), neutralized oxide 'i' surface ( $OX_iH$ ), deprotonated oxide 'i' surface ( $OX_i^-$ ), neutralized ' $j^{\text{th}}$ ' site of humic acid ( $OC_jH$ ) and deprotonated ' $j^{\text{th}}$ ' site of humic acid ( $OC_j^-$ ) including the proton and carbonate species production from biogeochemical reactions are as follows.

$$\begin{aligned} \frac{d[H^+]}{dt} = & (k_+[CO_2] - k_-[H^+][HCO_3^-]) + (k_+[HCO_3^-] - k_-[H^+][CO_3^{2-}]) \\ & + (k_+[OX_iH_2^+] - k_-[H^+][OX_iH]) + (k_+[OX_iH] - k_-[H^+][OX_i^-]) \\ & + (k_+[OC_jH] - k_-[OC_j^-][H^+]) + \Sigma rxn_{H^+} \end{aligned} \quad (6)$$

$$\frac{d[CO_2]}{dt} = (k_-[H^+][HCO_3^-] - k_+[CO_2]) + \Sigma rxn_{CO_2} \quad (7)$$

$$\frac{d[HCO_3^-]}{dt} = (k_+[CO_2] - k_-[H^+][HCO_3^-]) + (k_-[H^+][CO_3^{2-}] - k_+[HCO_3^-]) + \Sigma rxn_{HCO_3^-} \quad (8)$$

$$\frac{d[CO_3^{2-}]}{dt} = (k_+[HCO_3^-] - k_-[H^+][CO_3^{2-}]) + \Sigma rxn_{CO_3^{2-}} \quad (9)$$

$$\frac{d[OX_iH_2^+]}{dt} = (k_-[H^+][OX_iH] - k_+[OX_iH_2^+]) \quad (10)$$

$$\frac{d[OX_iH]}{dt} = (k_+[OX_iH_2^+] - k_-[H^+][OX_iH]) + (k_-[H^+][OX_i^-] - k_+[OX_iH]) \quad (11)$$

$$\frac{d[OX_i^-]}{dt} = (k_+[OX_iH] - k_-[H^+][OX_i^-]) \quad (12)$$

$$\frac{d[OC_jH]}{dt} = -(k_+[OC_jH] - k_-[OC_j^-][H^+]) \quad (13)$$

$$\frac{d[OC_j^-]}{dt} = (k_+[OC_jH] - k_-[OC_j^-][H^+]) \quad (14)$$

Where  $\sum rxn_{CO_2}$ ,  $\sum rxn_{HCO_3^-}$ ,  $\sum rxn_{CO_3^{2-}}$ ,  $\sum rxn_{H^+}$  represent the summation of production rates of  $CO_{2(aq)}$ ,  $HCO_3^-$ ,  $CO_3^{2-}$ ,  $H^+$  from biogeochemical reactions individually. Then, following mass balance is derived algebraically from the equations above for protons, carbonate species, oxides surfaces and organic carbon species.

$$\frac{d[H^+]}{dt} = -\frac{d[CO_2]}{dt} + \frac{d[CO_3^{2-}]}{dt} - \frac{d[OX_iH_2^+]}{dt} + \frac{d[OX_i^-]}{dt} + \frac{d[OC_i^-]}{dt} + rxn_{CO_2} - rxn_{CO_3^{2-}} + rxn_{H^+} \quad (15)$$

$$\frac{d[CO_2]}{dt} + \frac{d[HCO_3^-]}{dt} + \frac{d[CO_3^{2-}]}{dt} = rxn_{CO_2} + rxn_{HCO_3^-} + rxn_{CO_3^{2-}} \quad (16)$$

$$\frac{d[OX_iH_2^+]}{dt} + \frac{d[OX_iH]}{dt} + \frac{d[OX_i^-]}{dt} = 0.0 \quad (17)$$

$$\frac{d[OC_jH]}{dt} + \frac{d[OC_j^-]}{dt} = 0 \quad (18)$$

Note that all the kinetic terms are canceled out each other on the right side of the equations remaining only the production rates of  $CO_{2(aq)}$ ,  $HCO_3^-$ ,  $CO_3^{2-}$ ,  $H^+$  from biogeochemical reactions. The total oxides surfaces and organic surfaces don't change because there is no sink or source for the oxides in a closed system.

The (15), (16), (17), (18) can be rewritten in terms of proton( $H^+$ ), total carbonate concentrations ( $C_{t,CO_2} = [CO_{2(aq)}] + [HCO_3^-] + [CO_3^{2-}]$ ), total surface concentrations for

oxide 'i' ( $C_{t,OXi} = [OX_iH_2^+] + [OX_iH] + [OX_i^-]$ ), total surface concentrations for  $j^{\text{th}}$  surface of humic acid ( $C_{t,OCj} = [OC_jH] + [OC_j^-]$ ). For example, the  $[CO_2]$  in equation (15) can be replaced as follows introducing the fraction of  $[CO_2]$  among total carbonate species which are dependent on pH, so called alpha-notation (Snoeyink, 1980)

$$[CO_2] = \alpha_0 C_{t,CO_2}$$

$$\alpha_0 = \frac{[H^+]^2}{[H^+]^2 + K_{a1}[H^+] + K_{a1}K_{a2}} = \frac{[CO_2]}{C_{t,CO_2}}$$

where,  $C_{t,CO_2}$  is the total dissolved carbonate species concentrations. The derivative of  $[CO_2]$  in equation (15) can be rewritten with respect of total carbonate concentrations ( $C_{t,CO_2}$ ) and proton concentration ( $H^+$ ) as follows.

$$\frac{\partial[CO_2]}{\partial t} = \frac{\partial(\alpha_0 C_{t,CO_2})}{\partial t} = \alpha_0 \frac{\partial(C_{t,CO_2})}{\partial t} + C_{t,CO_2} \frac{\partial(\alpha_0)}{\partial t} = \alpha_0 \frac{\partial C_{t,CO_2}}{\partial t} + C_{t,CO_2} \frac{\partial \alpha_0}{\partial [H^+]} \frac{\partial [H^+]}{\partial t}$$

This derivation can be extended to all the other protonated and deprotonated species using fractions of each species depending on pH. The equations (15), (16), (17), (18) can be expressed as follows.

$$\begin{aligned} \frac{d[H^+]}{dt} = & (-\alpha_0 + \alpha_2) \frac{\partial C_{t,CO_2}}{\partial t} - C_{t,CO_2} \frac{\partial \alpha_0}{\partial H} \frac{d[H^+]}{dt} + C_{t,CO_2} \frac{\partial \alpha_2}{\partial H} \frac{d[H^+]}{dt} \\ & + (-\beta_{0,i} + \beta_{2,i}) \frac{\partial C_{t,OX,i}}{\partial t} - C_{t,OX,i} \frac{\partial \beta_{0,i}}{\partial H} \frac{d[H^+]}{dt} + C_{t,OX,i} \frac{\partial \beta_{2,i}}{\partial H} \frac{d[H^+]}{dt} \end{aligned} \quad (19)$$

$$\begin{aligned} & + \chi_{1,j} \frac{\partial C_{t,OC,j}}{\partial t} + C_{t,OC,j} \frac{\partial \chi_{1,j}}{\partial [H^+]} \frac{\partial [H^+]}{\partial t} + rxn_{CO_2} - rxn_{CO_3^{2-}} + rxn_{H^+} \\ & (\alpha_0 + \alpha_1 + \alpha_2) \frac{dC_{t,CO_2}}{dt} + C_{t,CO_2} \left( \frac{\partial \alpha_0}{\partial H} + \frac{\partial \alpha_1}{\partial H} + \frac{\partial \alpha_2}{\partial H} \right) \frac{d[H^+]}{dt} \end{aligned} \quad (20)$$

$$= rxn_{CO_2} + rxn_{HCO_3^-} + rxn_{CO_3^{2-}}$$

$$(\beta_{0,i} + \beta_{1,i} + \beta_{2,i}) \frac{dC_{t,OX,i}}{dt} + C_{t,OX,i} \left( \frac{\partial \beta_{0,i}}{\partial H} + \frac{\partial \beta_{1,i}}{\partial H} + \frac{\partial \beta_{2,i}}{\partial H} \right) \frac{d[H^+]}{dt} = 0.0 \quad (21)$$

$$(\chi_{0,j} + \chi_{1,j}) \frac{\partial C_{t,OC,j}}{\partial t} + C_{t,OC,j} \frac{\partial \chi_{0,j}}{\partial [H^+]} \frac{\partial [H^+]}{\partial t} + C_{t,OC,j} \frac{\partial \chi_{1,j}}{\partial [H^+]} \frac{\partial [H^+]}{\partial t} = 0.0 \quad (22)$$

The fractions  $\alpha$ ,  $\beta$ ,  $\chi$  and the derivative of  $\alpha$ ,  $\beta$ ,  $\chi$  with respect to proton ( $H^+$ ) concentrations are defined as follows.

$$\begin{aligned} \alpha_0 &= \frac{[H^+]^2}{[H^+]^2 + K_{a1}[H^+] + K_{a1}K_{a2}} = \frac{[CO_2]}{C_{t,CO2}} \\ \alpha_1 &= \frac{[H^+]K_{a1}}{[H^+]^2 + K_{a1}[H^+] + K_{a1}K_{a2}} = \frac{[HCO_3^-]}{C_{t,CO2}} \\ \alpha_2 &= \frac{K_{a1}K_{a2}}{[H^+]^2 + K_{a1}[H^+] + K_{a1}K_{a2}} = \frac{[CO_3^{2-}]}{C_{t,CO2}} \\ \beta_{0,i} &= \frac{[H^+]^2}{[H^+]^2 + K_{OX,a1,i}[H^+] + K_{OX,a1,i}K_{OX,a2,i}} = \frac{[OX_iH_2^+]}{C_{t,OX,i}} \\ \beta_{1,i} &= \frac{[H^+]K_{OX_i,a1}}{[H^+]^2 + K_{OX,a1,i}[H^+] + K_{OX,a1,i}K_{OX,a2,i}} = \frac{[OX_iH]}{C_{t,OX,i}} \\ \beta_{2,i} &= \frac{K_{OX_i,a1}K_{OX_i,a2}}{[H^+]^2 + K_{OX,a1,i}[H^+] + K_{OX,a1,i}K_{OX,a2,i}} = \frac{[OX_i^-]}{C_{t,OX,i}} \\ \chi_{0,j} &= \frac{[H^+]}{[H^+] + K_{OC,j}} = \frac{[OC_iH]}{C_{t,OC,j}} \\ \chi_{1,j} &= \frac{K_{OC_i}}{[H^+] + K_{OC,j}} = \frac{[OC_i^-]}{C_{t,OC,j}} \end{aligned}$$

$$\begin{aligned} \frac{\partial \alpha_0}{\partial [H^+]} &= \frac{(K_{a1}[H^+]^2 + 2K_{a1}K_{a2}[H^+])}{([H^+]^2 + K_{a1}[H^+] + K_{a1}K_{a2})^2} \\ \frac{\partial \alpha_1}{\partial [H^+]} &= \frac{(-K_{a1}[H^+]^2 + (K_{a1})^2K_{a2})}{([H^+]^2 + K_{a1}[H^+] + K_{a1}K_{a2})^2} \\ \frac{\partial \alpha_2}{\partial [H^+]} &= \frac{-K_{a1}K_{a2}(2[H^+] + K_{a1})}{([H^+]^2 + K_{a1}[H^+] + K_{a1}K_{a2})^2} \\ \frac{\partial \beta_{0,i}}{\partial [H^+]} &= \frac{(K_{OX,a1,i}[H^+]^2 + 2K_{OX,a1,i}K_{OX,a2,i}[H^+])}{([H^+]^2 + K_{OX,a1,i}[H^+] + K_{OX,a1,i}K_{OX,a2,i})^2} \end{aligned}$$

$$\begin{aligned}\frac{\partial\beta_{1,i}}{\partial[H^+]} &= \frac{(-K_{OX,a1,i}[H^+]^2 + (K_{OX,a1,i})^2 K_{OX,a2,i})}{([H^+]^2 + K_{OX,a1,i}[H^+] + K_{OX,a1,i}K_{OX,a2,i})^2} \\ \frac{\partial\beta_{2,i}}{\partial[H^+]} &= \frac{-K_{OX,a1,i}K_{OX,a2,i}(2[H^+] + K_{OX,a1,i})}{([H^+]^2 + K_{OX,a1,i}[H^+] + K_{OX,a1,i}K_{OX,a2,i})^2} \\ \frac{\partial\chi_{0,j}}{\partial[H^+]} &= \frac{K_{OC,j}}{([H^+] + K_{OC,j})^2} \\ \frac{\partial\chi_{1,j}}{\partial[H^+]} &= \frac{-1}{([H^+] + K_{OC,j})^2}\end{aligned}$$

$\alpha_0, \alpha_1, \alpha_2$  are fractions of  $[\text{CO}_2(\text{aq})], [\text{HCO}_3^-], [\text{CO}_3^{2-}]$  among total carbonate concentrations ( $C_{t,\text{CO}_2} = [\text{CO}_2(\text{aq})] + [\text{HCO}_3^-] + [\text{CO}_3^{2-}]$ ),  $\beta_{0,i}, \beta_{1,i}, \beta_{2,i}$  are fractions of  $[\text{OX}_i\text{H}_2^+], [\text{OX}_i\text{H}], [\text{OX}_i^-]$  among total 'i' oxide surface.  $\chi_{0,j}, \chi_{1,j}$  are fractions of  $[\text{OC}_j\text{H}], [\text{OC}_j^-]$  among total  $j^{\text{th}}$  surface of humic acid.

From the following definition of  $\alpha, \beta, \chi$

$$(\alpha_0 + \alpha_1 + \alpha_2) = 1 \quad (\beta_{0,i} + \beta_{1,i} + \beta_{2,i}) = 1 \quad (\chi_{0,j} + \chi_{1,j}) = 1$$

(19), (20), (21), (22) can be simplified as follows.

$$\begin{aligned}\frac{d[H^+]}{dt} &= (-\alpha_0 + \alpha_2) \frac{\partial C_{t,\text{CO}_2}}{\partial t} - C_{t,\text{CO}_2} \frac{\partial \alpha_0}{\partial H} \frac{d[H^+]}{dt} + C_{t,\text{CO}_2} \frac{\partial \alpha_2}{\partial H} \frac{d[H^+]}{dt} \\ &+ (-\beta_{0,i} + \beta_{2,i}) \frac{\partial C_{t,\text{OX},i}}{\partial t} - C_{t,\text{OX},i} \frac{\partial \beta_{0,i}}{\partial H} \frac{d[H^+]}{dt} + C_{t,\text{OX},i} \frac{\partial \beta_{2,i}}{\partial H} \frac{d[H^+]}{dt} \\ &+ \chi_{1,j} \frac{\partial C_{t,\text{OC},j}}{\partial t} + C_{t,\text{OC},j} \frac{\partial \chi_{1,j}}{\partial [H^+]} \frac{\partial [H^+]}{\partial t} + rxn_{\text{CO}_2} - rxn_{\text{CO}_3^{2-}} + rxn_{\text{H}^+}\end{aligned} \quad (23)$$

$$\frac{dC_{t,\text{CO}_2}}{dt} = -C_{t,\text{CO}_2} \left( \frac{\partial \alpha_0}{\partial H} + \frac{\partial \alpha_1}{\partial H} + \frac{\partial \alpha_2}{\partial H} \right) \frac{d[H^+]}{dt} + rxn_{\text{CO}_2} + rxn_{\text{HCO}_3^-} + rxn_{\text{CO}_3^{2-}} \quad (24)$$

$$\frac{dC_{t,\text{OX},i}}{dt} = -C_{t,\text{OX},i} \left( \frac{\partial \beta_{0,i}}{\partial H} + \frac{\partial \beta_{1,i}}{\partial H} + \frac{\partial \beta_{2,i}}{\partial H} \right) \frac{d[H^+]}{dt} \quad (25)$$

$$\frac{\partial C_{t,\text{OC},j}}{\partial t} = -C_{t,\text{OC},j} \frac{\partial \chi_{0,j}}{\partial [H^+]} \frac{\partial [H^+]}{\partial t} - C_{t,\text{OC},j} \frac{\partial \chi_{1,j}}{\partial [H^+]} \frac{\partial [H^+]}{\partial t} \quad (26)$$

The (23), (24), (25), (26) are coupled each other. Introducing (24), (25), (26) into (23) and rearranging (23) with respect to derivative of proton concentrations ( $H^+$ ) will lead to following equation.

$$\left( \begin{aligned} &1 + C_{t,CO_2} \left( (1 - \alpha_0 + \alpha_2) \frac{\partial \alpha_0}{\partial H} + (-\alpha_0 + \alpha_2) \frac{\partial \alpha_1}{\partial H} + (-1 - \alpha_0 + \alpha_2) \frac{\partial \alpha_2}{\partial H} \right) + \\ &C_{t,OX,i} \left( (1 - \beta_{0,i} + \beta_{2,i}) \frac{\partial \beta_{0,i}}{\partial H} + (-\beta_{0,i} + \beta_{2,i}) \frac{\partial \beta_{1,i}}{\partial H} + (-1 - \beta_{0,i} + \beta_{2,i}) \frac{\partial \beta_{2,i}}{\partial H} \right) \frac{d[H^+]}{dt} \\ &+ \chi_{1,j} C_{t,OC,j} \frac{\partial \chi_{0,j}}{\partial [H^+]} - \chi_{0,j} C_{t,OC,j} \frac{\partial \chi_{1,j}}{\partial [H^+]} \end{aligned} \right) \quad (27)$$

$$= (1 - \alpha_0 + \alpha_2) rxn_{CO_2} + (-\alpha_0 + \alpha_2) rxn_{HCO_3^-} + (-1 - \alpha_0 + \alpha_2) rxn_{CO_3^{2-}} + rxn_{H^+}$$

The equations can be generally rewritten including other oxides surfaces and other discrete surfaces of humic acid as follows.

$$\frac{d[H^+]}{dt} = \Gamma * \left\{ \begin{aligned} &(1 - \alpha_0 + \alpha_2) \Sigma rxn_{CO_2} + (-\alpha_0 + \alpha_2) \Sigma rxn_{HCO_3^-} \\ &+ (-1 - \alpha_0 + \alpha_2) \Sigma rxn_{CO_3^{2-}} + \Sigma rxn_{H^+} \end{aligned} \right\} \quad (28)$$

$$\Gamma = \left( \begin{aligned} &1 + C_{t,CO_2} \left( (1 - \alpha_0 + \alpha_2) \frac{\partial \alpha_0}{\partial H} + (-\alpha_0 + \alpha_2) \frac{\partial \alpha_1}{\partial H} + (-1 - \alpha_0 + \alpha_2) \frac{\partial \alpha_2}{\partial H} \right) + \\ &\sum_{i=1}^k \left\{ C_{t,OX,i} \left( (1 - \beta_{0,i} + \beta_{2,i}) \frac{\partial \beta_{0,i}}{\partial H} + (-\beta_{0,i} + \beta_{2,i}) \frac{\partial \beta_{1,i}}{\partial H} + (-1 - \beta_{0,i} + \beta_{2,i}) \frac{\partial \beta_{2,i}}{\partial H} \right) \right\} \\ &+ \sum_{j=1}^l \left\{ C_{t,OC,j} \left( \chi_{1,j} \frac{\partial \chi_{0,j}}{\partial [H^+]} - \chi_{0,j} \frac{\partial \chi_{1,j}}{\partial [H^+]} \right) \right\} \end{aligned} \right)^{-1}$$

Where  $k$  is the number of total oxides considered,  $l$  is the number of total organic carbon surface considered. The corresponding total dissolved carbonate species concentrations change can be derived by introducing (28) to (24) as follows.

$$\frac{\partial C_{t,CO_2}}{\partial t} = \{ \Lambda * (-1 + \alpha_0 - \alpha_2) + 1 \} \Sigma rxn_{CO_2} + \{ \Lambda * (\alpha_0 - \alpha_2) + 1 \} \Sigma rxn_{HCO_3^-} \\ + \{ \Lambda * (1 + \alpha_0 - \alpha_2) + 1 \} \Sigma rxn_{CO_3^{2-}} - \Lambda * \Sigma rxn_{H^+} \quad (29)$$

$$\Lambda = \Gamma * C_{t,CO_2} * \left( \frac{\partial \alpha_0}{\partial H} + \frac{\partial \alpha_1}{\partial H} + \frac{\partial \alpha_2}{\partial H} \right)$$

A. 2 FIGURES

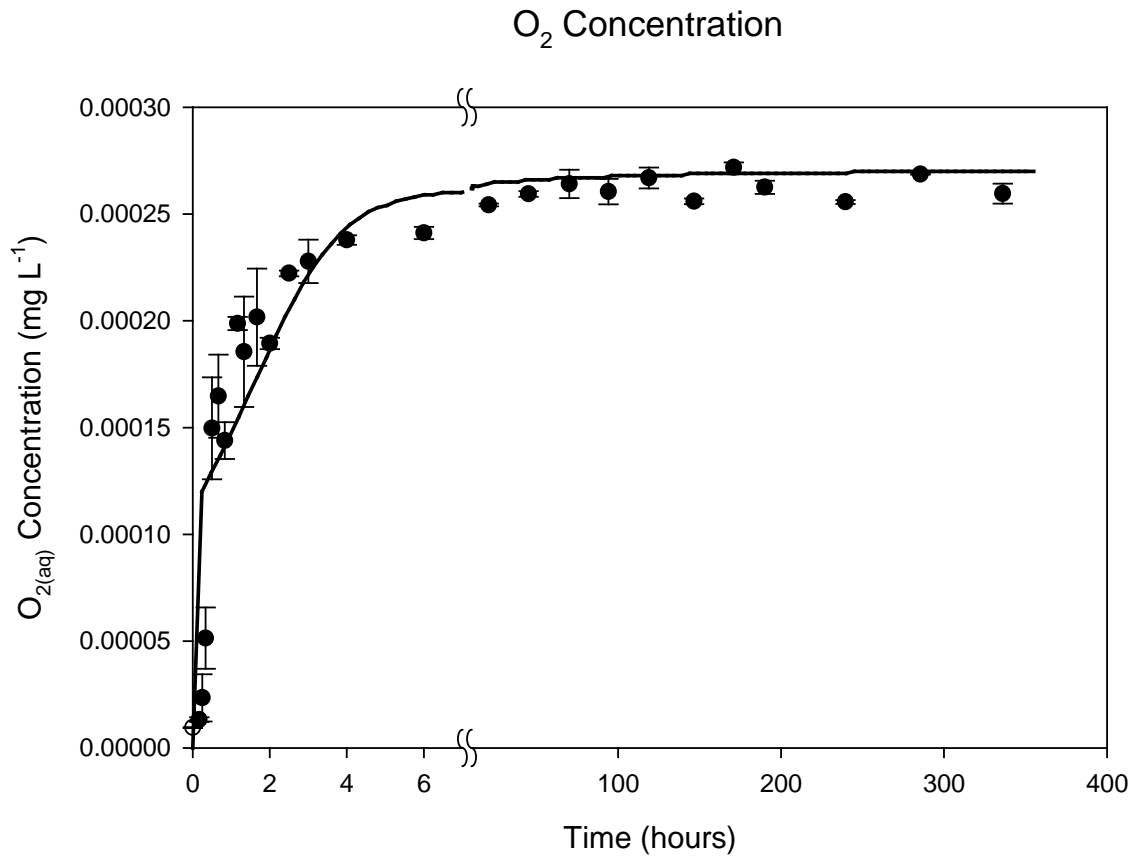


Figure A.1 Dissolved oxygen concentration changes in Anacostia Sediment  
Resuspension experiment

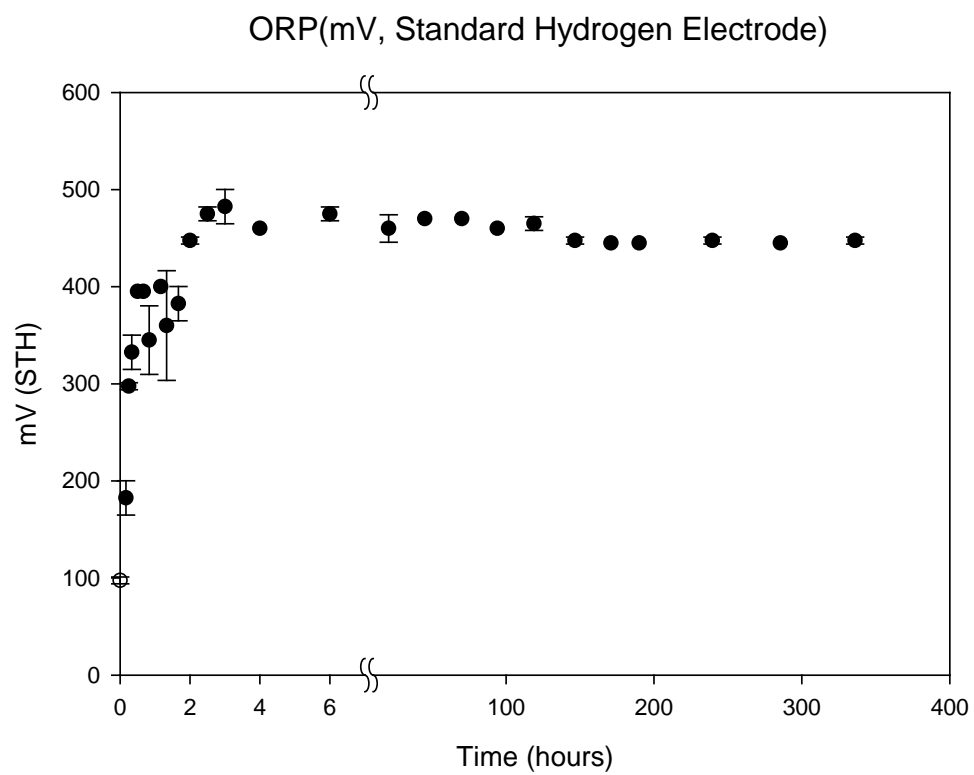


Figure A.2 Redox potential changes in Anacostia Sediment Resuspension experiment

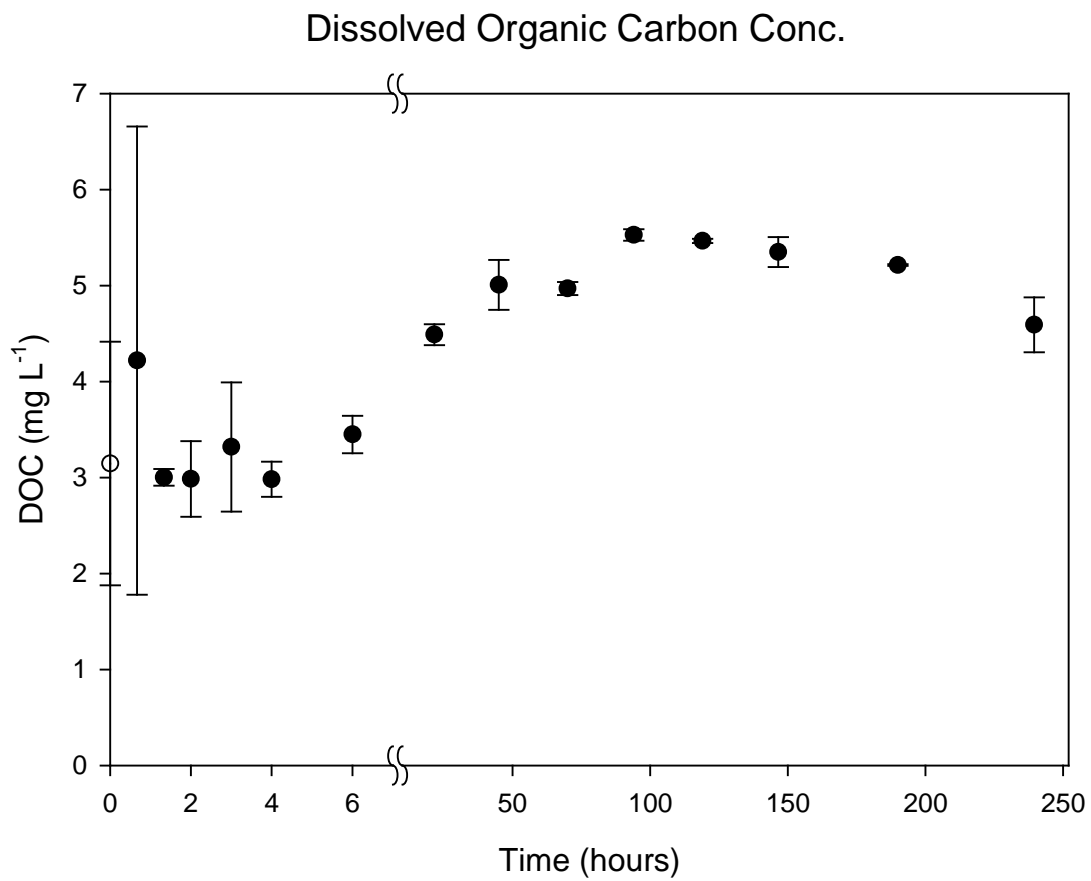


Figure A.3 Organic carbon concentration changes in Anacostia Sediment Resuspension experiment

### A.3 TABLES

Table A.1 Basic characteristics of sediments

Properties	Anacostia	Acid Sulfate
Wet sediment (g)	500	400
Suspension Water (mL)	2800	2000
Water Content (%)	53.4 (0.8)	70 (1.0)
Organic Matter (%)	7.0 (2.8)	4.7 (0.2)
Inorganic Carbon (%)	1.05 (0.21)	1.5 (0.2)
AVS ( $\mu\text{mol g}^{-1}$ )	54.03 (3.44)	220 (10.6)
$\text{S}^0_{(s)}$ ( $\mu\text{mol g}^{-1}$ )	---	113 (8.1)
$\text{NH}_4^+$ (M)	0.00016	---
Oxalate extractable $\text{Fe}^{2+}$ ( $\text{mg g}^{-1}$ )	3.05 (0.07)	15.4 (13.2~17.5)
Oxalate extractable $\text{Fe}^{3+}$ ( $\text{mg g}^{-1}$ )	20.85 (1.22)	33.0 (22.0~44.0)
Total Fe ( $\text{mg g}^{-1}$ )	53.42 (6.65)	98.6 (0.8)
Total Mn ( $\text{mg g}^{-1}$ )	0.24 (0.022)	0.19 (0.00032)
Total Zn ( $\text{mg g}^{-1}$ )	0.70 (0.087)	0.077 (0.0002)
Total Al ( $\text{mg g}^{-1}$ )	12.33 (3.98)	31.5 (1.1)
Total Ca ( $\text{mg g}^{-1}$ )	11.2 (2.74)	---
Total Mg ( $\text{mg g}^{-1}$ )	1.95 (0.45)	---
SEM Zn ( $\mu\text{mol g}^{-1}$ )	8.48 (0.76)	---
SEM Mn ( $\mu\text{mol g}^{-1}$ )	3.94 (0.46)	---
$\text{Fe}^{2+}$ (mM)	0.049	0.163
$\text{Ca}^{2+}$ (mM)	0.291	0.548
$\text{Mg}^{2+}$ (mM)	0.129	1.921
$\text{Cl}^-$ (mM)	0.272	13.657
$\text{SO}_4^{2-}$ (mM)	0.00063	2.385417
$\text{HCO}_3^-$ (mM)	0.7	0.7

## APPENDIX B: Supporting Information for Chapter 4

### B.1 FIGURES

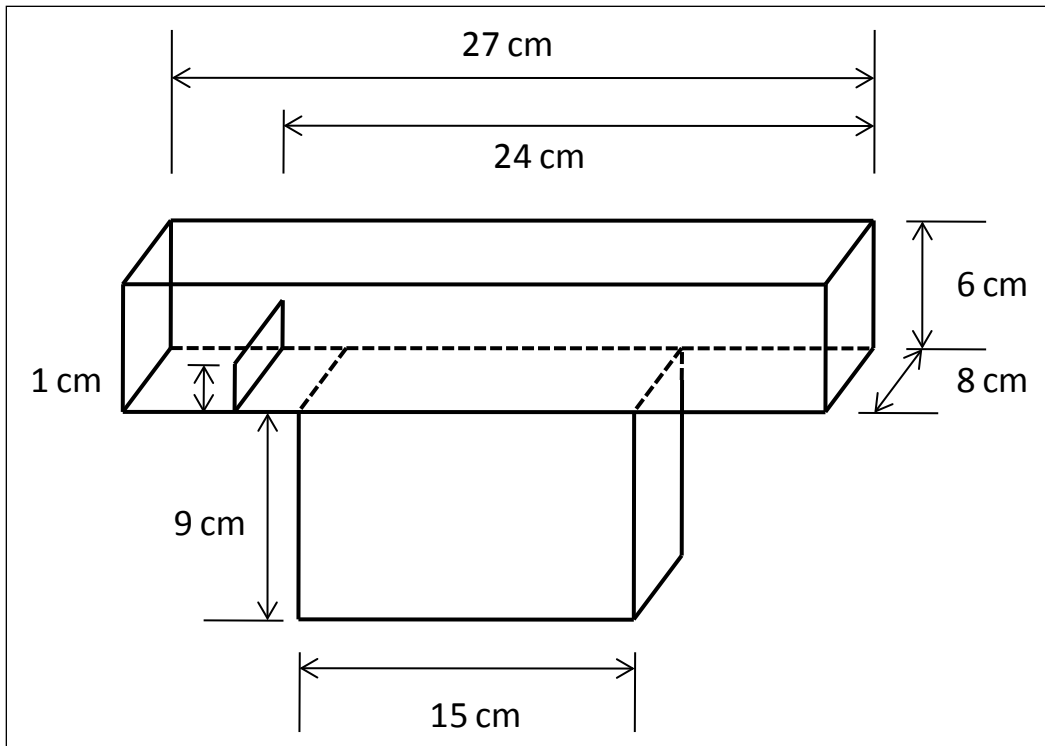


Figure B.1 Microcosm dimensions

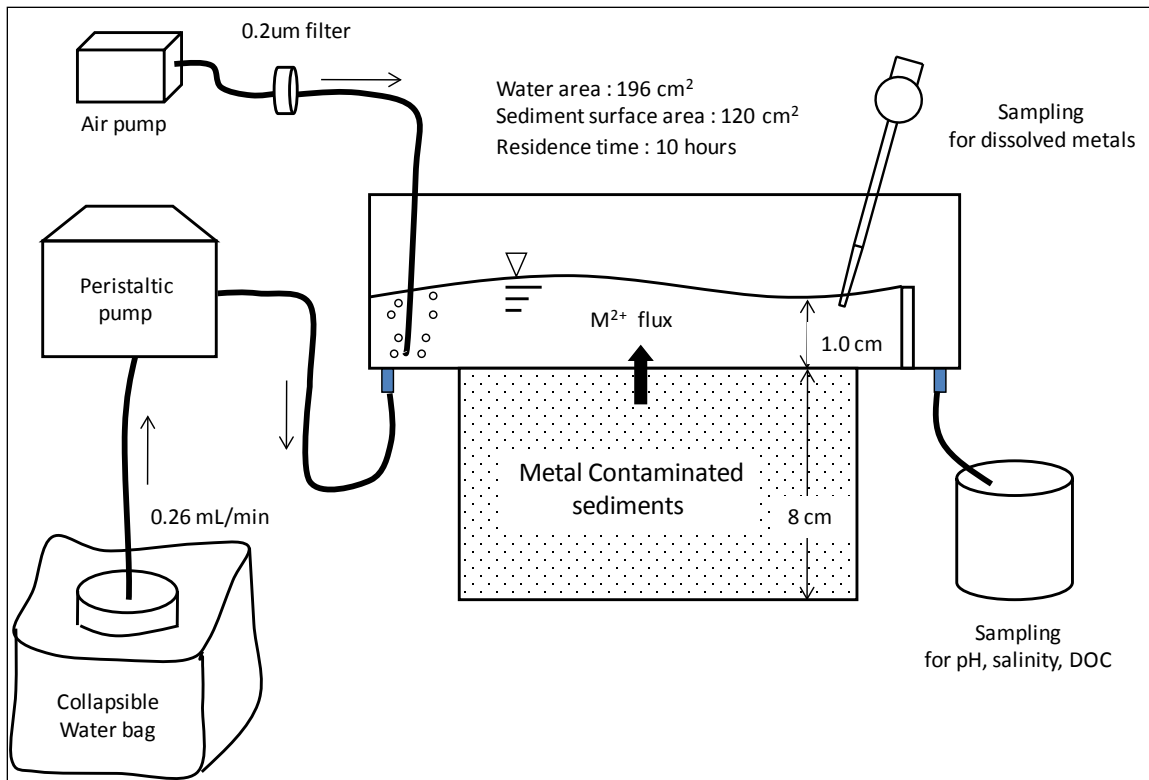


Figure B.2 Schematics and experimental setup of microcosms

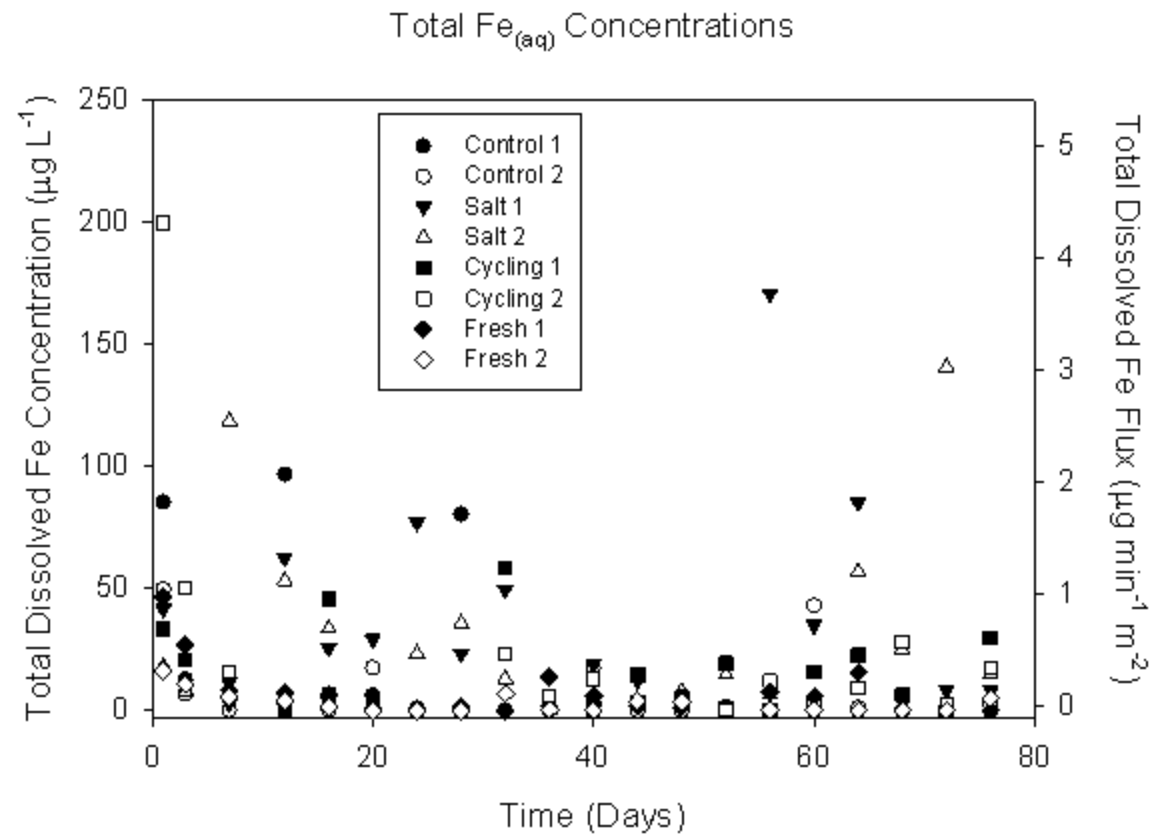


Figure B.3 Dissolved Fe concentrations in the overlying water.

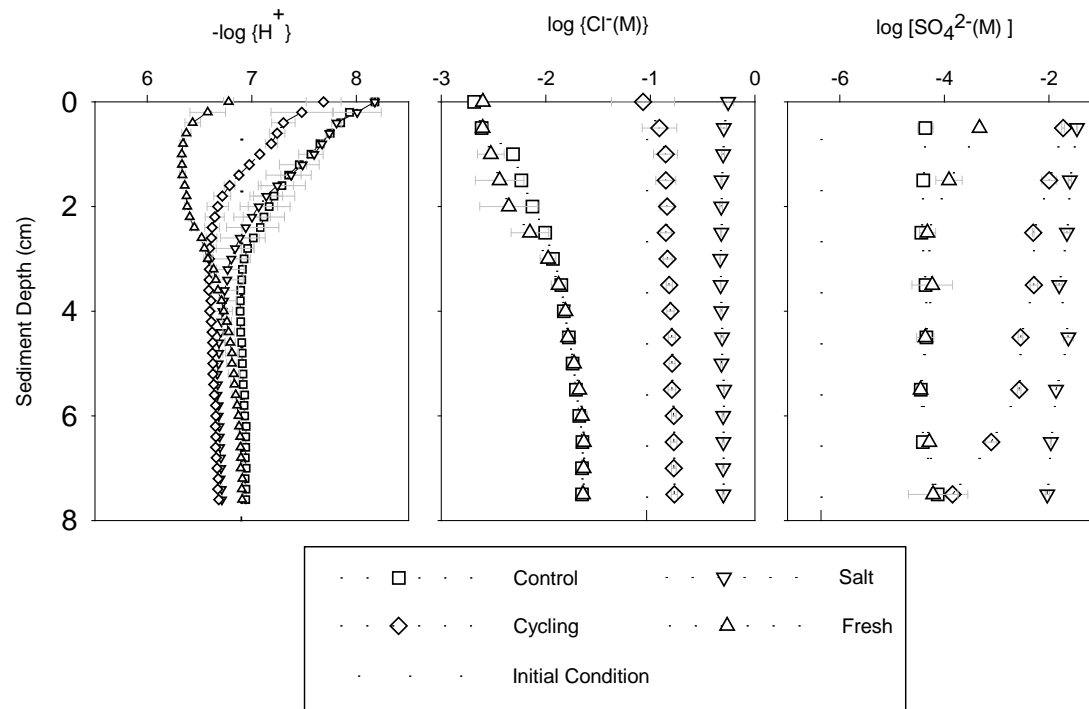


Figure B.4 Vertical profiles of porewater pH, Cl<sup>-</sup> and SO<sub>4</sub><sup>2-</sup> concentrations after 130 days sediments exposure to control, salt, fresh and cycling waters. pH and Cl<sup>-</sup> concentrations were determined in-situ using microelectrodes. SO<sub>4</sub><sup>2-</sup> concentrations were determined from centrifuged porewater. Symbols and error bars are the mean and standard deviations of duplicated experiments respectively.

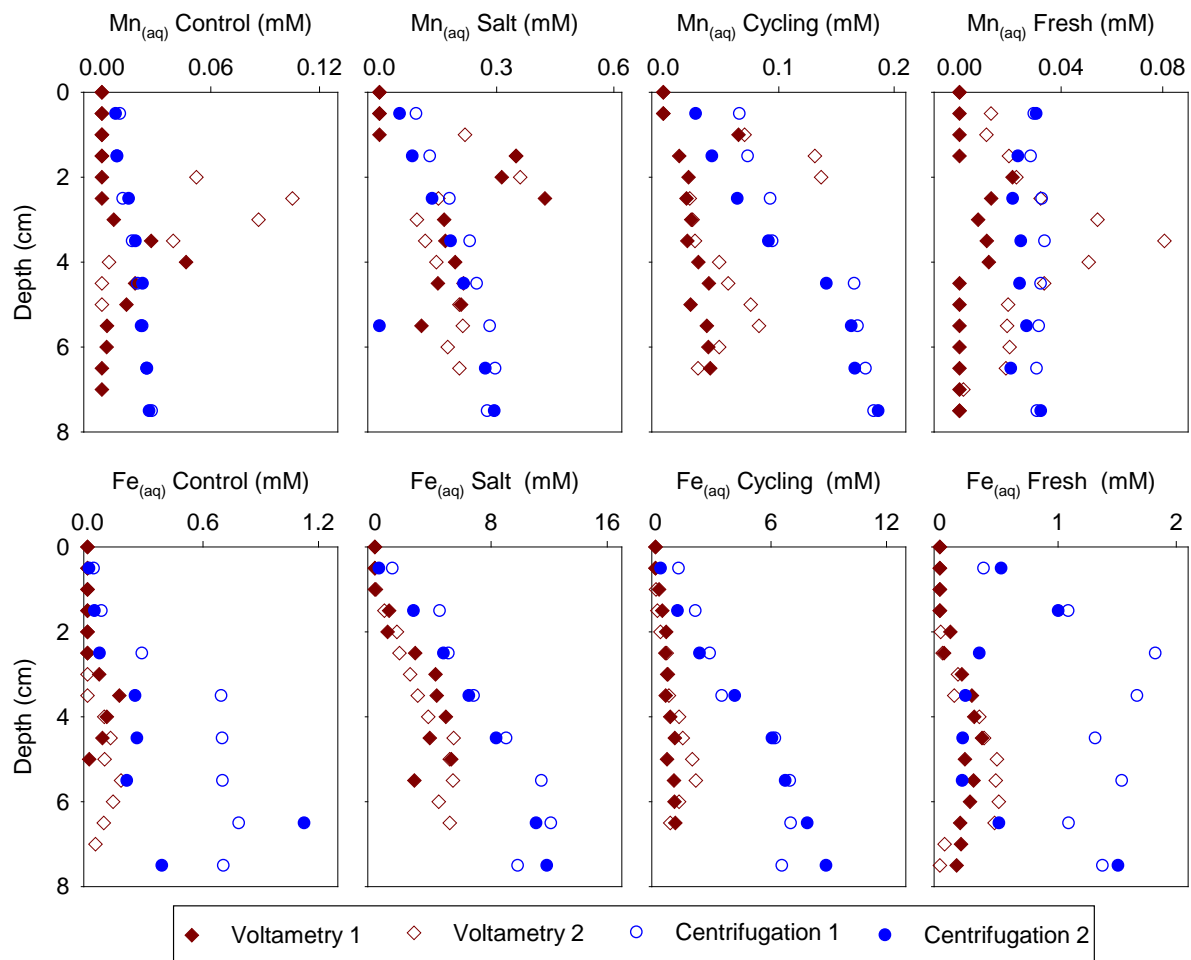


Figure B.5 Vertical profiles of porewater  $\text{Fe}_{(\text{aq})}$  and  $\text{Mn}_{(\text{aq})}$  determined by voltametric microelectrode and centrifugation.

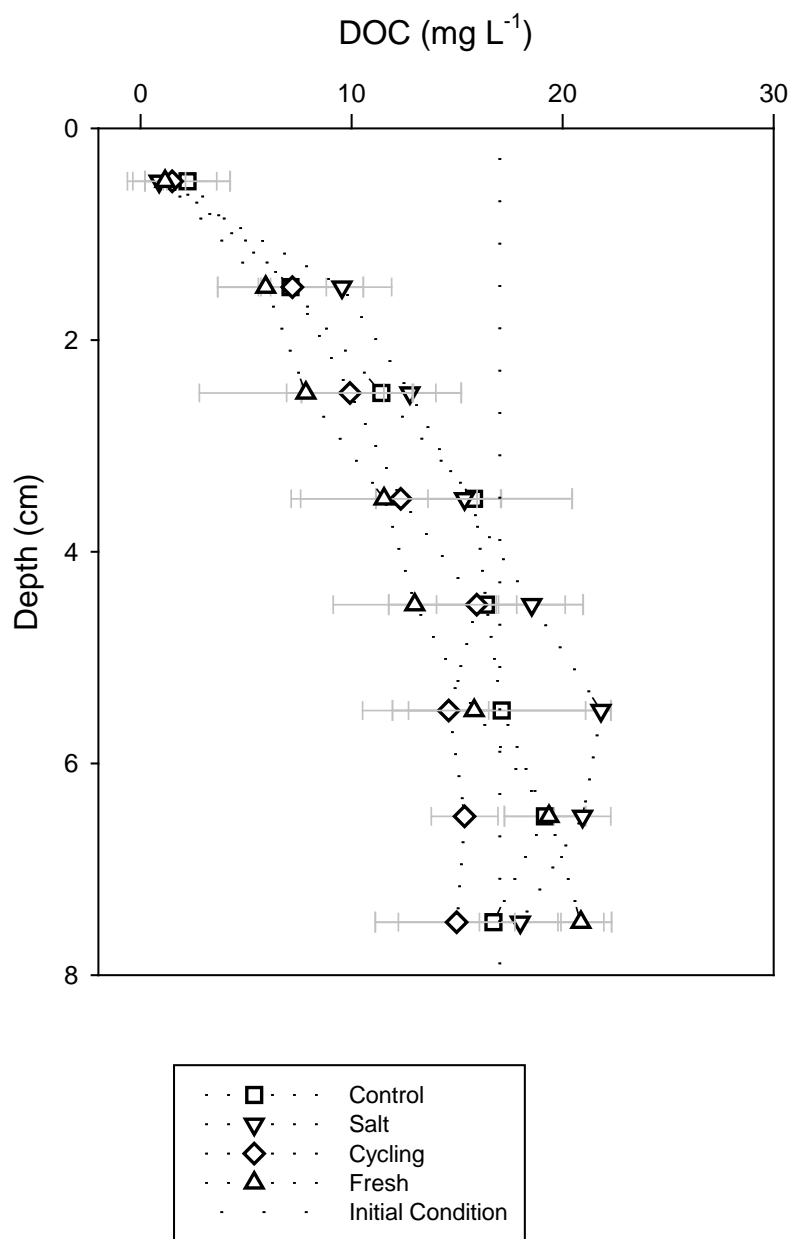


Figure B.6 Vertical profiles of porewater DOC concentrations. Symbols and error bars are the mean and standard deviations of duplicated experiments respectively.

## B.2 TABLES

Table B.1 Salts concentration in control, salt, and fresh water

	Control	Salt	Fresh
Ca <sup>2+</sup> (M)	6.03E-05	9.05E-03	6.03E-05
K <sup>+</sup> (M)	5.89E-05	8.83E-03	5.89E-05
Mg <sup>2+</sup> (M)	3.25E-04	4.87E-02	3.25E-04
Na <sup>+</sup> (M)	5.7E-03	3.90E-01	2.60E-03
SO <sub>4</sub> <sup>2-</sup> (M)	1.54E-04	2.31E-02	1.54E-04
Cl <sup>-</sup> (M)	3.1E-03	4.65E-01	3.1E-03
Total HCO <sub>3</sub> <sup>-</sup> (M)	3.15E-03	4.35E-03	4.40E-05
pH	8.1	8.3	6.5
Ionic Strength (M)	0.007	0.60	0.004
Salinity (g L <sup>-1</sup> )	0.45	29.6	0.30

## APPENDIX C: Supporting Information for Chapter 5

### C.2 FIGURES

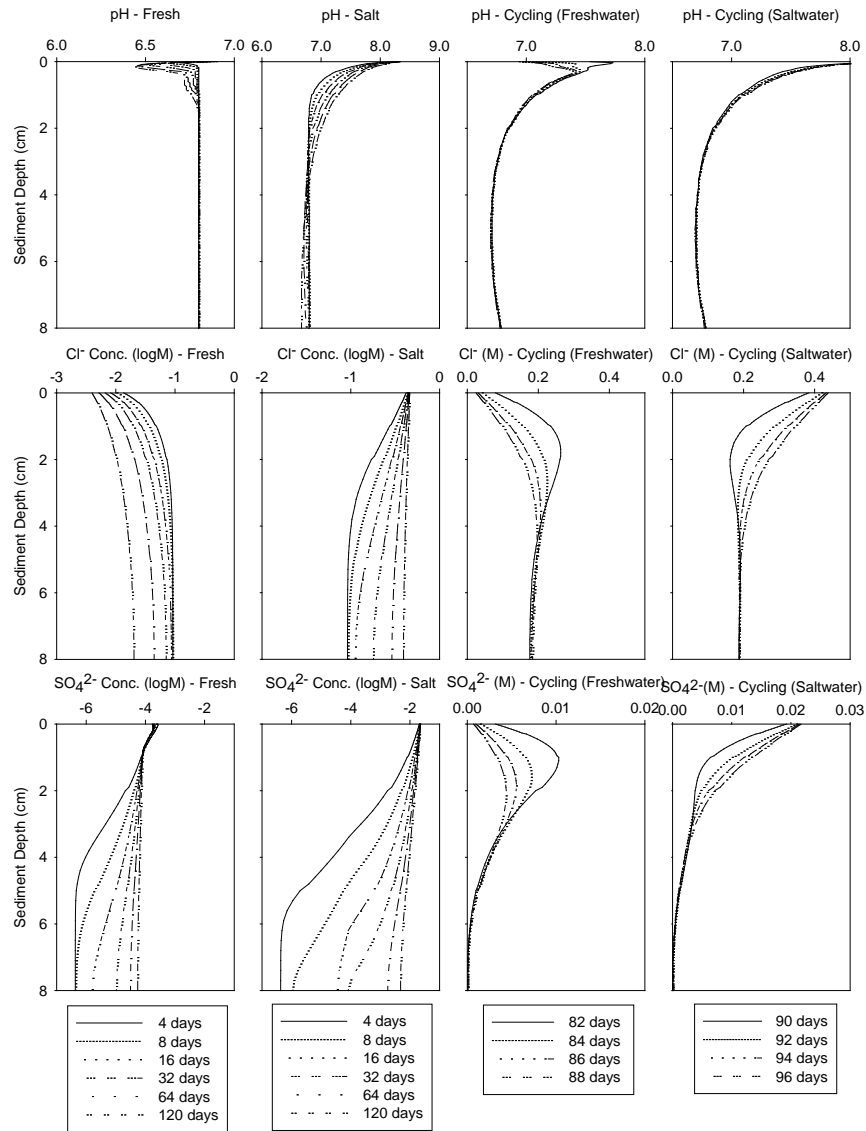


Figure C.1 Transient pH, Cl<sup>-</sup> and SO<sub>4</sub><sup>2-</sup> profiles developments in sediment porewaters under freshwater, saltwater, and cycling water conditions.

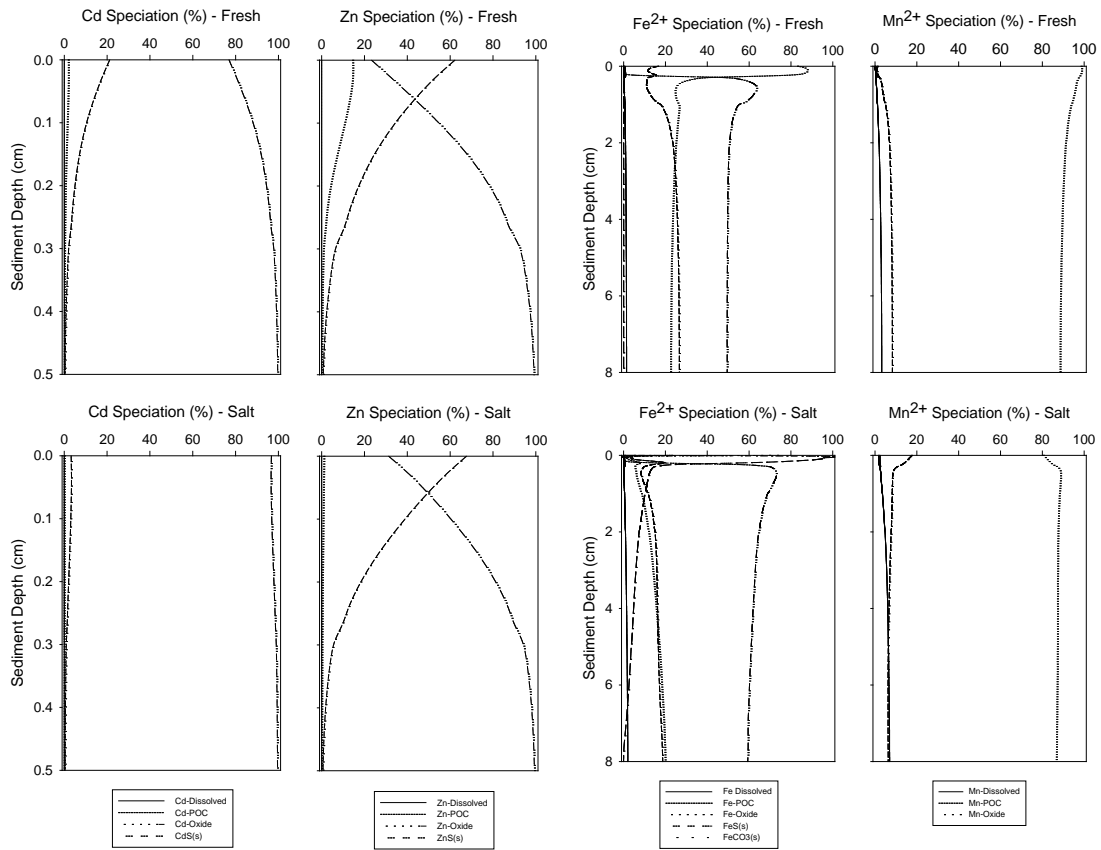


Figure C.2 Phase distribution of Cd, Zn, Fe and Mn to dissolved, particulate organic carbon, oxides, and sulfide (carbonate for Fe<sup>2+</sup>) under fresh water condition. The metals distributions are similar for other overlying water conditions.

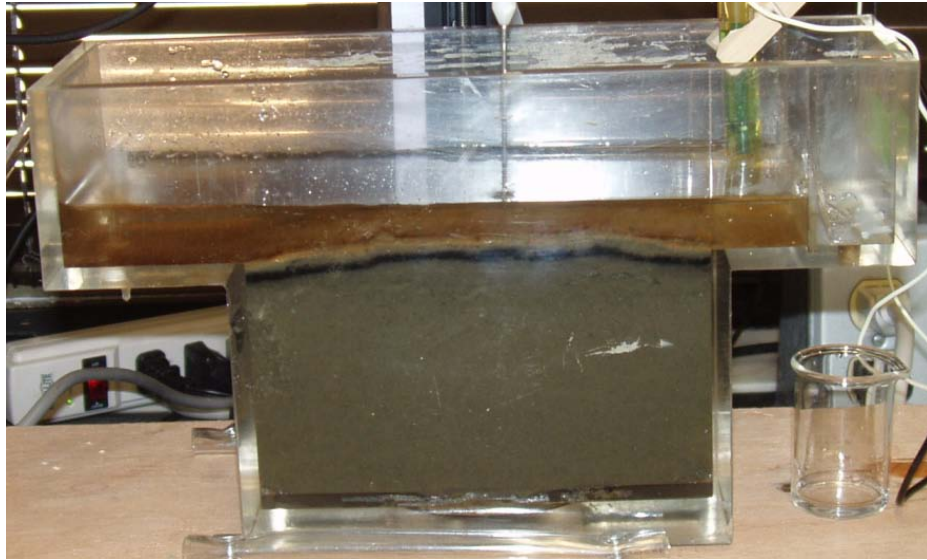


Figure C.3 T-Cell exposed to fresh water. Note the dark precipitates right below the surficial sediments.

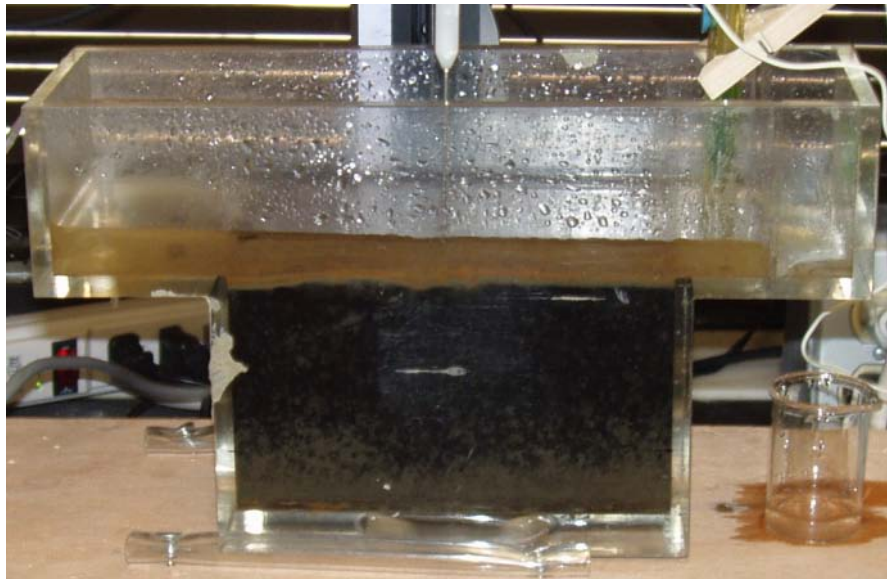


Figure C.4 T-Cell exposed to Salt water. Note the dark precipitates covering the whole sediment depth.

## C.2 TABLES

Table C.1 Sediment Characteristics

	Target Species	Values
Porewater	pH	6.9
	Conductivity (mS cm <sup>-1</sup> )	8.40
	ORP (mV, SHE)	-44.9
	Fe <sup>2+</sup> (M)	2.10 E-3
	Mn <sup>2+</sup> (M)	1.03 E-4
	Cd <sup>2+</sup> (M)	1.33 E-7
	Zn <sup>2+</sup> (M)	BDL <sup>(a)</sup>
	Ca <sup>2+</sup> (M)	8.53 E-3
	Mg <sup>2+</sup> (M)	2.49 E-3
	K <sup>+</sup> (M)	4.19 E-4
	Na <sup>+</sup> (M)	4.82 E-2
	S <sup>2-</sup> (M)	BDL <sup>(a)</sup>
	Cl <sup>-</sup> (M)	9.20 E-2
	SO <sub>4</sub> <sup>2-</sup> (M)	4.29 E-7
Bulk Sediment	Water Content (%)	55.77 (0.34)
	Organic Carbon (%)	7.0 (2.8)
	AVS (μmol g <sup>-1</sup> )	88.7 (6.2)
	Total Fe (mg g <sup>-1</sup> )	53.42 (6.65)
	Total Mn (mg g <sup>-1</sup> )	0.24 (0.022)
	Total Zn (mg g <sup>-1</sup> )	0.70 (0.087)
	Total Cd (mg g <sup>-1</sup> )	4.6 (0.16)
	H.H. <sup>(b)</sup> extractable Fe (mg g <sup>-1</sup> )	21.8 (0.75)
	H.H. <sup>(b)</sup> extractable Mn (mg g <sup>-1</sup> )	0.23 (0.056)
	H.H. <sup>(b)</sup> extractable Zn (mg g <sup>-1</sup> )	0.65 (0.07)
	H.H. <sup>(b)</sup> extractable Cd (mg g <sup>-1</sup> )	11.18 (2.09)
	SEM Zn (μmol g <sup>-1</sup> )	8.48 (0.76)
	SEM Cd (μmol g <sup>-1</sup> )	41.12 (1.84)
	Oxalate extractable Fe <sup>2+</sup> (mg g <sup>-1</sup> )	3.05 (0.07)
Oxalate extractable Fe <sup>3+</sup> (mg g <sup>-1</sup> )	20.85 (1.22)	

(a) H.H. Hydroxylamine Hydrochloride.

(b) BDL : below detection limit (1.0E-6 M)

## APPENDIX D: Metal – Inorganic Ligands Complexation Reactions

Reaction	Log K <sub>L</sub> (25°C)
$\{\text{Ca}^{2+}\} + \{\text{OH}^{-}\} = \{\text{Ca}(\text{OH})^{+}\}$	1.15
$\{\text{Ca}^{2+}\} + \{\text{CO}_3^{2-}\} = \{\text{CaCO}_3\}$	3.2
$\{\text{Ca}^{2+}\} + \{\text{H}^{+}\} + \{\text{CO}_3^{2-}\} = \{\text{Ca}(\text{HCO}_3)^{+}\}$	11.6
$\{\text{Ca}^{2+}\} + \{\text{SO}_4^{2-}\} = \{\text{Ca}(\text{SO}_4)\}$	2.31
$\{\text{Mg}^{2+}\} + \{\text{OH}^{-}\} = \{\text{Mg}(\text{OH})^{+}\}$	1.15
$\{\text{Mg}^{2+}\} + \{\text{CO}_3^{2-}\} = \{\text{MgCO}_3\}$	3.2
$\{\text{Mg}^{2+}\} + \{\text{H}^{+}\} + \{\text{CO}_3^{2-}\} = \{\text{Mg}(\text{HCO}_3)^{+}\}$	11.6
$\{\text{Mg}^{2+}\} + \{\text{SO}_4^{2-}\} = \{\text{Mg}(\text{SO}_4)\}$	2.31
$\{\text{Mn}^{2+}\} + \{\text{OH}^{-}\} = \{\text{Mn}(\text{OH})^{+}\}$	3.4
$\{\text{Mn}^{2+}\} + 2\{\text{OH}^{-}\} = \{\text{Mn}(\text{OH})_2\}$	5.8
$\{\text{Mn}^{2+}\} + 3\{\text{OH}^{-}\} = \{\text{Mn}(\text{OH})_3^{-}\}$	7.2
$\{\text{Mn}^{2+}\} + 4\{\text{OH}^{-}\} = \{\text{Mn}(\text{OH})_4^{2-}\}$	7.7
$\{\text{Mn}^{2+}\} + \{\text{H}^{+}\} + \{\text{CO}_3^{2-}\} = \{\text{Mn}(\text{HCO}_3)^{+}\}$	12.1
$\{\text{Mn}^{2+}\} + \{\text{SO}_4^{2-}\} = \{\text{Mn}(\text{SO}_4)\}$	2.31
$\{\text{Mn}^{2+}\} + \{\text{Cl}^{-}\} = \{\text{MnCl}^{+}\}$	0.6
$\{\text{Fe}^{2+}\} + \{\text{OH}^{-}\} = \{\text{Fe}(\text{OH})^{+}\}$	4.5
$\{\text{Fe}^{2+}\} + 2\{\text{OH}^{-}\} = \{\text{Fe}(\text{OH})_2\}$	7.4
$\{\text{Fe}^{2+}\} + 3\{\text{OH}^{-}\} = \{\text{Fe}(\text{OH})_3^{-}\}$	11.0
$\{\text{Fe}^{2+}\} + \{\text{SO}_4^{2-}\} = \{\text{Fe}(\text{SO}_4)\}$	2.2
$\{\text{Zn}^{2+}\} + \{\text{OH}^{-}\} = \{\text{Zn}(\text{OH})^{+}\}$	5.0
$\{\text{Zn}^{2+}\} + 2\{\text{OH}^{-}\} = \{\text{Zn}(\text{OH})_2\}$	11.1
$\{\text{Zn}^{2+}\} + 3\{\text{OH}^{-}\} = \{\text{Zn}(\text{OH})_3^{-}\}$	13.6
$\{\text{Zn}^{2+}\} + 4\{\text{OH}^{-}\} = \{\text{Zn}(\text{OH})_4^{2-}\}$	14.8
$\{\text{Zn}^{2+}\} + \{\text{SO}_4^{2-}\} = \{\text{Zn}(\text{SO}_4)\}$	2.1
$\{\text{Zn}^{2+}\} + 2\{\text{SO}_4^{2-}\} = \{\text{Zn}(\text{SO}_4)_2^{2-}\}$	3.1
$\{\text{Zn}^{2+}\} + \{\text{Cl}^{-}\} = \{\text{ZnCl}^{+}\}$	0.4
$\{\text{Zn}^{2+}\} + 2\{\text{Cl}^{-}\} = \{\text{ZnCl}_2\}$	0.2
$\{\text{Zn}^{2+}\} + 3\{\text{Cl}^{-}\} = \{\text{ZnCl}_3^{-}\}$	0.5

Reaction	Log K <sub>L</sub> (25°C)
$\{\text{Ni}^{2+}\} + \{\text{OH}^{-}\} = \{\text{Ni}(\text{OH})^{+}\}$	4.1
$\{\text{Ni}^{2+}\} + 2\{\text{OH}^{-}\} = \{\text{Ni}(\text{OH})_2\}$	9.0
$\{\text{Ni}^{2+}\} + 3\{\text{OH}^{-}\} = \{\text{Ni}(\text{OH})_3^{-}\}$	12.0
$\{\text{Ni}^{2+}\} + \{\text{SO}_4^{2-}\} = \{\text{Ni}(\text{SO}_4)\}$	2.3
$\{\text{Ni}^{2+}\} + \{\text{Cl}^{-}\} = \{\text{NiCl}^{-}\}$	0.6
$\{\text{Pb}^{2+}\} + \{\text{OH}^{-}\} = \{\text{Pb}(\text{OH})^{+}\}$	6.3
$\{\text{Pb}^{2+}\} + 2\{\text{OH}^{-}\} = \{\text{Pb}(\text{OH})_2\}$	10.9
$\{\text{Pb}^{2+}\} + 3\{\text{OH}^{-}\} = \{\text{Pb}(\text{OH})_3^{-}\}$	13.9
$\{\text{Pb}^{2+}\} + \{\text{SO}_4^{2-}\} = \{\text{Pb}(\text{SO}_4)\}$	2.8
$\{\text{Pb}^{2+}\} + \{\text{Cl}^{-}\} = \{\text{PbCl}^{-}\}$	1.6
$\{\text{Pb}^{2+}\} + 2\{\text{Cl}^{-}\} = \{\text{PbCl}_2\}$	1.8
$\{\text{Pb}^{2+}\} + 3\{\text{Cl}^{-}\} = \{\text{PbCl}_3^{-}\}$	1.7
$\{\text{Pb}^{2+}\} + 4\{\text{Cl}^{-}\} = \{\text{PbCl}_4^{-}\}$	1.4
$\{\text{Cd}^{2+}\} + \{\text{OH}^{-}\} = \{\text{Cd}(\text{OH})^{+}\}$	3.9
$\{\text{Cd}^{2+}\} + 2\{\text{OH}^{-}\} = \{\text{Cd}(\text{OH})_2\}$	7.6
$\{\text{Cd}^{2+}\} + \{\text{SO}_4^{2-}\} = \{\text{Cd}(\text{SO}_4)\}$	2.3
$\{\text{Cd}^{2+}\} + 2\{\text{SO}_4^{2-}\} = \{\text{Cd}(\text{SO}_4)_2^{2-}\}$	3.2
$\{\text{Cd}^{2+}\} + \{\text{Cl}^{-}\} = \{\text{CdCl}^{+}\}$	2.0
$\{\text{Cd}^{2+}\} + 2\{\text{Cl}^{-}\} = \{\text{CdCl}_2\}$	2.6
$\{\text{Cd}^{2+}\} + 3\{\text{Cl}^{-}\} = \{\text{CdCl}_3^{-}\}$	2.4
$\{\text{Cd}^{2+}\} + 4\{\text{Cl}^{-}\} = \{\text{CdCl}_4^{2-}\}$	1.7

## APPENDIX E: Microcosm Tracer Test

To characterize the overlying water hydraulics of microcosm (T-cell) and to know the effect of overlying water aeration, tracer test was conducted with food coloring. Few drops of food coloring are well mixed in 2 L of water. The concentrations of dyed water were measured by spectrophotometer (absorbance at 500 nm) and the response was as follows.

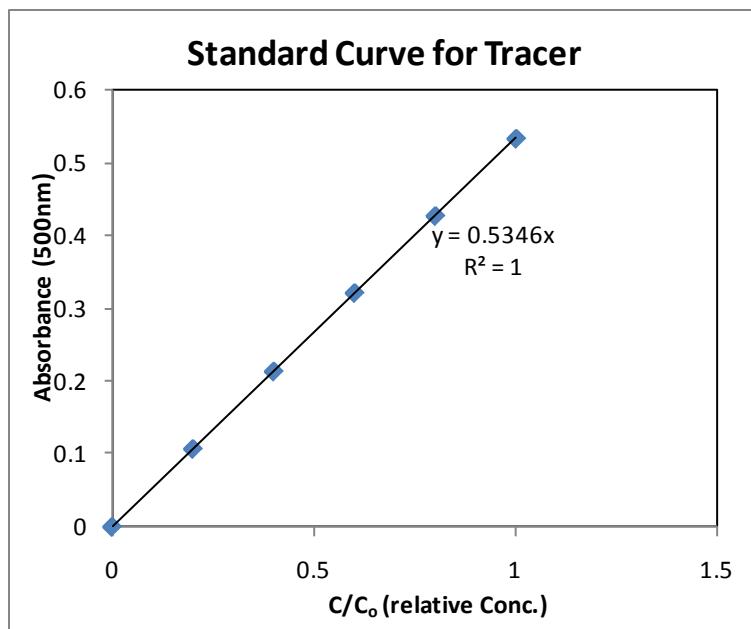


Figure E.1 Standard curve for food coloring.

Two microcosms (T-cell) were filled with sand and distilled water was continuously pumped with water for 2 days to stabilize the flow and to settle down suspended sand particles. One of the microcosms was gently aerated without disturbing sand and the other was not aerated. The depth and volume of overlying water depth was 1.5 cm and 288 mL, respectively. Dyed water was continuously pumped (step input) to

the microcosm with a flow rate of 1.41mL/min for 8 hours. The flow rate is measured with graduated mass cylinder and timer. The calculated hydraulic residence time of a tracer is 3.4 hours.

From control volume mass balance, the effluent dye concentration could be calculated as follows

$$\frac{C_e}{C_o} = 1 - \exp(-k_r / t)$$

where  $C_e$  is the effluent dye concentration,  $C_o$  is the influent dye concentration,  $k_r$  is the overlyingwater hydraulic residence time,  $t$  is the time. Following figure shows the measured effluent tracer concentration when the overlying water is aerated and when it is not aerated.

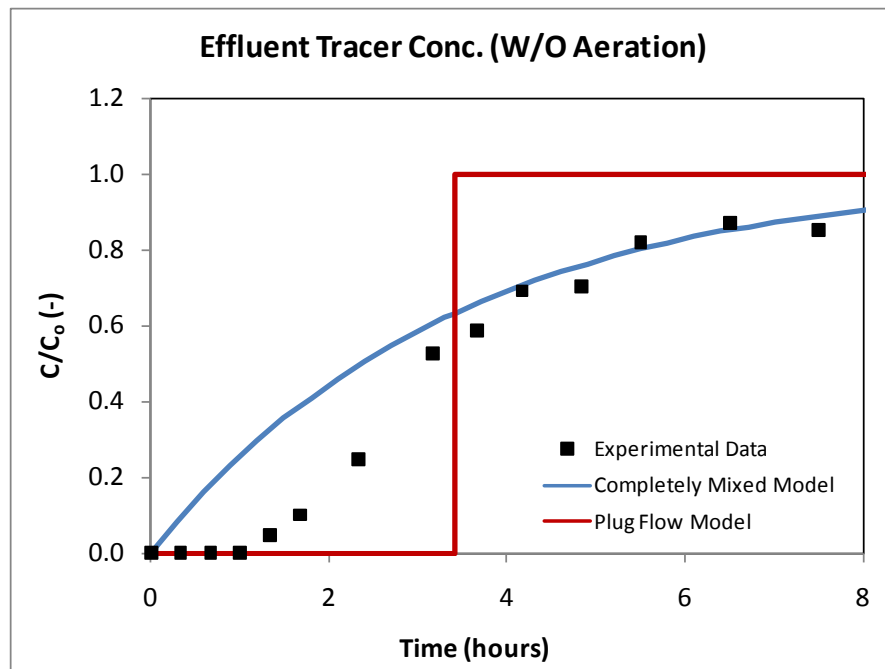


Figure E.2 Tracer test without overlyingwater aeration.

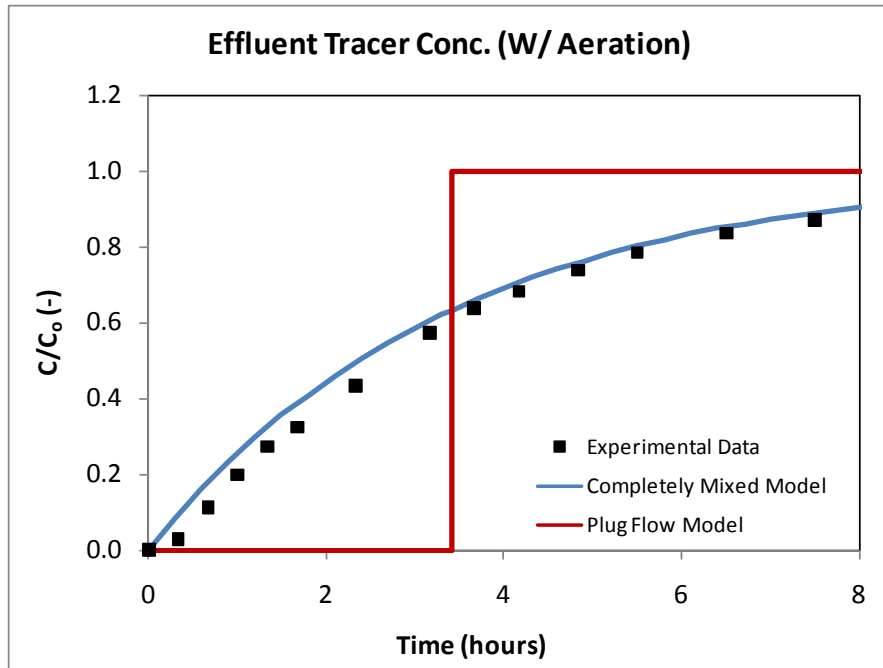


Figure E.3 Tracer test with overlying water aeration.

Non ideal behavior of tracer was observed when the overlying water was not aerated while the reactor behaved similar with a completely stirred reactor when it was aerated. Hence, the overlying waters were gently aerated in all microcosms to facilitate mixing the overlying water homogeneously as well as to transfer the oxygen to the overlying water.

## APPENDIX F: Dissolved Organic Carbon Complexation with Metals

### F.1 THE EFFECT OF DISSOLVED ORGANIC CARBON ON METALS RELEASE

In both resuspension and microcosm experiments, dissolved organic carbon concentrations were characterized with ultraviolet absorbance at 270 nm. The concentrations of DOC were around 4 mg/L in resuspension experiments (Figure A.3) and were less than 2 mg L<sup>-1</sup> and 20 mg L<sup>-1</sup> in the overlying water and sediment porewater, respectively, for microcosm experiments (Figure 4.4, Figure B.5). The potential for this concentration of organic carbon to influence metals speciation (organic complexation was evaluated with WinHumic V (<http://www.lwr.kth.se/english/OurSoftware/WinHumicV/index.htm>). The model is based on the Humic Ion-Binding Model V, originally created by Dr. Edward Tipping in 1992.

DOC was modeled as colloidal Fulvic acid. This may overestimate DOC-metal complex because 65% of DOC was typically considered as active as colloidal FA (Thakali et al., 2006). Temperature was fixed at 25 °C. From WHAM V modeling analysis, Zn and Cd complexation with DOC was not significant in all experimental conditions. Table F.1 summarizes the input parameters to investigate Zn speciation in Anacostia River sediment resuspension experiment.

Table F.1 Simulation conditions for resuspension experiments

Parameters	Values	Parameters	Values
DOC (mg L <sup>-1</sup> )	4	Na <sup>+</sup> (M)	2.30E-3
Fulvic acid (mg L <sup>-1</sup> )	2.6	SO <sub>4</sub> <sup>2-</sup> (M)	2.0E-3
pH fixed at	6	Cl <sup>-</sup> (M)	2.7E-3
Ca <sup>2+</sup> (M)	4.99E-5	CO <sub>3</sub> <sup>2-</sup> (M)	0
K <sup>+</sup> (M)	5.12E-5	Zn <sup>2+</sup> (M)	3.1E-06
Mg <sup>2+</sup> (M)	2.72E-4		

All parameters were experimentally determined. Measured DOC concentrations were between 3 to 5 mg/L and median is used for simulations. pH was changed from 6.5 to 5.5 and median was used. All other parameters were experimentally measured. The following Zn distribution was predicted at 4 mg/L organic carbon concentration.

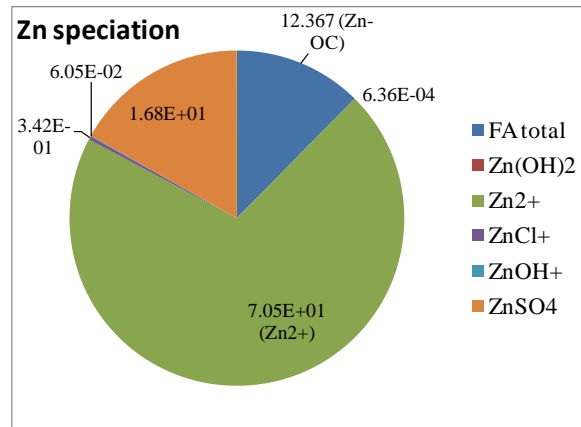


Figure F.1 The distribution of Zn in resuspension experiments.

Similarly, the Cd and Zn complexation with DOC can be investigated for microcosm experiments. Table F.2 summarizes the concentration of ions in both fresh and salt water.

Table F.2 Simulation conditions for microcosm experiments

	Fresh Water	Salt Water
pH	7	8
Ca <sup>2+</sup> (M)	0.00006	0.00905
K <sup>+</sup> (M)	0.00006	0.00883
Mg <sup>2+</sup> (M)	0.000325	0.0487
Na <sup>+</sup> (M)	0.0026	0.39
SO <sub>4</sub> <sup>2-</sup> (M)	0.000145	0.0218
Cl <sup>-</sup> (M)	0.00293	0.439
CO <sub>3</sub> <sup>2-</sup> (M)	0.00021	0.0314
Cd, Zn (μM)	1.0	1.0

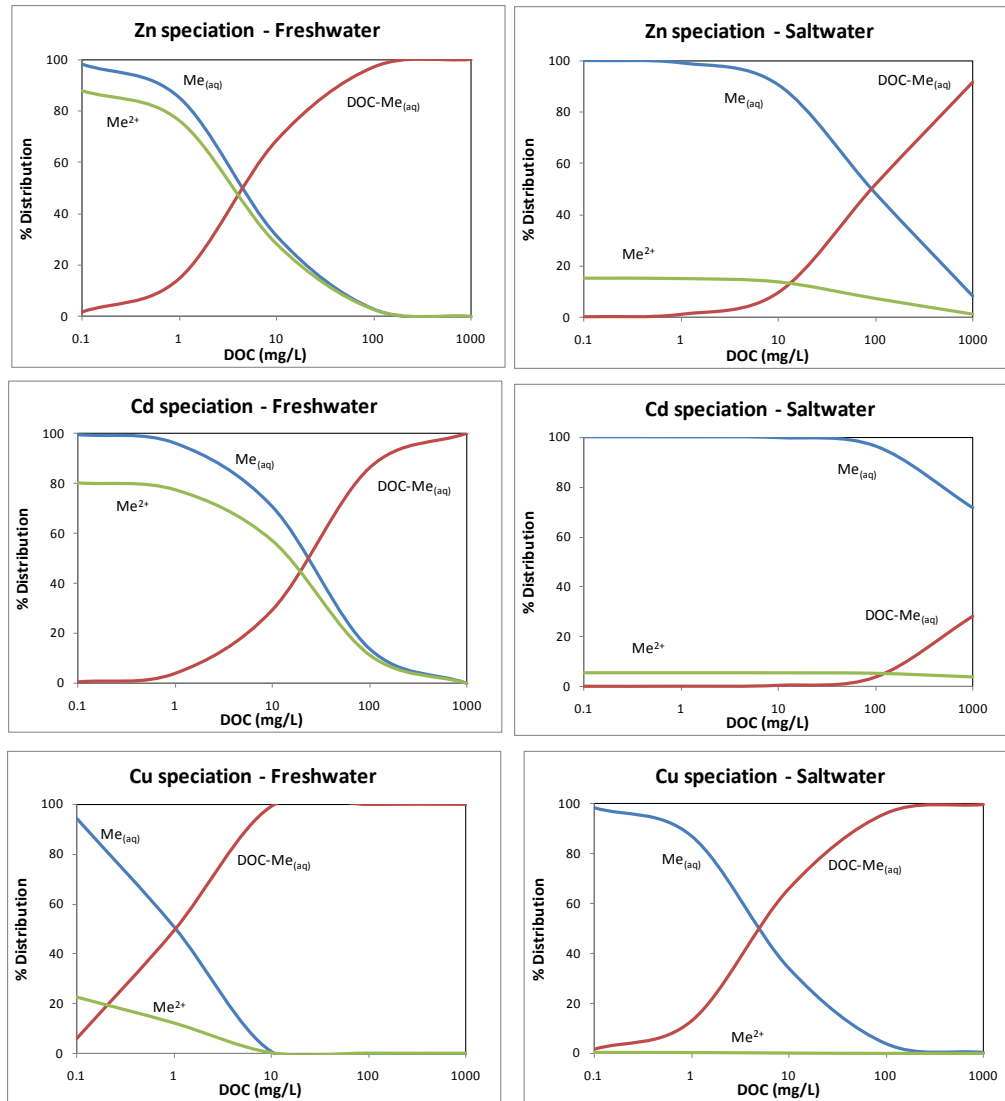


Figure F.2 The DOC dependent distribution of Zn, Cd, and Cu in fresh and saltwater. Cu is simulated to compare the strength of metal complexation with DOC. Typical DOC concentration in the overlying water was less than 3 mg/L only for the first 10 days. The DOC complexation with Cd and Zn with DOC were not significant.

The simulation results are shown in Figure F.2. Dissolved organic carbon concentration in the overlying water was less than 3 mg L<sup>-1</sup> and this concentration only lasted for the first 20 days (Figure 4.4). The results indicate that for the species

simulated in Chapter 4 (Zn and Cd), organic matter at the observed concentrations does not play a significant role in metal speciation. For other metals, notably copper, however, even this level of organic matter will give rise to substantial complexation of the metal. For these species and for higher organic carbon concentrations it is important to include organic carbon complexation in the simulation results in the overlying water.

In sediment porewater, however, organic complexation may not be important even if present at significantly higher concentrations. In these experiments, porewater DOC concentrations were around 15 mg L<sup>-1</sup>. Figure F.3 and F.4 show that even at this DOC concentration, the dissolved metals concentration of Zn and Cd is controlled by sulfide concentrations and metal sulfide solubility products.

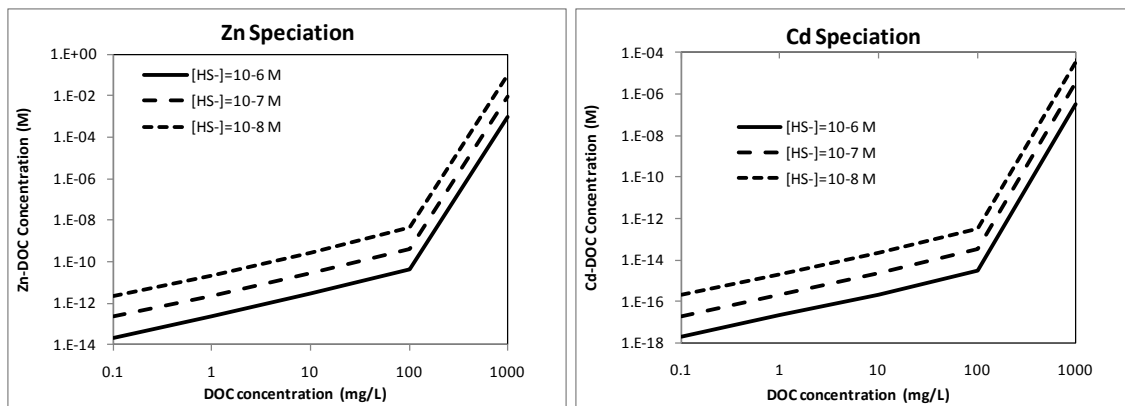


Figure F.3 The metal-DOC complex concentrations in sediment porewater where metal sulfides are present.  $[M^{2+}]$  were calculated from solubility products of metal sulfides when sulfide concentrations were 10E-6,-7,-8M.  $[DOC-M]$  were calculated from the  $K_d$  which were calculated from Figure F.2 in freshwater composition. In anoxic sediments, sulfide minerals control the solubility of dissolved metals concentrations even when DOC concentration is close to 100 mg/L.

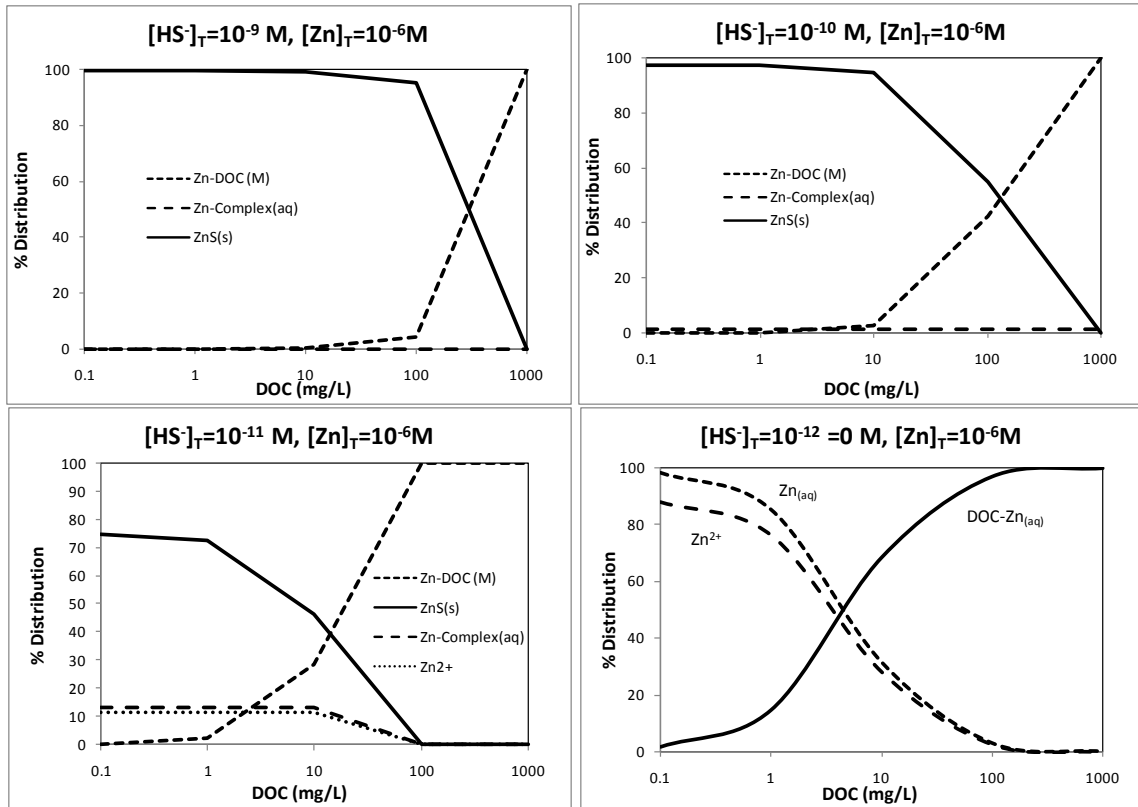
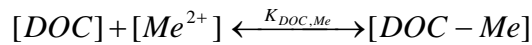


Figure F.4 Zn speciation when  $10^{-6}$  M of Zn is introduced to sediment porewater.  $[\text{HS}^-]$  were changed from  $10^{-9}$  to  $10^{-12}$  M. When  $[\text{HS}^-]$  is greater than  $10^{-10}$  M and when DOC is less than 100 mg/L, almost all Zn would be precipitated as  $\text{ZnS}_{(s)}$ . However, when  $[\text{HS}^-]$  is less than  $10^{-12}$  M,  $\text{ZnS}_{(s)}$  will not precipitate and aqueous phase complexation will determine Zn speciation.

## F.2 EXTENDING THE PROPOSED MODEL TO OTHER SITES WHERE HIGH DISSOLVED ORGANIC CARBON CONCENTRATIONS ARE EXPECTED.

For higher dissolved organic carbon concentrations it is important to include the effect of DOC on the fraction of truly dissolved metal in the overlying water. DOC has been modeled as composed of eight fractions, each with a characteristic  $\text{pK}_a$  which are evenly and widely distributed in the pH range of 3 to 10 (Tipping, 1998). By this model,

DOC doesn't change its surface characteristics dramatically in the neutral pH (7 to 8). This may allow us to model the DOC as though it were another inorganic ligands, such as Cl<sup>-</sup> and SO<sub>4</sub><sup>2-</sup>, with an effective DOC metal partition coefficient calculated by the WinHumic V model (Tipping, 1994). Simple DOC – metal complexation reaction can be defined as follows.



Complexation constant  $K_{DOC,Me}$  [L mg<sup>-1</sup>] can be estimated as follows.

$$K_{DOC,Me} = \frac{[DOC - Me]}{[DOC][Me^{2+}]} = \frac{1}{[DOC]} \frac{[DOC - Me]}{[Me^{2+}]} = \frac{1}{[DOC]} K_d$$

$K_d$  [-] can be calculated from WinHumic V and values are included in Table F.1 for 1, 10, 50 and 100 mg L<sup>-1</sup> DOC. The resulting complexation constant  $K_{DOC,Me}$  [L mg<sup>-1</sup>] by this approach is also shown in Table F.1. 10 mg L<sup>-1</sup> DOC were not different from the earlier modeling neglecting DOC although some deviation would be expected at 50 and 100 mg L<sup>-1</sup> DOC. Even at these higher DOC levels, however, the effects of DOC on metal speciation are only significant in the overlying water and not within the sediments, where association with sulfides dominates the metal solubility.

Table F.3  $K_{DOC,Me}$  from WinHumic V (WHAM V)

DOC (mg L <sup>-1</sup> )	Zn		Cd	
	Freshwater	Saltwater	Freshwater	Saltwater
1	1.92E-01	6.91E-02	4.89E-02	7.05E-03
10	2.43E-01	6.94E-02	5.09E-02	7.06E-03
50	3.04E-01	7.02E-02	6.00E-02	7.08E-03
100	3.60E-01	7.08E-02	7.58E-02	7.06E-03

## References

- Adriano, D.C., 2001. Trace elements in terrestrial environments. Springer. New York. P56.
- Allen H.E., Fu G. and Deng B., 1993. Analysis of acid volatile sulfide(AVS) and simultaneously extracted metals(SEMs) for the estimation of potential toxicity in aquatic sediments. *Environ. Toxicol. Chem.* 12: 1441-1453
- Ankley G.T., Di Toro DM, Hansen DJ., Berry WJ. 1996. Technical basis and proposal for deriving sediment quality criteria for metals. *Environ. Toxicol. Chem.* 15:2056-2066
- Archer, D., Kheshgi, H., and Maier-Reimer E., 1998. Dynamics of fossil fuel CO<sub>2</sub> neutralization by marine CaCO<sub>3</sub>. *Global Biogeochemical Cycles.* 12:259-276
- Atkinson, CA., Jolly, DF., and Simpson, SL., 2007. Effect of overlying water pH, dissolved oxygen, salinity and sediment disturbances on metal release and sequestration from metal contaminated marine sediments. *Chemosphere*, 69:1428-1437
- Audry, S., Blanc, G., Schäfer, J., Chaillou, G., Robert, S., 2006. Early diagenesis of trace metals (Cd, Cu, Co, Ni, U, Mo, and V) in the freshwater reaches of a macrotidal estuary. *Geochim. Cosmochim. Acta.* 70:2264-2282.
- Baumann, E.W. 1973. Determination of pH in concentrated salt solutions. *Anal. Chim. Acta* 64: 284 - 288.
- Berner RA. 1980. Early Diagenesis: A Theoretical Approach. Princeton Univ. Press.
- Berry WJ, Boothman WS, Serbst JR and Edwards PA, 2004. Predicting the toxicity of chromium in sediments. *Environ. Toxicol. Chem.* 23:2981-2992
- Berry WJ, Hansen DJ, Mahony DL, Robson DM, Di Toro DM, Shipley BP, Rogers B, Corbin JM, Boothman WS. 1996. Predicting the toxicity of metal spiked laboratory sediments using acid-volatile sulfide and interstitial water normalizations. *Environ. Toxicol. Chem.* 15:2067-2079
- Boudreau BP. 1991. Modeling the sulfide-oxygen reaction and associated pH gradients in porewaters. *Geochim. Cosmochim. Acta*, 55:5145-159
- Boudreau, B.P., 1997. Diagenetic Models and Their Implementation: Modeling Transport Reactions in Aquatic Sediments. Springer-Verlag, New York.
- Boudreau, B.P. 1987. A steady state diagenetic model for dissolved carbonate species and pH in the porewaters of oxic and suboxic sediments. *Geochim. Cosmochim. Acta.* 51:1985-1996

- Boussrhrine N., Gasser UG., Jeanroy E., and Berthelin J. 1999. Bacterial and chemical reductive dissolution of Mn-, Co-, Cr- and Al-substituted goethites. *Geomicrobiology J.* 16:245-258
- Bowles, KC., Bell, RA., Ernste, MJ., Kramer, JR., Manolopoulos, HM., and Ogden, N., 2002. Synthesis and characterization of metal sulfide clusters for toxicological studies. *Environ. Toxicol. Chem.* 31:693-699
- Bradl HB., 2005. Heavy metals in the environment: origin, interaction and remediation. *Interface science and technology*. Volume 6. Elsevier Academic press..
- Brendel, PJ., Luther, GW., 1995. Development of a gold amalgam voltammetric microelectrodes for the determination of dissolved Fe, Mn, O<sub>2</sub>, and S(-II) in porewaters of marine and freshwater sediments. *Environ. Sci. Tech.* 29:751-761
- Brouwer, H., and Murphy, TP., 1994. Diffusion method for the determination of acid-volatile sulfides (AVS) in sediment. *Environ. Toxicol. Chem.* 13:1273-1275
- Brown, P.N., Byrne, G. D., Hindmarsh, A.C., 1989. VODE: A Variable Coefficient ODE Solver. *J. Sci. Stat. Comput.* 10: 1038-1051.
- Burden, R., Faires J.D., 2005. Numerical Analysis. 8th edition. Thomson Brooks/Cole.
- Burton, E.D., Bush, R.T. and Sullivan, L.A. 2006 Acid-volatile sulfide oxidation in coastal flood plain drains: iron-sulfur cycling and effects on water quality. *Environ. Sci. Technol.* 40: 1217-1222
- Burton, ED., Bush, RT, and Sullivan LA., 2006. Reduced inorganic sulfur speciation in drain sediments from acid sulfate soil landscapes. *Environ. Sci. Technol.* 40:888-893
- Cai, W-J. , P. Zhao, S. M. Theberge, A. Witter, Y. Wang, G. Luther III. 2002. Porewater redox species, pH and *p* CO<sub>2</sub> in aquatic sediments—Electrochemical sensor studies in Lake Champlain and Sapelo Island . In “Environmental Electrochemistry: Analyses of Trace Element Biogeochemistry” ACS Symposium Volume on Electrochemistry. M. Taillefert and T. Rozan (ed.)
- Cai, WJ., and Wang YC., 1998. The chemistry, fluxes, and sources of carbon dioxide in the estuarine waters of the Satilla and Altamaha Rivers, Georgia. *Limnol. Oceanogr.*, 43:657-668
- Canavan, RW, Van Cappellen, P., Zwolsman, JJG, Van Den Berg, GA., Slomp, CP., 2007. Geochemistry of trace metals in a fresh water sediment: Field results and diagenetic modeling. *Science of Total Environment.* 381:263-279
- Cantwell, MG., Burgess, RM., and Kester, DR., 2002. Release and phase partitioning of metals from anoxic estuarine sediments during periods of simulated resuspension. *Environ. Sci. Technol.* 36:5328-5334

- Cappuyns, V., Swennen, R., 2005. Kinetics of element release during combined oxidation and pHstat leaching of anoxic river sediments. *Appl. Geochem.* 20:1169-1179.
- Carbonaro R.F., Mahony J.D., Water A.D., Halper E.B., Di Toro D.M., 2005. Experimental and modeling investigation of metal release from metal-spiked sediments. *Environ. Toxicol. Chem.* 24:3007-3019.
- Chapman P.M., Wang F., Janssen C., Perssone G., Allen H.E., 1998. Ecotoxicology of metals in aquatic sediments binding and release, bioavailability, risk assessment, and remediation. *Can. J. Fish. Aquat. Sci.* 55: 2221-2243.
- Chapman PM, Wang F, Adams WJ, and Green A. 1999. Appropriate applications of sediment quality values for metals and metalloids. *Environ. Sci. Technol.* 33:3937-3941
- Chapman PM, Wang F, Janssen C, Perssone G, and Allen HE. 1998. Ecotoxicology of metals in aquatic sediments binding and release, bioavailability, risk assessment, and remediation. *Can. J. Fish. Aquat. Sci.* 55:2221-2243
- Chapman, P.M. and Wang, F., 2001. Assessing sediment contamination in estuaries, *Environ. Toxicol. Chem.* 20:3-22
- Choi JH, Park SS and Jaffe PR. 2006. Simulating the dynamics of sulfur species and zinc in wetland sediments. *Ecological Modeling.* 199:315-323
- Chou, L., Garrels, R.M., Wollast, R., 1989. Comparative study of the kinetics and mechanisms of dissolution of carbonate minerals. *Chem. Geol.* 78:269-282.
- Cooper DC, Neal AL, Kukkadapu RK, Brewe D, Coby A. and Picadal FW. 2005. Effects of sediment iron mineral composition on microbially mediated changes in divalent metal speciation:importance of ferrihydrite. *Geochim. Cosmochim. Acta*, 69:1739-1754
- Davis, J.A., Coston, J.A., Kent D.B., Fuller C.C., 1998. Application of the surface complexation concept to complex mineral assemblages. *Environ. Sci. Technol.* 32: 2820-2828.
- Di Toro D.M., Mahony J.D., Hansen D.J., Scott K.J., Carlson A.R. and Ankley G.T. 1992. Acid-volatile sulfide predicts the acute toxicity of cadmium and nickel in sediments. *Environ. Sci. Technol.* 26: 96–101.
- Di Toro, D.M. Sediment flux modeling. 2001. Wiley-Interscience
- Di Toro, D.M., Mahony, J.D., Gonzalez A.M., 1996. Particle oxidation model of synthetic FeS and sediment acid-volatile sulfide. *Environ. Toxicol. Chem.* 15:2156-2167.

- Di Toro, D.M., Mahony, J.D., Hansen, D.J., Scott, K.J., Hicks, M.B., Mayr, S.M., Redmond, M.S., 1990. Toxicity of cadmium in sediments: the role of acid volatile sulfide. *Environ. Toxicol. Chem.* 9: 1487-1502.
- Di Toro, D.M., Mahony, J.D., Hansen, D.J., and Berry, W.J., 1996. A model of the oxidation of iron and cadmium sulfide in sediments. *Environ. Toxicol. Chem.* 15: 2168-2186.
- Di Toro, DM., Allen, HE., Bergman, HL., Meyer, JS., Paquin, PR., and Santore, RC., 2001. Biotic ligand model of the acute toxicity of metals. 1. Technical basis. *Environ. Toxicol. Chem.* 20:2383-2396
- Di Toro, DM., McGrath, JA., Hansene, DJ., Berry, WJ., and Paquine, PR., 2005. Predicting sediment metal toxicity using a sediment biotic ligand model: methodology and initial application. *Environ. Toxicol. Chem.* 24:2410-2427
- Duffus JH. 2002. "Heavy metals"-a meaningless term?. *Pure Appl. Chem.* 74:793-807.
- Dzombak DA. And Morel FMM. 1990. Surface complexation modeling. Hydrous ferric oxide. Wiley Interscience
- Furrer G, Wehrli B.1996. Microbial reactions, chemical speciation, and multicomponent diffusion in porewaters of a eutrophic lake. *Geochim. Cosmochim. Acta*, 60:2333-2346
- Gao, Y., Kan, A.T., Tomson, M.B., 2003. Critical evaluation of desorption phenomena of heavy metals from natural sediments. *Environ. Sci. Technol.* 37: 5566-5573.
- Grabowski, LA, Houpis JJJ., Woods WI. And Johnson KA. 2001. Seasonal bioavailability of sediment-associated heavy metals along the Mississippi river floodplain. *Chemosphere.* 45:643-651
- Gustafsson, J.P., 2001. Modeling the acid-base properties and metal complexation of humic substances with the Stockholm Humic Model. *Journal of Colloid and Interface Science*, 244: 102-112
- Hansen DJ., Berry WJ., Mahony JD., Boothman WS, Di Toro DM, Robson DL., Ankley GT, Ma D, Yan Q and Pesch CE. 1996. Predicting the toxicity of metal contaminated field sediments using interstitial concentration of metals and acid volatile sulfide normalizations. *Environ. Toxicol. Chem.* 15:2080-2094
- Hart, B.T., 1981. Trace metal complexing capacity of natural waters: a review. *Environ. Technol. Lett.* 2: 95-110.
- Himmelherber, D.W., Taillefert, M., Pennell, K.D., and Hughes, J.B., 2008. Spatial and temporal evolution of biogeochemical processes following in-situ capping of contaminated sediments. *Environ. Sci. Technol.* 42: 4113-4120.

- Hseih, Y.P., Chung, S.W., Tsau, Y.J., Sue, C.T., 2002. Analysis of sulfides in the presence of ferric minerals by diffusion methods. *Chem. Geol.* 182: 195-201.
- Hutchins, CM., Teasdale, PR., Lee, J., and Simpson, SL., 2007. The effect of manipulating sediment pH on the porewater chemistry of copper and zinc – spiked sediments. *Chemosphere.* 69:1089-1099
- Hutchins, CM., Teasdale, PR., Lee, J., and Simpson, SL., 2008. Cu and Zn concentration gradients created by dilution of pH neutral metal-spiked marine sediment: A comparison of sediment geochemistry with direct methods of metal addition. *Environ. Sci. Technol.* 42:2912-2918
- Jaffé, P.R., Wang, S., Kallin, P.L., Smith, S.L., 2001. The dynamics of arsenic in saturated porous medial: fate and transport modeling for deep-water sediments, wetland sediments, and groundwater environments. In: Hellman, R., Wood, S.A. (Eds.), *Water Rock Interactions, Ore Deposits, and Environmental Geochemistry: A tribute to David Crerar, Special Publication, No.7.* The Geochemical society, pp. 379-397
- Jourabchi, P., Van Cappellen, P, and Regnier P., 2005. Quantitative interpretation of pH distributions in aquatic sediments: a reaction-transport modeling approach. *American Journal of Science.* 305: 919-956
- Kalnejais, L.H., Martin, W.R., Signell, R.P., Bothner, M.H., 2007. Role of sediment resuspension in the remobilization of particulate-phase metals from coastal sediments. *Environ. Sci. Technol.* 41: 2282-2288.
- Kinniburgh, DG., Milne, CJ., Benedetti, MF, Pinheiro, JP, Filius, J., Koopal, LK., and Reimdsdijk, WH., 1996. Metal ion binding by humic acid: application of the NICA-Donnan Model. *Environ. Sci. Technol.* 30:1687-1698
- Komlos, J., Moon, HS., and Jaffé. P.R., 2008. Effect of Sulfate on the Simultaneous Bioreduction of Iron and Uranium. *Journal of Environmental Quality.* 37:2058-2062
- Lee BG, Lee JS, Luoma SN., Choi HJ, and Koh CH. 2000. Influence of acid volatile sulfide and metal concentrations on metal bioavailability to marine invertebrates in contaminated sediment. *Environ. Sci. Technol.* 34:4517-4523, b
- Li, YH. and Gregory, S., 1974. Diffusion of ions in sea water and in deep-sea sediments. *Geochim. Cosmochim. Acta.* 38:703-714
- Liber K, Call DJ, Markee TP, Schmude JL., Balcer MD, Whiteman FW and Ankley GT., 1996. Effects of acid volatile sulfide on zinc bioavailability and toxicity to benthic macroinvertebrates: a spiked sediment field experiment. *Environ. Toxicol. Chem.* 15:2113-2125

- Liu, C., Jay, J.A., Ika, R., Shine, J.P., and Ford, T.E., 2001. Capping efficiency for metal-contaminated marine sediment under conditions of submarine groundwater discharge. *Environ. Sci. Technol.* 35:2334-2340.
- Liu, WC, Chang, SW., Jiann, KT., Wen, LS., and Lu KK. 2007. Modeling diagnosis of heavy metal (copper) transport in an estuary. *Sci Total Environ*, 388:234-249
- Lofts, S. and Tipping, E., 1998. An assemblage model for cation binding by natural particulate matter. *Geochim. Cosmochim. Acta*, 62:2609-2625
- Lofts, S., Spurgeon, DJ., Svendsen, C. and Tipping, E. 2004. Deriving soil critical limits for Cu, Zn, Cd, and Pb: a method based on free ion concentrations. *Environ. Sci. Technol.* 38:3623-3631
- Long ER. And Morgan LG. 1991. The potential for biological effects of sediment-sorbed contaminants tested in the national status and trends program. NOAA Technical Memorandum NOSOMA 52. National Oceanic and Atmospheric Administration, Seattle, WA. USA.
- Lors, C., Tiffreau, C., Laboudigue, A., 2004. Effects of bacterial activities on the release of heavy metals from contaminated dredged sediments. *Chemosphere*, 56: 619-630.
- Loft, S. and Tipping, E., 1998. An assemblage model for cation binding by natural particulate matter. *Geochim. Cosmochim. Acta*, 62:2609-2625
- Lovely DR., 1991. Dissimilatory Fe(III) and Mn(IV) reduction. *Microbial. Rev.* 55:259-287
- Lovely, DR and Klug MJ.1986. Model for the distribution of sulfate reduction and methanogenesis in freshwater sediments. *Geochim. Cosmochim. Acta*, 50:11-18
- Lowson, R.T., 1982. Aqueous oxidation of pyrite by molecular oxygen. *Chem. Rev.* 82: 461-499
- Luoma SN and Davis JA. 1983. Requirements for modeling trace metal partitioning in oxidized estuarine sediments. *Mar. Chem.* 12:159-181
- MacDonald, DD., Carr RS, Calder FD, Long ER and Ingersoll CG. 1996. Development and evaluation of sediment quality guidelines for Florida coastal waters. *Ecotoxicology* 5:253-278.
- Madigan, M.T., Martinko, J.M., Parker J., 2003. Brock biology of microorganisms. Tenth edition. Prentice Hall.
- Mahony JD, Di Toro DM, Gonzalez AM, Curto M, Dilg M, Rosa LDD, and Sparrow LA ,1996, Partitioning of metals to sediment organic carbon. *Environ. Toxicol. Chem.* 15: 2187-2197
- Morel, F.M.M., 1993. Principles of Aquatic Chemistry, Wiley-Interscience, New York.

- Mosley, LM., Husheer, SLG., Hunter, KA., 2004. Spectrophotometric pH measurement in estuaries using thymol blue and m-cresol purple. *Mar. Chem.*, 91:175-186
- Nelson M.B. 1978. Kinetics and mechanisms of the oxidation of ferrous sulfide. Ph.D thesis. Stanford University, Palo Alto, Ca. USA.
- Peltier E., Dahl, AL., and Gaillard JF. 2005. Metal speciation in anoxic sediments: when sulfides can be construed as oxides. *Environ. Sci. Technol.* 39:311-316
- Persaud D., Jacqumagi R. And Hayton A. 1989. Development of provincial sediment quality guidelines. Ontario Ministry of the Environment. Toronto. ON. Canada.
- Peterson, G.S., Ankley, G.T., and Leonard, E.N., 1996. Effect of bioturbation on metal sulfide oxidation in surficial freshwater sediments. *Environ. Toxicol. Chem.* 15:2147-2155
- Philips, EJP. And Lovely, D.R., 1998. Determination of Fe(II) and Fe(III) in oxalate extracts of sediments. *Soil Sci. Soc. Am. J.*, 51:938-941
- Pivovarov, S., 1998. Acid-base properties and heavy and alkaline earth metal adsorption on the oxide-solution interface: Non-electrostatic model. *Journal of Colloid and Interface Science*, 206: 122-130
- Pritchard, D.W., 1967. What is an estuary; physical viewpoint. In Lauff GH, ed, Estuaries. American Association for the Advancement of Science, Washington, DC, pp 3-5.
- Radovanovic, H., Koelmans, AA. 1998. Prediction of in-situ trace metal distribution coefficients for suspended solids in natural waters. *Environ. Sci. Technol.* 32:753-759
- Reible, D. and Mohanty, S., 2002. A levy flight-random walk model for bioturbation. *Environ. Toxicol. Chem.* 21:875-881
- Reible, D., Lampert, D, Constant, D, Mutch Jr. RD., Zhu, Y., 2006 Active capping demonstration in the Anacostia River, Washington, D.C., *Remediation*, Winter, 39-53
- Reible, D.D., 2000. Contaminated sediment management: Still an oxymoron? *Environmental Progress*, 19: 2 -3
- Riba, I., Valls, AD., Forja, JM., and Gomez-Parra, A., 2004. The influence of pH and salinity on the toxicity of heavy metals in sediment to the estuarine clam *Ruditapes Philippinarum*. *Environ. Toxicol. Chem.* 32:1100-1107
- Rickard, D., Morse JW, 2005. Acid Volatile Sulfide (AVS), *Mar. Chem.* 97:141-197
- Riedel, GF., Sanders, JG., and Osman, RW., 1997. Biogeochemical control on the flux of trace elements from estuarine sediments: water column oxygen concentrations and benthic infauna. *Estuarine, Coastal and Shelf Science.* 44:23-38

- Ringwood, AH. And Keppler CJ., 2002. Water Quality variation and clam growth: Is pH really a non-issue in estuaries?. *Estuaries*, 25:901-907
- Robert, S., Blanc, G., Schäfer, J., Lavaux, G., Abril, G., 2004. Metal mobilization in the Gironde Estuary (France): the role of the soft mud layer in the maximum turbidity zone. *Mar. Chem.* 87:1-13
- Roden, E.E. and Urritia, M.M., 1999. Ferrous iron removal promotes microbial reduction of crystalline iron(III) oxides. *Environ. Sci. Technol.* 33:1847-1853
- Saulnier, I., Mucci, A., 2000. Trace metal remobilization following the resuspension of estuarine sediments: Sauenay Fjord, Canada. *Appl. Geochem.* 15:191-210.
- Schnitzer, M, Kahn SW. Humic substances in the environment. Marcel Dekker; New York, 1972.
- Schulz, K.G., Riebesell, U., Rost, B., Thoms, S., Zeebe R.E., 2006. Determination of the rate constants for the carbon dioxide to bicarbonate inter-conversion in pH-buffered seawater systems. *Mar. Chem.* 100:53-65.
- Schwertmann U. and Taylor RM. 1989. Iron Oxides. In minerals in Soils Environments, 2<sup>nd</sup> ed. Soil Science Society American Journal Book Series No.1 (eds. J.B. Dixon and S.B. Weed), pp 379-438.
- Sevinc Sengor, S., Spycher, NF., Ginn TR., Sani, RK., and Peyton, B., 2007. Biogeochemical reaction-diffusive transport of heavy metals in Lake Coeur d'Alene sediments. *Appl. Geochem*, 22:2569-2594
- Shank, GC., Skrabal, SA., Whitehead, RF., and Kieber, RJ., 2004. Strong copper complexation in an organic-rich estuary: the importance of allochthonous dissolved organic matter. *Mar. Chem.* 88: 21-39
- Shi, Z., Allen, H.E., Di Toro, D.M., Lee, S.Z., Flores Meza, D.M., Lofts, S., 2007. Predicting cadmium adsorption on soils using WHAM VI. *Chemosphere.* 69: 605-612.
- Shine, JP., Ika, R. and Ford TE., 1998. Relationship between oxygen consumption and sediment-water fluxes of heavy metals in coastal marine sediments. *Environ. Toxicol. Chem.* 17:2325-2337
- Simpson S.L., Apte S.C., and Batley G.E. 1998. Effect of short term resuspension events on trace metal speciation in polluted anoxic sediments. *Environ. Sci. Technol.* 32: 620-625
- Simpson S.L., Apte S.C., and Batley G.E. 2000. Effect of short term resuspension events on the oxidation of cadmium, lead, and zinc sulfide phases in anoxic estuarine, *Environ. Sci. Technol.* 34: 4533-4537

- Simpson, S.L., Maher, E.J., and Jolley, D.F., 2004. Processes controlling metal transport and retention as metal-contaminated groundwaters efflux through estuarine sediments. *Chemosphere*. 56:821-831.
- Simpson, S.L., Pryor, I.C., Mewburn, B.R., Batley, G.E., and Jolley, D., 2002. Considerations for Capping Metal-Contaminated Sediments in Dynamic Estuarine Environments. *Environ. Sci. Technol.*, 2002, 36: 3772–3778
- Slaton, N.A., Norman, R.J., Gilmour, J.T., 2001. Oxidation rates of commercial elemental sulfur products applied to an alkaline silt loam from Arkansas. *Soil Sci. Soc. Am. J.* 65: 239-243.
- Smith, S.L. and Jaffé, P.R., 1998. Modeling the transport and reaction of trace metals in water-saturated soils and sediments. *Water Resour. Res.* 34:3135-3147
- Snoeyink VL and Jenkins D. 1980. Water chemistry. Wiley Interscience
- Soetaert, K., Hofmann, A.F., Middelburg, J.J., Meysman, F.J.R. and Greenwood, J. 2007. Reprint of “the effect of biogeochemical processes on pH”. *Mar. Chem.* 106:380-401
- Sorensen J. 1982. Reduction of ferric iron in anaerobic, marine sediment and interaction with reduction of nitrate and sulfate. *App. Environ. Micro.* 43:319-324
- Standard methods, 1998. Standard methods for the examination of water and wastewater, 20th ed.; American Public Health Association: Baltimore, Maryland.
- Stumm W., Morgan J.J., 1996. Aquatic chemistry. Third edition. Wiley Interscience
- Sullivan, J., Ball J., Brick E., Hausmann S., Pilarski G. and Sopcich D. 1985. Report of the technical subcommittee on determination of dredge material suitability of in-water disposal. Wisconsin Department of Natural Resources, Madison, WI. USA
- Tessier, A, Campbell PGC, and Bisson M. 1979. Sequential extraction procedure for the speciation of particulate trace metals. *Analytical Chemistry*. 51:844-851.
- Tessier, A. Couillard Y., Campbell, PGC., and Auclair JC. 1993. Modeling Cd partitioning in oxic lake sediments and Cd concentrations in the freshwater bivalves *Anodonta gradis*. *Limnol. Oceanogr.* 38:1-17.
- Tessier, A., Rapin F., and Carignan R. 1985. Trace metals in oxic lake sediments: possible adsorption onto iron oxyhydroxides. *Geochim. Cosmochim. Acta*, 49:183-194
- Thakali, S., Allene, HE., Di Toro, DM., Ponizovsky, AA., Rooney, CP., Zhao, FJ., and McGrath, SP., 2006. A terrestrial biotic ligand model. 1. Development and application to Cu and Ni toxicities to barely root elongation in soils. *Environ. Sci. Technol.* 40:7085-7093

- Thamdrup B, Fossing, H and Jorgensen BB. 1994. Manganese, iron, and sulfur cycling in a coastal marine sediment, Aarhus bay, Denmark. *Geochim. Cosmochim. Acta*. 58:5115-5129.
- Thurman, EM., Malcom RL. 1981. Preparative isolation of aquatic humic substances. *Environ. Sci. Tech.* 15:463-466
- Tipping E., 1998. Humic ion-binding Model VI: an improved description of the interactions of protons and metal ions with humic substances. *Aquat. Geochem.* 4: 3-48.
- Turner, A., Martino M., and Roux, SM. 2002. Trace metal distribution coefficients in the Mersey Estuary, UK: evidence for salting out metal complexes. *Environ. Sci. Technol.* 36:4578-4584
- Turner, A., Millward, GE. And Roux, SM., 2004. Significance of oxides and particulate organic matter in controlling trace metal partitioning in a contaminated estuary. *Mar. Chem.* 88:179-192
- USEPA report, 1998, EPA's contaminated sediment management strategy. EPA-823-R-98-001
- USEPA report, 2005, Procedures for the derivation of equilibrium partitioning sediment benchmarks (ESBs) for the protection of benthic organisms: metal mixtures (cadmium, copper, lead, nickel, silver and zinc). EPA-600-R-02-011.
- USEPA, SW 846-3051, Test Methods for Evaluating Solid Waste, Physical/Chemical Methods, Microwave Assisted Acid Digestion of Sediments, Sludges, Soils, and Oils
- Van Leeuwen, H.P., Town, R.M., Buffle, J., Cleven, R.F.M.J., Davison, W., Puy, J., Van Riemsdijk, W.H., and Sigg, L., 2005. Dynamic Speciation Analysis and Bioavailability of Metals in Aquatic Systems, *Environ. Sci. Technol.*, 39:8545-8556
- Wang Y and Van Cappellen P. 1996. A multicomponent reactive transport model of early diagenesis: application to redox cycling in coastal marine sediments. *Geochim. Cosmochim. Acta*, 60:2993-3014
- Wang, F. And Chen, J. 1997. Modeling sorption of trace metals on natural sediments by surface complexation model. *Environ. Sci. Technol.* 31:448-453
- Wang, F., Chen, J., 1997. Modeling sorption of trace metals on natural sediments by surface complexation model. *Environ. Sci. Technol.* 31: 448-453.
- Zachara JM., Fredrickson JK., Smith SC and Gassman PL. 2001. Solubilization of Fe(III) oxide-bound trace metals by a dissimilatory Fe(III) reducing bacterium. *Geochim. Cosmochim. Acta*, 65:75-93

- Zeebe, R.E., Wolf-Gladrow, D.A., Jansen, H., 1999. On the time required to establish chemical and isotope equilibrium in the carbon dioxide system in seawater. *Mar. Chem.* 65:135-153.
- Zeebe, RE. 2007. Modeling CO<sub>2</sub> chemistry,  $\delta^{13}\text{C}$ , and oxidation of organic carbon and methane in sediment porewater: Implications for paleo-proxies in benthic foraminifera. *Geochim. Cosmochim. Acta*, 71:3238-32
- Zhang, H. and Davison, W. 1995. Performance characteristics of diffusion gradients in thin films for the in situ measurement of trace metals in aqueous solution. *Anal. Chem.* 67:3391-3400
- Zsecsody, J.E., Fruchter, J.S., Williams, M.D., Vermeul, V.R., and Sklarew, D., 2004. In situ chemical reduction of aquifer sediments: Enhancement of reactive iron phases and TCE dechlorination. *Environ. Sci. Technol.* 38:4656-4663.

## **Vita**

Yongseok Hong was born in Seoul, Korea in December, 1977. He had lived in Chamsil-dong for more than 20 years since he was 7 years old. After completing high school, he entered the Department of Civil and Environmental Engineering at Korea University and received his Bachelor's degree in January, 2002. During his college years, he went to the demilitarized zone (DMZ) in Korea and served for his country as an artillery specialist. He received his Master's of Environmental Engineering and Science degree from Korea University in January, 2004. He took a one and half year break as a project engineer at Dea-lim Industrial Company. He had been a doctoral student in the department of Civil, Architectural and Environmental engineering at the University of Texas at Austin since fall semester in 2005.

Permanent Address : 521 dong 605 ho, Jamsil 3 dong, SongpaGu, Seoul, Korea, 138-917

This manuscript was typed by the author.